EFFECT OF PRIOR EXPOSURE AT ELEVATED TEMPERATURES ON TENSILE PROPERTIES AND STRESS-STRAIN BEHAVIOR OF THREE OXIDE/OXIDE CERAMIC MATRIX COMPOSITES

THESIS

Christopher J. Hull, Captain, USAF

AFIT-ENY-MS-15-M-228

DEPARTMENT OF THE AIR FORCE
AIR UNIVERSITY

AIR FORCE INSTITUTE OF TECHNOLOGY

Wright-Patterson Air Force Base, Ohio

AFIT-ENY-MS-15-M-228

EFFECT OF PRIOR EXPOSURE AT ELEVATED TEMPERATURES ON TENSILE PROPERTIES AND STRESS-STRAIN BEHAVIOR OF THREE OXIDE/OXIDE CERAMIC MATRIX COMPOSITES

THESIS

Presented to the Faculty

Department of Aeronautics and Astronautics

Graduate School of Engineering and Management

Air Force Institute of Technology

Air University

Air Education and Training Command

In Partial Fulfillment of the Requirements for the

Degree of Master of Science in Aeronautical Engineering

Christopher J. Hull, BS

Captain, USAF

March 2015

AFIT-ENY- MS-15-M-228

EFFECT OF PRIOR EXPOSURE AT ELEVATED TEMPERATURES ON TENSILE PROPERTIES AND STRESS-STRAIN BEHAVIOR OF THREE OXIDE/OXIDE CERAMIC MATRIX COMPOSITES

Christopher J. Hull, BS

Captain, USAF

Committee Membership:

Dr. Marina Ruggles-Wrenn
Chair

Lt Col Chad Ryther, PhD
Member

Dr. Richard Hall
Member

AFIT-ENY-MS-15-M-228

Abstract

Thermal stability of three oxide-oxide ceramic matrix composites was studied. The materials studied were Nextel™610/aluminosilicate (N610/AS), Nextel™720/aluminosilicate (N720/AS), and Nextel™720/Alumina (N720/A), commercially available oxide-oxide ceramic composites (COI Ceramics, San Diego, CA). The N610/AS composite consists of a porous aluminosilicate matrix reinforced with laminated woven alumina N610 fibers. The N720/AS and N720/A composites consist of a porous oxide matrix reinforced with laminated, woven mullite/alumina (Nextel™720) fibers. The matrix materials are aluminosilicate in N720/AS and alumina in N720/A. All three composites have no interface between the fibers and matrix, and rely on the porous matrix for flaw tolerance. The N610/AS and N720/AS CMCs were heat treated in laboratory air for 100 h at 1100°C and for 10, 20, 40 and 100 h at 1200°C. The N720/A CMC was heat treated in laboratory air for 100 h at 1200°C and for 10, 20, 40 and 100 h at 1300°C. The room-temperature tensile properties of all composites were measured after each type of heat treatment. Effects of prior heat treatment on tensile strength were evaluated. Heat treatment at 1100°C had little effect on tensile strength of the N610/AS and N720/AS composites, while heat treatment at 1200°C caused dramatic loss of tensile strength. Poor strength retention after heat treatment at 1200°C is attributed to degradation of the aluminosilicate matrix. The N720/A composite exhibited excellent thermal stability, retaining about 90% of its tensile strength after heat treatment at

1300°C. Results indicate that the aluminosilicate matrix is considerably more susceptible to localized densification and coarsening of the porosity than the alumina matrix.

Acknowledgments

First and foremost, I would like to give my sincerest thanks and appreciation to Dr. Marina Ruggles-Wrenn as my thesis advisor. She has provided me with countless hours of guidance, not only through the process of writing this thesis, but also through the course work of my entire master's program. Ultimately, this thesis would not have been possible without her, and I cannot thank her enough. I would also like to thank Dr. Kathleen Shugart (AFRL/RXCC), Dr. Kristen Keller (AFRL/RXCCM) and Mr. Randy Corns (AFRL/RXCCM) for their equipment training, support and access to resources that without, I would have not been able to complete this research. I would also like to recognize and thank the AFIT machine shop for putting in the extra time to get me my test specimens early in order to avoid major delays due to construction. Additionally, thanks to Mr. Barry Page and Mr. Wilber Lacy for their constant support and willingness to immediately help when equipment needed to be fixed or reconfigured to continue my testing. Finally, I would like to thank my wife for her continued love and support while I devoted so much of my free time to research.

Christopher J. Hull

Table of Contents

Page

List of Figures

List of Tables

Nomenclature

σ	Stress
A	Cross-Sectional Area (mm^2)
E	Young's modulus (GPa)
P	Load (Pa)

List of Acronyms

AFIT	Air Force Institute of Technology
AFRL	Air Force Research Laboratory
CMC	Ceramic matrix composite
MTS	Material Test System
MPT	Multi-Purpose Testware
SEM	Scanning Electron Microscope
TEM	Transmission Electron Microscope
TPS	Thermal Protection Systems
UTS	Ultimate Tensile Strength

EFFECT OF PRIOR EXPOSURE AT ELEVATED TEMPERATURES ON TENSILE PROPERTIES AND STRESS-STRAIN BEHAVIOR OF THREE OXIDE/OXIDE CERAMIC MATRIX COMPOSITES

I. Introduction

1.1 Motivation

As aircraft performance increases, so does the demand for new material systems. Composites have helped to reduce cost and weight of many aircraft components. As of 2008, half of the components used to construct new generation aircraft are composites [1].

Advances in missiles and military aircraft, recently hypersonic aircraft, have also caused several components to be exposed to elevated temperatures and corrosive environments (primarily moisture) during operations. Examples of components include engine ducts, exhaust flaps, and large acreage thermal protection systems (TPS). This drives a demand for materials that can maintain mechanical properties, be thermally resistance, and have damage tolerance. All these requirements make ceramic matrix composites (CMC) prime candidates for such uses [2]. It is therefore necessary to study the effects of prolonged exposure, both at and above the manufacturer's recommended use temperatures, on CMC mechanical properties and microstructure.

1.2 Research Objective

The objective of this thesis was to determine the mechanical properties and capabilities of three oxide/oxide ceramic matrix composites (CMC) that have been subjected to controlled time-temperature histories.

The materials were be subjected to heat exposures that exceed their recommended use temperature threshold. Exposure was controlled for specific time intervals before being allowed to cool to room temperature. Room temperature tensile testing of each material was conducted in laboratory air to determine the effects that the time-temperature history had on the materials. Similar thermal exposures were conducted on each material at the maximum recommended use temperature to allow for a comparison between the mechanical properties and to evaluate the sensitivity that the temperature exceedance created.

The first two materials examined utilize an aluminosilicate matrix with Nextel™ fibers: Nextel™ 610/aluminosilicate (N610/AS) and Nextel™ 720/aluminosilicate (N720/AS). Both materials had a manufacturer maximum recommended use temperature of 1100°C. The third materials was Nextel™ 720/alumina (N720/A) which had a maximum recommended use temperature of 1200°C.

1.3 Methodology

In order to accomplish the objective of the research, the following process was used:

- Specimen preparation to include heat soak each of the CMC plates both at the maximum recommended temperature and over-temperature conditions for various controlled time intervals
- Perform monotonic tensile testing to failure on specimens to determine various material characteristics.

- Perform microscopy observations on the fracture surface using an optical microscope and SEM.

II. Background

2.1 Ceramics

Ceramics are inorganic and nonmetallic materials and have existed for centuries. Human and animal figurines have been found from as early as 24,000 B.C. made from clay and other materials [3]. The original uses for ceramic were primarily decorative, until more utilitarian purposes were discovered. Pottery was developed around 9,000 – 10,000 B.C. and became a means for transporting water and food storage. Eventually, ceramics were used to create thermal and electrical insulators [3]. The high strength, electrical insulation properties and the ability to handle relatively high temperature compared to many metallic materials have made ceramics a staple in modern life. It is because of these properties that engineers have incorporated ceramics into many advanced automotive, aerospace, and military designs. One of the largest drawbacks to monolithic ceramics is low fracture toughness and susceptibility to catastrophic failure [4].

2.2 Ceramic Matrix Composite

Composite materials are not a new idea. Straw was mixed with mud by the Egyptians as early as 1500 B.C. to construct buildings. The combination of the two materials provides many superior properties that the individual materials could not provide independently. This consolidation of materials helped to mitigate catastrophic modes of failure; one of the largest disadvantages that ceramics face. Reinforcing fibers provide strength to the material by carrying loads unattainable by the ceramic matrix itself. The ceramic matrix operates as a way of deflecting the crack propagation around

the fibers. It is accepted that for CMCs, weak bonding between the fiber and matrix is needed to allow this crack deflection to occur. Strong matrix/fiber bonding allows the crack propagation to continue through the matrix material into the fiber. Fiber coating reduces the adhesion between the fiber and the matrix material. Another philosophy for crack deflection is through the use of a porous matrix. The relatively high porosity allows a path for the crack to propagate around the CMC fibers instead of through it. This reduces coordinated fiber failures and allows the CMC to fail gracefully.

The components of CMCs are generally divided into two different categories; oxide and non-oxides. Corrosive environments, like steam, can oxidize materials. Oxide CMC components tend to resist this oxidation even at elevated temperatures. Non-oxide components, while prone to oxidation, are generally much stronger than oxide components. [5].

III. Material and Test Specimen

3.1 Material

The objective of this research is to characterize the mechanical properties and composite microstructure of oxide-oxide CMC systems subjected to various controlled time-temperature histories. Three material systems studied in this work consisted of a porous oxide matrix reinforced with oxide fibers. There is no fiber coating. The damage tolerance of all three composites is enabled by the porous matrix. The composites were fabricated by ATK-COIC (San Diego, CA) and supplied in a form of plates comprised of 0/90 woven layers. The fibers were woven in an eight-harness satin weave (8HSW). The fiber fabric was infiltrated with the matrix in a sol-gel process. The laminate was dried with a "vacuum bag" technique under low pressure and low temperature, then pressureless sintered [6]. The oxide CMC fabrication process used by COIC is shown schematically in Figure 1 [7]. No exterior coating was added to the fabricated CMC panels.

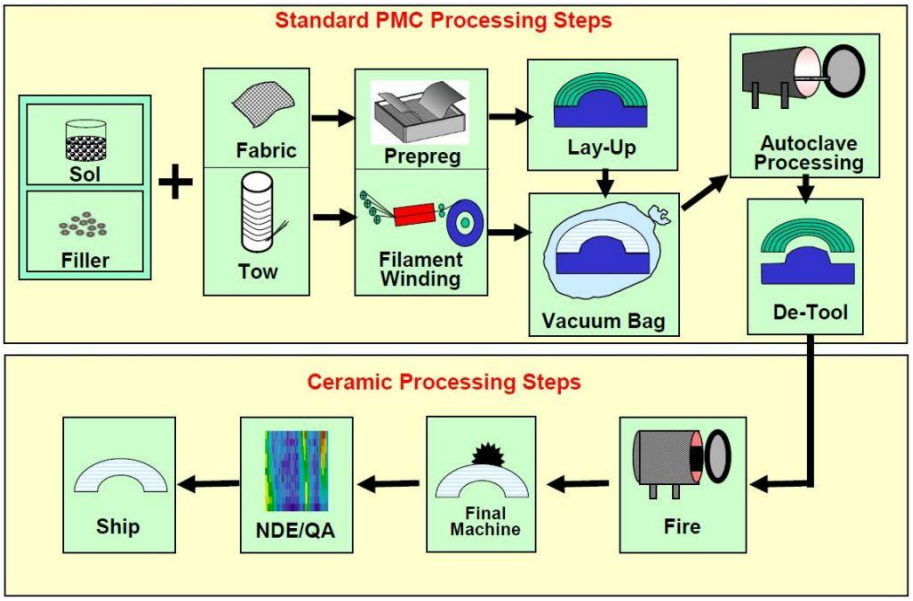

Figure 1 – Oxide CMC Fabrication Process [7]

A detailed description of each oxide-oxide CMC studied in this work is given below.

3.1.1 Nextel™610/Aluminosilicate (N610/AS)

The Nextel™610/aluminosilicate (N610/AS) is an oxide-oxide CMC consisting of a porous aluminosilicate matrix reinforced with Nextel™610 fibers. There is no fiber coating. The Nextel™610 is a high-purity alumina fiber (> 99% Al_2O_3) manufactured by 3M™ Corporation (Minneapolis, MN). Fiber properties are extensively reported elsewhere [8, 9, 10, 11]. The aluminosilicate matrix was comprised of the Al_2O_3 particles bonded together by a continuous SiO_2 film. The matrix derives its porosity from incomplete filling of the interparticle voids [12].

The N610/AS composite was supplied in a form of a 2.63-mm thick panel comprised of 14 0°/90° woven layers, with a density of 2.83 g/cm^3, a fiber volume of 51%, and matrix porosity of 25% [7].

3.1.2 Nextel™720/Aluminosilicate (N720/AS)

The Nextel™720/aluminosilicate (N720/AS) is an oxide-oxide CMC consisting of a porous aluminosilicate matrix reinforced with Nextel™720 fibers. There is no fiber coating. The Nextel™ 720 is an alumina-mullite fiber (85 wt% Al_2O_3 and 15 wt% SiO_2) manufactured by 3M™ Corporation (Minneapolis, MN) with an α-alumina – mullite volume fraction ratio of 57:43 [13]. Nextel™720 fibers is comprised of alumina grains with an approximate diameter of 0.1 μm distributed among larger (0.5 μm) mullite grains, consisting of many smaller subgrains [14]. It is recognized that Nextel™720 fiber has the best creep performance of any commercially available polycrystalline oxide fiber. The superior high-temperature creep performance of the Nextel™720 fibers results from

the high content of mullite, which has a much better creep resistance than alumina [10]. An extensive review of fiber properties can be found elsewhere [9, 10, 13, 14, 15, 16, 17, 18]. A brief description of the aluminosilicate matrix is provided in Section 3.1.1 above.

The N720/AS composite was supplied in a form of a 2.54-mm thick panel comprised of 12 0°/90° woven layers, with a density of 2.80 g/cm^3, a fiber volume of 39%, and matrix porosity of 25% [7].

3.1.3 Nextel^{TM}720/Alumina (N720/A)

The Nextel^{TM}720/alumina (N720/A) is an oxide-oxide CMC consisting of a porous alumina matrix reinforced with Nextel^{TM}720 fibers. There is no fiber coating. The N720/A composite was supplied in a form of a 2.74-mm thick panel comprised of 12 0°/90° woven layers, with a density of 2.73 g/cm^3, a fiber volume of 45%, and matrix porosity of 25% [7].

3.2. Specimen Geometry

Each CMC was fabricated in a form of a 200 mm × 200 mm square panel. These panels were each cut into four smaller plates. Hence four 100 mm × 100 mm plates of each composite were available for this work. Each 100 mm × 100 mm plate was subjected to a controlled time-temperature history prior to specimen machining. Six dogbone-shaped specimens were cut from each plate. The cutting plan is shown in Figure 2. Test specimens were cut using an abrasive waterjet according to the specifications in Figure 3.

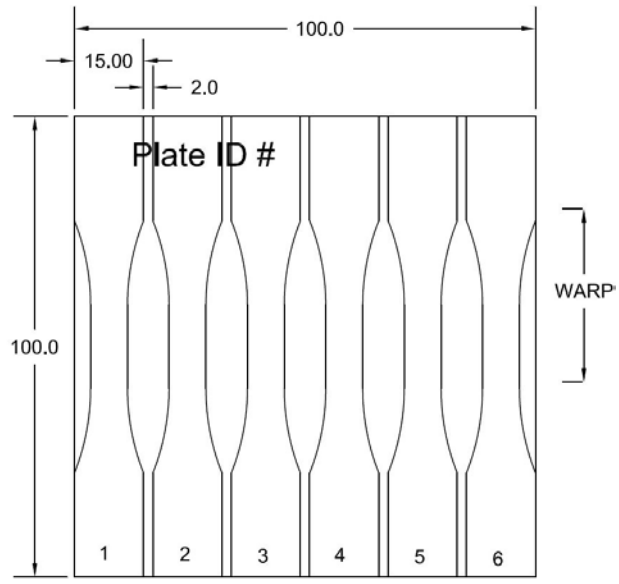

Figure 2 – Cutting plan (all dimensions in mm)

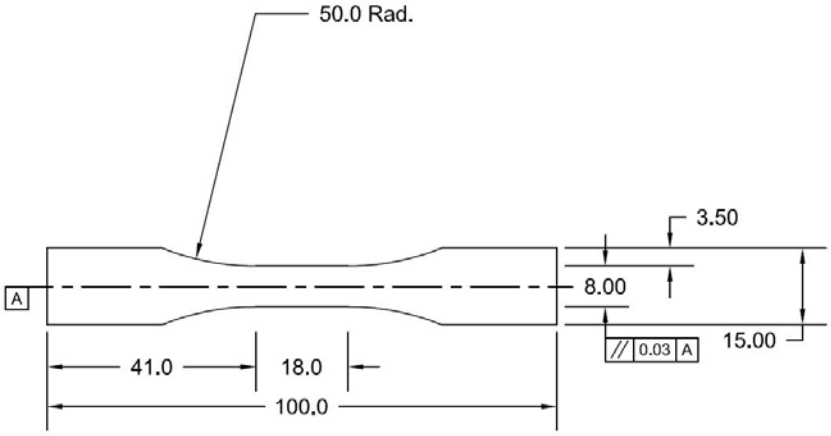

Figure 3 – Dogbone-shaped specimen (all dimensions in mm)

Width and thickness of the gage section of each specimen were measured (using a Mitutoyo Corporation Digital Micrometer) and recorded prior to testing. Based on these measurements, the cross sectional area of each specimen was determined. Stress was calculated using the standard expression:

$$\sigma = \frac{P}{A} \tag{1}$$

where P is the applied load and A is the cross-sectional area of the test specimen.

IV. Experimental Setup and Test Procedures

This section provides a description of the equipment used for mechanical testing and for microstructural examination. Preparation of test specimens, as well as test procedures, are described in detail.

4.1. Mechanical Test Equipment

Uniaxial mechanical testing was completed using a MTS 810 Material Test Systems of 13.3 kN (3 kip) capacity (Figure 4) equipped with hydraulic wedge grips. An MTS FlexTest^{TM} 40 digital controller was used for input signal generation and data collection.

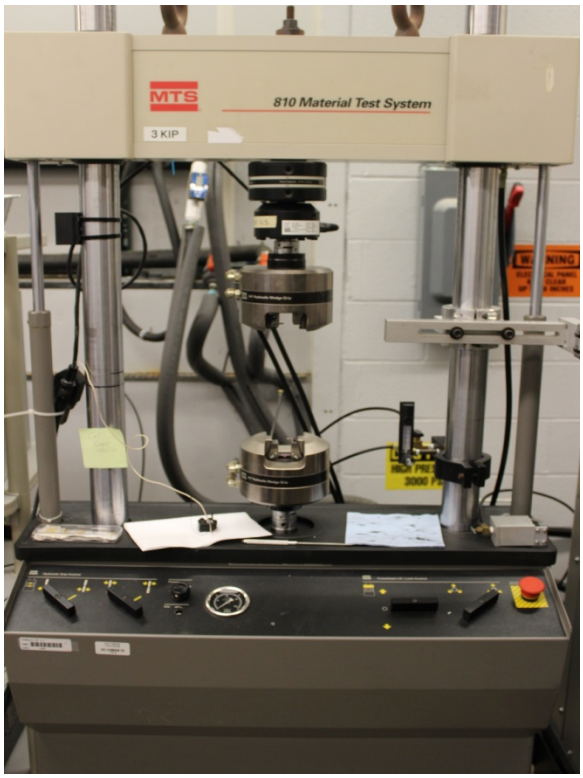

Figure 4 – MTS 810 Material Test System utilized for uniaxial tensile testing

Strain measurement was accomplished with a clip-on, uniaxial extensometer (MTS model 632.13E-20) with 12.7 mm gage section (Figure 5).

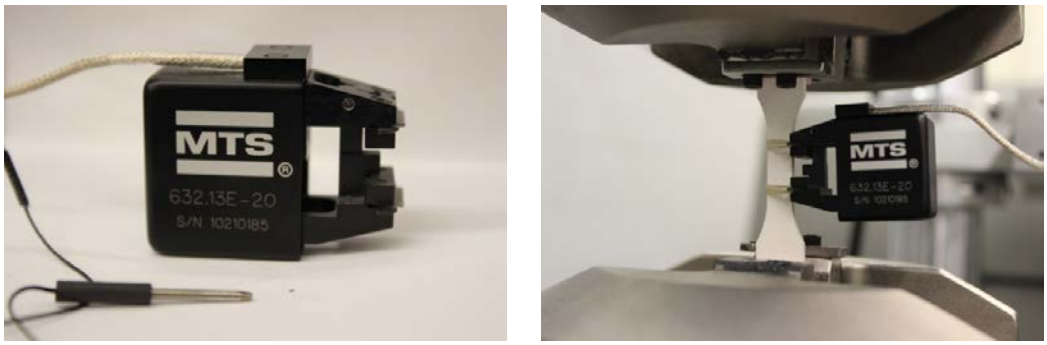

Figure 5 – (a) MTS extensometer and (b) extensometer installed on test specimen

4.2. Microstructural Characterization

The post-test microstructure was examined using both an optical microscope and a scanning electron microscope (SEM). Microstructure of the as-processed CMCs was also examined. The resulting micrographs were used to characterize the dominant damage mechanisms and microstructural changes caused by prior time-temperature histories.

4.2.1 Optical Microscope

Optical microscopy was completed with a Zeiss Discovery V12 (Jena, Germany) equipped with an AxioCam HRc digital camera to capture the images (Figure 6).

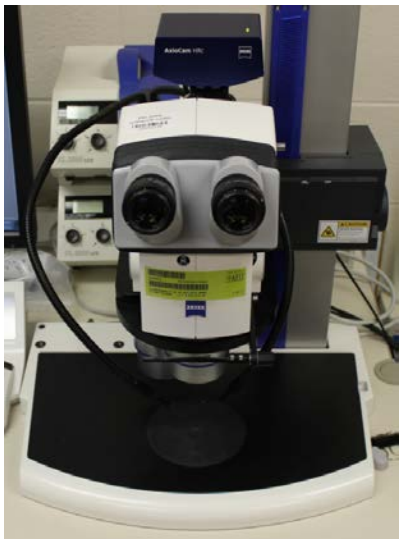

Figure 6 – Zeiss Discovery V12 optical microscope equipped with an AxioCam HRc digital camera

4.2.2 Scanning Electron Microscope

For greater magnification than that available from the optical microscope, a FEI Quanta 450 SEM was used (Figure 7). To prepare the specimens for viewing with the SEM, a Buehler IsoMet 5000 Linear Precision Saw (Figure 8) was used to cut the specimen.

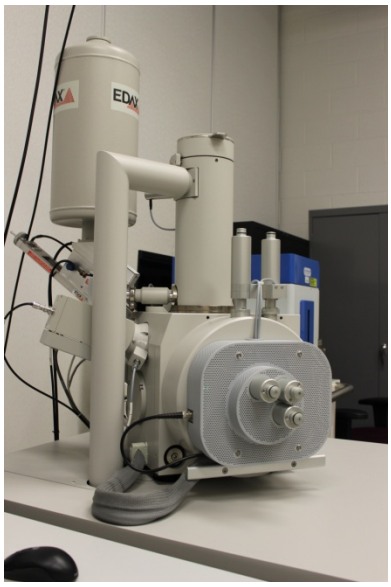

Figure 7 – FEI Quanta 450 scanning electron microscope

Figure 8 – IsoMet 5000 linear precision saw

4.3. Specimen Preparation

Eight plates and three dogbone-shaped specimens of each material system were provided by AFRL for this research. A summary of plates and specimens of each material system is depicted in Figure 9.

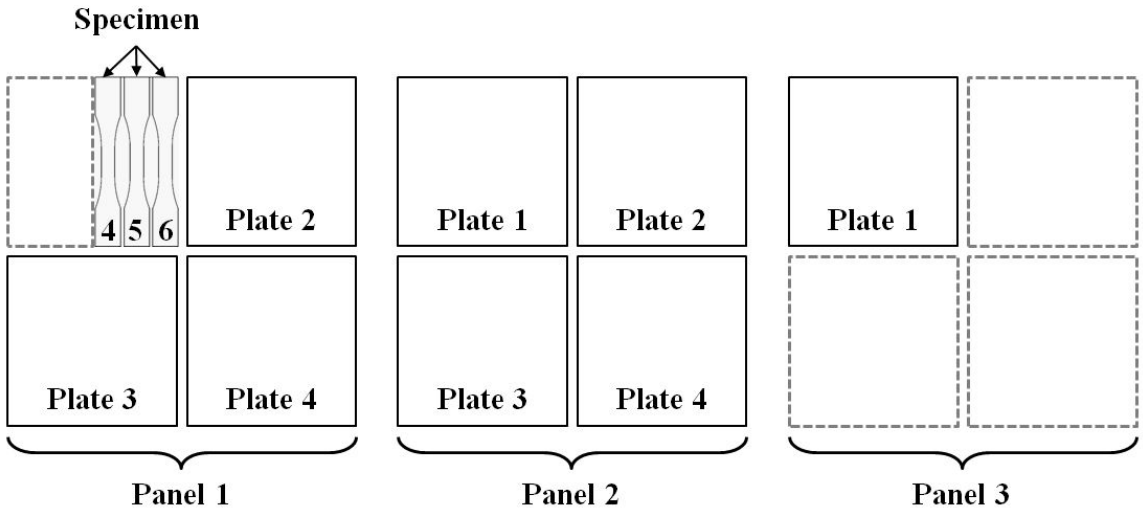

Figure 9 – Plates and specimens of a given material system provided for this research

The thickness of each plate was measured in four locations and recorded. The length and width of each plate were measured in two locations. The measured dimensions were averaged to calculate an approximate volume of each plate. The weight of each plate was measured and an approximate density was calculated. Then, the plates were dried in a vacuum oven (Lab Companion Vacuum Oven OV-11) at 120°C for approximately 24 hours to ensure a near zero moisture content in the material. After drying, the plates were weighed and measured again to calculate the dry density. Next, the plates were subjected to prescribed time-temperature histories in a furnace (Thermolyne 46100). The furnace was heated to the target temperature at 10°C/min. Table 1 shows exposure temperature and exposure time for each plate. After the plates

were heat treated and allowed to cool, they were weight and measured again to calculate a post-heat treated density. The recorded weights and measurements collected during specimen preparation are shown in Appendix A along with a more in-depth discussion on how the densities were calculated.

Table 1 –Exposure Temperature and Time Conditions

Material	*Panel*	*Plate*	*Exposure Temperature (°C)*	*Exposure Time (h)*
N610/AS	2	3	1100	100
N610/AS	1	4	1200	10
N610/AS	1	3	1200	20
N610/AS	2	1	1200	40
N610/AS	2	2	1200	100
N720/AS	2	3	1100	100
N720/AS	1	1	1200	10
N720/AS	1	3	1200	20
N720/AS	2	1	1200	40
N720/AS	2	2	1200	100
N720/A	2	3	1200	100
N720/A	1	1	1300	10
N720/A	1	3	1300	20
N720/A	2	1	1300	40
N720/A	2	4	1300	100

Test specimens were cut from the plates following heat treatment. Prior to testing, all specimens were cleaned using a process previously employed at AFIT [12]:

1. Rinsed with isopropyl alcohol
2. Immersed in a sonic bath (Branson 5510) of isopropyl alcohol for 20 minutes
3. Soaked in separate bath of isopropyl alcohol for 10 minutes
4. Rinsed with isopropyl alcohol
5. Dried in oven (Yamato Drying Oven DVS 602) for 20-24 h at 120°C in ambient pressure

4.4. Test Preparation

Each specimen was measured to determine the cross sectional area of the gage section. Immediately before testing, fiberglass tabs were attached with cyanacrylate adhesive (M-Bond 200) to the gripping sections of each specimen. These tabs were used to protect specimens from the grip wedges/pressure when using the MTS machine.

Initially, several N610/AS specimens heat treated at 1200°C for various durations were prepared for testing with thin (0.79 mm) fiberglass tabs. Three specimens were tested. In all tests, specimens failed prematurely in the gripping section. Reduction in the grip pressure did not solve this problem. Therefore, it was concluded that the thin fiberglass tabs were not providing sufficient protection to the heat treated specimens. Thicker (6.35 mm) fiberglass tabs were bonded to the remaining specimens to provide more protection. Specimens outfitted with thicker tabs failed consistently in the gage section. Figure 10 shows a side by side comparison of the two different fiberglass tabs that were used to protect the specimens.

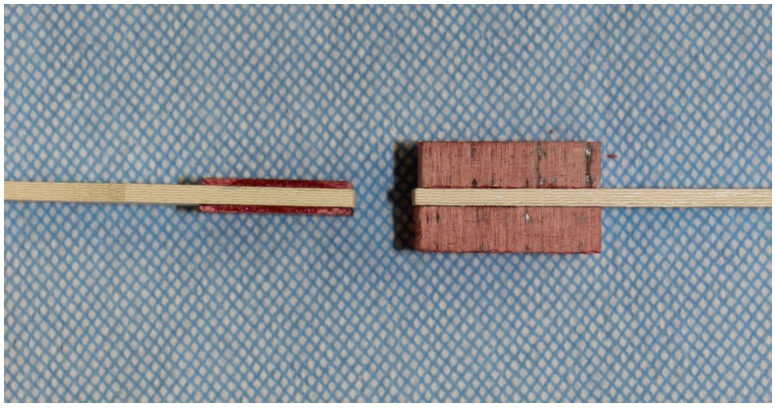

Figure 10 – Comparison of the two different fiberglass tabs used during tensile testing

4.5. Test Procedures

The MTS testing system was placed in displacement control and the actuator was moved to accept the test specimen. Then, the top of the prepared test specimen was gripped. The MTS testing system was then placed into force control and set to command zero load. Then, the bottom of the specimen was gripped.

A locking pin was inserted into the extensometer to keep the extensometer at zero strain. The extensometer was mounted on the side of the test section of the specimen using rubber bands. The surface of the specimens were rough enough that the specimens did not need any surface treatment or notching for accurate measurements, but enough tension in the rubber bands was needed to ensure the knife edge of the strain gauge did not slip along the edge of the specimen during testing. Once the extensometer was installed, the locking pin was removed and the strain reading was tared so that zero initial strain was being measured.

The MTS testing system was then set back to displacement control. Tensile tests to failure were performed in displacement control at a rate of 0.05 mm/s. This process was repeated for each of the specimens for each of the materials. All testing was completed at room temperature in laboratory air. The test data was retrieved from the MTS FlexTest^{TM} software for further analysis.

After specimen failure, visual inspection of the test specimens was completed to identify a representative sample from each material and heat treatment condition. The representative specimens were then examined under an optical microscope.

V. Results and Discussion

5.1. Effect of Heat Treatment on Composite Density

Density of each material system was calculated before and after drying in a vacuum oven. The recorded weights and measurements collected during testing are shown in Appendix A along with a more in-depth discussion on how the densities were calculated. The average as-received density of each material system is compared to its average dry density in Table 2. Average density of all material systems increased slightly due to vacuum drying. The percent change in average density due to the vacuum drying is shown in Figure 11 for each material.

Table 2 – Comparison of average as-received density and average dry density for each material system.

Material	*As-received density (g/cm^3)*	*Dry density (g/cm^3)*
N610/AS	2.89	2.93
N720/AS	2.66	2.70
N720/A	2.74	2.78

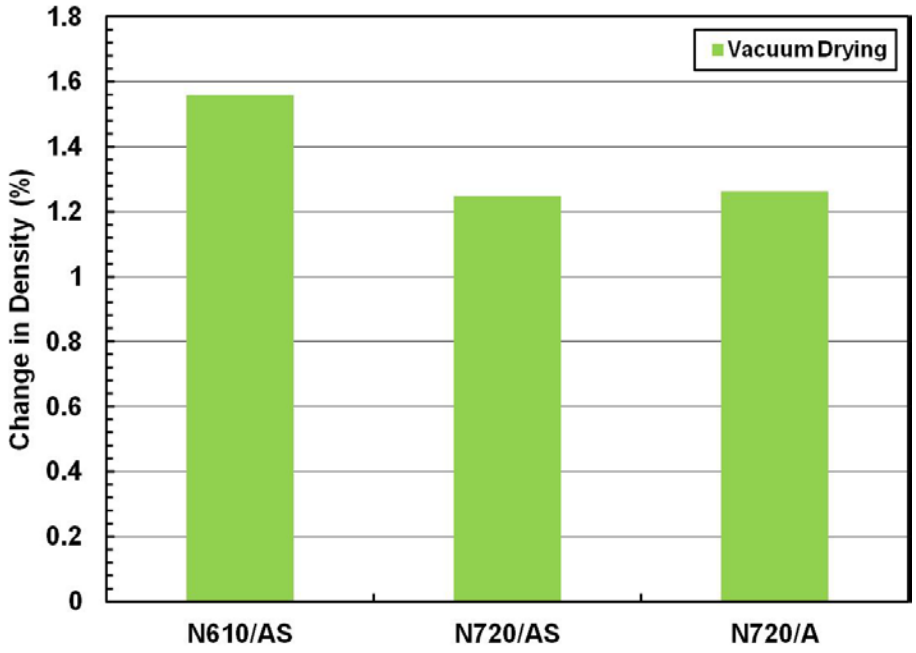

Figure 11 – Average change in density due to vacuum drying of N610/AS, N720/AS, and N720/A composites

Notably, heat treatment had a more significant effect on density of each CMC. Recall that two exposure temperatures were used for each of the materials: the maximum recommended use temperature (T_{max}) and a temperature 100°C above the maximum recommended use temperature (T_{max}+100°C). One plate of each CMC was heat treated for 100 h at T_{max}. Remaining plates of each CMC were heat treated for various durations at T_{max}+100°C. Figure 12 shows the percent change in CMC density due to the vacuum drying process followed by heat treatment for 100 h at T_{max}. Note that the results in Figure 12 are based on a single plate for each CMC. Hence, the percent change in density due to vacuum drying and heat treatment for 100 h at T_{max} in Figure 12 represents a single data point. While this limited amount of data does not allow for final determination of material characteristics, it does allow for observations to be made. The materials that utilized the aluminosilicate matrix showed either no increase, as is the case with

N610/AS, or an actual decrease in density, as is the case with N720/AS. In contrast, the density of the CMC containing alumina matrix continued to increase during the heat treatment. At the end of the 100 h heat treatment, percent increase in density of the N720/A CMC with an alumina matrix was nearly twice that of the N610/AS CMC with an aluminosilicate matrix.

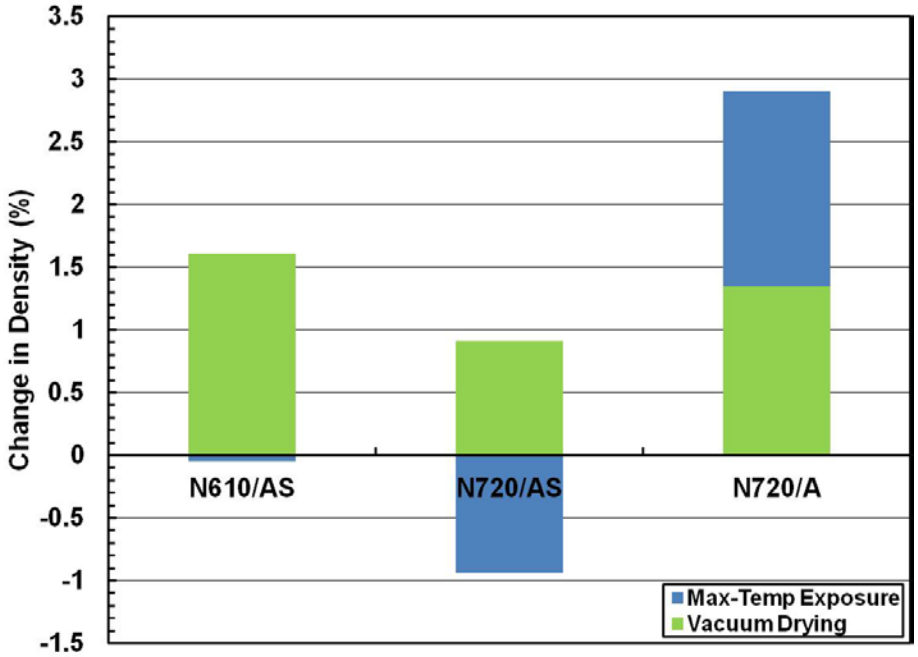

Figure 12 – Change in average density due to vacuum drying followed by 100 h at T_{max} of N610/AS, N720/AS, and N720/A composite

Four plates of each CMC were exposed to over-temperature (T_{max} + 100°C) conditions for various durations. Figure 13 shows the average percent change in density due to the vacuum drying process followed by 100 h at over-temperature (T_{max} + 100°C) for each CMC. In this case, all the CMCs exhibited an increase in density. Furthermore, the increases in average density of the CMCs with aluminosilicate matrix were noticeably above the increase in average density of the N720/alumina composite.

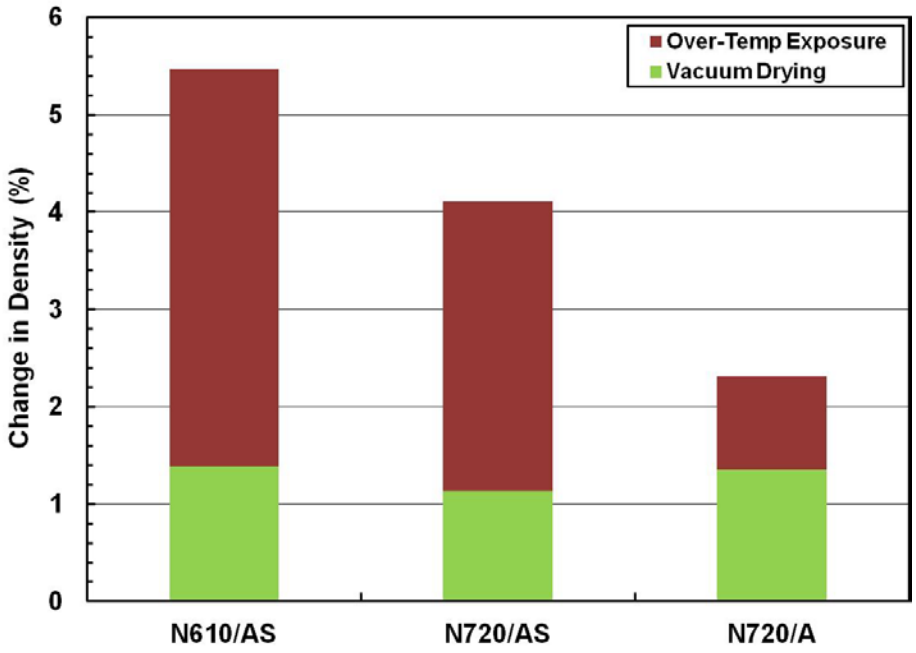

Figure 13 – Change in average density due to vacuum drying followed by 100 h at over-temperature (T_{max}+100°C) of N610/AS, N720/AS and N720/A composites

Figure 14 compares the percent changes in density due to heat treatment only. Results reveal that the aluminosilicate matrix exhibits significant densification when exposed at temperatures above the maximum recommended use temperature T_{max}. In contrast, the alumina matrix exhibits densification when heat treated at either T_{max} or T_{max}+100°C. However, density of the alumina matrix is less sensitive to the increase in heat treatment temperature from T_{max} to T_{max}+100°C. Note that the changes in density due to 100 h of exposure at T_{max} shown in Figure 14 are the same as those presented previously in Figure 12.

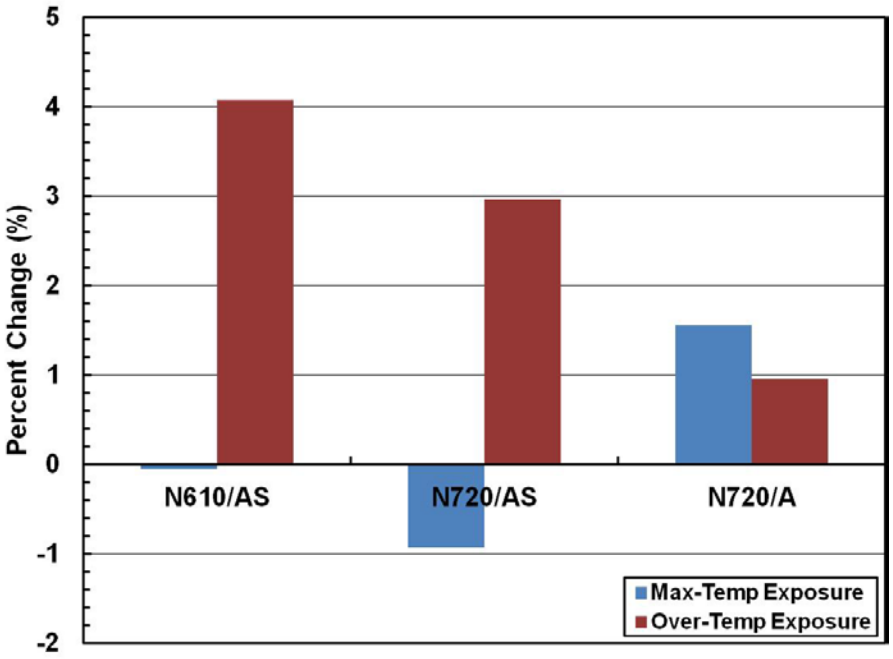

Figure 14 – Change in average density due to 100 h at T_{max} and at over-temperature (T_{max}+100°C) of N610/AS, N720/AS and N720/A composites

The change in weight and the change in the volume of each plate due to drying and subsequent heat treatment were also examined. The weight change was negligible in all cases. In contrast, considerable changes in volume were observed. The increases in density reported above were caused by slight shrinking of the composite plates.

Figure 15 – Figure 17 show the percent change in volume and weight of the plates at room temperature due to vacuum drying and subsequent heat treatment. Also depicted is the change in the overall density resulting from changes in volume and/or weight of each material. Due to the limited number of plates, a trend in volume, weight, or density change cannot be determined with statistical confidence. However, the density is expected to vary with exposure time in a non-linear manner and to ultimately reach an asymptotic solution.

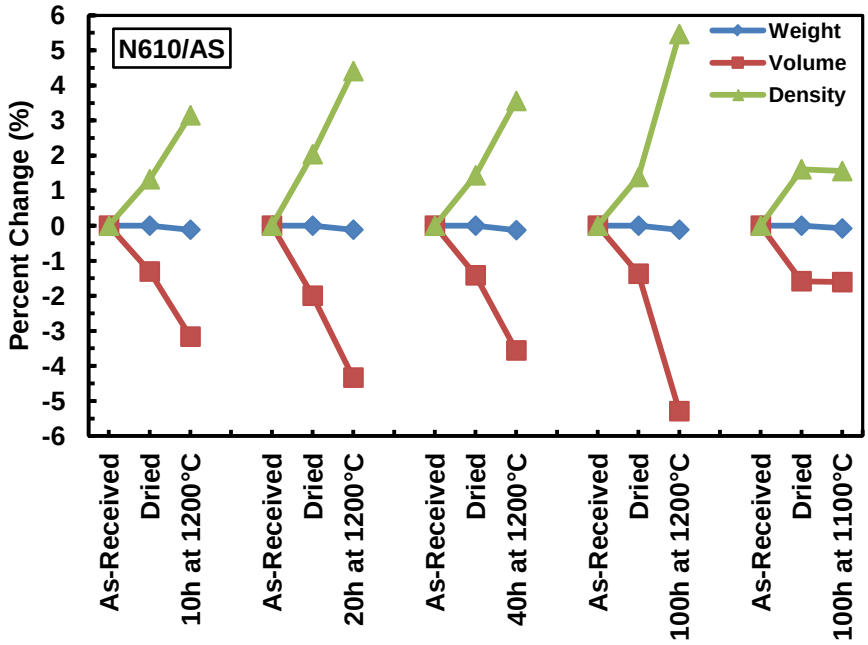

Figure 15 – Change in weight, volume and density due to vacuum drying and subsequent heat treatment for N610/AS ceramic composite

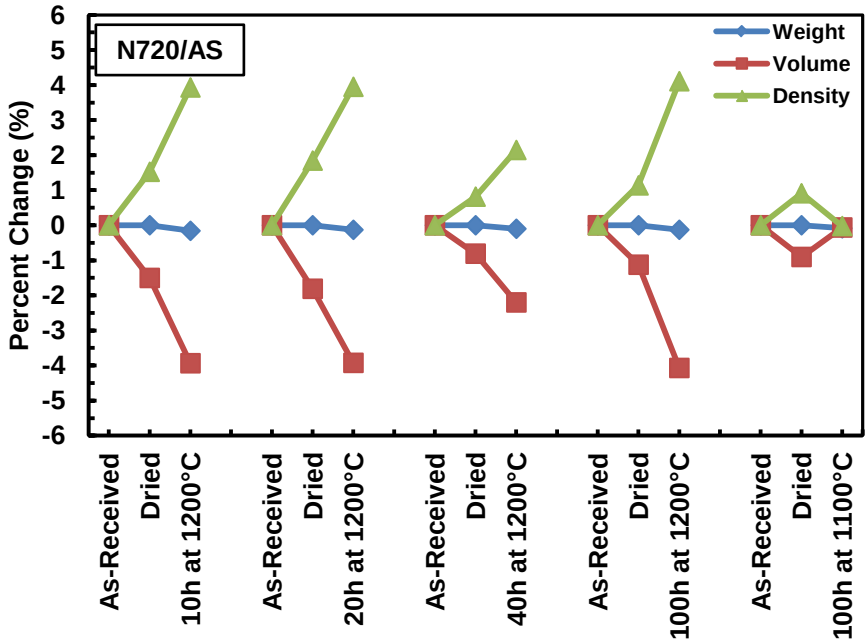

Figure 16 – Change in weight, volume and density due to vacuum drying and subsequent heat treatment for N720/AS ceramic composite

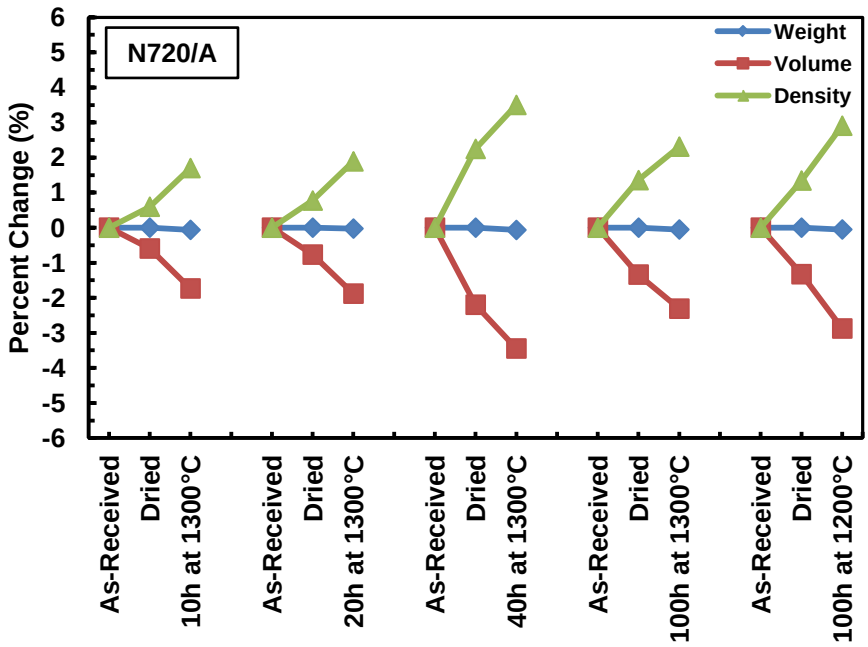

Figure 17 – Change in weight, volume and density due to vacuum drying and subsequent heat treatment for N720/A ceramic composite

5.2. Effect of Heat Treatment on Composite Tensile Properties

The as-received specimens of each material system were tested to determine baseline tensile properties. The as-received tensile properties obtained in this work were compared with unpublished results of as-received strength and modulus values obtained at AFRL for the same batch of the three CMCs (Table 3). Results in Table 3 reveal a good agreement between the two sets of data.

Table 3 – Tensile strength and modulus values obtained for the as-received N610/AS, N720/AS, and N720/A composites at AFIT and at AFRL

Material	*AFRL UTS (MPa)*	*Report UTS (MPa)*	*AFRL Modulus (GPa)*	*Report Modulus (GPa)*
N610/AS	397	410.7	110	116.6
N720/AS	229	225.9	78.7	81.4
N720/A	161	159.9	83	83.8

Stress-strain curves were generated for each of the specimens tested in this research. These curves are shown in Appendix B. For each material system, representative stress-strain curves for each prior heat treatment were selected in order to determine and compare the effects of the different time-temperature histories. Results are presented below for each CMC.

5.2.1 Effect of Heat Treatment on Tensile Properties of N610/AS Composite

Figure 18 shows the representative tensile stress-strain curves obtained for the N610/AS specimens heat treated at 1200°C for various durations. The representative stress-strain curve for the as-received N610/AS composite is included in Figure 18 for comparison. Results in Figure 18 reveal that the tensile strength decreased and the elastic modulus increased with increased exposure time.

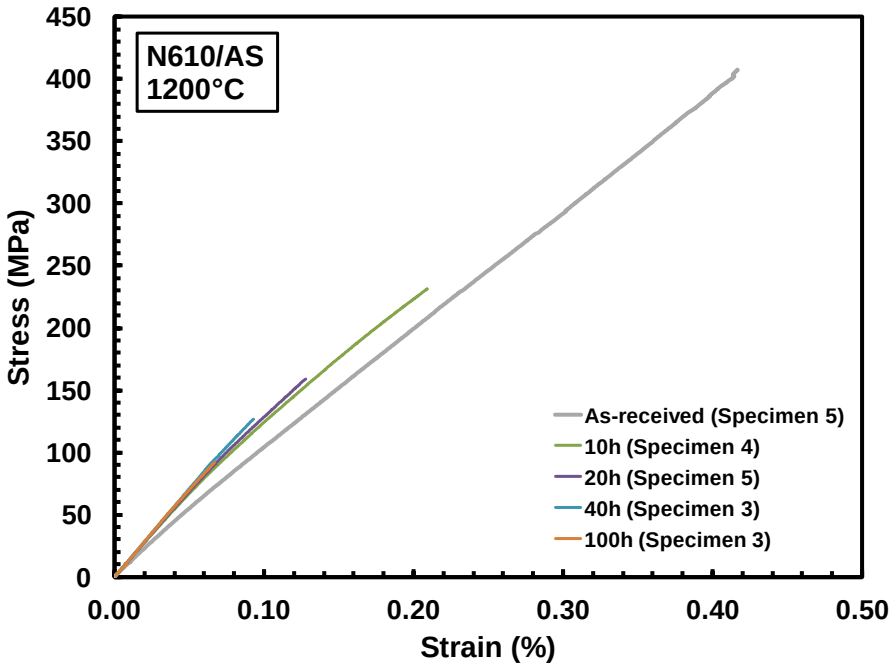

Figure 18 – Effect of prior heat treatment at 1200°C on tensile stress-strain behavior of N610/AS composite

Notably, the majority of the tensile strength is lost during the first 10 h of exposure at 1200°C. Figure 19 shows the percentage of retained strength vs. exposure time.

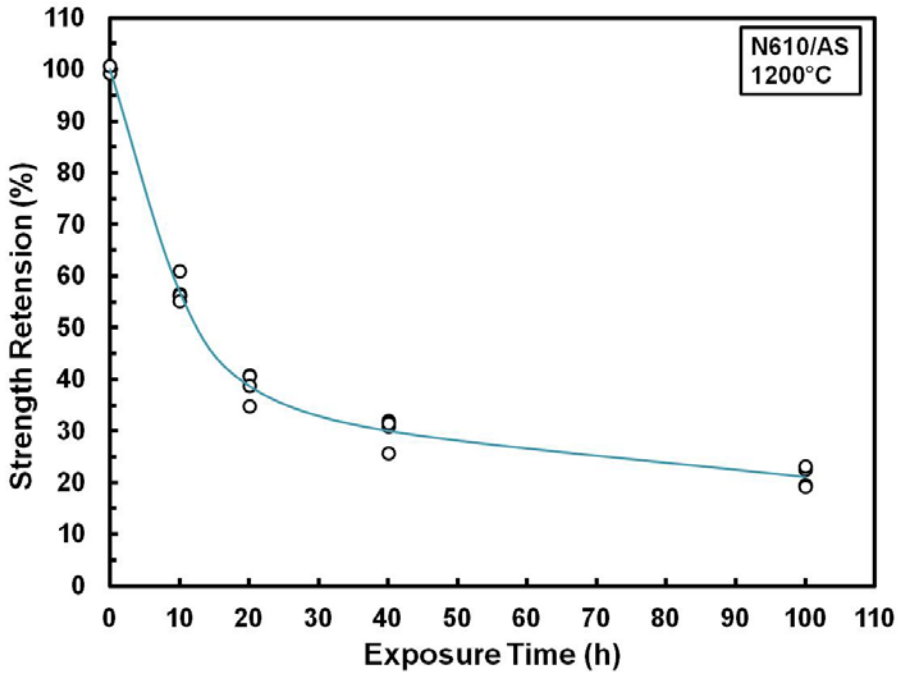

Figure 19 – Tensile strength retention as a function of exposure time at 1200°C for N610/AS composite

Figure 20 shows the representative tensile stress-strain curve obtained for N610/AS specimens heat treated for 100 h at 1100°C together with those obtained for specimens heat treated at 1200°C for 10 and 100 h. The representative stress-strain curve for the as-received N610/AS composite is included in Figure 20 for comparison. Prior heat treatment at 1100°C also causes a decrease in tensile strength and an increase in elastic modulus of the N610/AS composite. However, results in Figure 20 demonstrate that 10 h at 1200°C had a far more degrading effect on tensile strength than 100 h at 1100°C.

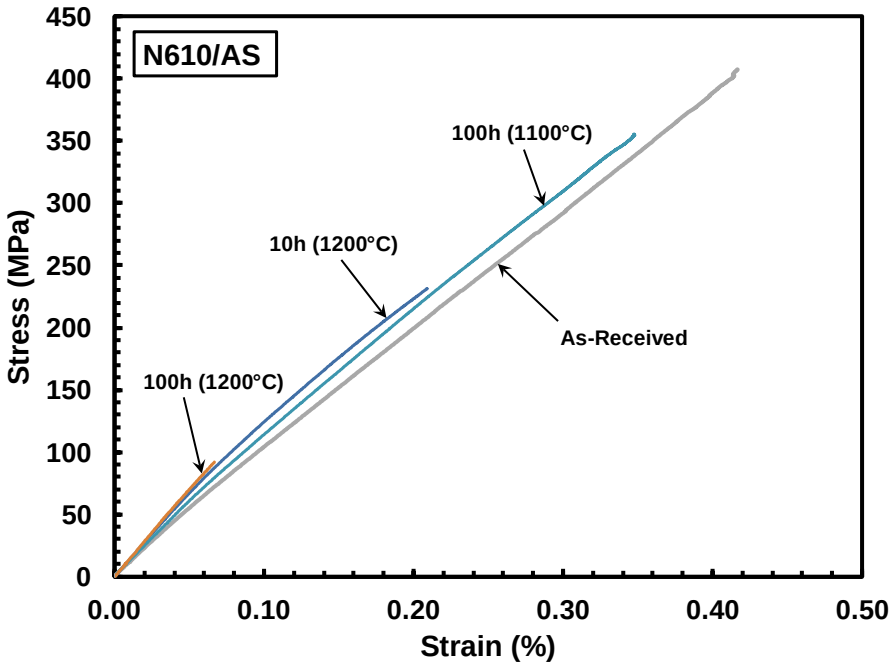

Figure 20 – Effect of prior heat treatment at 1100°C and at 1200°C on tensile stress-strain behavior of N610/AS composite

Tensile strength, modulus, and failure strain values obtained for the N610/AS specimens subjected to the different time-temperature histories are summarized in Table 4, Table 5, and Table 6, respectively.

Table 4 – Effect of prior heat treatment on tensile strength of N610/AS composite

Exposure Time (h)	*Exposure Temp (°C)*	*Average UTS (MPa)*	*Individual Specimen UTS (MPa)*			
			3	*4*	*5*	*6*
0	N/A	410.7	N/A	N/A	407.7	413.6
100	1100	351.1	355.6	340.0	355.5	353.4
10	1200	234.3	230.6	231.2	226.5	250.7
20	1200	154.7	168.0	166.8	159.2	142.9
40	1200	123.4	127.0	131.5	105.3	129.6
100	1200	86.7	92.4	94.9	80.6	78.8

Table 5 – Effect of prior heat treatment on tensile modulus of N610/AS composite

Exposure Time (h)	*Exposure Temp (°C)*	*Average E (GPa)*	*Individual Specimen E (GPa)*					
			1	*2*	*3*	*4*	*5*	*6*
0	N/A	116.6	N/A	N/A	N/A	118.1	111.9	119.9
100	1100	122.6	131.7	122.2	120.1	120.1	121.2	120.4
10	1200	132.3	131.0	140.5	128.3	138.4	127.5	127.9
20	1200	135.4	138.1	134.2	136.9	135.3	140.8	127.3
40	1200	142.2	143.0	148.9	144.0	149.0	134.8	133.8
100	1200	134.4	135.1	130.0	143.1	133.5	139.8	124.8

Table 6 – Effect of prior heat treatment on tensile failure strain of N610/AS composite

Exposure Time (h)	*Exposure Temp (°C)*	*Average Failure Strain (%)*	*Individual Specimen Failure Strain (%)*			
			3	*4*	*5*	*6*
0	N/A	0.417	N/A	N/A	0.417	0.418
100	1100	0.358	0.369	0.338	0.348	0.375
10	1200	0.212	0.216	0.209	0.204	0.235
20	1200	0.128	0.138	0.140	0.128	0.124
40	1200	0.094	0.093	0.094	0.083	0.108
100	1200	0.067	0.067	0.075	0.060	0.065

Generally, results in Table 4 – Table 6 show little specimen-to-specimen variability for a given property and time-temperature history. However, specimen-to-specimen variability increases somewhat with increasing exposure time.

5.2.2 Effect of Heat Treatment on Tensile Properties of N720/AS Composite

Figure 21 shows the representative tensile stress-strain curves obtained for the N720/AS specimens heat treated at 1200°C for various durations. The representative stress-strain curve for the as-received N720/AS composite is included in Figure 21 for comparison. Tensile strength decreases with exposure time. The elastic modulus of the

heat treated specimens was higher than that of the as-received composites. However, the elastic modulus shows little change with exposure time.

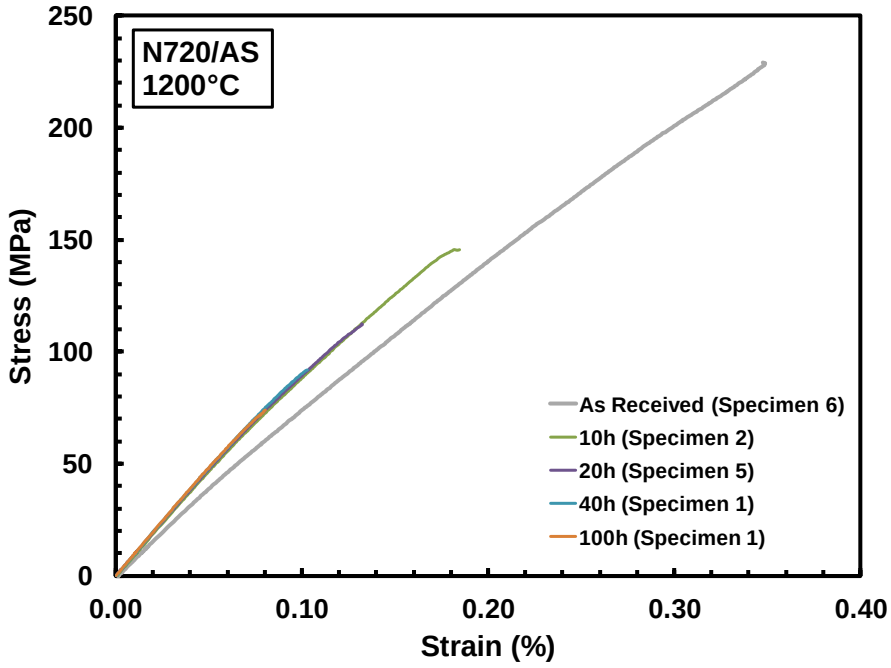

Figure 21 – Effect of prior heat treatment at 1200°C on tensile stress-strain behavior of N720/AS composite

As in the case of the N610/AS composite, the majority of the tensile strength of N720/AS was lost during the first 10 h of heat treatment at 1200°C. Figure 22 shows the strength retention as a nonlinear function of exposure time.

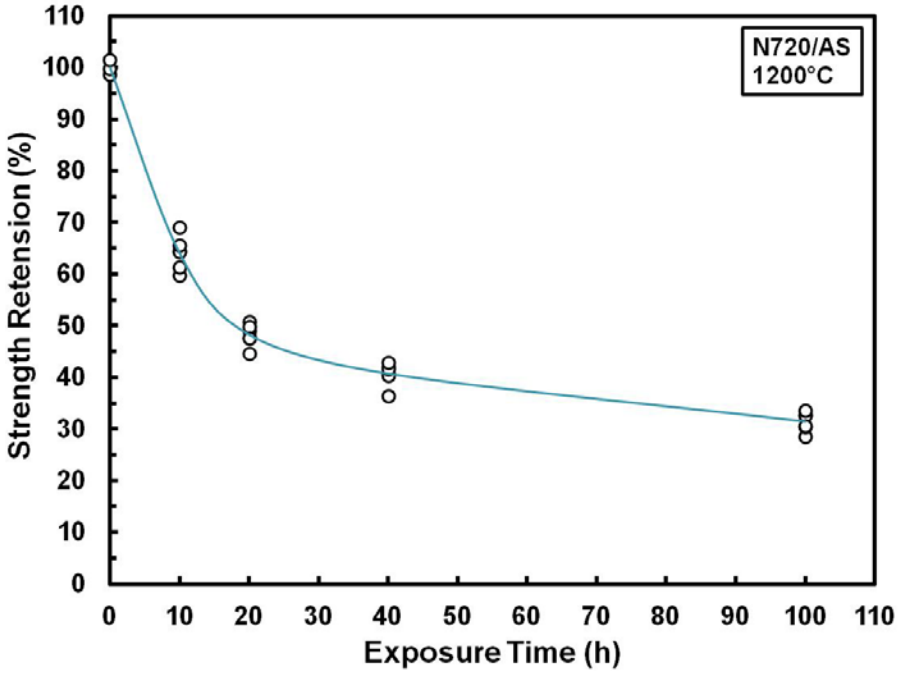

Figure 22 – Tensile strength retention as a function of exposure time at 1200°C for N720/AS composite

Figure 23 shows the representative tensile stress-strain curve obtained for N720/AS specimens heat treated for 100 h at 1100°C together with those obtained for specimens heat treated at 1200°C for 10 and 100 h. The representative stress-strain curve for the as-received N720/AS composite is included in Figure 23 for comparison. Effect of the exposure temperature on tensile properties of N720/AS composite is evident. Elastic modulus increased with exposure temperature. It is noteworthy that 100 h of 1100°C had little effect on tensile strength. In contrast, 10 h at 1200°C decreased the tensile strength 36%.

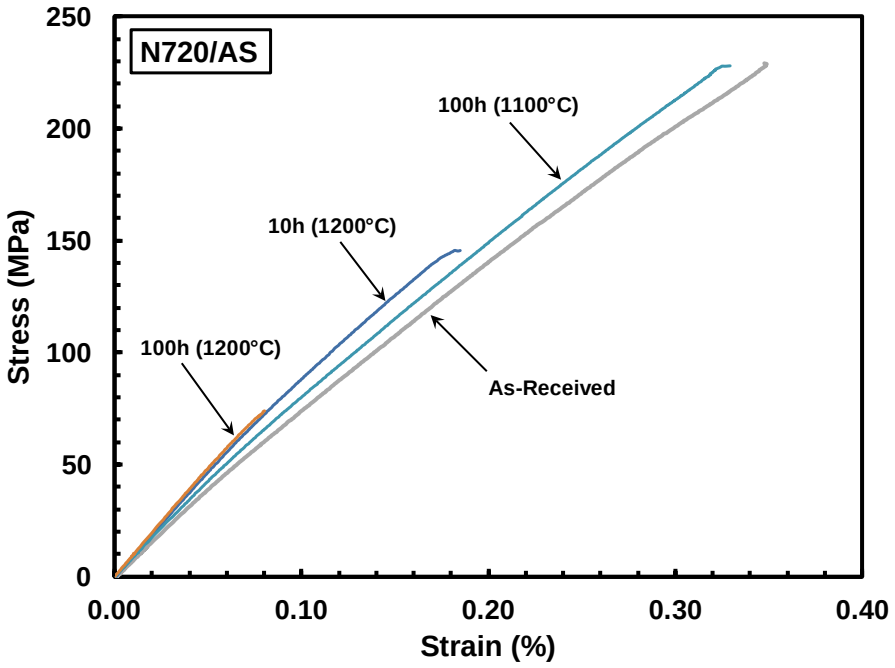

Figure 23 – Effect of prior heat treatment at 1100°C and at 1200°C on tensile stress-strain behavior of N720/AS composite

Tensile strength, modulus, and failure strain values obtained for the N720/AS specimens subjected to different time-temperature histories are summarized in Table 7, Table 8, and Table 9, respectively.

Table 7 – Effect of prior heat treatment on tensile strength of N720/AS composite

Exposure Time (h)	*Exposure Temp (°C)*	*Average UTS (MPa)*	*Individual Specimen UTS (MPa)*					
			1	*2*	*3*	*4*	*5*	*6*
0	N/A	225.9	N/A	N/A	N/A	223.1	225.5	229.3
100	1100	228.8	226.2	237.1	229.4	227.9	232.5	219.9
10	1200	144.7	155.9	145.6	134.8	145.2	148.3	138.4
20	1200	109.0	107.4	110.9	100.9	114.9	112.4	107.5
40	1200	91.9	92.1	91.1	95.1	82.4	94.1	96.8
100	1200	71.0	74.1	64.6	73.6	68.9	75.8	69.1

Table 8 – Effect of prior heat treatment on tensile modulus of N720/AS composite

Exposure Time (h)	*Exposure Temp (°C)*	*Average E (GPa)*	*Individual Specimen E (GPa)*					
			1	*2*	*3*	*4*	*5*	*6*
0	N/A	81.4	N/A	N/A	N/A	80.8	81.3	82.2
100	1100	89.6	88.3	91.2	102.4	87.9	84.8	82.7
10	1200	95.9	95.7	95.9	93.0	94.3	94.6	102.3
20	1200	95.4	90.7	93.8	101.5	97.0	96.3	92.9
40	1200	98.5	98.7	97.1	98.7	94.4	99.8	102.2
100	1200	99.4	98.1	101.0	102.8	99.8	97.9	97.1

Table 9 – Effect of prior heat treatment on tensile failure strain of N720/AS composite

Exposure Time (h)	*Exposure Temp (°C)*	*Average Failure Strain (%)*	*Individual Specimen Failure Strain (%)*					
			1	*2*	*3*	*4*	*5*	*6*
0	N/A	0.340	N/A	N/A	N/A	0.329	0.342	0.349
100	1100	0.325	0.322	0.343	0.284	0.329	0.336	0.336
10	1200	0.181	0.207	0.185	0.169	0.182	0.183	0.159
20	1200	0.134	0.140	0.150	0.110	0.141	0.133	0.129
40	1200	0.104	0.103	0.102	0.109	0.092	0.117	0.105
100	1200	0.076	0.080	0.068	0.075	0.073	0.085	0.075

5.2.3 Effect of Heat Treatment on Tensile Properties of N720/A Composite

Figure 24 shows the representative tensile stress-strain curves obtained for the N720/A specimens heat treated at 1300°C for various durations. The representative stress-strain curve for the as-received N720/A composite is included in Figure 24 for comparison. Exposure up to 100 h at 1300°C appears to have little influence on tensile strength.

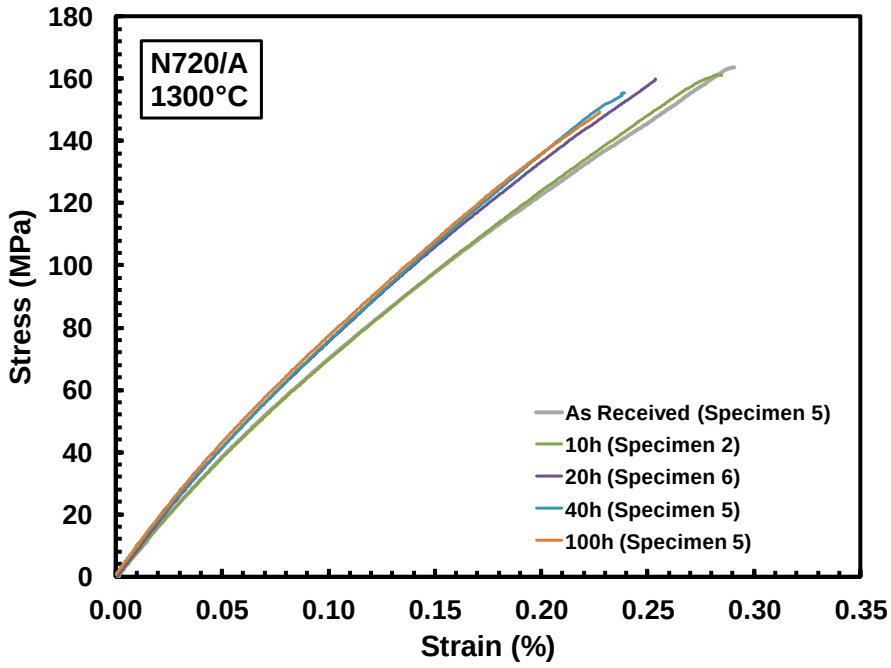

Figure 24 – Effect of prior heat treatment at 1300°C on tensile stress-strain behavior of N720/A composite

Figure 25 shows the strength retention as a function of exposure time. There is a slight decrease in the tensile strength as exposure time is increased. However, after 100 h at 1300°C, the material retained over 90% of its tensile strength on average.

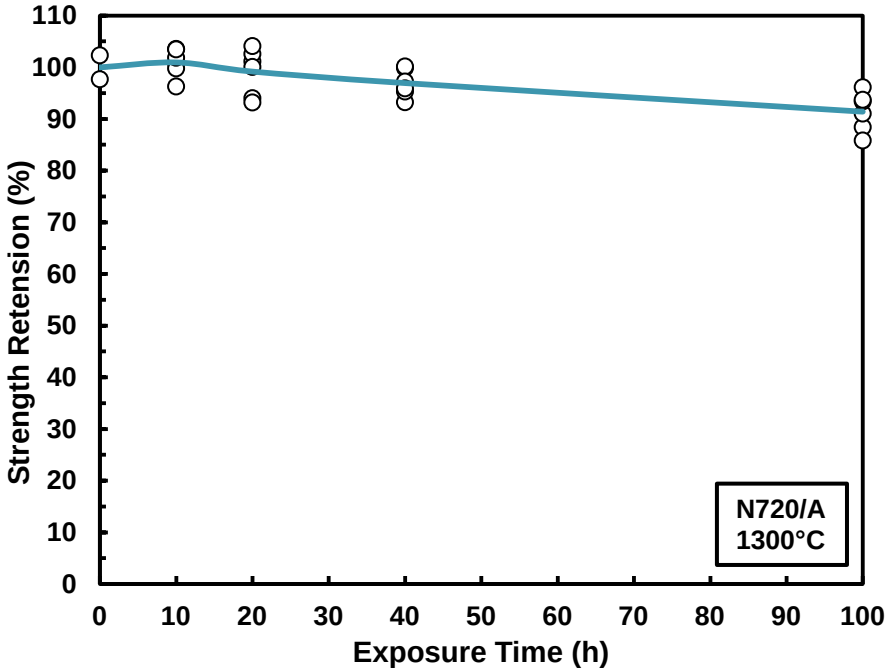

Figure 25 – Tensile strength retention as a function of exposure time at 1300°C for N720/A composite

Figure 26 shows the representative tensile stress-strain curve obtained for N720/A specimens heat treated for 100 h at 1200°C together with those obtained for specimens heat treated at 1300°C for 10 and 100 h. The representative stress-strain curve for the as-processed N720/A composite is included in Figure 26 for comparison. Heat treatment at 1200°C resulted in higher tensile strength and modulus values. Heat treatment at 1300°C resulted in higher modulus values, but some loss in tensile strength.

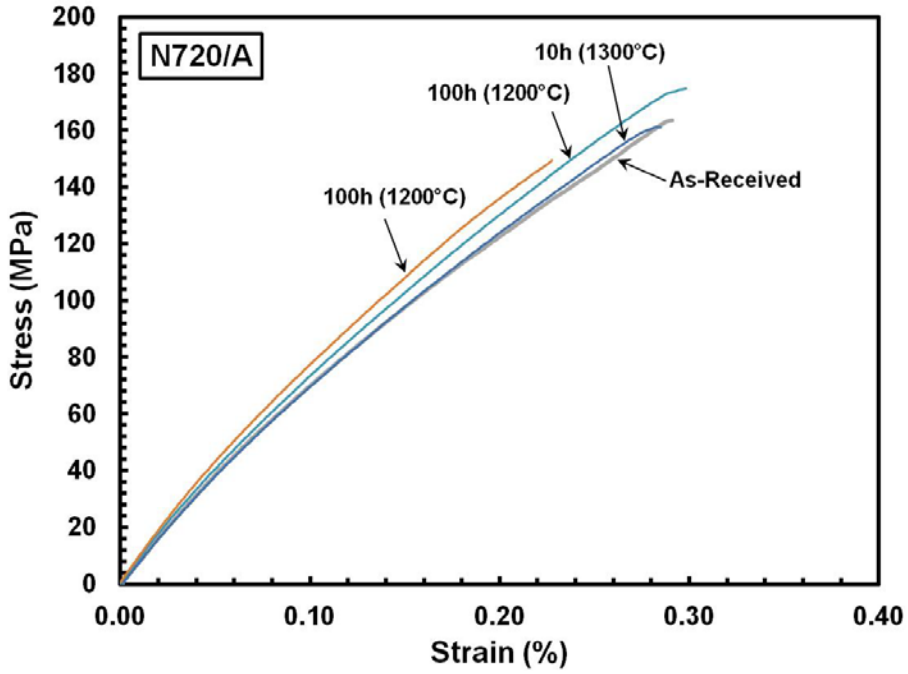

Figure 26 – Effect of prior heat treatment at 1200°C and at 1300°C on tensile stress-strain behavior of N720/A composite

Tensile strength, modulus, and failure strain values obtained for the N720/A specimens subjected to different time-temperature histories are summarized in Table 10, Table 11, and Table 12, respectively

Table 10 – Effect of prior heat treatment on tensile strength of N720/A composite

Exposure Time (h)	*Exposure Temp (°C)*	*Average UTS (MPa)*	*Individual Specimen UTS (MPa)*					
			1	*2*	*3*	*4*	*5*	*6*
0	N/A	159.9	N/A	N/A	N/A	N/A	163.6	156.2
100	1200	175.9	177.2	174.0	178.3	184.2	174.7	167.2
10	1300	161.4	165.6	161.1	159.5	162.8	154.0	165.4
20	1300	158.6	161.7	164.0	166.5	150.3	149.0	160.0
40	1300	155.0	159.7	149.1	152.4	160.1	155.5	153.4
100	1300	146.2	153.7	141.4	137.2	145.6	149.3	149.8

Table 11 – Effect of prior heat treatment on tensile modulus of N720/A composite

Exposure Time (h)	*Exposure Temp (°C)*	*Average E (GPa)*	*Individual Specimen E (GPa)*					
			1	*2*	*3*	*4*	*5*	*6*
0	N/A	83.8	N/A	N/A	N/A	N/A	83.4	84.2
100	1200	86.8	85.9	87.2	83.7	88.1	88.2	87.8
10	1300	83.4	81.6	83.1	82.7	81.3	85.1	86.8
20	1300	88.5	87.4	90.2	85.1	84.9	92.9	90.4
40	1300	91.5	89.0	90.5	95.7	92.6	89.8	91.5
100	1300	91.0	89.7	91.2	95.3	91.1	92.3	86.1

Table 12 – Effect of prior heat treatment on tensile failure strain of N720/A composite

Exposure Time (h)	*Exposure Temp (°C)*	*Average Failure Strain (%)*	*Individual Specimen Failure Strain (%)*					
			1	*2*	*3*	*4*	*5*	*6*
0	N/A	0.281	N/A	N/A	N/A	0.329	0.342	0.349
100	1100	0.301	0.307	0.313	0.307	0.298	0.281	0.303
10	1200	0.282	0.285	0.268	0.312	0.259	0.276	0.295
20	1200	0.258	0.256	0.285	0.246	0.226	0.254	0.281
40	1200	0.238	0.225	0.231	0.240	0.239	0.240	0.252
100	1200	0.226	0.212	0.208	0.221	0.228	0.249	0.242

5.2.4 Comparison of Results for Different Material Systems

The N610/AS and N720/AS contained the same aluminosilicate matrix, but were reinforced with different fibers. Both CMCs were processed in the same manner and were subjected to the same time-temperatures histories. Figure 27 shows the change in elastic modulus with heat treatment duration for each material system. Recall that for a composite with 0/90 fiber orientation, elastic modulus measured in a tensile test is a fiber-dominated property. Hence it is not surprising that prior heat treatment had similar effect on the elastic moduli of N720/AS and N720/A composites.

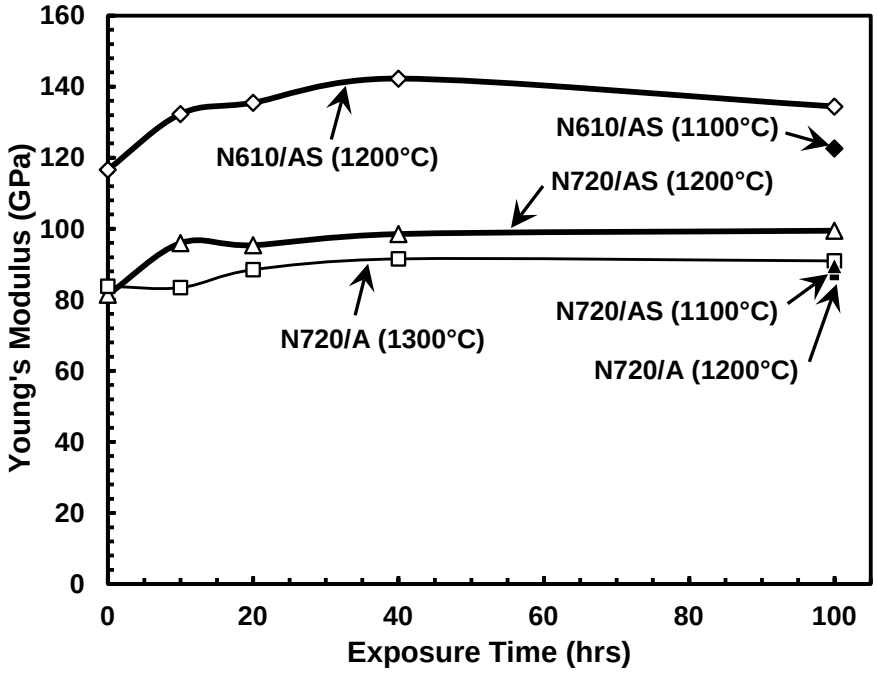

Figure 27 – Elastic modulus vs. exposure time at elevated temperature for N610/AS, N720/AS, and N720/A ceramic composites

Figure 28 shows the strength retention as a function of exposure time for the three material systems studied in this work. The N610/AS and N720/AS CMCs with aluminosilicate matrix exhibited significant loss of tensile strength with increased exposure times at 1200°C. As expected, the CMC reinforced with N720 fibers had better strength retention than the CMC reinforced with N610 fibers. The N720/A CMC showed little loss of tensile strength with increased exposure time. Results in Figure 28 suggested that the matrix played a considerable role in the retention of tensile strength after heat treatment. Results in Figure 28 also show that exposing the CMCs with aluminosilicate matrix to temperature above the maximum recommended use temperature dramatically reduces tensile strength. This observation suggested that changes in the microstructure of the materials (primarily those containing the aluminosilicate matrix) occurred during the

over-temperature exposures. Furthermore, it appeared that these changes may be time dependent. The changes in volume of the CMCs with aluminosilicate matrix noted earlier in this report also suggest that considerable changes to the microstructure take place during heat treatment.

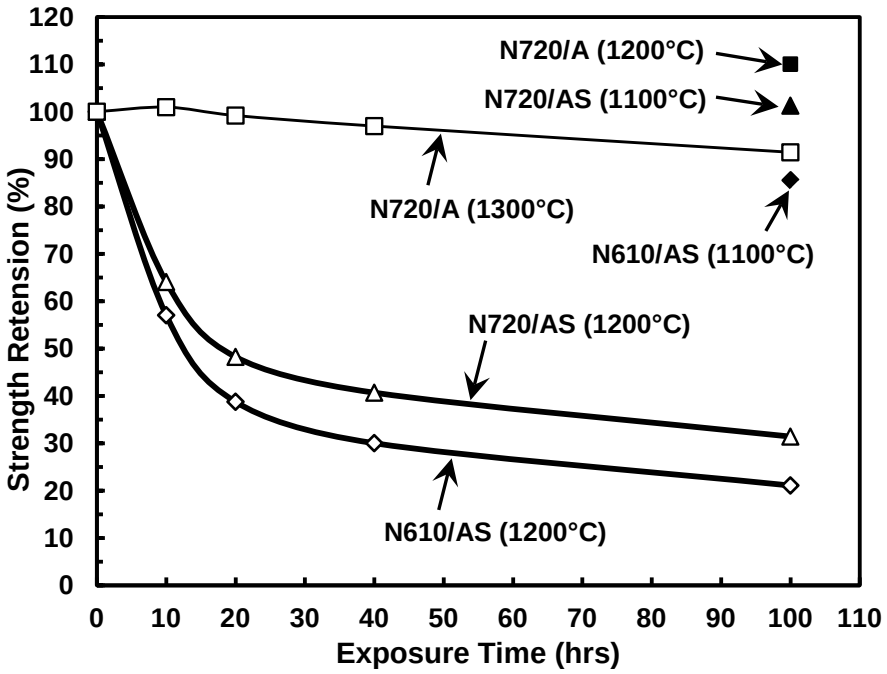

Figure 28 – Tensile strength retention as a function of exposure time at elevated temperature for N610/AS, N720/AS, and N720/A ceramic composites

Results obtained for the three CMCs were also compared using Ashby-style plots. Figure 29 compares the effects of heat treatment on strength and stiffness of the N610/AS and N720/AS composites. It is evident that N610/AS consistently exhibits higher values of tensile strength and modulus than the N720/AS composite. The strength and stiffness values obtained for both materials follow similar trends as exposure time is increased. Note that strength and modulus data obtained for N720/AS show less scatter than the data obtained for N610/AS.

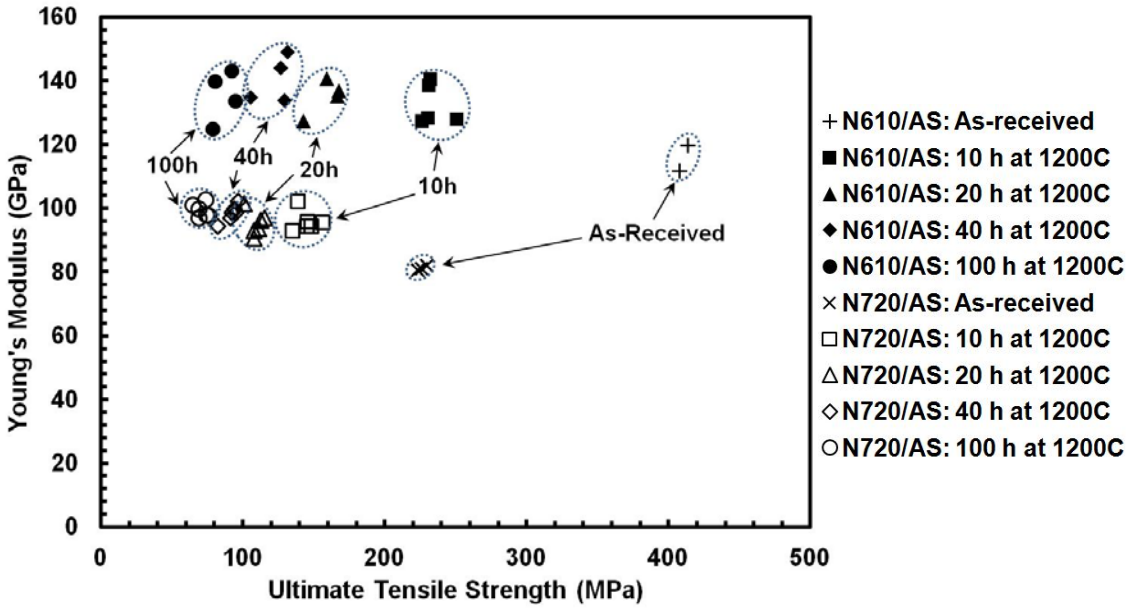

Figure 29 – The Young's modulus plotted vs. the UTS for N610/AS and N720/AS composites heat treated at 1200°C

It is instructive to compare the strength and modulus data obtained for the two composites reinforced with N720 fibers. Results obtained for the N720/AS composite heat treated at 1200°C and those obtained for the N720/A composite heat treated at 1300°C are shown in Figure 30. It is seen that prior heat treatment at 1300°C had little effect on the tensile strength and modulus of the N720/A composite. In fact, it is difficult to discern the individual groups of data corresponding to each exposure time. The N720/A composite was stable even after 100-h exposure at 1300°C, a temperature above the maximum recommended use temperature. Conversely, tensile strength and modulus of N720/AS composite were strongly influence by the prior heat treatment at 1200°C.

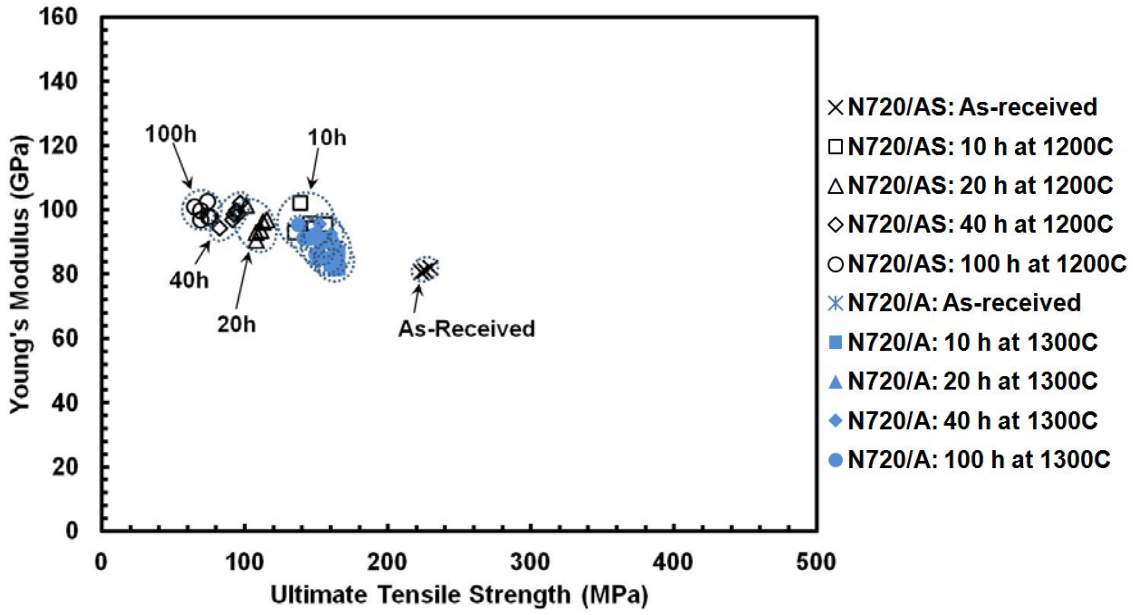

Figure 30 – The Young's modulus plotted vs. the UTS for N720/AS composite heat treated at 1200°C and N720/A composite heat treated at 1300°C

5.4. Composite Microstructure – Optical Microscopy

5.4.1 Effect of Heat Treatment on Microstructure of N610/AS Composite

Optical micrographs of the fracture surfaces obtained in tension tests of the as-received specimen and specimens subjected to 100 h at 1100 and 1200°C are shown in Figure 31. The fracture surface of the as-received composite was brushy with considerable fiber pullout. Excellent crack deflection is evident. The fracture surface of the specimen heat treated for 100 h at 1100°C was considerably more planar, although some fiber pullout was still observed. Note that most of the plies failed at different locations resulting in a jagged fracture surface. The appearance of the fracture surface still suggested some crack deflection and graceful failure. The fracture surface of the specimen heat treated for 100 h at 1200°C was drastically different. The fracture surface was entirely planar and indicative of brittle failure. Note that all the plies failed in

concert. Prior heat treatment significantly degraded the crack deflection capability of the composite.

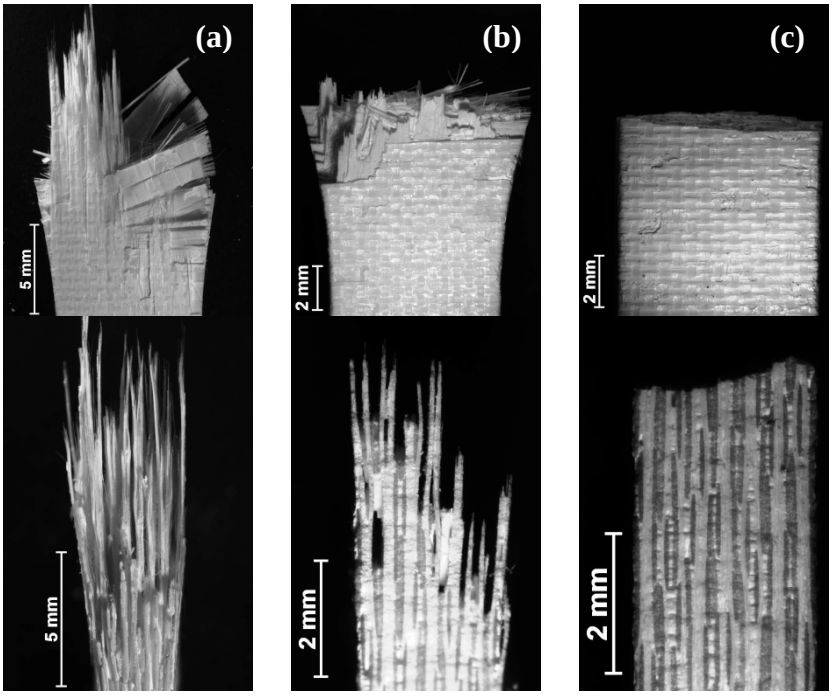

Figure 31 – Fracture surfaces of the N610/AS composite obtained in tensile tests. (a) as-received composite, (b) composite heat treated for 100 h at 1100°C, and (c) composite heat treated for 100 h at 1200°C

Figure 32 shows the fracture surfaces obtained in tensile tests of the specimens exposed to 1200°C for different durations. The effects of exposure duration at 1200°C on the N610/AS microstructure were readily seen. A planar fracture surface characteristic of brittle failure was produced in all tests. Evidently even 10-h exposure at 1200°C was sufficient to dramatically alter the crack deflection capabilities of the N610/AS composite. However, a side view of the fracture surface of the specimen heat treated for 10 h still showed that the individual plies failed at different locations indicating some desired composite behavior. In contrast, the fracture surfaces of the specimens heat treated for 20 h exhibited coordinated fiber and ply failure. These observations were

consistent with the strength retention results presented earlier. The N610/AS composite retains less than 40% of its tensile strength after 20 h at 1200°C. Additional optical micrographs of fracture surfaces of N610/AS composite are shown in Appendix C.

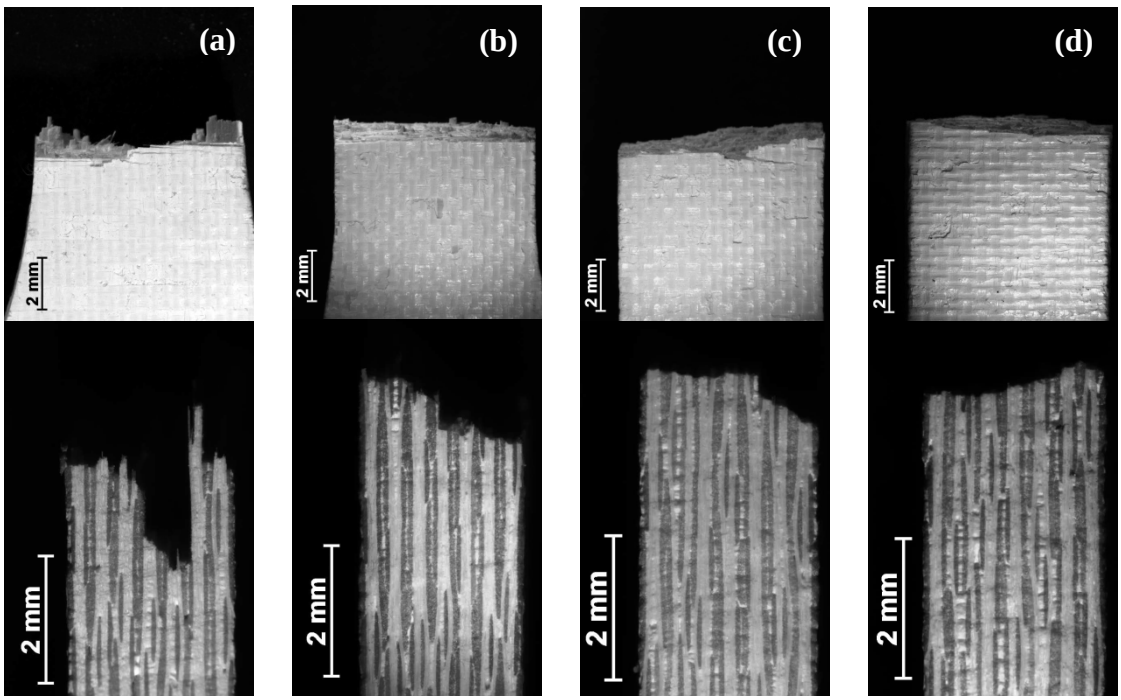

Figure 32 – Fracture surfaces obtained in tensile tests of the N610/AS specimens heat treated at 1200°C for: (a) 10 h, (b) 20 h, (c) 40 h, and (d) 100 h

5.4.2 Effect of Heat Treatment on Microstructure of N720/AS Composite

Optical micrographs of the fracture surfaces obtained in tension tests of the as-received specimen and specimens subjected to 100 h at 1100 and 1200°C are shown in Figure 33. As was the case with the N610/AS composite (Figure 31a), the fracture surface of the as-received N720/AS composite was brushy with considerable amount of fiber pullout. Excellent flaw tolerance and graceful failure were evident. The fracture surface of the specimen heat treated for 100 h at 1100°C exhibited large regions of planar fracture, although some regions of fibrous fracture and fiber pullout were also seen. The

appearance of the fracture surface suggested a transition from graceful failure to brittle fracture. The fracture surface of the specimen heat treated for 100 h at 1200°C was strikingly different. The fracture surface was entirely planar with all the plies failing in concert. The composite exhibited brittle fracture.

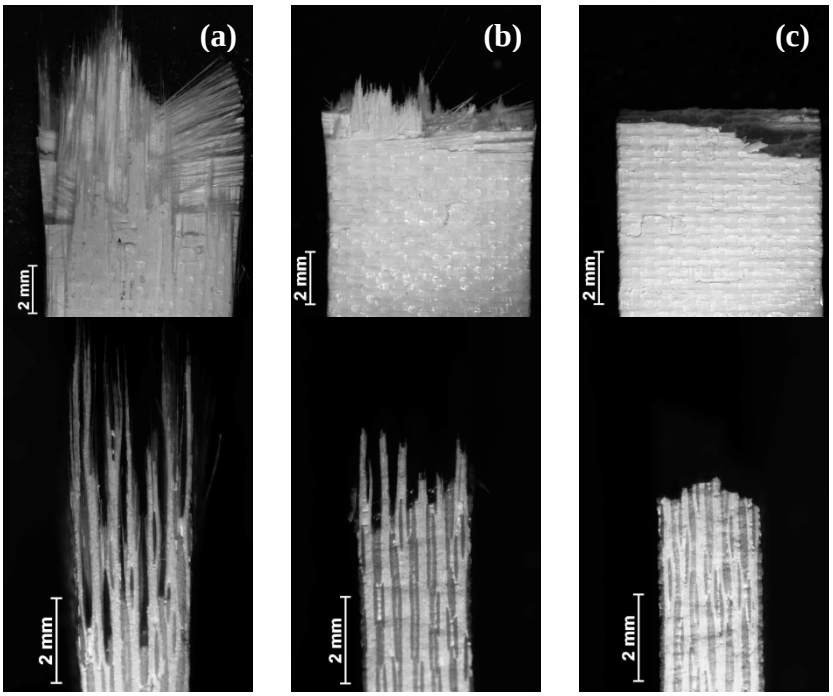

Figure 33 – Fracture surfaces of the N720/AS composite obtained in tensile tests. (a) as-received composite, (b) composite heat treated for 100 h at 1100°C, and (c) composite heat treated for 100 h at 1200°C

The effects of the exposure duration at 1200°C on the composite microstructure were also examined. Figure 34 shows the fracture surfaces obtained in tensile tests of the specimens exposed to 1200°C for different durations. As in the case of the N610/AS composite (Figure 32), all N720/AS specimens heat treated at 1200°C produced planar fracture surfaces characteristic of brittle failure. Furthermore, fracture surfaces obtained after 40-h and 100-h heat treatments were virtually indistinguishable. All fiber tows and

plies failed in a coordinated fashion. Additional optical micrographs of fracture surfaces of N720/AS composite are shown in Appendix D.

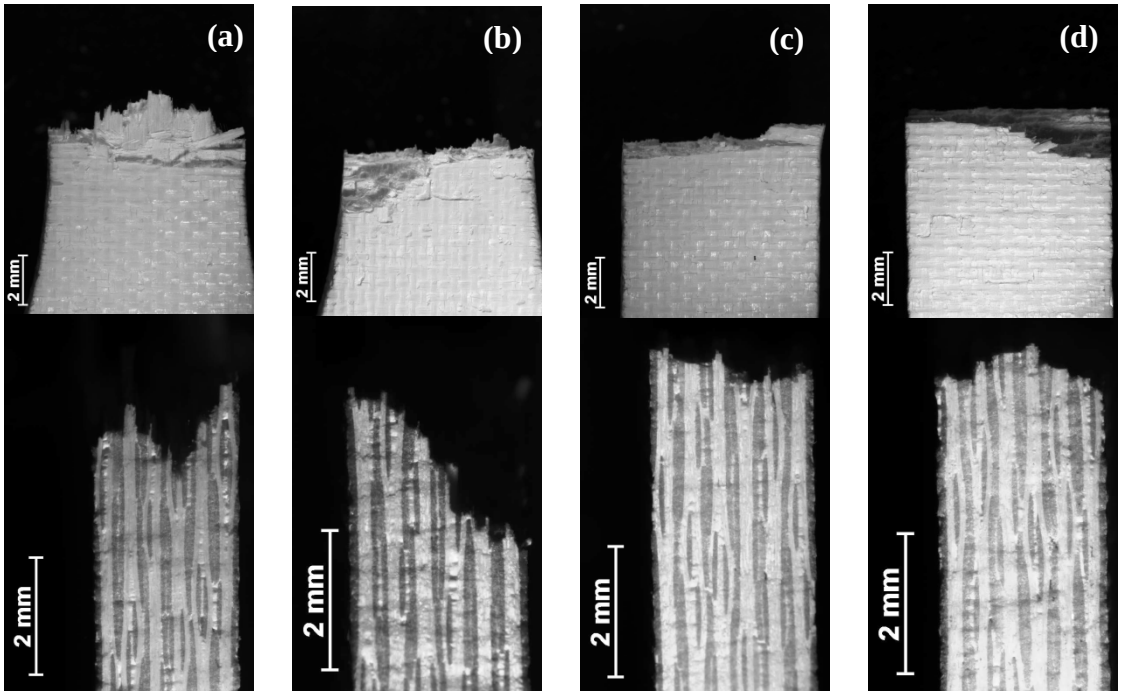

Figure 34 – Fracture surfaces obtained in tensile tests of the N720/AS specimens heat treated at 1200°C for: (a) 10 h, (b) 20 h, (c) 40 h, and (d) 100 h

5.4.3 Effect of Heat Treatment on Microstructure of N720/A Composite

Effects of the prior heat treatment on the microstructure of the N720/A composite were profoundly different from the effects on the microstructure of the CMCs with the aluminosilicate matrix. All N720/A specimens showed considerably longer damage zones than the N610/AS or N720/AS specimens. Optical micrographs of the N720/A fracture surfaces obtained in tension tests of the as-received specimen and specimens subjected to 100 h at 1200°C and 1300°C are shown in Figure 35. The fracture surfaces of the as-received composite and of the specimen heat treated at 1200°C were brushy with considerable fiber pullout. The fracture surface appearance indicated active crack deflection and graceful failure. Even the fracture surface of the specimen heat treated at

1300°C still showed regions of brushy failure and noticeable fiber pullout. Apparently 100 h at 1300°C did not completely degrade the composite microstructure.

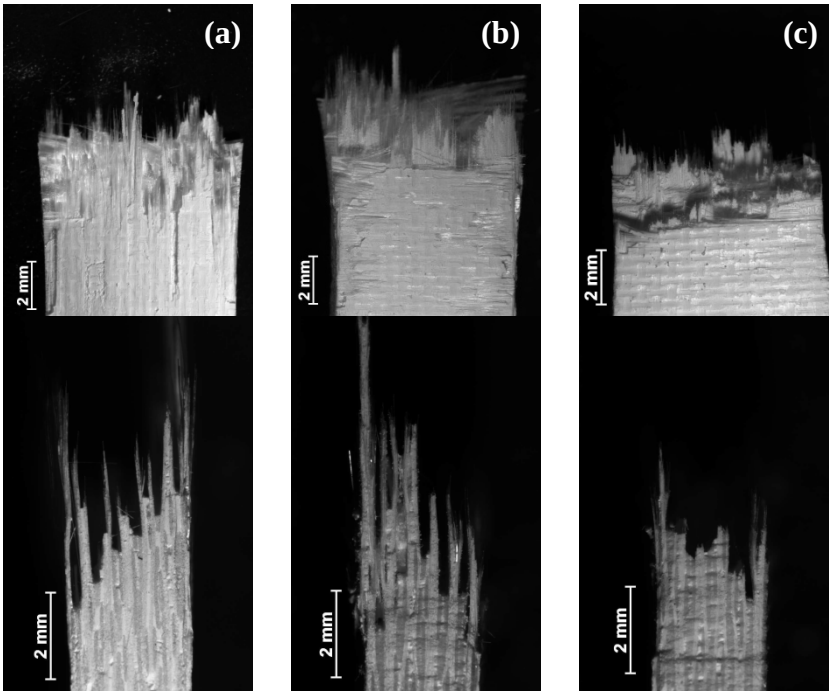

Figure 35 – Fracture surfaces of the N720/A composite obtained in tensile tests. (a) as-received composite, (b) composite heat treated for 100 h at 1200°C, and (c) composite heat treated for 100 h at 1300°C

Figure 36 shows the fracture surfaces obtained in tensile tests of the specimens exposed to 1300°C for different durations. Exposure duration at 1300°C had limited influence on the N720/A microstructure. All fracture surfaces show regions of brushy uncoordinated fiber fracture. In all cases some fiber pullout was observed. Recall that exposure duration also had little influence on tensile strength of the N720/A composite. Additional optical micrographs of fracture surfaces of N720/A composite are shown in Appendix E.

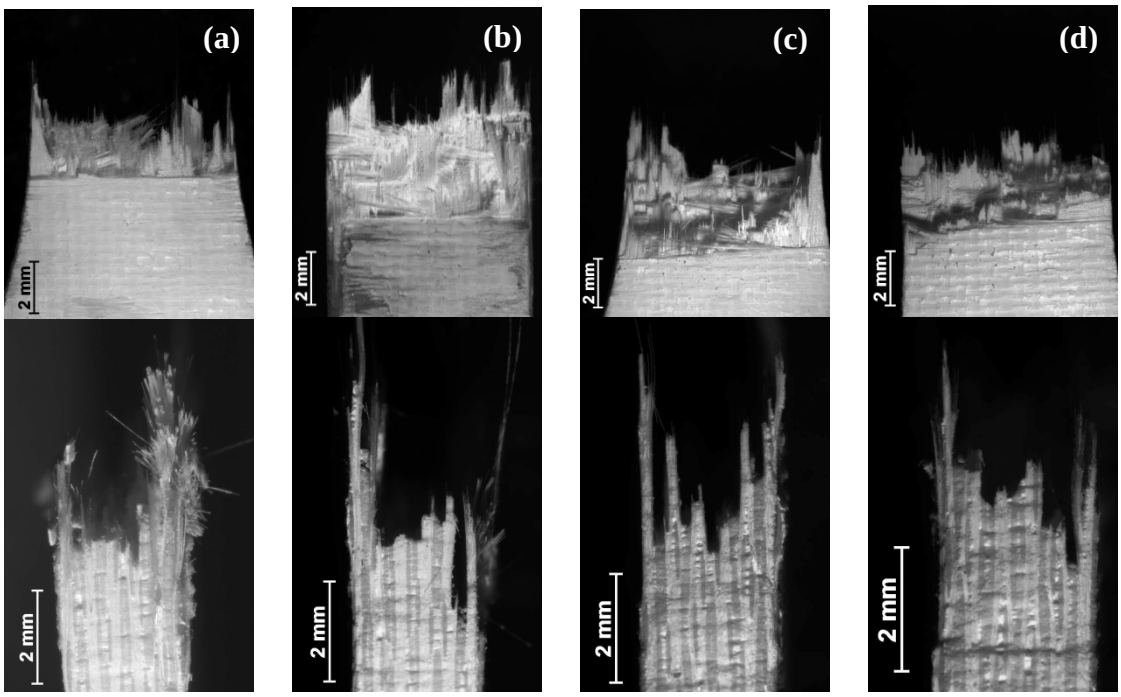

Figure 36 – Fracture surfaces obtained in tensile tests of the N720/A specimens heat treated at 1300°C for: (a) 10 h, (b) 20 h, (c) 40 h, and (d) 100 h

5.4.4 Comparison of Results for Different Material Systems

Examination of the post-heat treatment fracture surfaces suggested conclusions consistent with the tensile strength and modulus data presented earlier in this report. Heat treatment had similar effects on the microstructure of N610/AS and N720/AS, the two composites with the aluminosilicate matrix. All fracture surfaces of the heat treated N610/AS and N720/AS specimens were predominantly planar, suggesting brittle failure. Contrastingly, prior heat treatment had very different effects on the microstructure of the two composites reinforced with N720 fibers. All fracture surfaces of the N720/A composite with the alumina matrix exhibited fibrous fracture and considerable degree of fiber pullout. Conversely, all fracture surfaces of the heat treated N720/AS specimens were largely planar, indicating the loss of crack deflection capabilities. These results suggested that matrix performance played a significant role in the thermal stability of the

N720/A and N720/AS composites. Furthermore, the matrix appeared to be the limiting factor for thermal stability in these material systems.

5.5 Composite Microstructure - Scanning Electron Microscopy

Further understanding of the influence of exposure temperature and duration on the composite microstructure can be gained by examining the fracture surfaces with a SEM. In preparation for SEM examination, carbon tape was used to secure the specimens to the stage platform. The specimens were not coated.

5.5.1 Effect of Heat Treatment on Microstructure of N610/AS Composite – SEM Examination

It is noteworthy that the SEM examination of the N610/AS fracture surfaces obtained in this work confirmed the conclusions reached when these fracture surfaces were examined with an optical microscope. The fracture surface of the as-received specimen in Figure 37a was dominated by regions of uncorrelated fiber fracture, where individual fibers were clearly discernible. Prior heat treatment at 1100°C significantly changed the appearance of the fracture surface indicating a change from graceful to brittle failure. The fracture surface of the specimen heat treated for 100 h at 1100°C (Figure 37b) was nearly planar, although some isolated areas of fibrous fracture may be observed under higher magnification. The near planar fracture surface suggested a decrease in matrix porosity. Recall that the N610/AS composite derives its flaw tolerance from the porous matrix. A minimum level of matrix porosity is required for this approach to work. Evidently, 100 h at 1100°C decreased the matrix porosity enough to cause reduction in composite tensile strength from 410.7 MPa (UTS for the as-processed

composite) to 351.1 MPa on average. The fracture surfaces of the N610/AS specimens heat-treated at 1200°C (Figure 37c-f) were dominated by planar regions of coordinated fiber failure. Prior heat treatment at 1200°C has changed the failure mode of the composite from graceful (for as-processed material) to brittle.

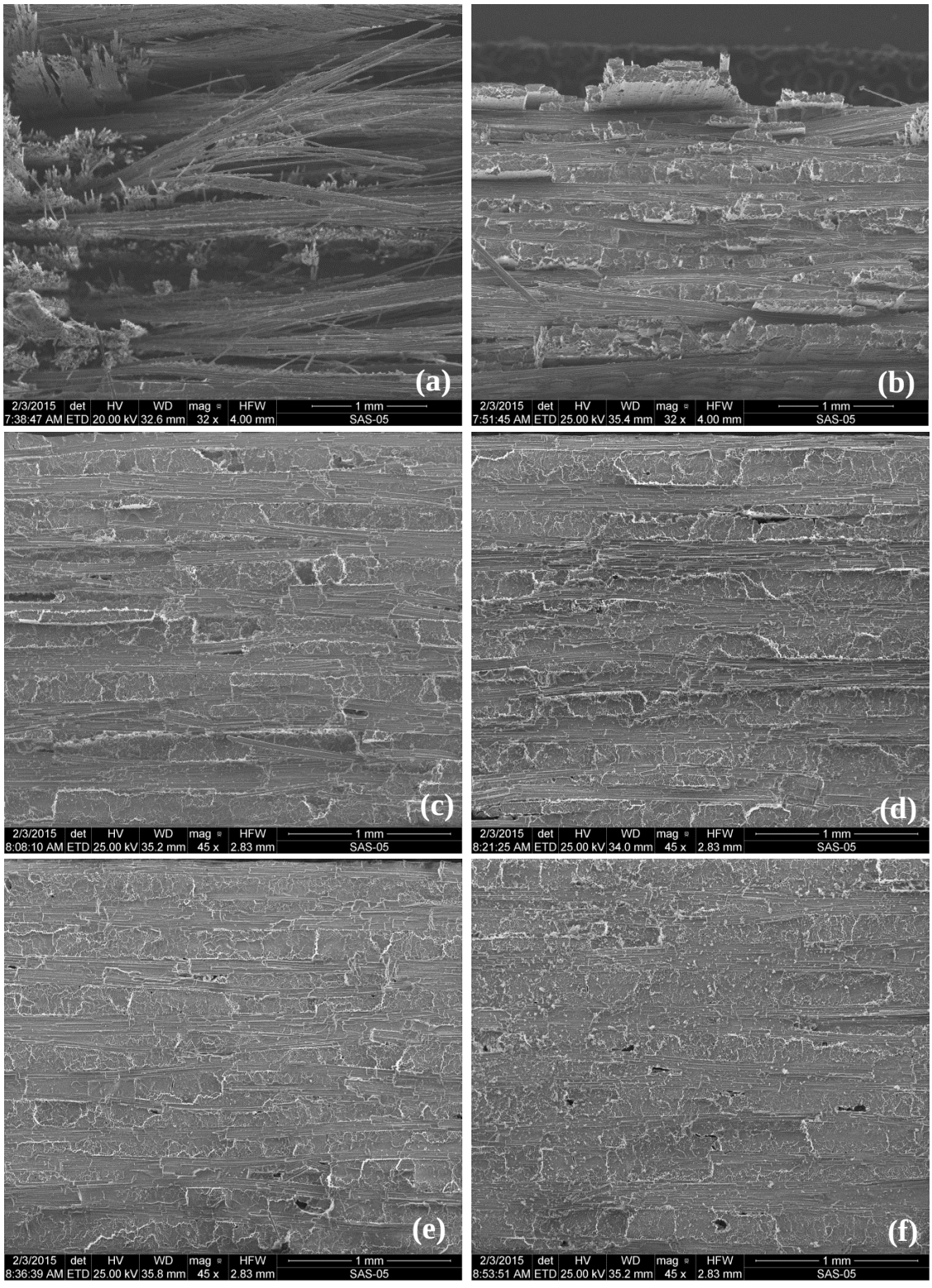

Figure 37 – SEM micrographs of the N610/AS fracture surfaces produced in tensile tests. (a) as-received, (b) 100 h at 1100°C, (c) 10 h at 1200°C, (d) 20 h at 1200°C, (e) 40 h at 1200°C, and (f) 100 h at 1200°C

Higher magnification SEM images of the fracture surfaces of the N610/AS specimens heat treated at 1200°C (Figure 38) also exhibit features characteristic of brittle failure. The fracture surfaces in Figure 38 show no fiber pullout, increased fiber-matrix bonding was apparent, and fibers and matrix fail in a coplanar fashion. Additionally, large voids were seen throughout the fracture surfaces (Figure 38). The aluminosilicate matrix of the N610/AS composite was comprised of the Al_2O_3 particles bonded together by a continuous SiO_2 film. The matrix derived its porosity from incomplete filling of the interparticle voids. The SiO_2 film in the matrix is under a near hydrostatic constraint from the tightly packed Al_2O_3 grains and the surrounding N610 fibers. Under this three-dimensional constraint, heat treatment at 1200°C causes coarsening of the pore-size distribution, rather than the densification of the matrix [19]. Pore-coarsening occurred as the regions of high capillary pressure caused small pores to contract and larger pores to expand [20]. The total volume of the composite was dimensionally constrained by the fiber skeleton and cannot change significantly. At the same time, the smaller matrix pores shrink forcing the larger ones to grow. As a result, some matrix regions densified while others dilate forming large voids [21] as those seen in Figure 38.

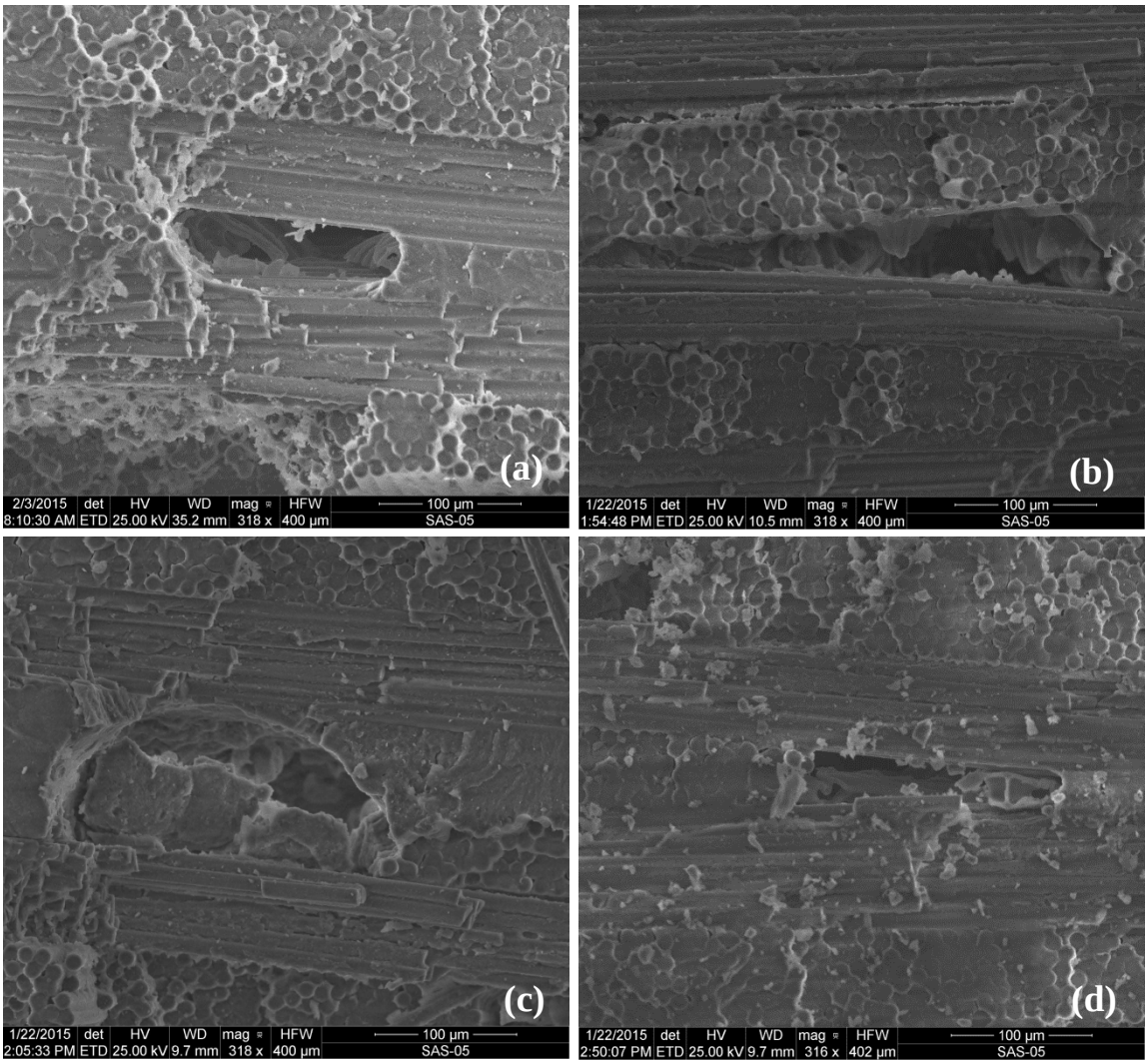

Figure 38 – Higher magnification SEM micrographs of the N610/AS fracture surfaces produced in tensile tests after heat treatment at 1200°C for (a) 10 h, (b) 20 h, (c) 40 h, (d) 100 h. Large matrix voids are clearly visible.

It is noteworthy that large matrix voids are observed in all specimens heat treated at 1200°C (Figure 38) including the specimens with the shortest heat treatment of 10 h. Apparently, 10-h exposure at 1200°C was sufficiently long to cause substantial changes in the aluminosilicate matrix. Most of the matrix porosity was lost during the first 10 h of exposure. These observations can be further confirmed by examining the fracture surface of the specimen heat treated for 10 h in Figure 39. Planar fracture topography with no

visible fiber pullout and increased matrix-fiber bonding, seen in Figure 39, are indicative of a loss in matrix porosity. The changes in matrix porosity can be linked to changes in tensile strength of the composite. Recall that the N610/AS specimens heat treated for 10 h at 1200°C retained only 57.0% of their of their tensile strength on average. The specimens heat treated for 100 h retained 21.1% of their tensile strength. Evidently, the greatest reduction in tensile strength occurred during the first 10 h at 1200°C. Additional SEM micrographs of the fracture surfaces of N610/AS composite are shown in Appendix F.

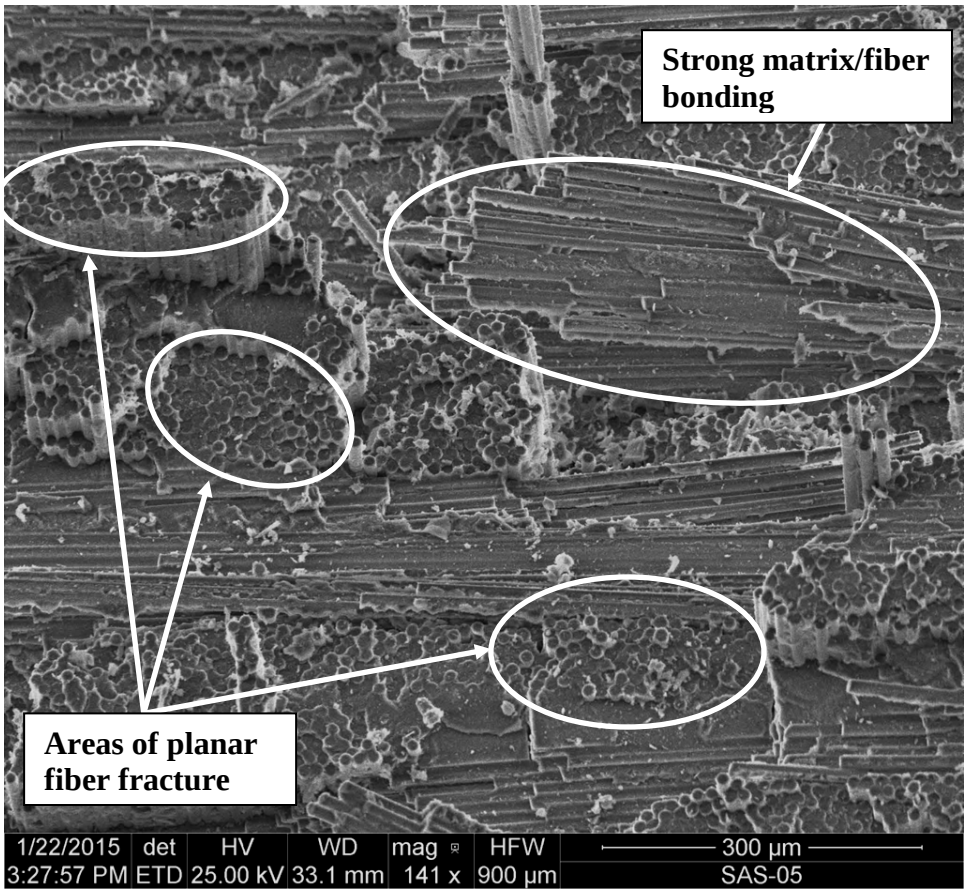

Figure 39 – Higher magnification SEM micrograph of the N610/AS fracture surfaces produced in tensile tests after 10 h at 1200°C. Multiple regions of coordinated fiber fracture and fiber-matrix bonding are clearly visible.

5.5.2 Effect of Heat Treatment on Microstructure of N720/AS Composite – SEM Examination

Figure 40 compares the fracture surfaces of N720/AS specimens subjected to different time-temperature histories. Not surprisingly, the SEM images in Figure 40 were similar to those obtained for N610/AS composite (Figure 37). The thermal stability of the N610/AS and N720/AS composites were limited by their aluminosilicate matrix.

The fracture surface of the as-received composite in Figure 40a was dominated by regions of fibrous fracture and extensive fiber pullout. These microstructural features indicated robust crack deflection and graceful failure of the composite. The fracture surface obtained after 100 h at 1100°C (Figure 40b) exhibited some regions of fibrous fracture and fiber pullout. However, coordinated fiber failure and planar fracture were becoming prevalent. The appearance of the fracture surface changed significantly due to prior heat treatment at 1200°C (Figure 40c – f). All fracture surfaces obtained after heat treatment at 1200°C were dominated by planar fracture. Little or no fiber pullout was observed. In contrast, strong bonding between the fibers and the matrix was seen throughout the fracture surfaces. A typical area of fiber-matrix bonding is shown in Figure 41. Note the significant amount of matrix material that remained bonded to the fibers. The discussion of the porosity loss in the aluminosilicate matrix of the N610/AS composite also applied to the N720/AS composite. Additional SEM micrographs of fracture surfaces of N720/AS composite are shown in Appendix G.

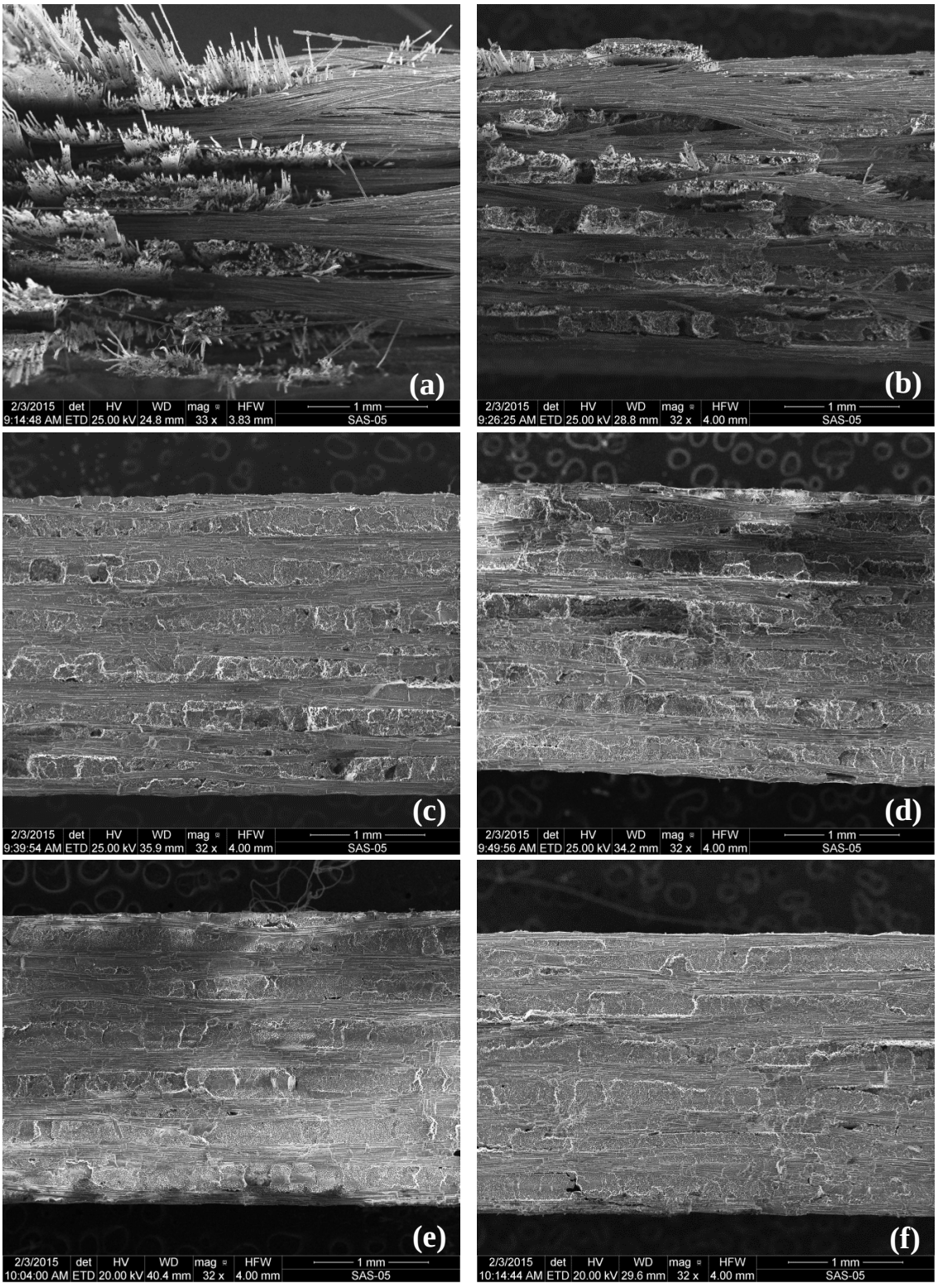

Figure 40 – SEM micrographs of the N720/AS fracture surfaces produced in tensile tests. (a) as-received, (b) 100 h at 1100°C, (c) 10 h at 1200°C, (d) 20 h at 1200°C, (e) 40 h at 1200°C, and (f) 100 h at 1200°C

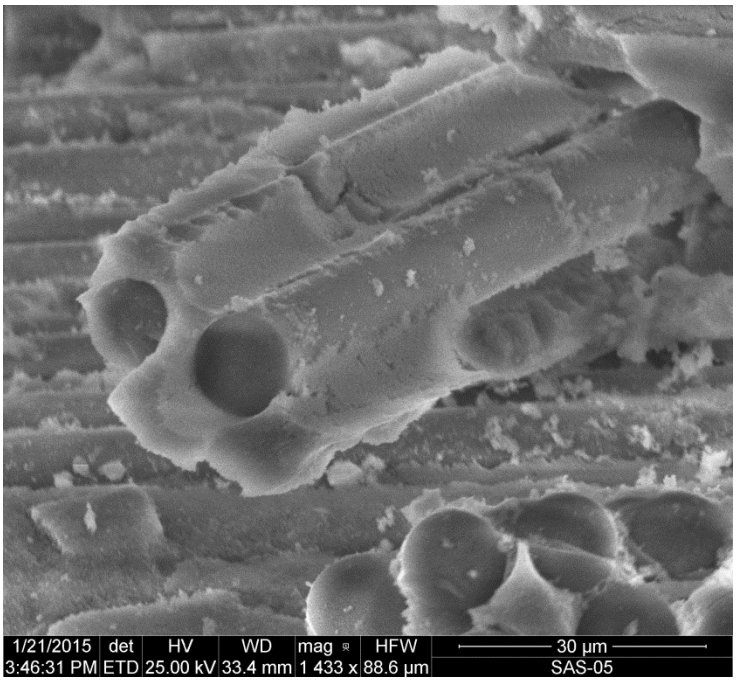

Figure 41 – Higher magnification SEM micrograph of the N720/AS fracture surfaces produced in tensile test after 20 h at 1200°C. Strong fiber/matrix bonding is evident.

5.5.3 Effect of Heat Treatment on Microstructure of N720/A Composite – SEM Examination

The fracture surfaces of the N720/A specimens subjected to different time-temperature histories are presented in Figure 42. The fracture surface of the N720/A as-received specimen was similar to those obtained for the N610/AS and N720/AS as-received specimens. The fracture surface of the as-received composite (Figure 42a) was dominated by fibrous fracture and extensive fiber pullout. Such fracture surface topography indicated that porous matrix adequately provided for crack deflection to promote graceful failure of the composite.

Notably, the fracture surfaces of the heat treated N720/A specimens (Figure 42b-f) exhibited areas of uncoordinated, brushy failure along with areas of planar fracture. As

the heat treatment temperature increased from 1200 to 1300°C, the extent of the correlated fiber failure also increased (compare Figure 42b and f). The same increase in correlated fiber failure and planar fracture was seen when the heat treatment time increased from 10 h (Figure 42c) to 100 h (Figure 42f). Still, even after 100 h at 1300°C, the fracture surface exhibited some areas of fibrous fracture and fiber pullout (Figure 42f and Figure 43a), although fiber-matrix bonding, coordinated fiber failure, and planar fracture become prevalent (Figure 42f and Figure 43b). It was recognized that planar fracture surface and increase in the spatial correlation of the fiber failure locations were among the main manifestations of the matrix densification [22, 23]. The progressively more planar N720/A fracture surfaces indicated that progressive loss of matrix porosity and subsequent matrix densification due to additional sintering. As a result, when the duration of heat treatment at 1300°C increased from 10 to 100 h, the N720/A composite exhibited decreased damage tolerance and increased loss of tensile strength. Still, even after 100 h at 1300°C, the N720/A composite retained about 90% of its tensile strength.

As mentioned earlier, the thermal stability of the N610/AS and N720/AS composites were limited by their aluminosilicate matrix. The N720/A composite with the alumina matrix exhibited improved thermal stability compared to the N610/AS and N720/AS CMCs. Additional SEM micrographs of fracture surfaces of N720/A composite are shown in Appendix H.

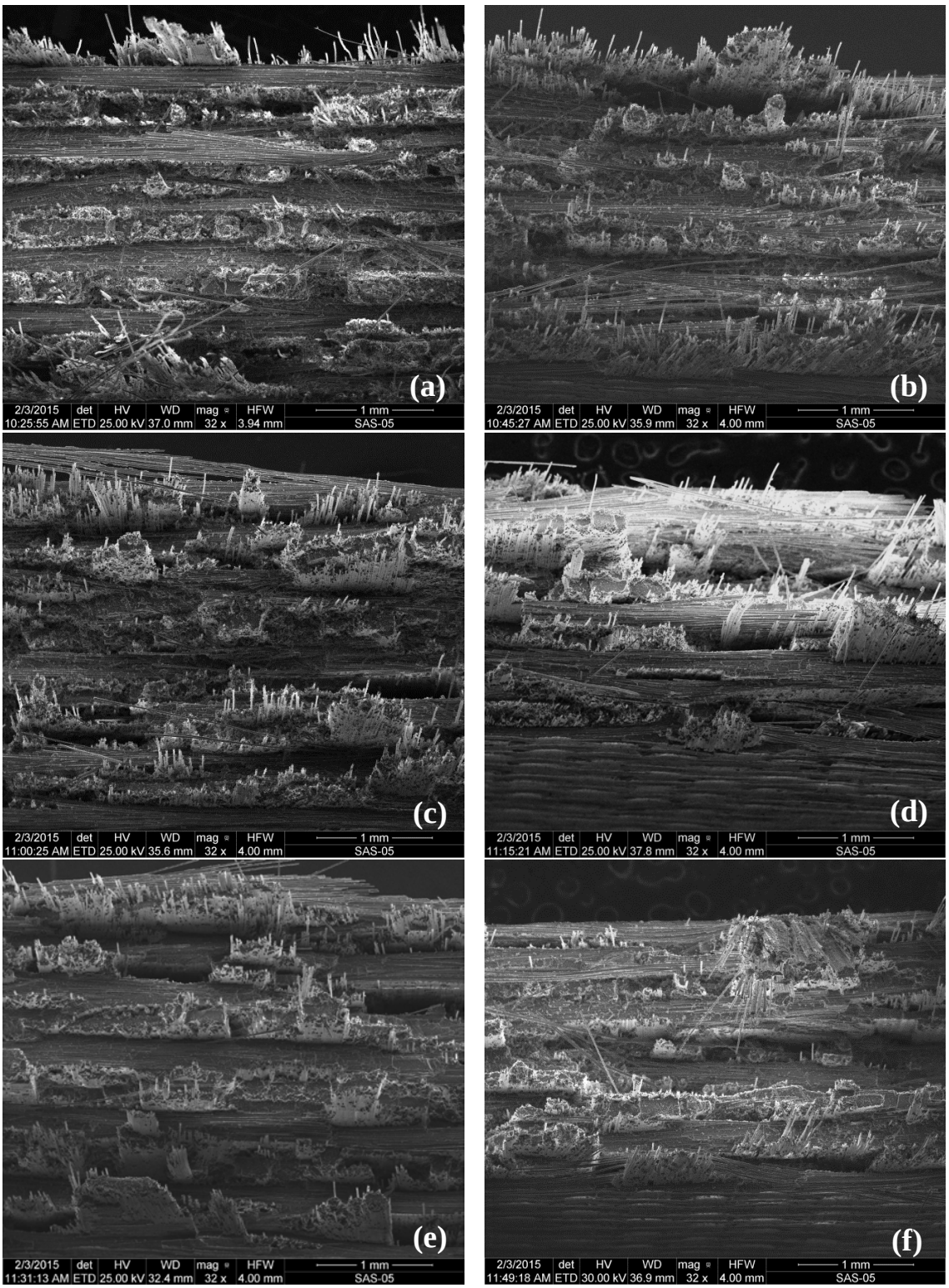

Figure 42 – SEM micrographs of the N720/A fracture surfaces produced in tensile tests. (a) as-received, (b) 100 h at 1200°C, (c) 10 h at 1300°C, (d) 20 h at 1300°C, (e) 40 h at 1300°C, (f) 100 h at 1300°C

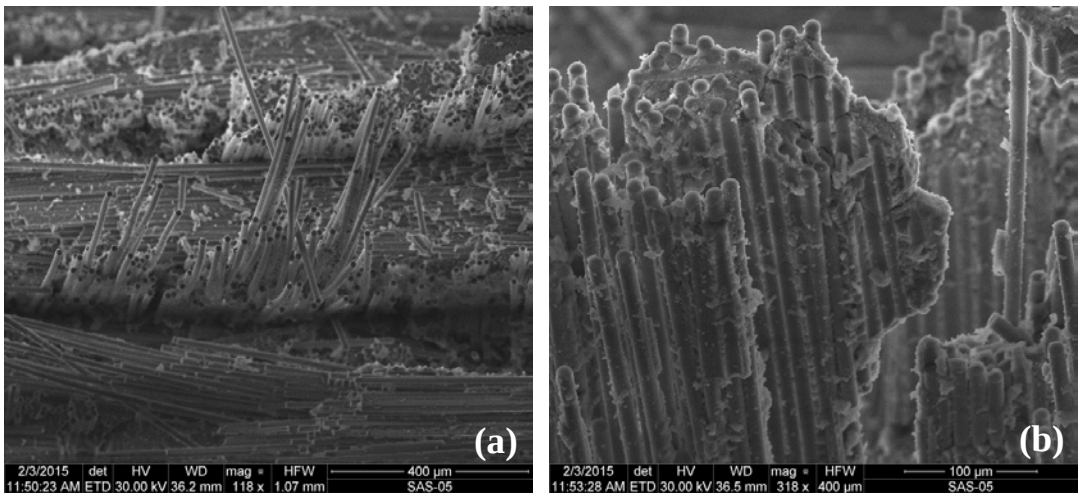

Figure 43 – SEM micrographs of the N720/A fracture surface produced in tensile tests after 100 at 1300°C showing (a) area of fibrous fracture and (b) area of strong fiber-matrix bonding.

VI. Conclusions and Recommendations

Effects of prior time-temperature histories on tensile properties of N610/AS, N720/AS, and N720/A oxide/oxide ceramic matrix composites were evaluated in this work. The N610/AS and N720/AS CMCs with aluminosilicate matrix were heat treated in laboratory air for 100 h at 1100°C and for 10, 20, 40 and 100 h at 1200°C. The N720/A CMC was heat treated in laboratory air for 100 h at 1200°C and for 10, 20, 40, and 100 h at 1300°C. The tensile properties of each composite were evaluated after each type of heat treatment. The baseline tensile properties were also obtained for comparison.

After 100 h at 1100°C, the N610/AS composite retained about 86% of its tensile strength, while the N720/AS CMC showed no loss of tensile strength. Heat treatment at 1200°C caused dramatic degradation in tensile strength of N610/AS and N720/AS, the two CMCs with aluminosilicate matrix. After 100 h at 1200°C, N610/AS retained only ~21% of its tensile strength, while N720/AS retained ~31% of its tensile strength. For both N610/AS and N720/AS composites, the majority of strength loss occurred during the first 10 h at 1200°C. The dramatic degradation in tensile strength was attributed to significant loss of porosity in aluminosilicate matrix. The N720/A composite with alumina matrix exhibited improved thermal stability. After 100 h at 1200°C, the N720/A composite retained 100% of its tensile strength. After 100 h at 1300°C the N720/A CMC retained ~90% of its tensile strength. The strength loss increased with increasing duration at 1300°C.

More extensive microstructural characterization of the heat treated composites is recommended for a follow-on effort. Changes in matrix porosity could be assessed and quantified using TEM examination. Additionally, effects of exposure at elevated

temperature, but in water vapor or combustion environments on tensile properties should be studied.

Appendix A - Plate Measurements

The density for each of the CMC plate was approximated by first approximating the volume of each plate. This was completed by first measuring the width of two opposite edges of the plate using a Mitutoyo Corporation Digital Micrometer. Measurements were recorded to the nearest hundredth of a millimeter. These two width measurement were then averaged together to determine an average plate width. Next, the lengths of two opposite edges of the plate were measured using the same micrometer were measured and recorded. Again, these two values were averaged to determine an average length. Finally, the thickness of the plate was measure in four locations near the corners of the plate. The four values were recorded and averaged together to determine an average thickness for the plate. The average length, width, and thickness values were multiplied together to calculate an approximate volume for the plate. Figure A.1 is a diagram depicting the approximate locations on each plate where the dimensions were measured.

Each of the plates were then weighed on a digital scale (OHaus Precision Balance, 3100g × 0.01g) and recorded. The approximate volume was divided by the weight to then calculate an approximate plate density. This process was repeated for each of the plates. The recorded values for each of the dimensions and weight of each plate before vacuum drying, after vacuum drying, and post heat treatment, are shown in Table A.1, Table A.2, and Table A.3 respectively.

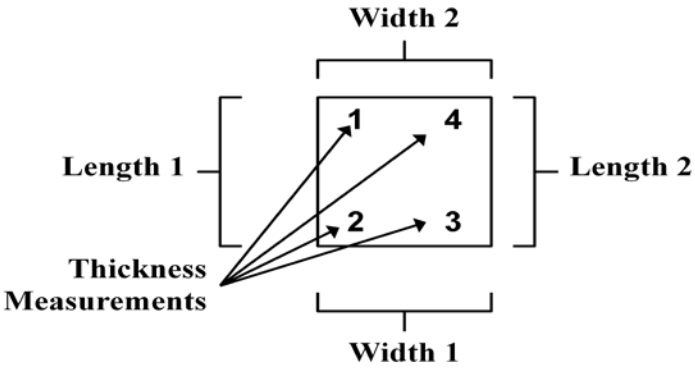

Figure A.1 - Diagram of the approximate location where each dimension on the plates were measured

Table A.1 - Plate measurement prior to drying in vacuum oven

			Thickness (mm)				*Length (mm)*		*Width (mm)*		
Material	***Panel***	***Plate***	***1***	***2***	***3***	***4***	***1***	***2***	***1***	***2***	***Weight (g)***
N610/AS	1	1	2.64	2.54	2.58	2.73	101.47	101.42	101.43	101.52	77.94
N610/AS	1	3	2.52	2.65	2.73	2.66	101.53	101.46	101.43	101.50	78.32
N610/AS	2	1	2.59	2.52	2.67	2.76	101.56	101.57	101.54	101.59	78.22
N610/AS	2	2	2.76	2.65	2.54	2.60	101.54	101.46	101.52	101.55	78.81
N610/AS	2	3	2.46	2.57	2.75	2.64	101.58	101.50	101.60	101.76	77.71
N720/AS	1	1	2.50	2.42	2.60	2.66	101.40	101.40	101.39	101.64	69.21
N720/AS	1	3	2.47	2.49	2.64	2.58	101.44	101.47	101.41	101.66	69.20
N720/AS	2	1	2.50	2.45	2.54	2.63	101.47	101.46	101.39	101.57	69.84
N720/AS	2	2	2.61	2.53	2.49	2.54	101.43	101.46	101.48	101.43	69.88
N720/AS	2	3	2.42	2.52	2.62	2.50	101.53	101.52	101.41	101.58	69.75
N720/A	1	1	2.76	2.76	2.86	2.83	101.36	101.43	101.38	101.60	79.43
N720/A	1	3	2.67	2.70	2.81	2.80	101.40	101.36	101.38	101.54	77.86
N720/A	2	1	2.70	2.75	2.72	2.75	101.28	101.32	101.35	101.67	76.16
N720/A	2	2	2.77	2.73	2.70	2.76	101.33	101.37	101.37	101.45	77.38
N720/A	2	3	2.69	2.67	2.75	2.75	101.54	101.55	101.36	101.66	76.89
N720/A	2	4	2.77	2.76	2.73	2.75	101.59	101.58	101.43	101.54	77.93

Table A.2 - Plate measurements after drying in vacuum oven, but prior to heat exposure

			Thickness (mm)				*Length (mm)*		*Width (mm)*		
Material	***Panel***	***Plate***	***1***	***2***	***3***	***4***	***1***	***2***	***1***	***2***	***Weight (g)***
N610/AS	1	1	2.62	2.48	2.55	2.71	101.44	101.37	101.40	101.49	77.94
N610/AS	1	3	2.47	2.58	2.71	2.59	101.50	101.46	101.44	101.50	78.32
N610/AS	2	1	2.52	2.48	2.65	2.75	101.52	101.49	101.47	101.60	78.22
N610/AS	2	2	2.70	2.63	2.51	2.57	101.52	101.45	101.49	101.52	78.81
N610/AS	2	3	2.41	2.54	2.74	2.57	101.54	101.48	101.57	101.75	77.71
N720/AS	1	1	2.48	2.35	2.55	2.65	101.39	101.40	101.37	101.61	69.21
N720/AS	1	3	2.36	2.44	2.64	2.56	101.43	101.44	101.38	101.64	69.20
N720/AS	2	1	2.49	2.43	2.52	2.60	101.46	101.44	101.39	101.56	69.84
N720/AS	2	2	2.60	2.51	2.44	2.51	101.41	101.41	101.47	101.42	69.88
N720/AS	2	3	2.40	2.50	2.58	2.49	101.56	101.49	101.39	101.58	69.75
N720/A	1	1	2.74	2.75	2.85	2.81	101.35	101.39	101.35	101.56	79.43
N720/A	1	3	2.66	2.70	2.79	2.75	101.38	101.35	101.35	101.52	77.86
N720/A	2	1	2.67	2.63	2.68	2.71	101.24	101.27	101.30	101.62	76.16
N720/A	2	2	2.73	2.71	2.66	2.71	101.30	101.36	101.36	101.42	77.38
N720/A	2	3	2.65	2.64	2.70	2.73	101.51	101.52	101.34	101.64	76.89

Table A.3 - Plate measurement after heat exposure

			Thickness (mm)				*Length (mm)*		*Width (mm)*		
Material	***Panel***	***Plate***	***1***	***2***	***3***	***4***	***1***	***2***	***1***	***2***	***Weight (g)***
N610/AS	1	1	2.54	2.68	2.58	2.43	101.06	101.15	101.08	101.12	77.85
N610/AS	1	3	2.55	2.65	2.54	2.44	101.13	101.09	101.04	101.11	78.23
N610/AS	2	1	2.51	2.43	2.60	2.71	101.13	101.12	101.10	101.22	78.12
N610/AS	2	2	2.65	2.53	2.39	2.51	101.09	101.05	101.07	101.08	78.72
N610/AS	2	3	2.60	2.40	2.54	2.74	101.40	101.43	101.62	101.44	77.65
N720/AS	1	1	2.78	2.85	2.73	2.72	101.31	101.08	101.12	101.08	79.38
N720/AS	1	3	2.31	2.51	2.60	2.40	101.23	101.22	101.17	101.37	69.10
N720/AS	2	1	2.40	2.59	2.52	2.33	101.09	101.36	101.18	101.12	69.11
N720/AS	2	2	2.41	2.49	2.59	2.47	101.13	101.16	101.07	101.25	69.77
N720/AS	2	3	2.55	2.44	2.39	2.47	100.96	100.94	100.99	100.97	69.79
N720/A	1	1	2.52	2.43	2.51	2.61	101.44	101.45	101.49	101.33	69.69
N720/A	1	3	2.71	2.78	2.75	2.62	101.01	101.01	100.96	101.08	77.84
N720/A	2	1	2.68	2.71	2.64	2.62	100.81	101.14	100.83	100.81	76.11
N720/A	2	3	2.61	2.70	2.71	2.63	101.45	101.14	101.37	101.37	76.85
N720/A	2	4	2.68	2.71	2.73	2.71	100.93	100.93	100.85	100.86	77.89

Appendix B - Tensile Stress-Strain Curves

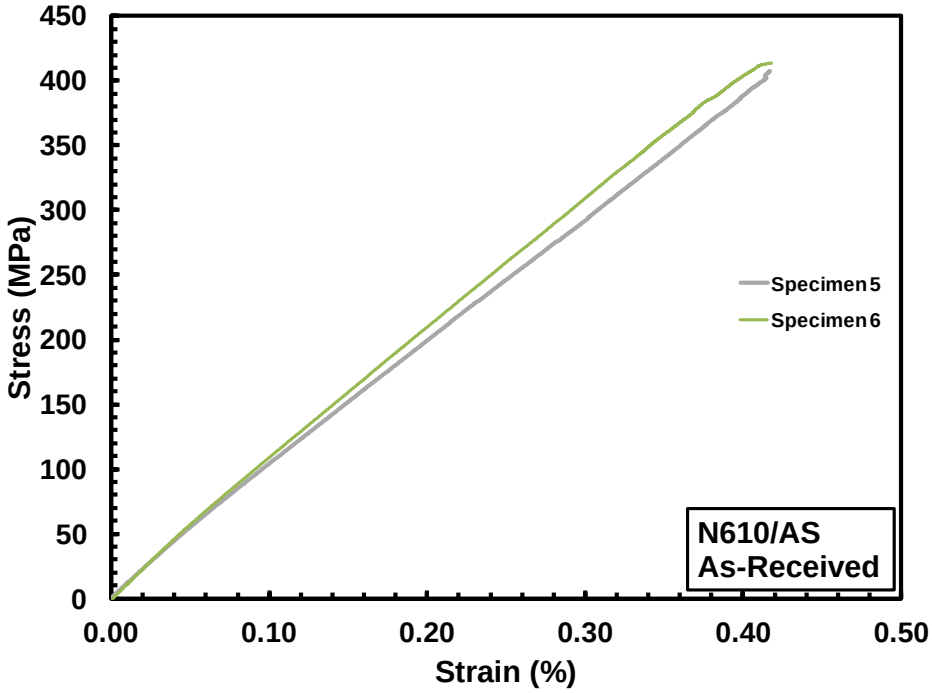

Figure B.1 – Tensile stress-strain curve for as-received specimens of N610/AS composite

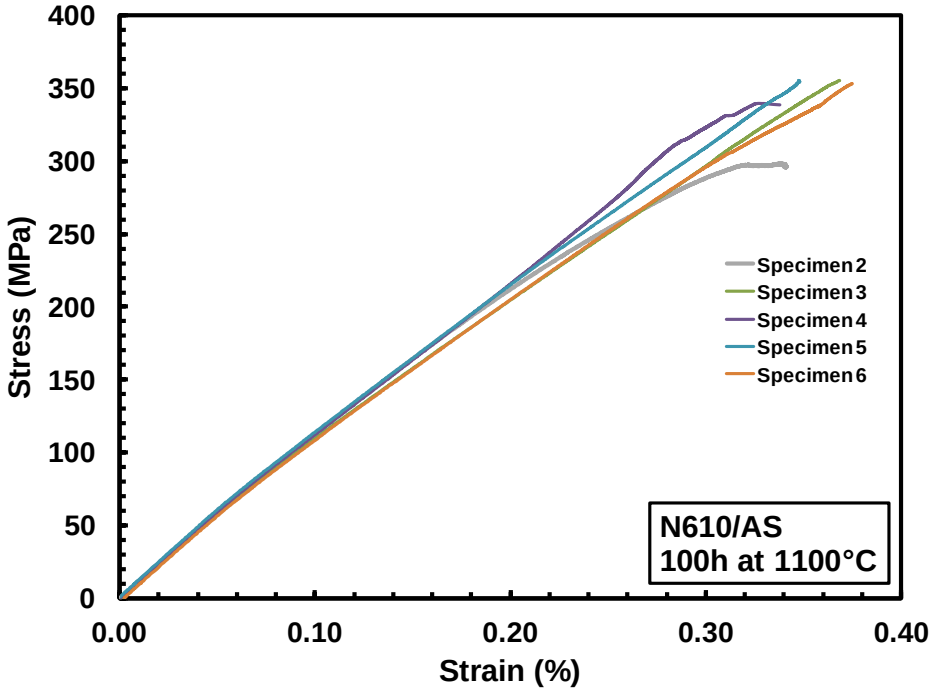

Figure B.2 – Tensile stress-strain curve for specimens of N610/AS composite with prior heat treatment for 100 h at 1100°C

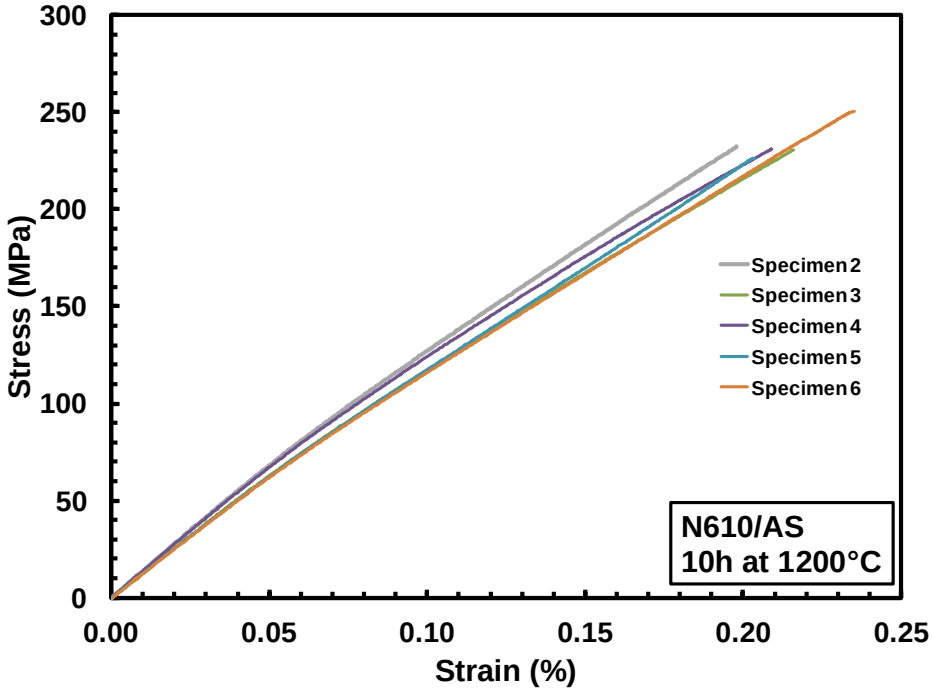

Figure B.3 – Tensile stress-strain curve for specimens of N610/AS composite with prior heat treatment for 10 h at 1200°C

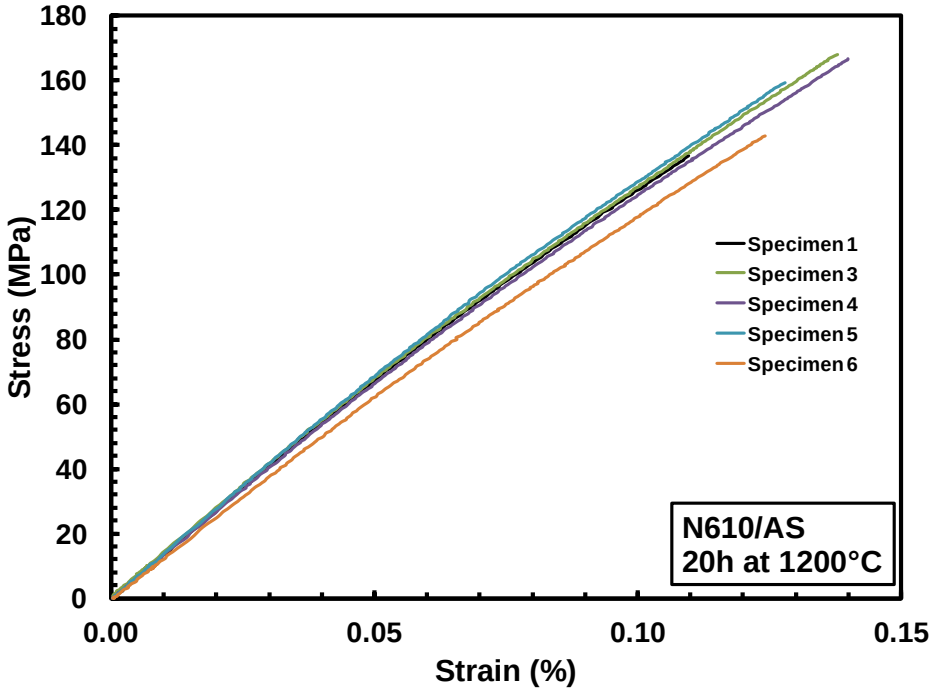

Figure B.4 – Tensile stress-strain curve for N610/AS composite with prior heat treatment for 20 h at 1200°C

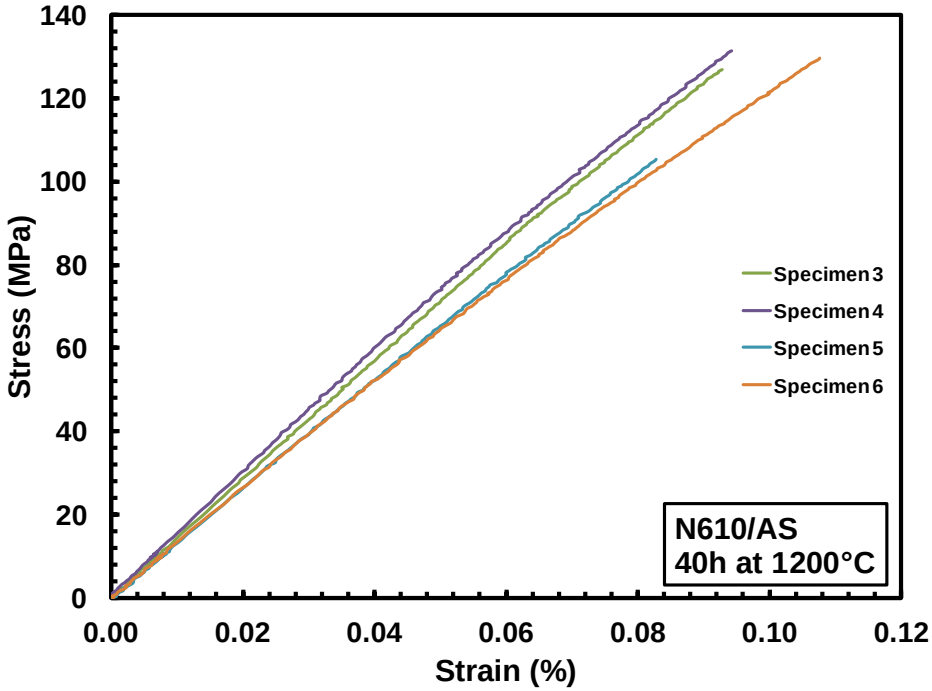

Figure B.5 – Tensile stress-strain curve for N610/AS composite with prior heat treatment for 40 h at 1200°C

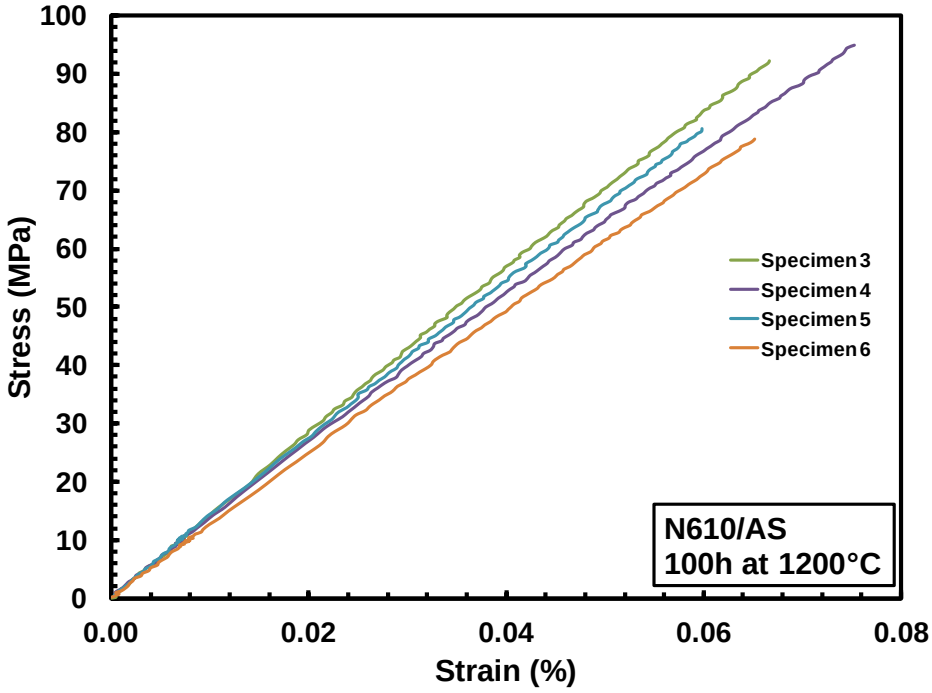

Figure B.6 – Tensile stress-strain curve for N610/AS composite with prior heat treatment for 100 h at 1200°C

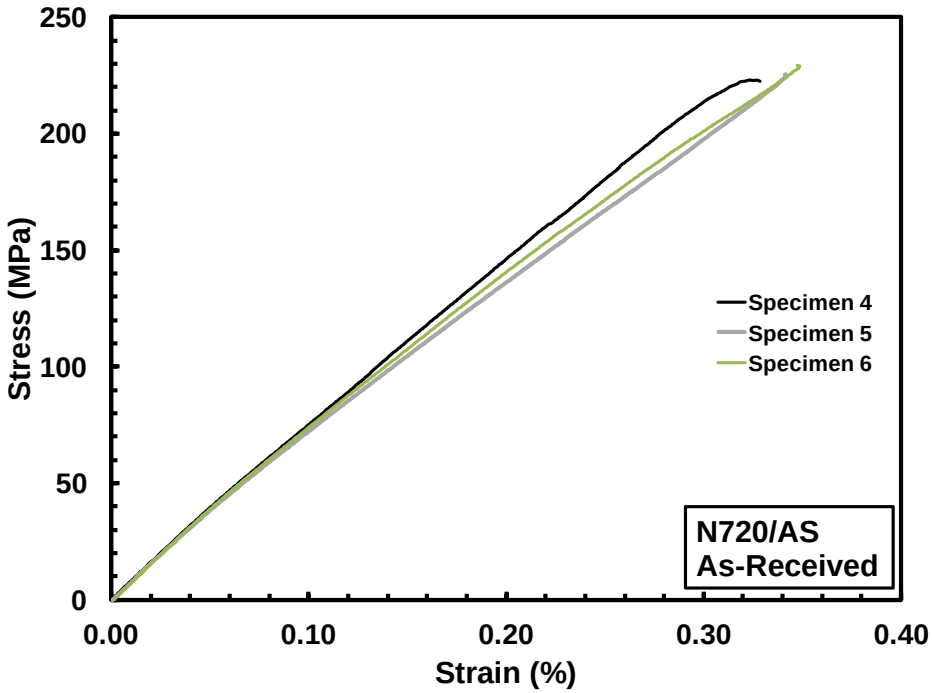

Figure B.7 – Tensile stress-strain curve for as-received specimens of N720/AS composite

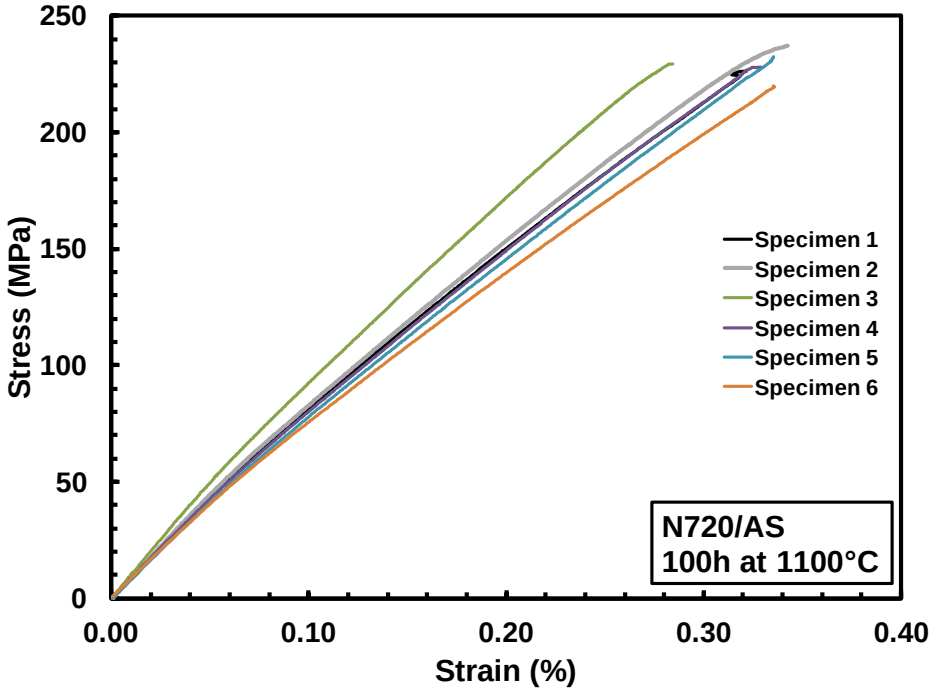

Figure B.8 – Tensile stress-strain curve for N720/AS composite with prior heat treatment for 100 h at 1100°C

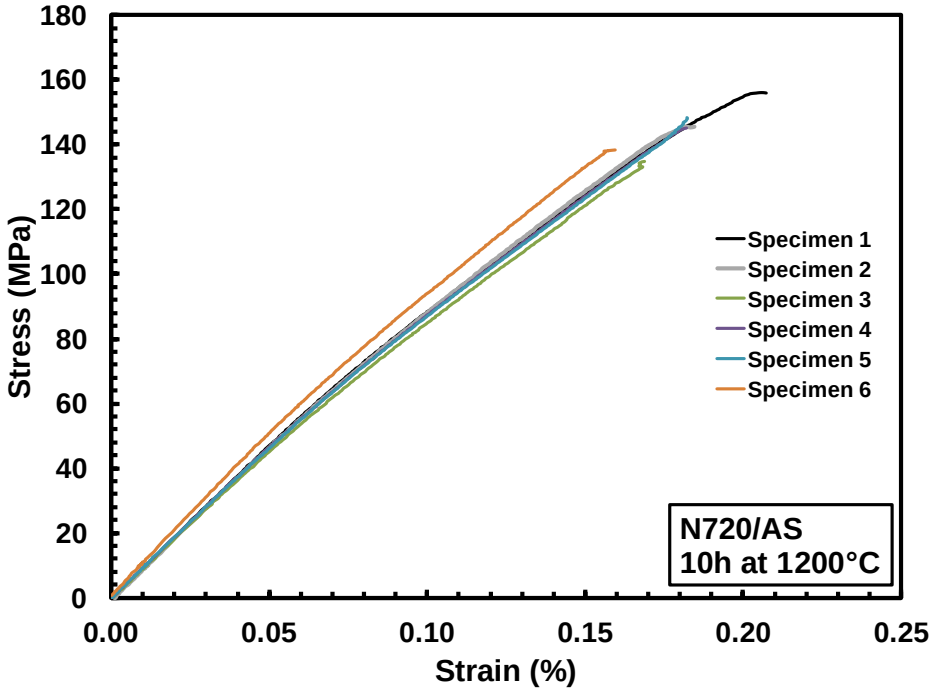

Figure B.9 – Tensile stress-strain curve for N720/AS composite with prior heat treatment for 10 h at 1200°C

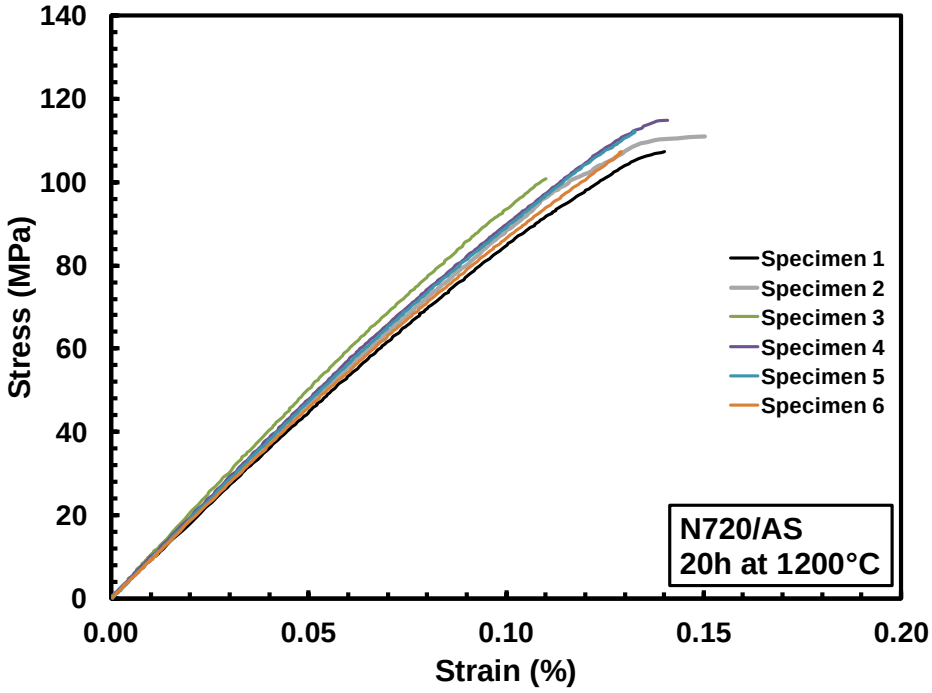

Figure B.10 – Tensile stress-strain curve for N720/AS composite with prior heat treatment for 20 h at 1200°C

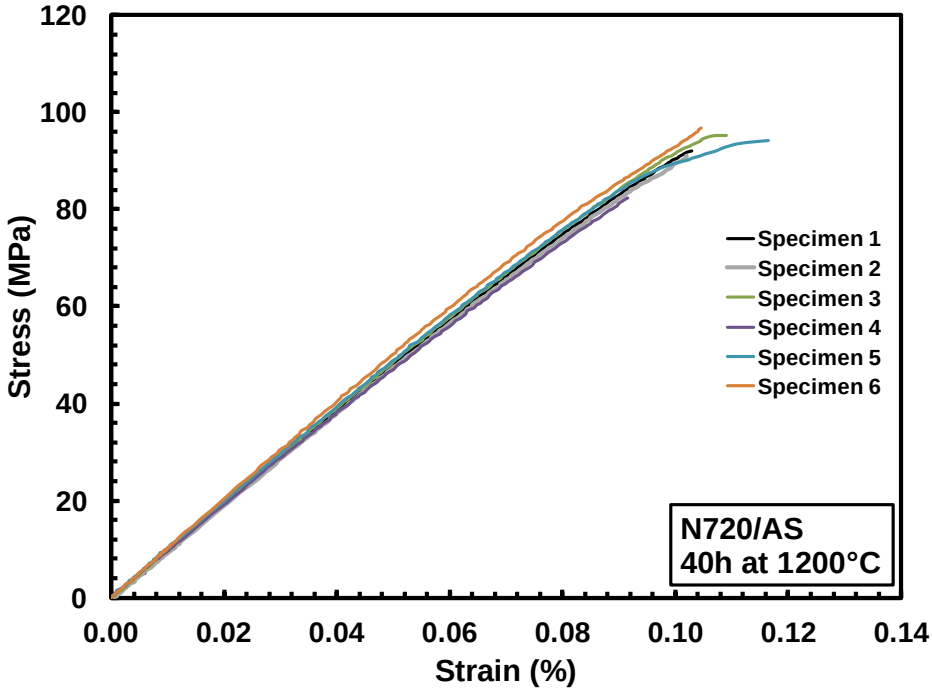

Figure B.11 – Tensile stress-strain curve for N720/AS composite with prior heat treatment for 40 h at 1200°C

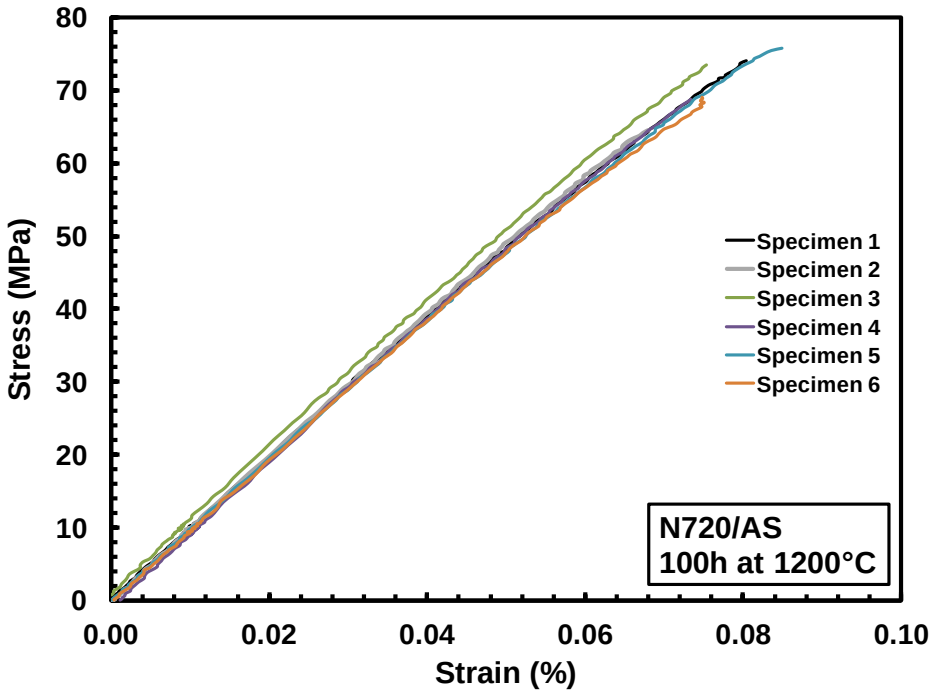

Figure B.12 – Tensile stress-strain curve for N720/AS composite with prior heat treatment for 100 h at 1200°C

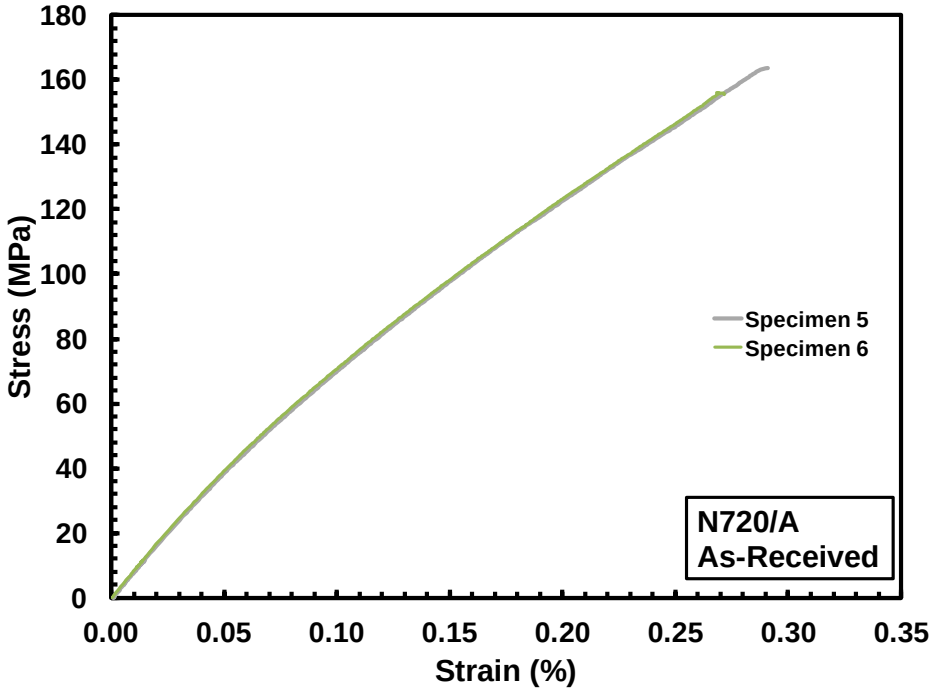

Figure B.13 – Tensile stress-strain curve for as-received specimens of N720/A composite

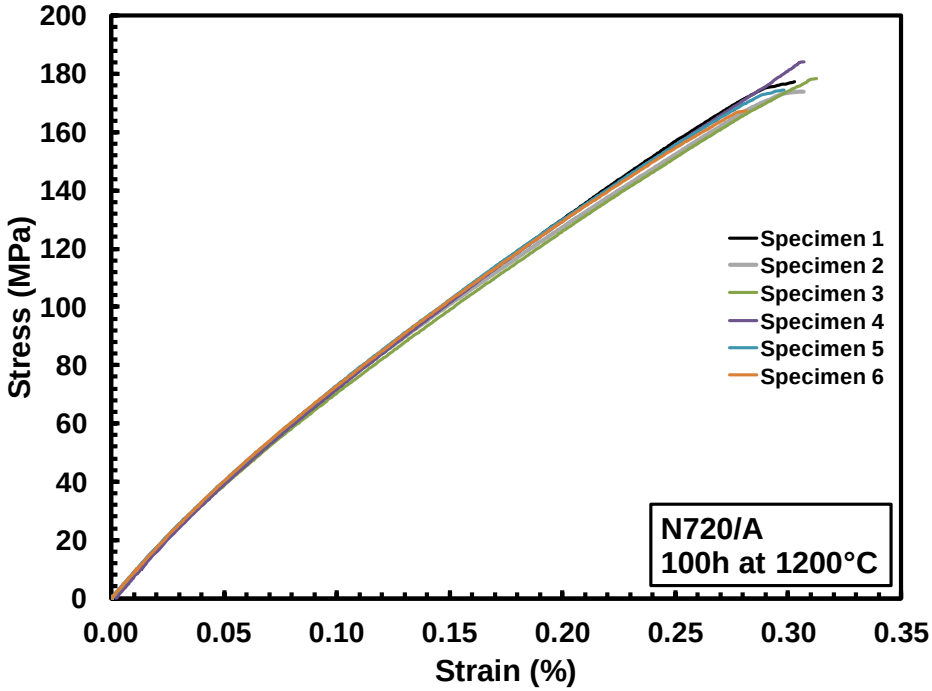

Figure B.14 – Tensile stress-strain curve for N720/A composite with prior heat treatment for 100 h at 1200°C

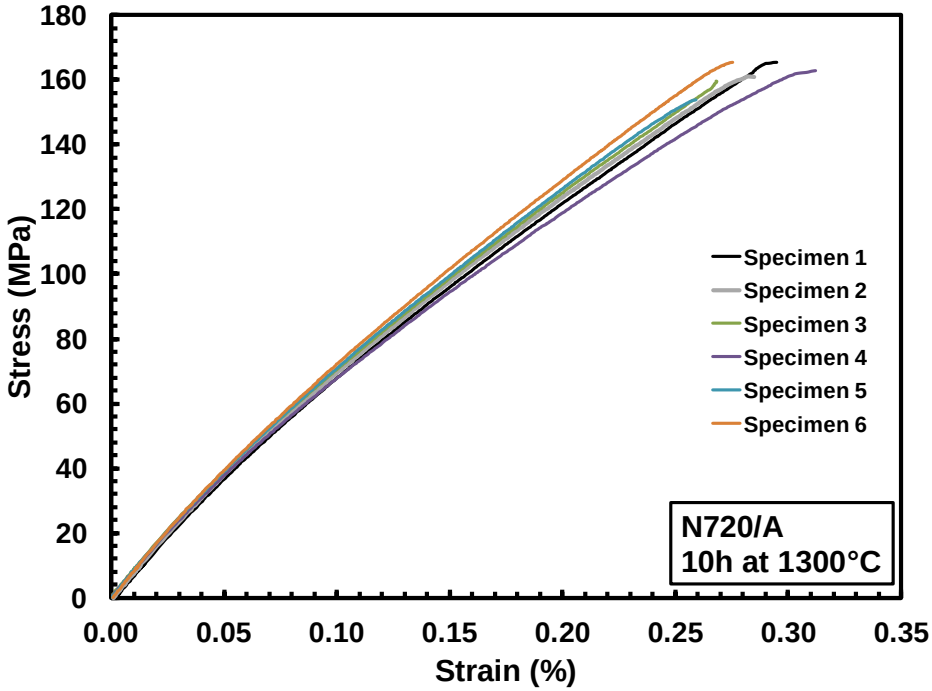

Figure B.15 – Tensile stress-strain curve for N720/A composite with prior heat treatment for 10 h at 1300°C

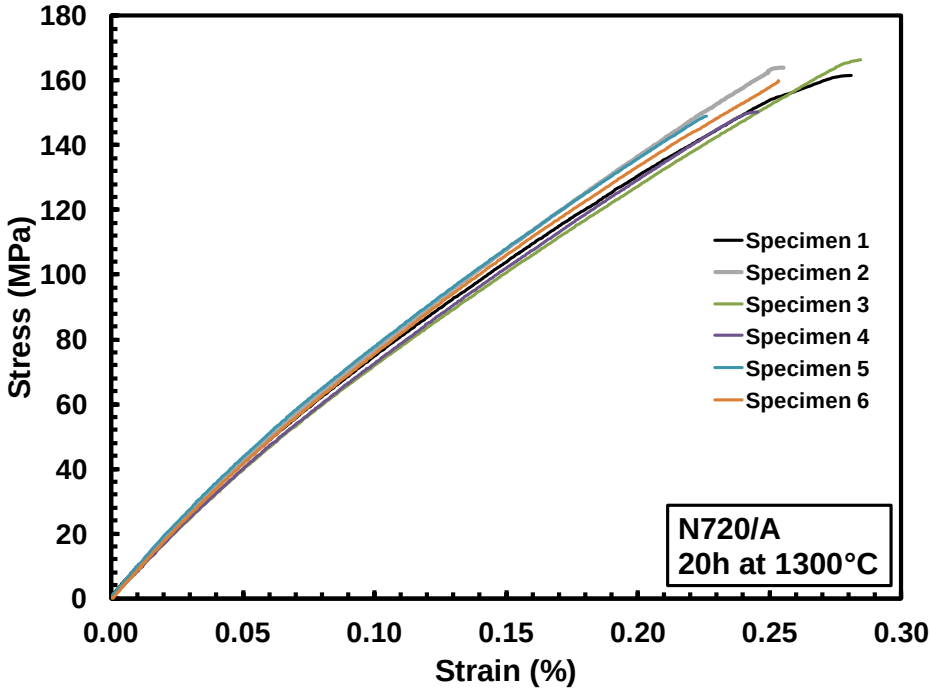

Figure B.16 – Tensile stress-strain curve for N720/A composite with prior heat treatment for 20 h at 1300°C

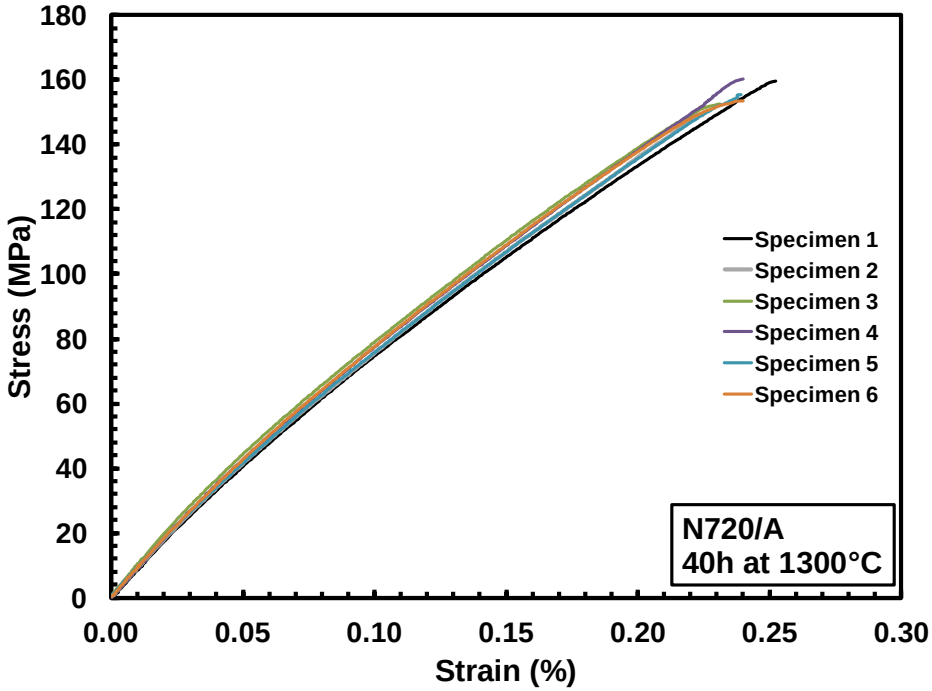

Figure B.17 – Tensile stress-strain curve for N720/A composite with prior heat treatment for 40 h at 1300°C

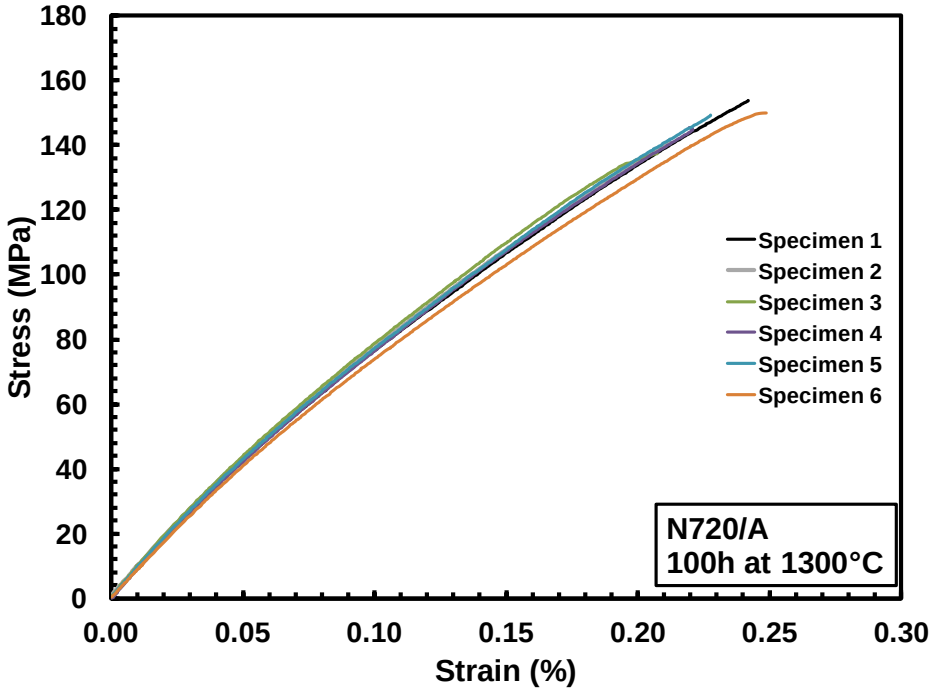

Figure B.18 – Tensile stress-strain curve for N720/A composite with prior heat treatment for 100 h at 1300°C

Appendix C - Additional Optical Micrographs of N610/AS Fracture Surfaces

Appendix C presents additional optical micrographs of the fracture surfaces of N610/AS specimens produced in tensile tests.

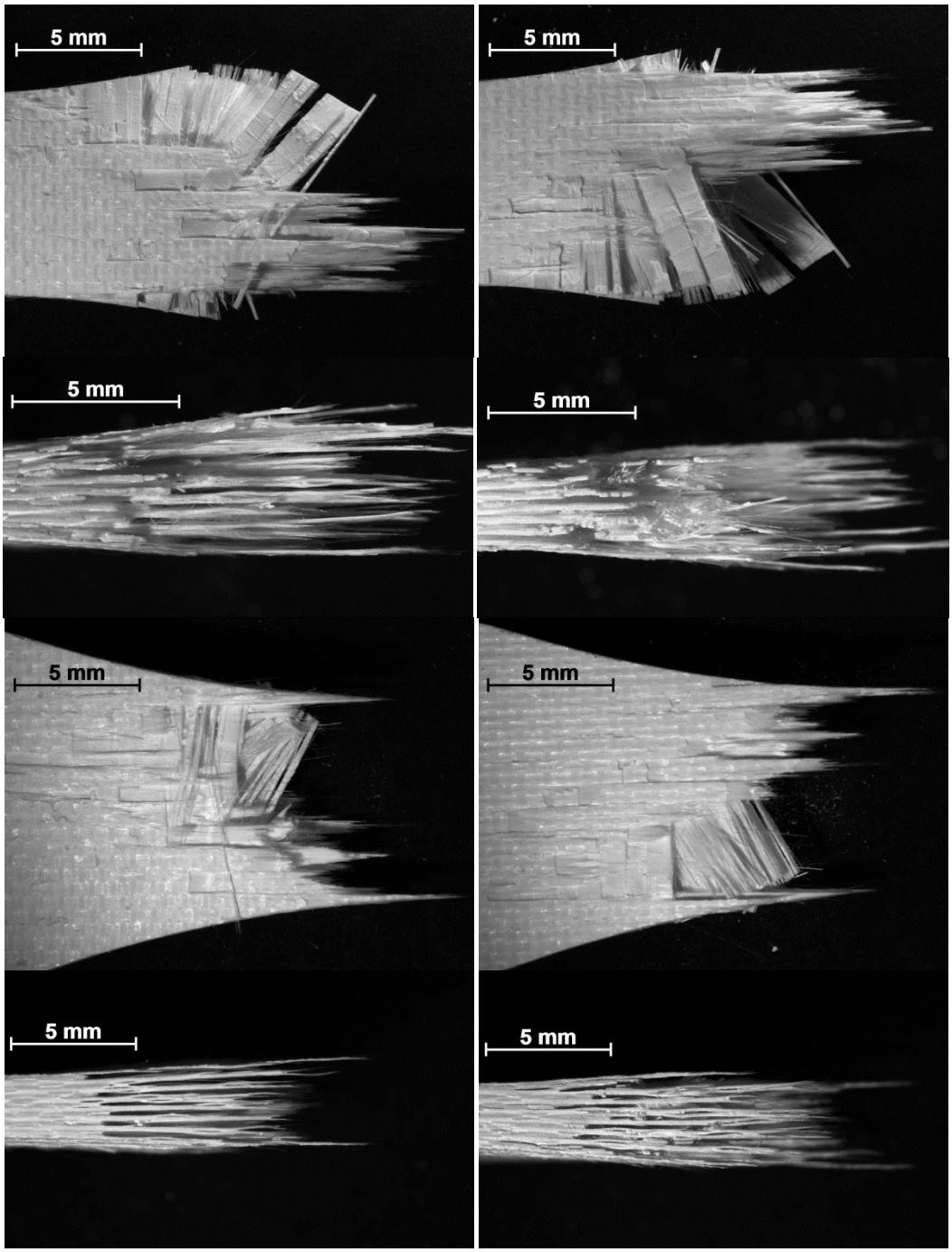

Figure C.1 - Optical micrographs of fracture surface of as-received N610/AS composite obtained in tensile tests (Specimen 5)

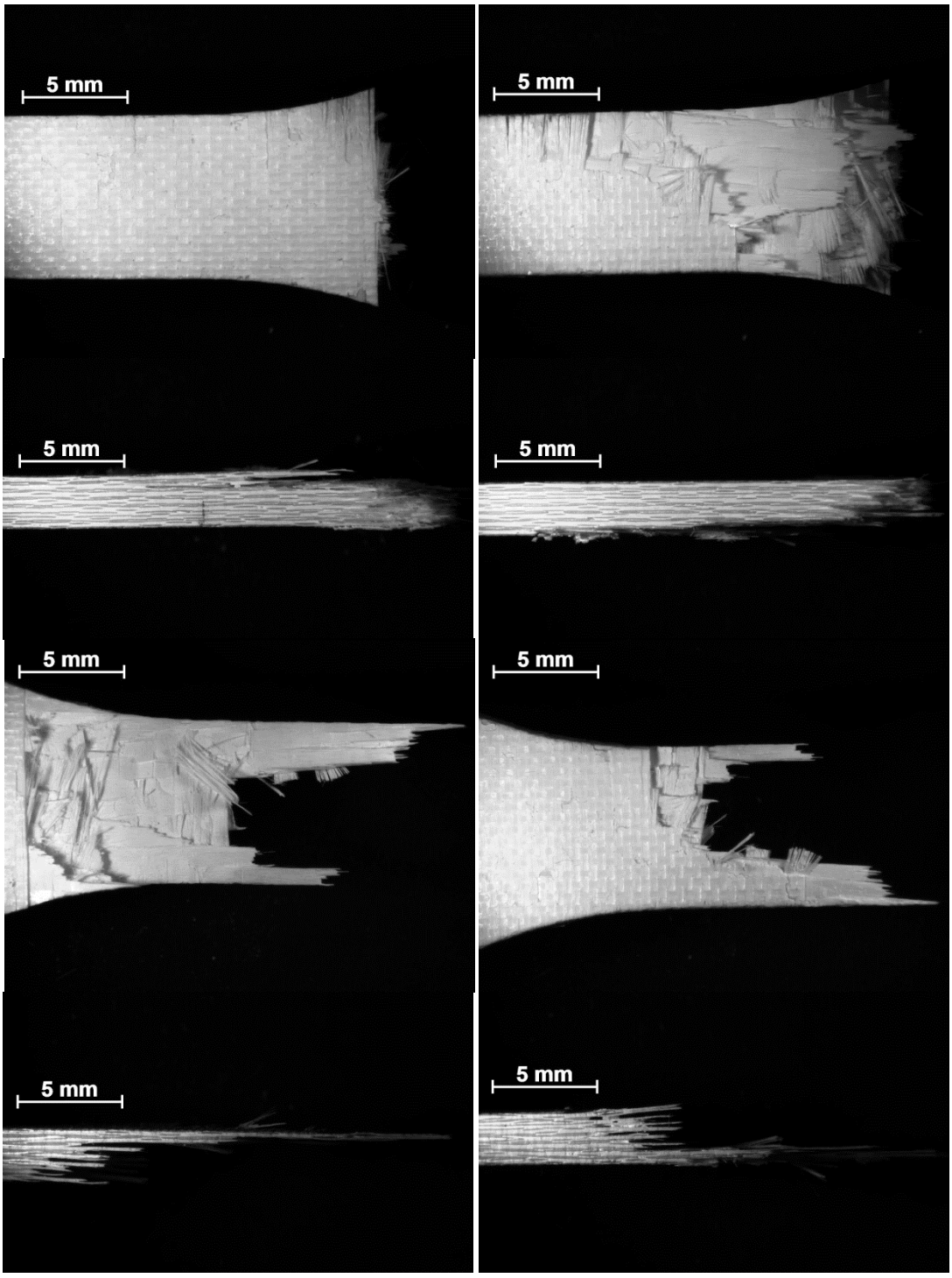

Figure C.2 - Optical micrographs of fracture surface of N610/AS composite obtained in tensile tests after prior heat treatment of 100 h at 1100°C (Specimen 3)

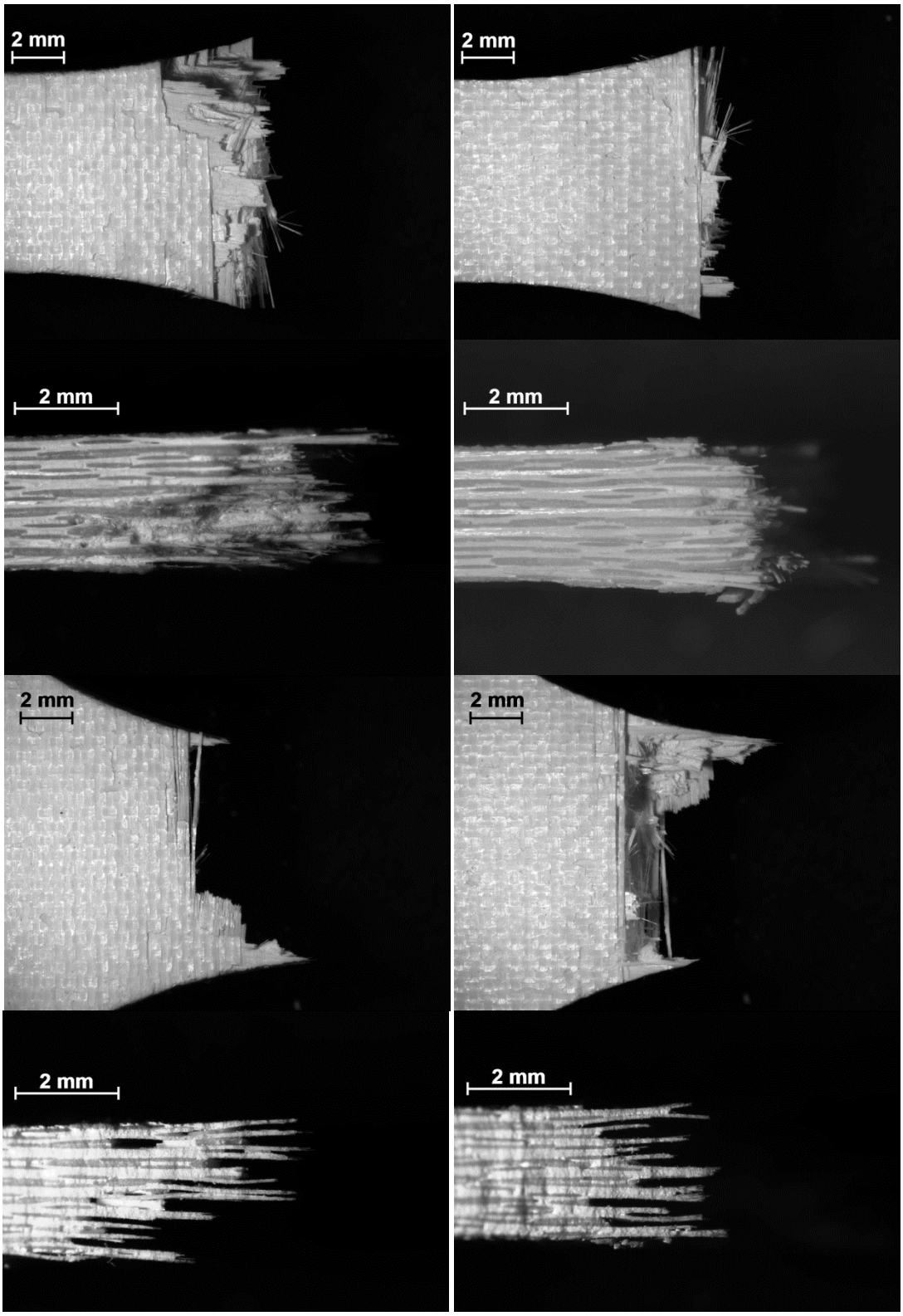

Figure C.3 - Optical micrographs of fracture surface of N610/AS composite obtained in tensile tests after prior heat treatment of 100 h at 1100°C (Specimen 5)

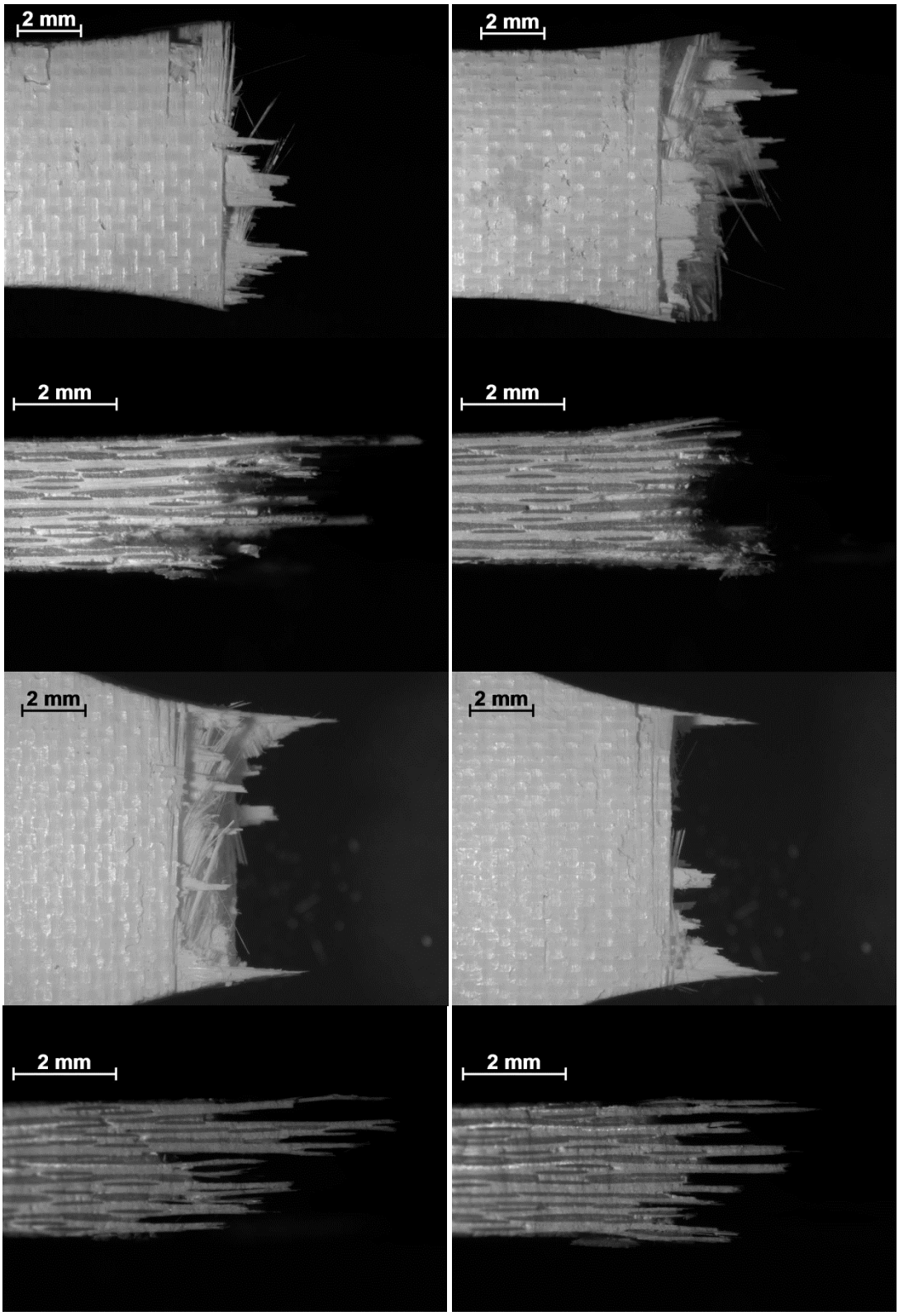

Figure C.4 - Optical micrographs of fracture surface of N610/AS composite obtained in tensile tests after prior heat treatment of 100 h at 1100°C (Specimen 6)

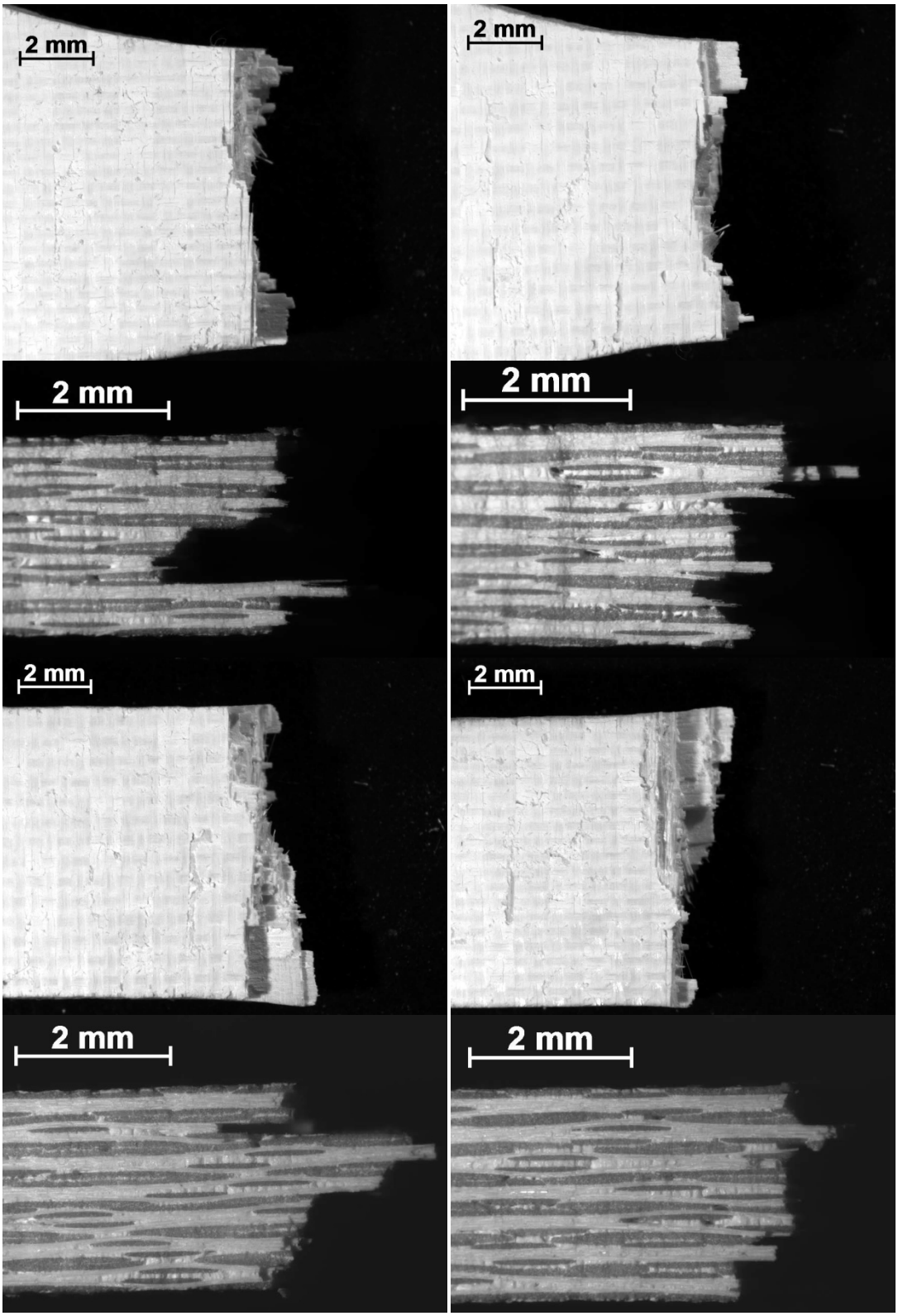

Figure C.5 - Optical micrographs of fracture surface of N610/AS composite obtained in tensile tests after prior heat treatment of 10 h at 1200°C (Specimen 2)

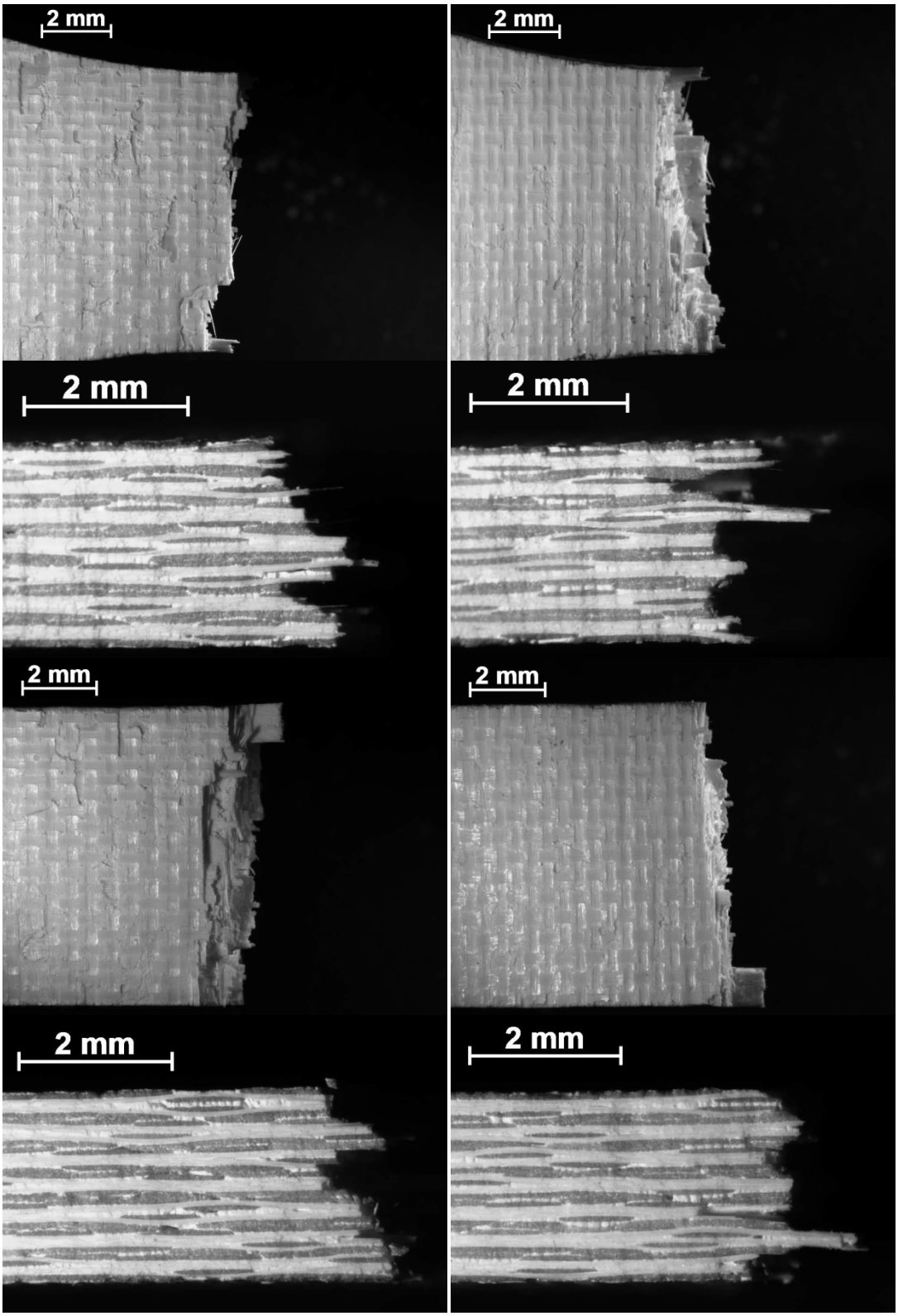

Figure C.6 - Optical micrographs of fracture surface of N610/AS composite obtained in tensile tests after prior heat treatment of 10 h at 1200°C (Specimen 4)

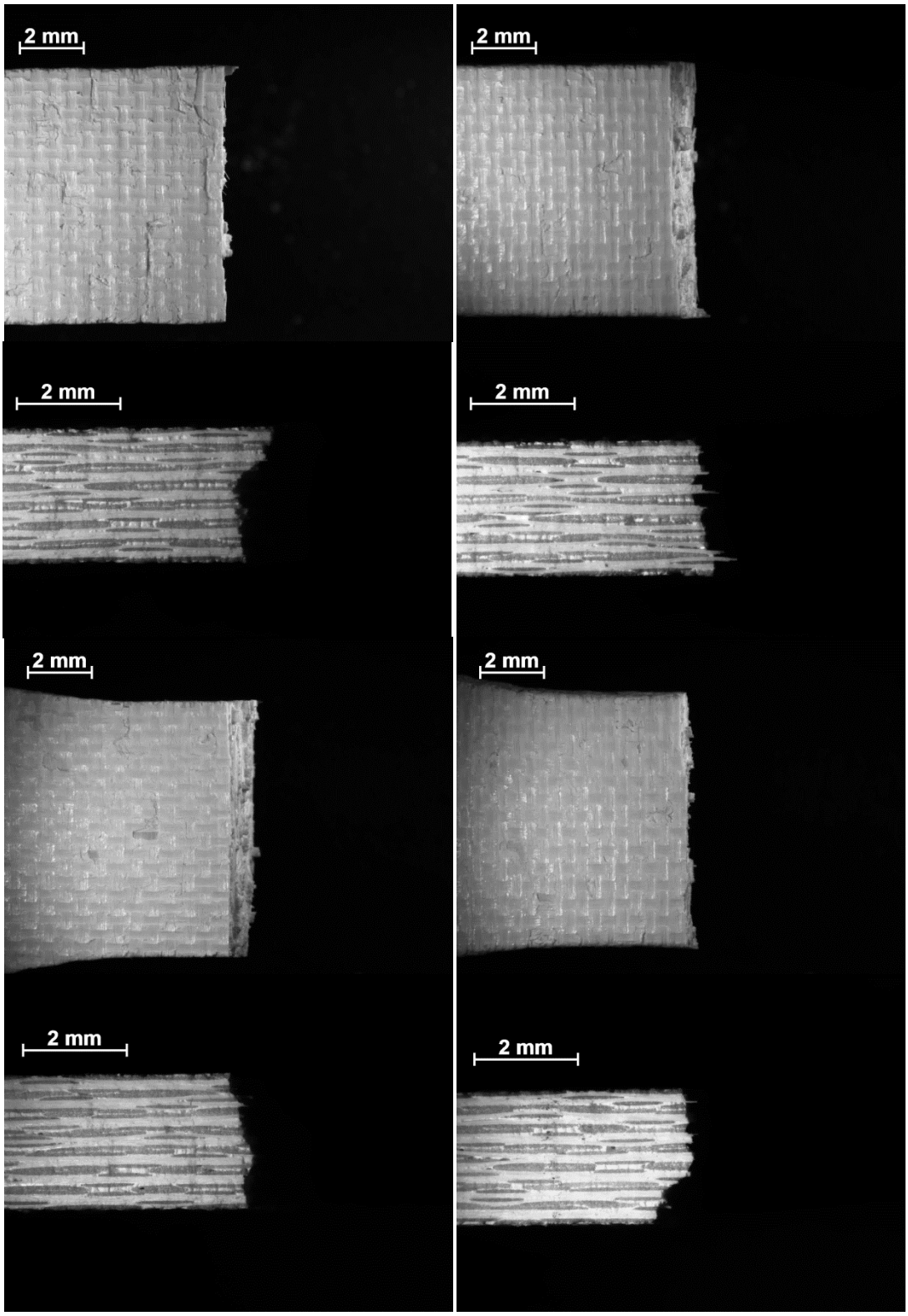

Figure C.7 - Optical micrographs of fracture surface of N610/AS composite obtained in tensile tests after prior heat treatment of 20 h at 1200°C (Specimen 3)

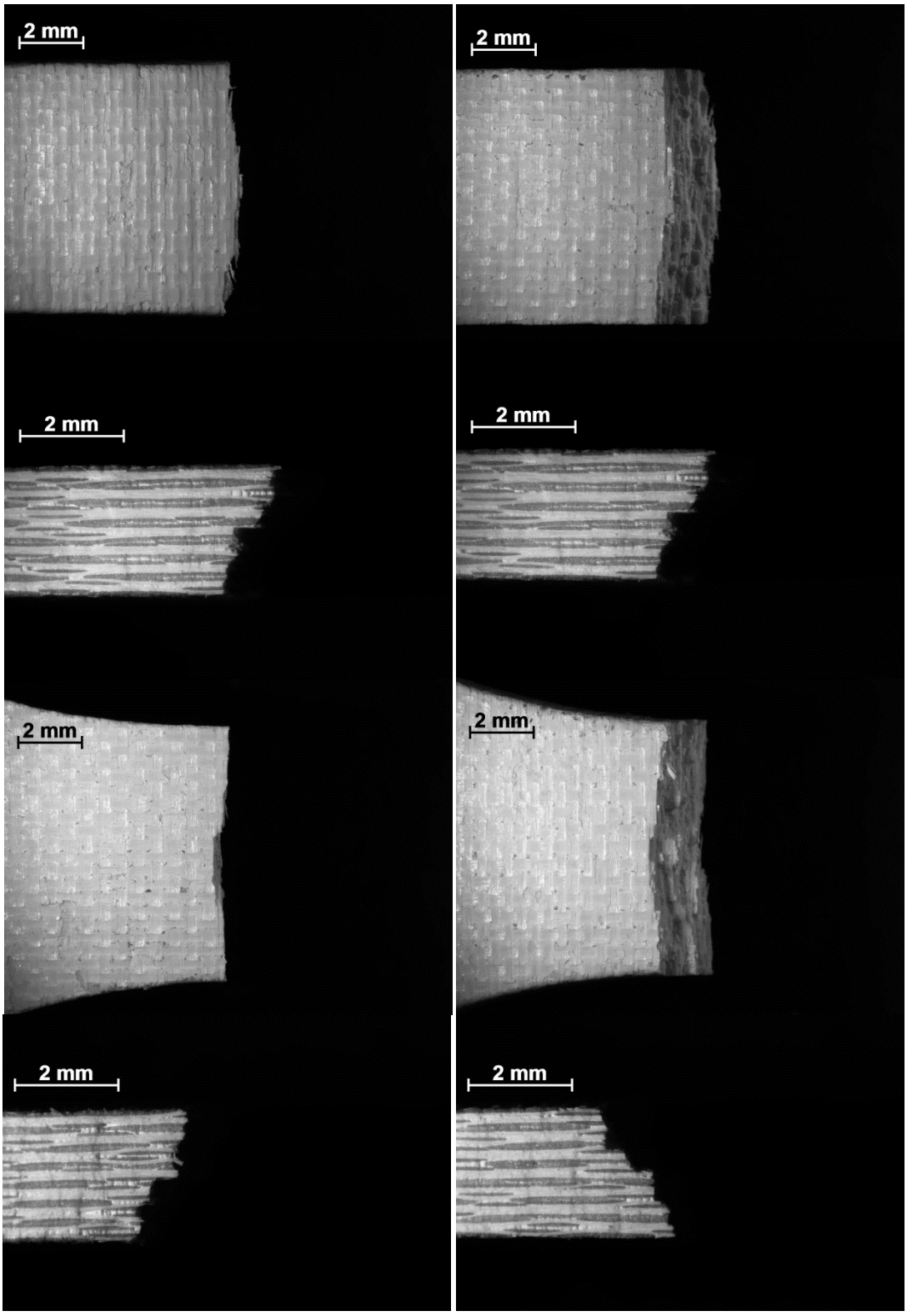

Figure C.8 - Optical micrographs of fracture surface of N610/AS composite obtained in tensile tests after prior heat treatment of 20 h at 1200°C (Specimen 5)

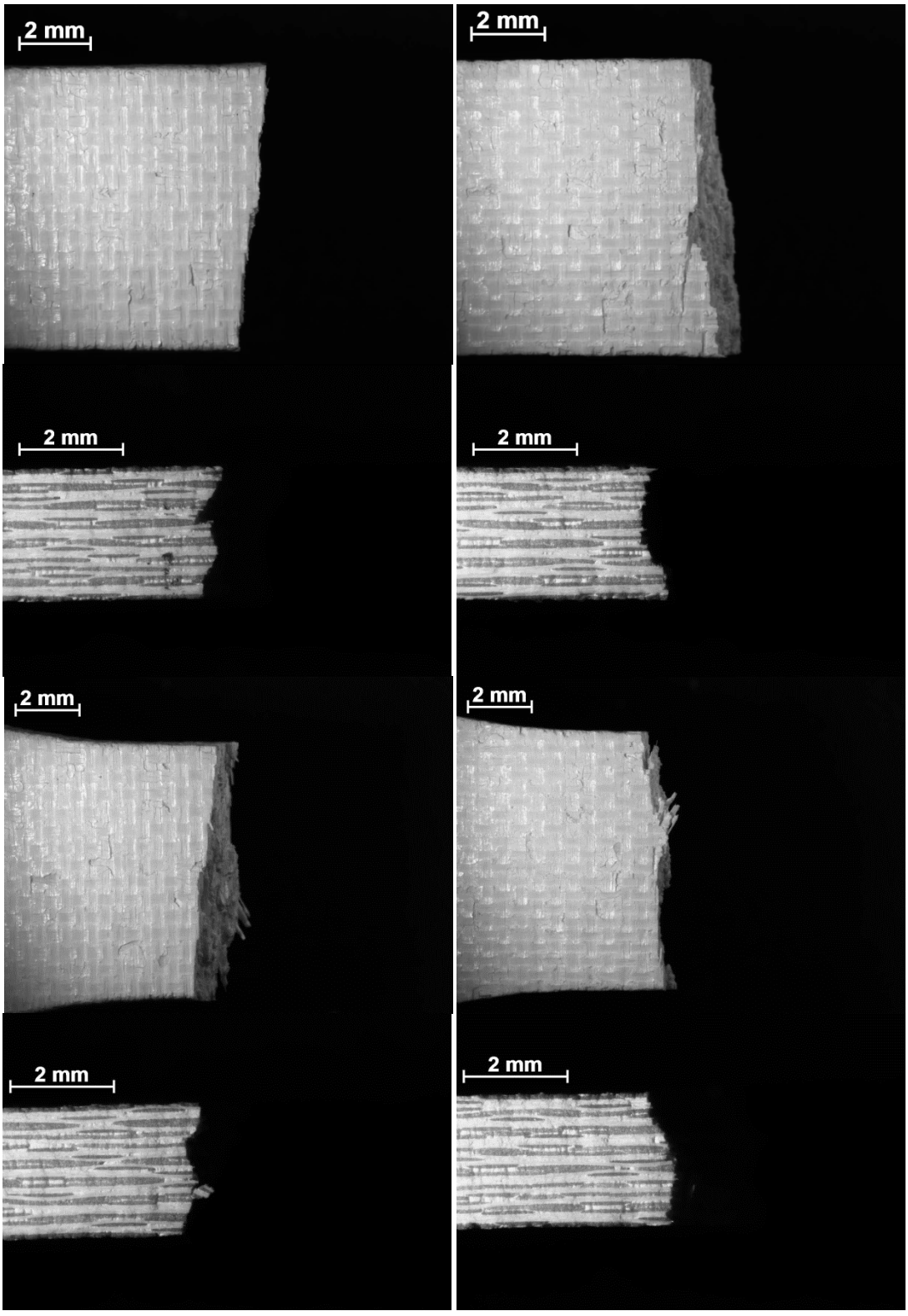

Figure C.9 - Optical micrographs of fracture surface of N610/AS composite obtained in tensile tests after prior heat treatment of 40 h at 1200°C (Specimen 5)

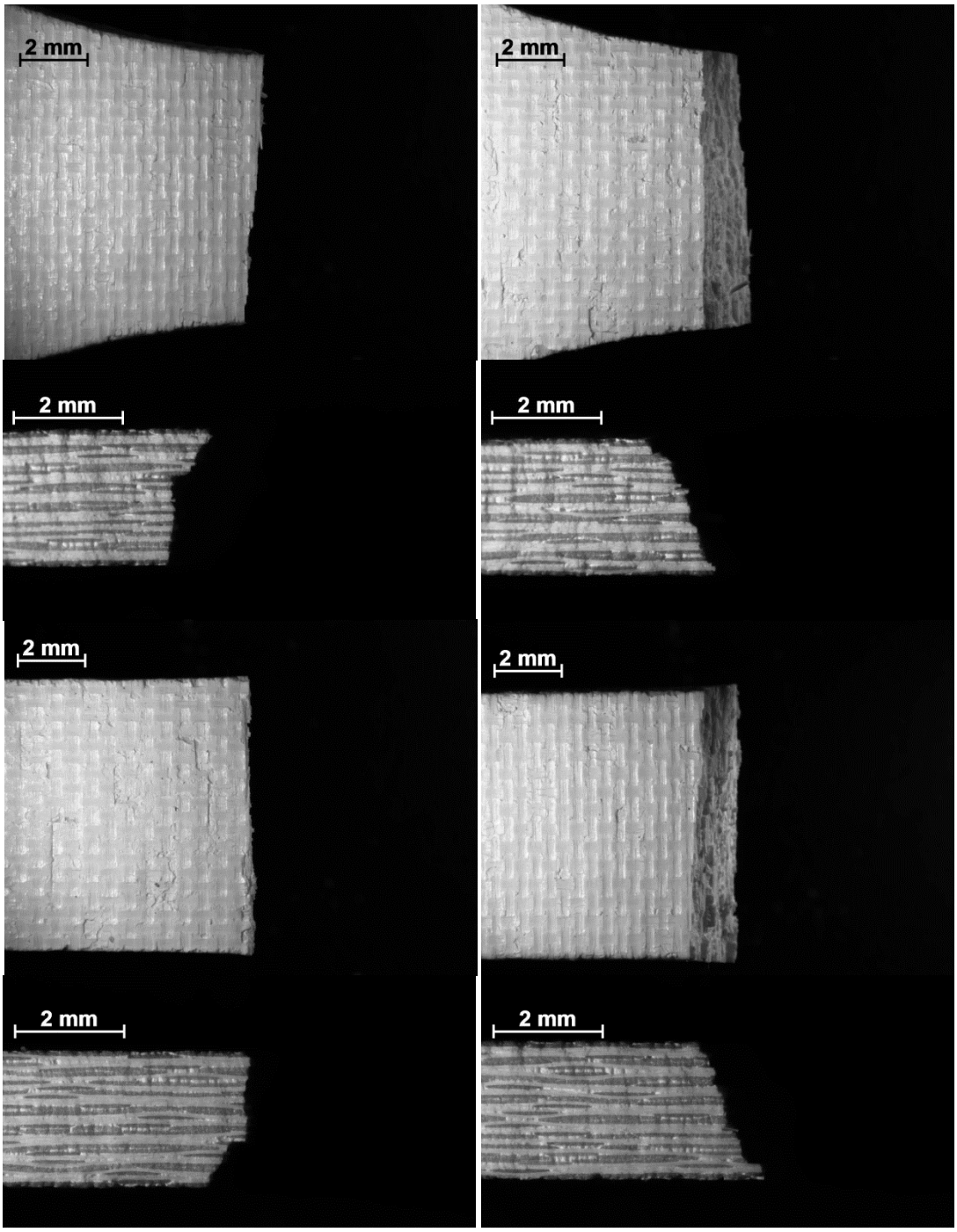

Figure C.10 - Optical micrographs of fracture surface of N610/AS composite obtained in tensile tests after prior heat treatment of 40 h at 1200°C (Specimen 6)

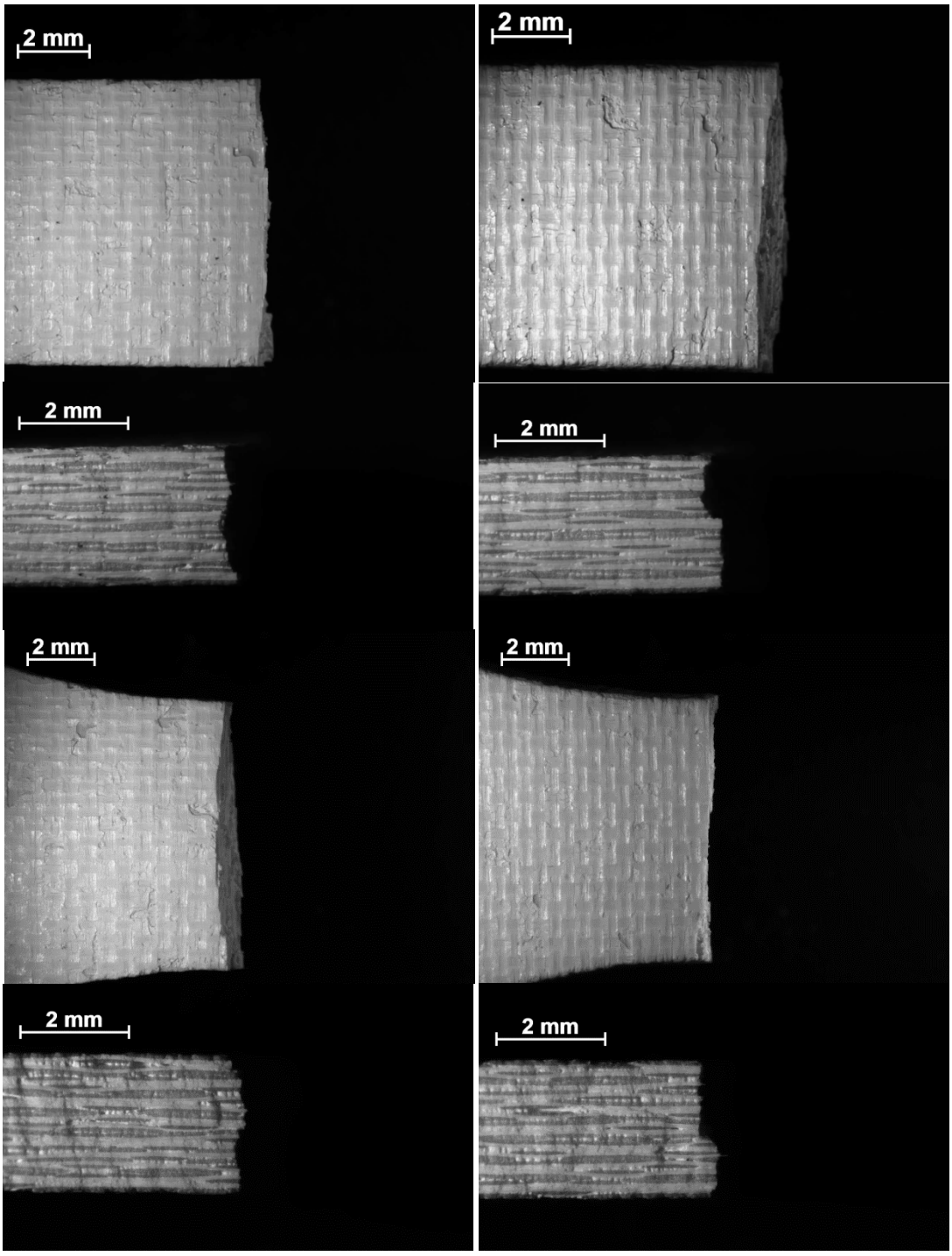

Figure C.11 - Optical micrographs of fracture surface of N610/AS composite obtained in tensile tests after prior heat treatment of 100 h at 1200°C (Specimen 3)

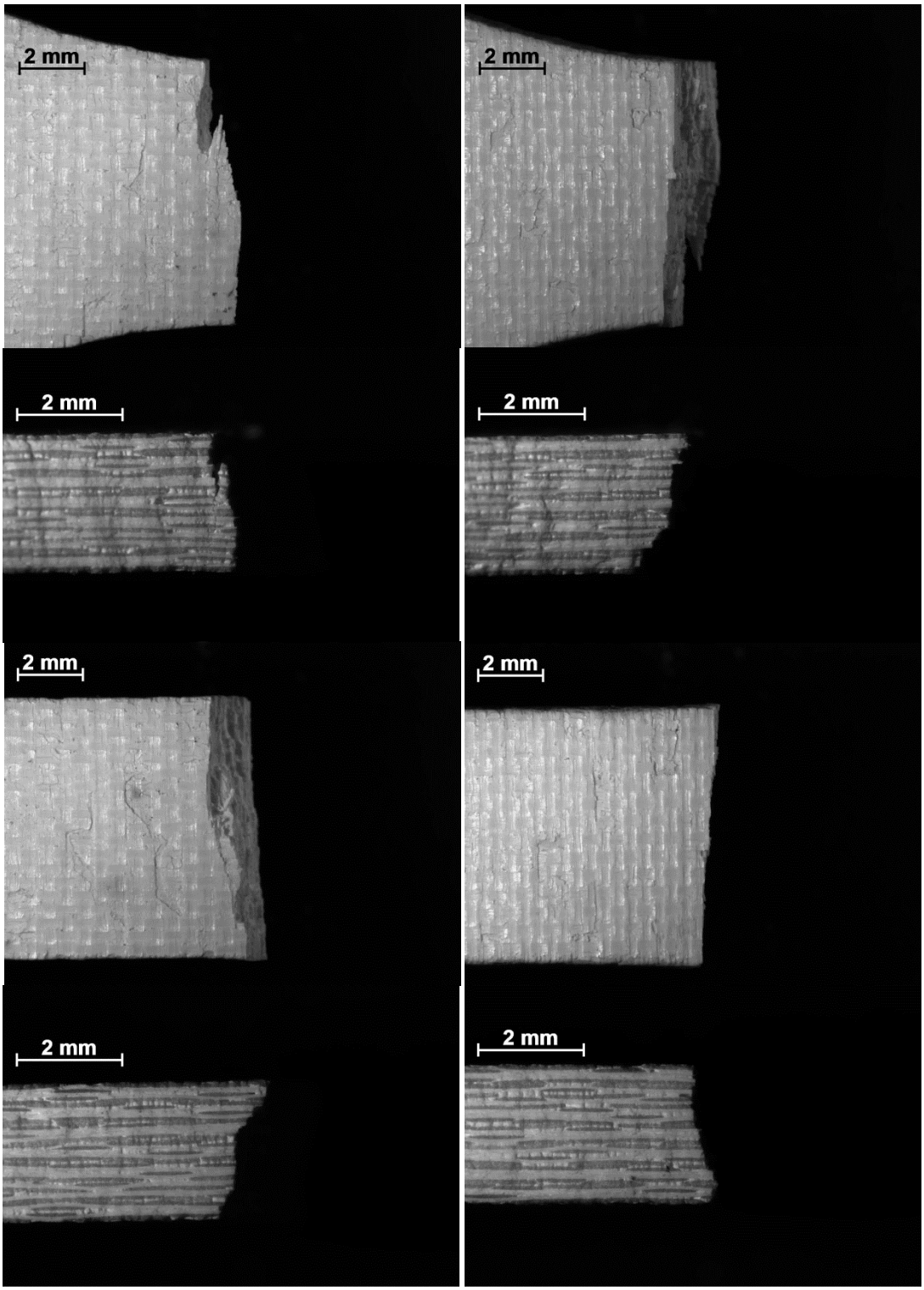

Figure C.12 - Optical micrographs of fracture surface of N610/AS composite obtained in tensile tests after prior heat treatment of 100 h at 1200°C (Specimen 5)

Appendix D - Additional Optical Micrographs of N720/AS Fracture Surfaces

Appendix D presents additional optical micrographs of the fracture surfaces of N720/AS specimens produced in tensile tests.

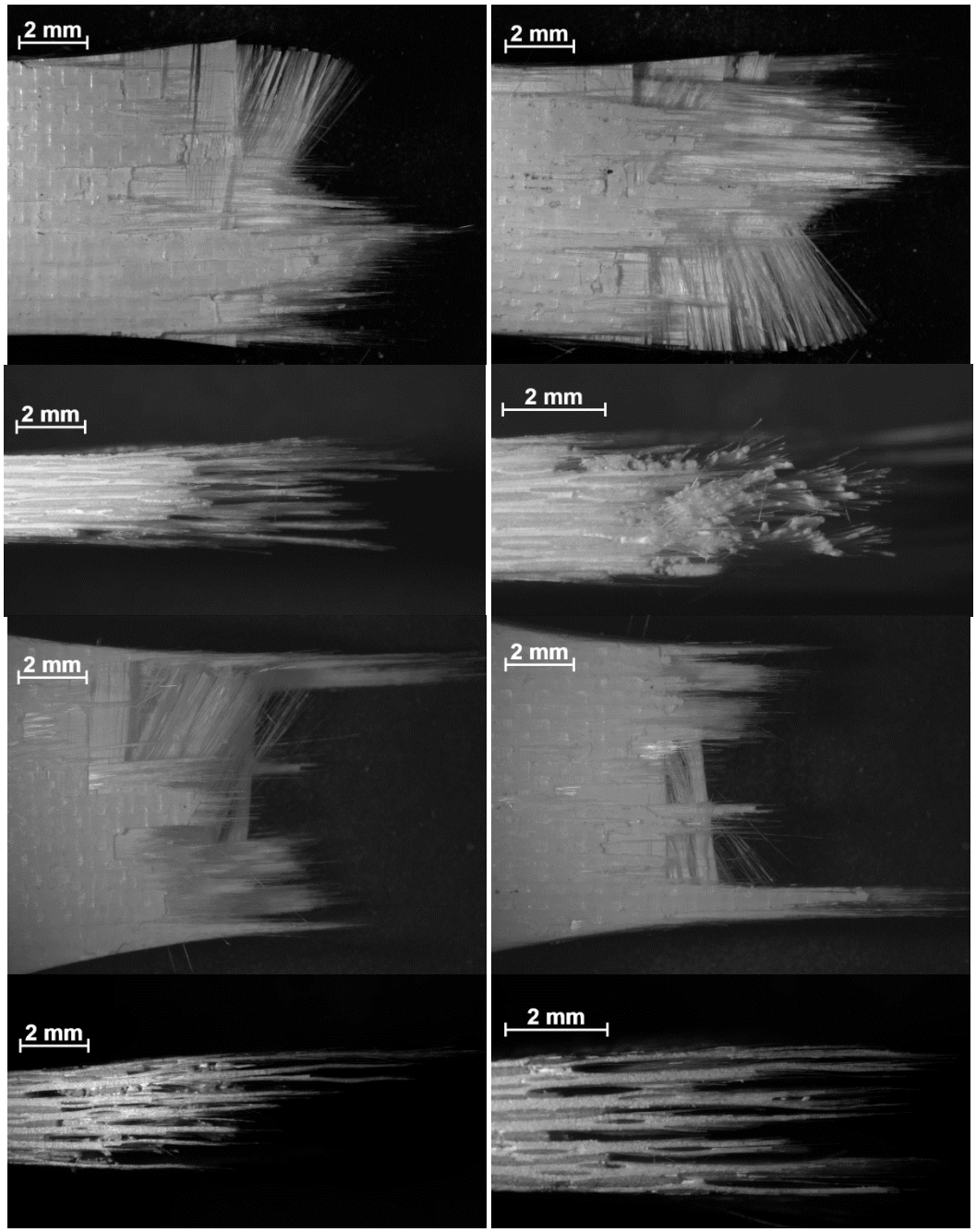

Figure D.1 - Optical micrographs of fracture surface of as-received N720/AS composite obtained in tensile tests (Specimen 6)

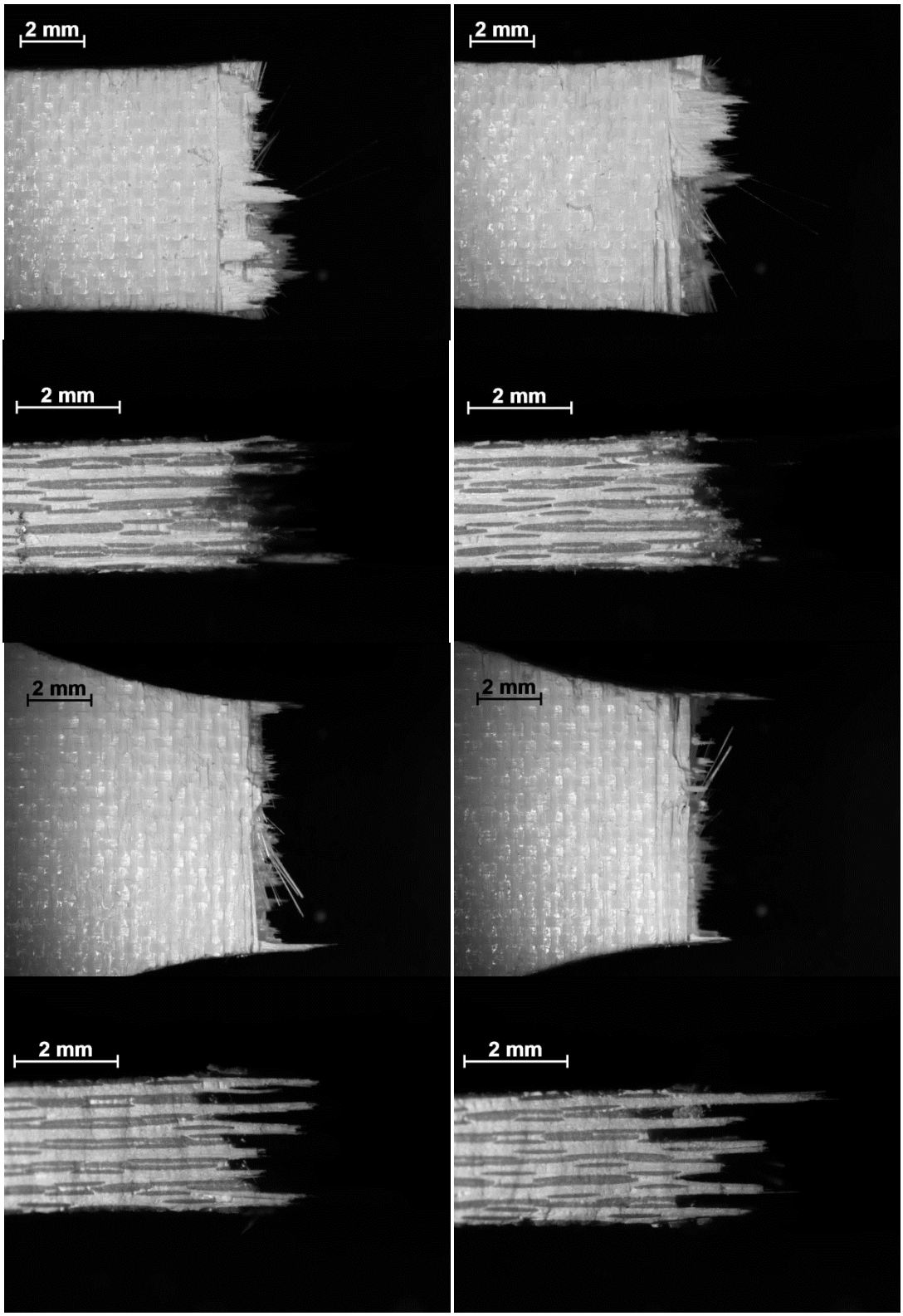

Figure D.2 - Optical micrographs of fracture surface of N720/AS composite obtained in tensile tests after prior heat treatment of 100 h at 1100°C (Specimen 4)

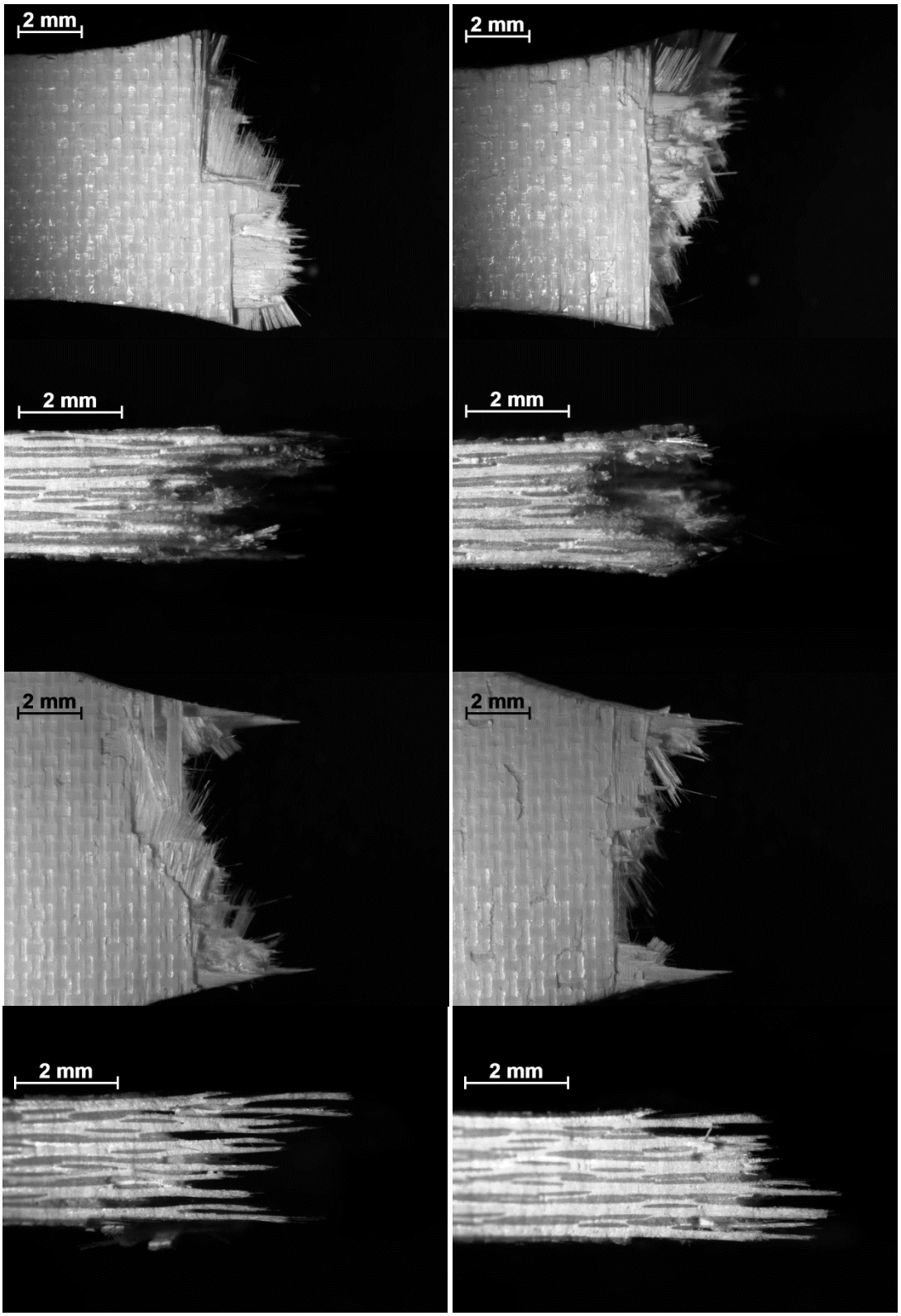

Figure D.3 - Optical micrographs of fracture surface of N720/AS composite obtained in tensile tests after prior heat treatment of 100 h at 1100°C (Specimen 5)

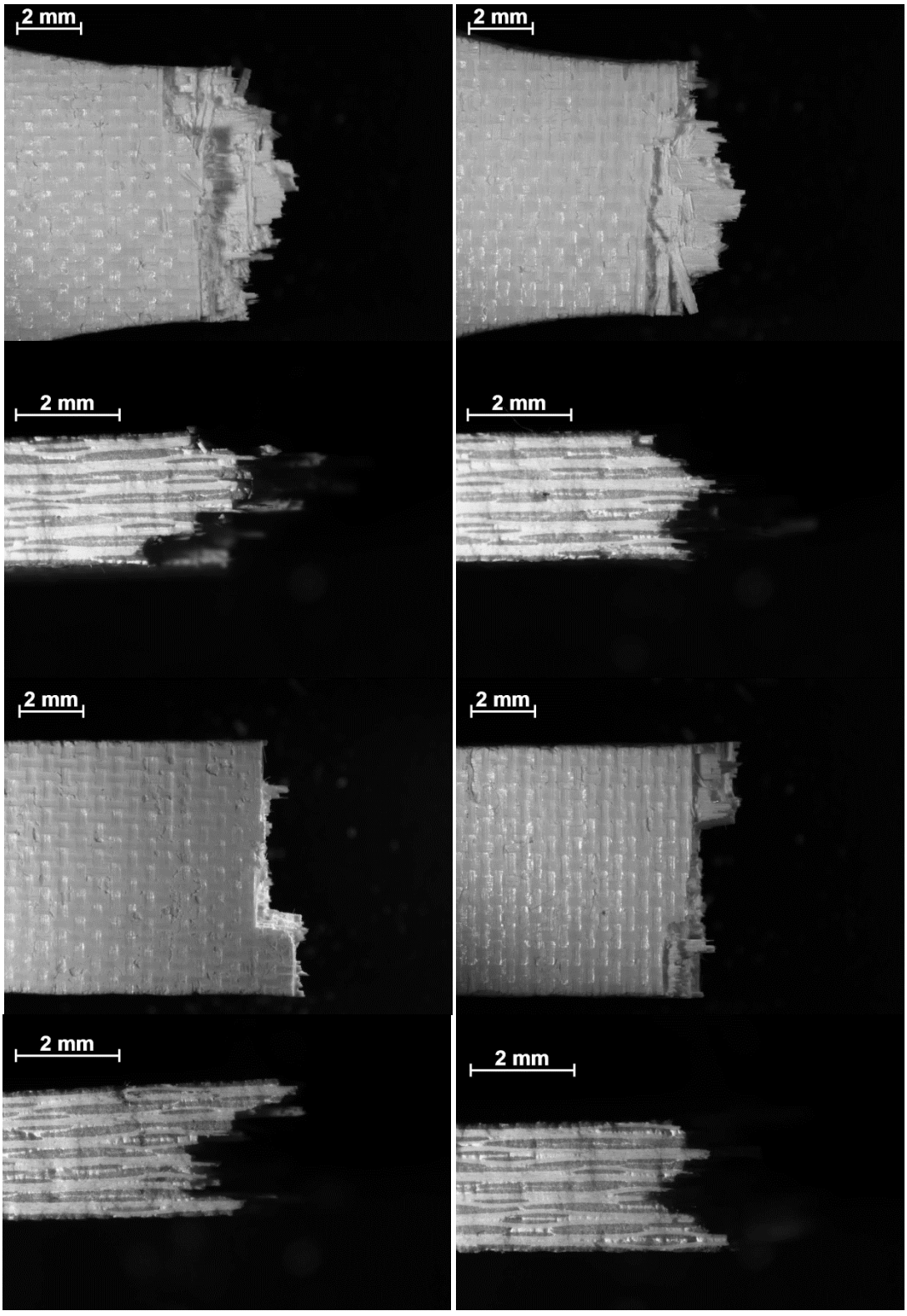

Figure D.4 - Optical micrographs of fracture surface of N720/AS composite obtained in tensile tests after prior heat treatment of 10 h at 1200°C (Specimen 2)

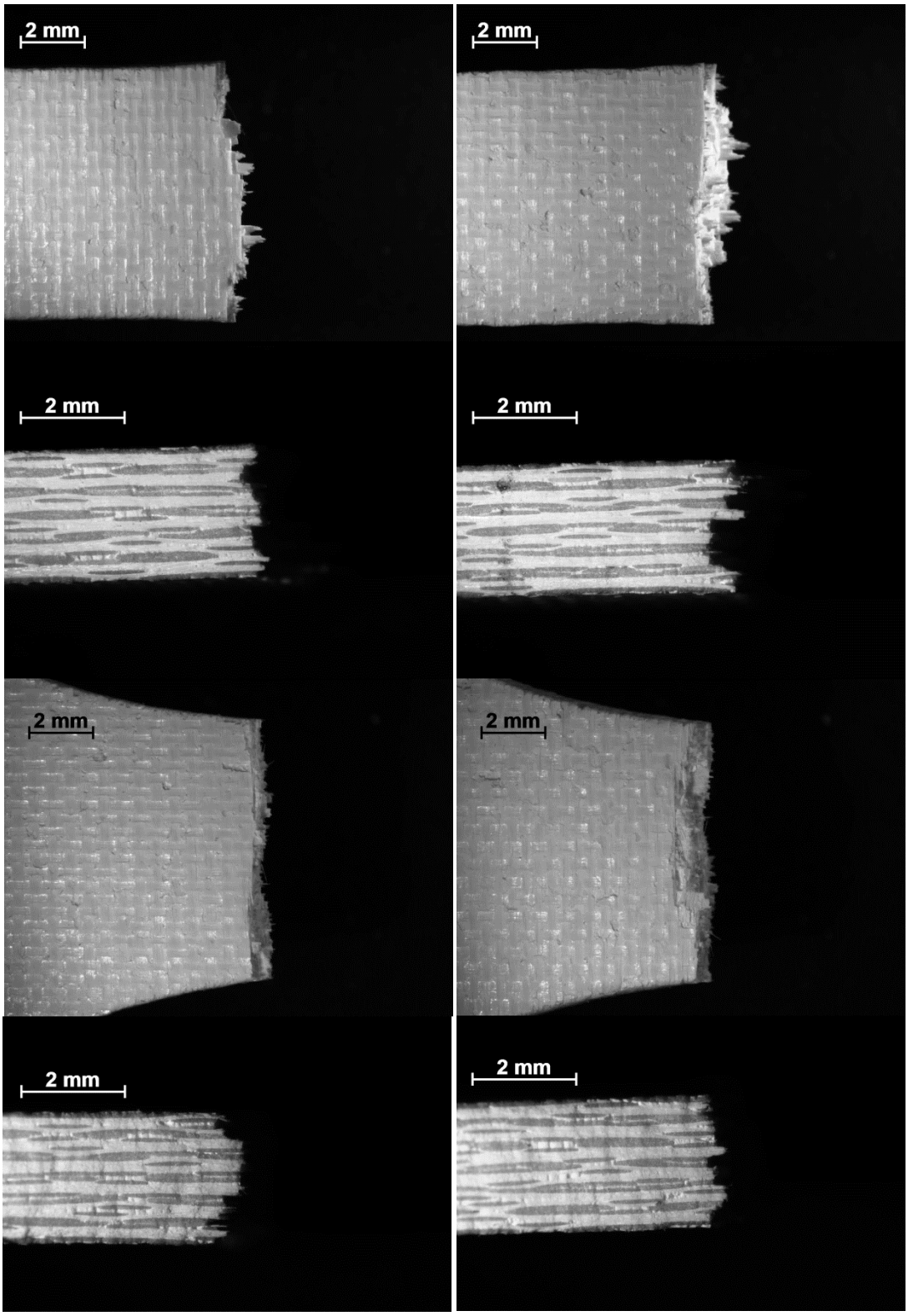

Figure D.5 - Optical micrographs of fracture surface of N720/AS composite obtained in tensile tests after prior heat treatment of 10 h at 1200°C (Specimen 5)

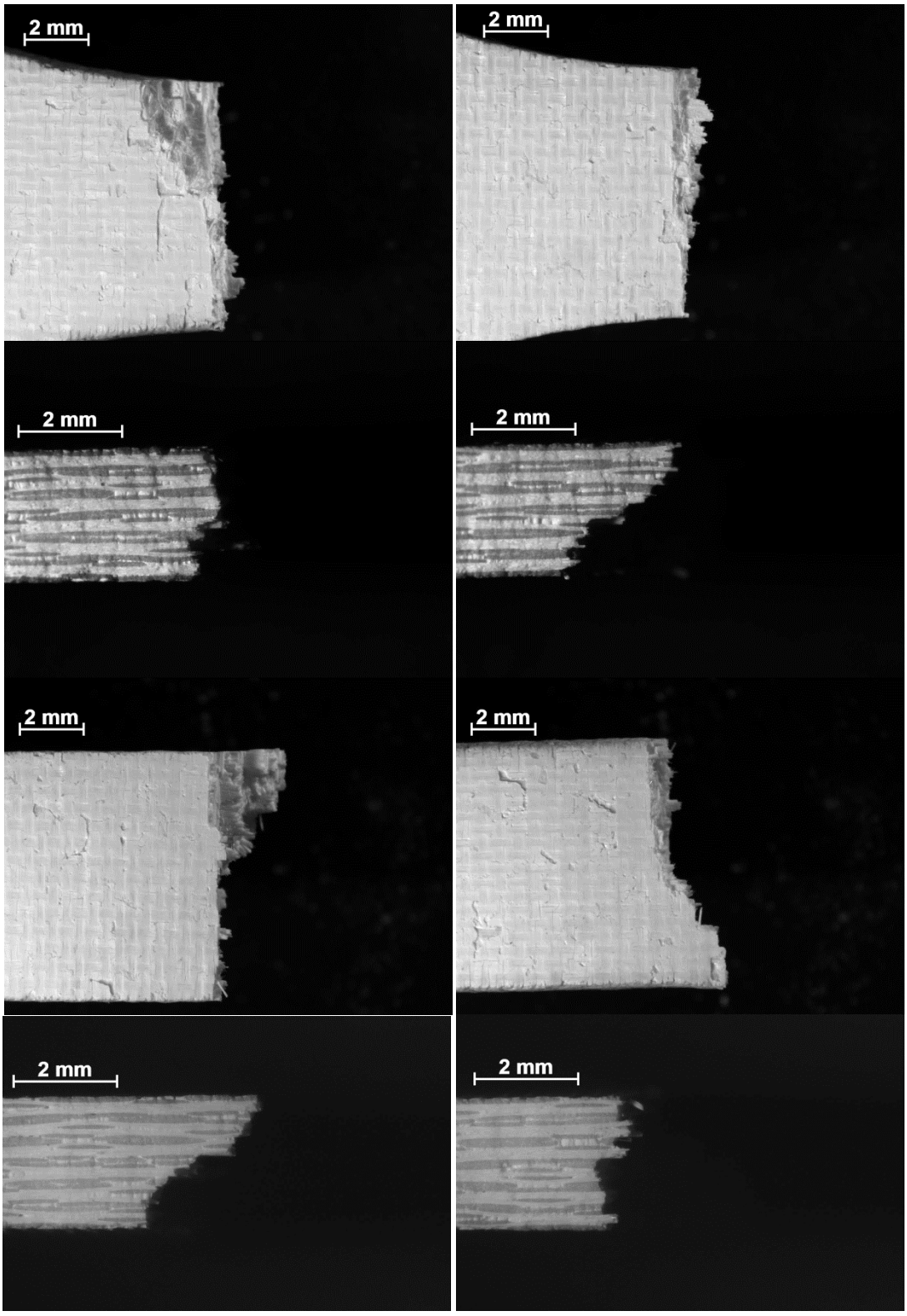

Figure D.6 - Optical micrographs of fracture surface of N720/AS composite obtained in tensile tests after prior heat treatment of 20 h at 1200°C (Specimen 1)

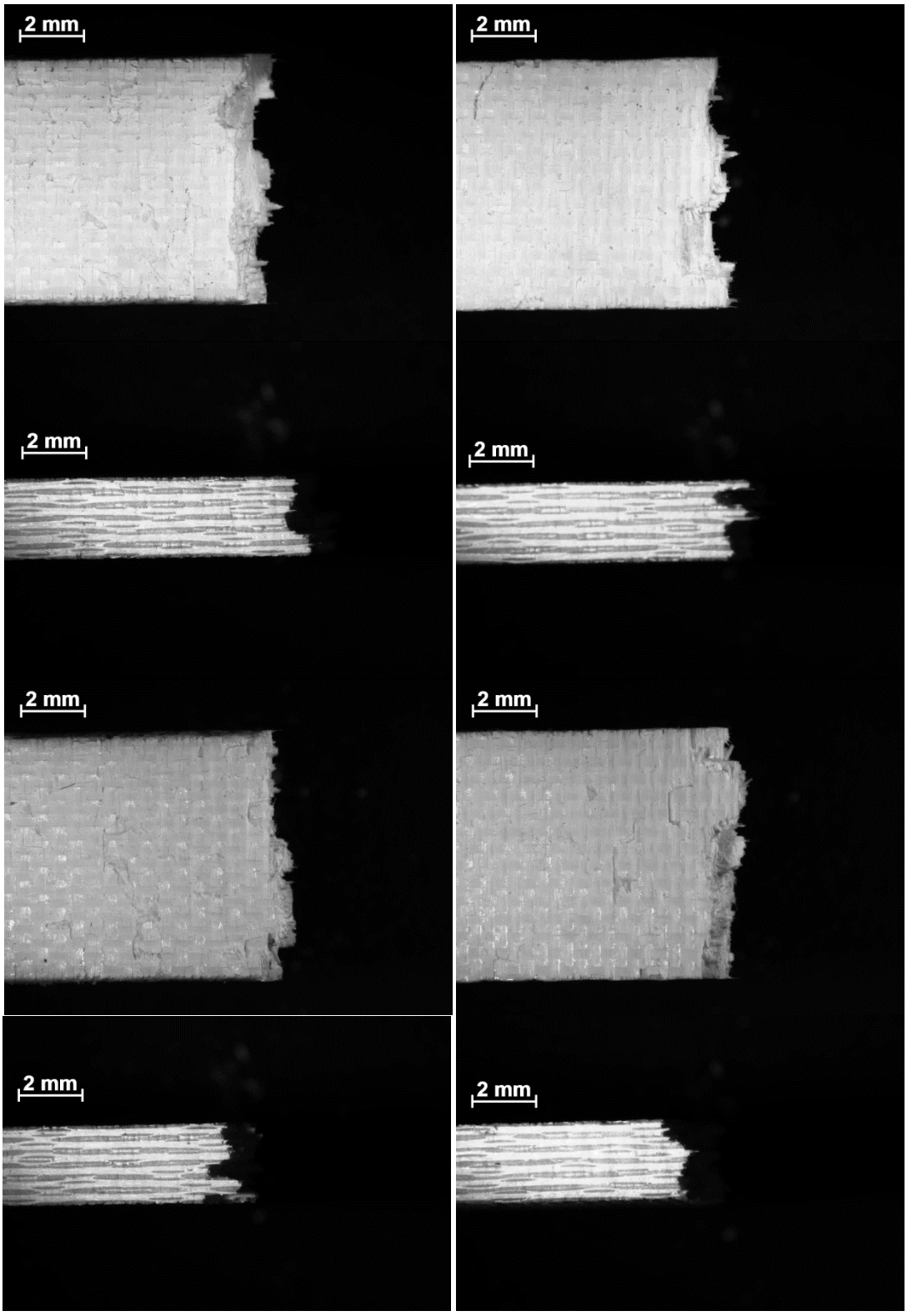

Figure D.7 - Optical micrographs of fracture surface of N720/AS composite obtained in tensile tests after prior heat treatment of 20 h at 1200°C (Specimen 2)

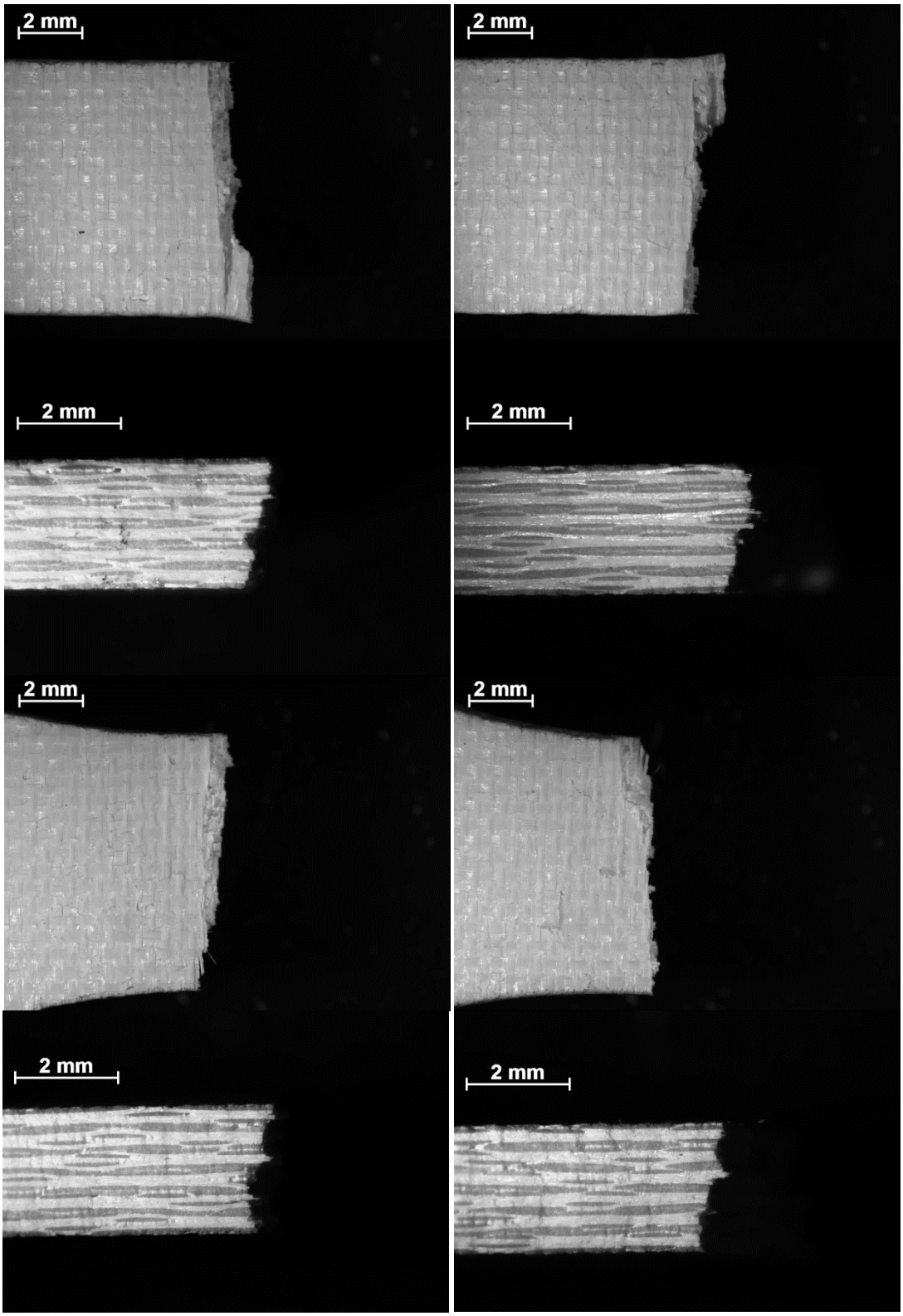

Figure D.8 - Optical micrographs of fracture surface of N720/AS composite obtained in tensile tests after prior heat treatment of 40 h at 1200°C (Specimen 3)

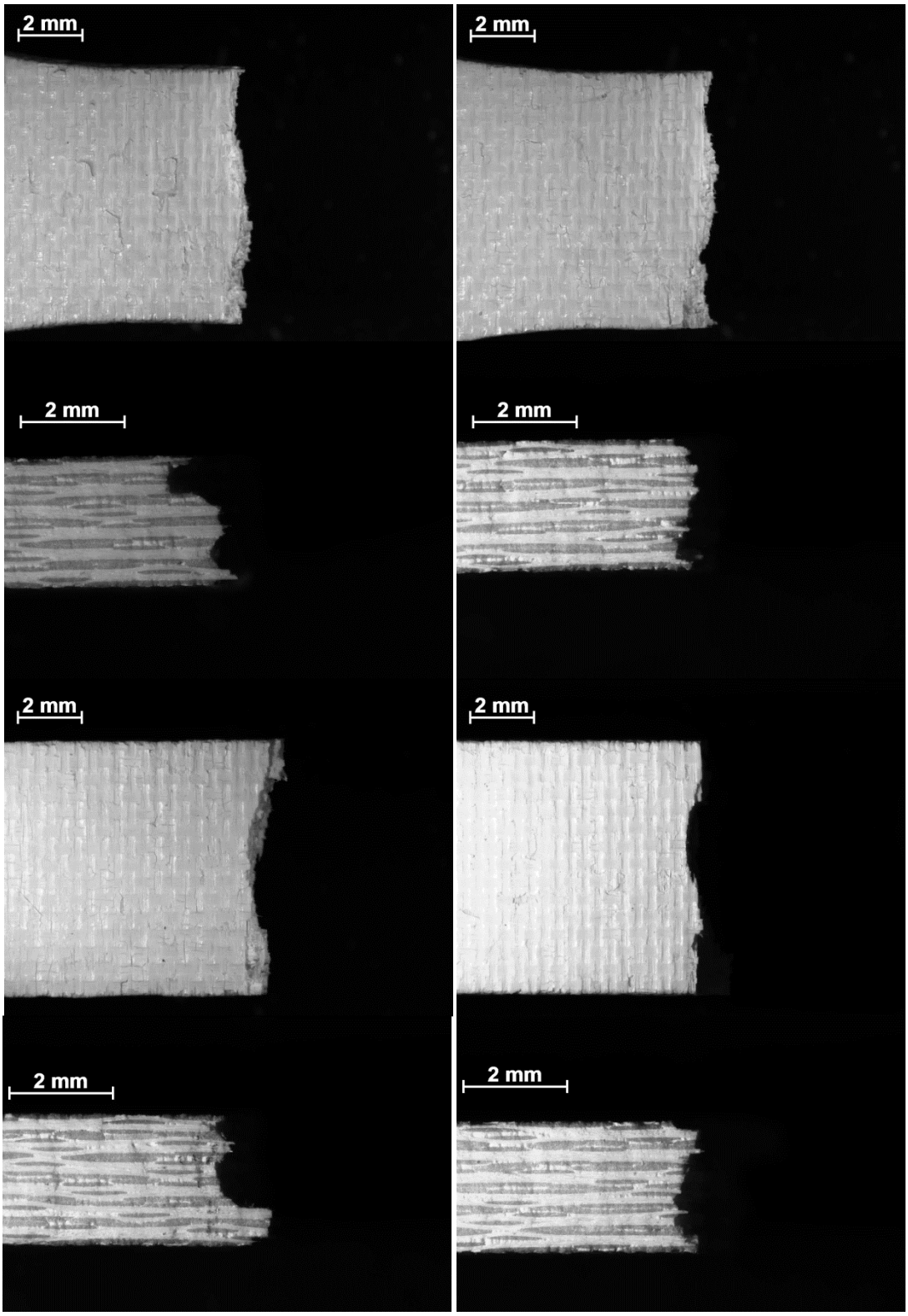

Figure D.9 - Optical micrographs of fracture surface of N720/AS composite obtained in tensile tests after prior heat treatment of 40 h at 1200°C (Specimen 5)

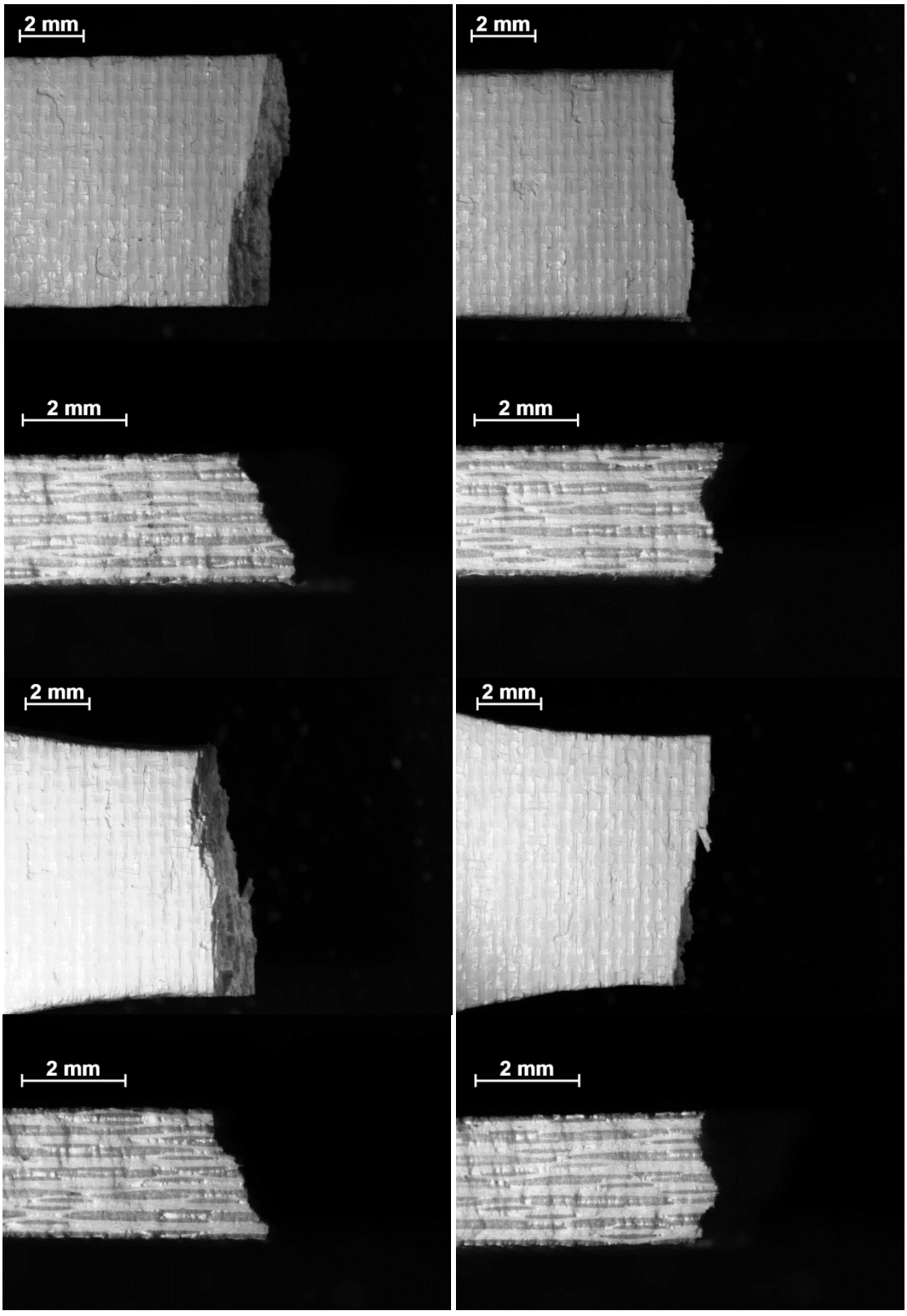

Figure D.10 - Optical micrographs of fracture surface of N720/AS composite obtained in tensile tests after prior heat treatment of 100 h at 1200°C (Specimen 2)

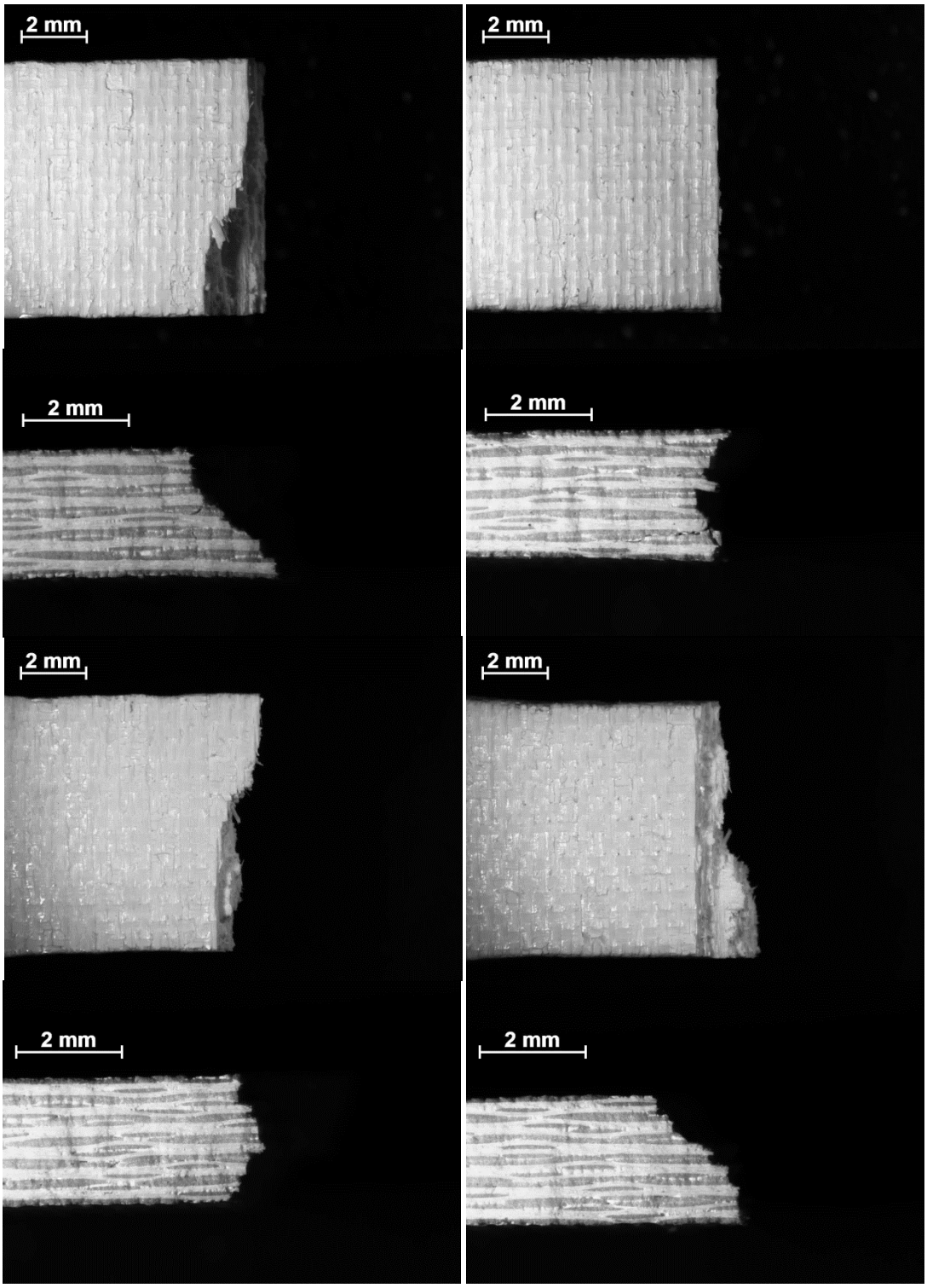

Figure D.11 - Optical micrographs of fracture surface of N720/AS composite obtained in tensile tests after prior heat treatment of 100 h at 1200°C (Specimen 4)

Appendix E - Additional Optical Micrographs of N720/A Fracture Surfaces

Appendix E presents additional optical micrographs of the fracture surfaces of N720/A specimens produced in tensile tests

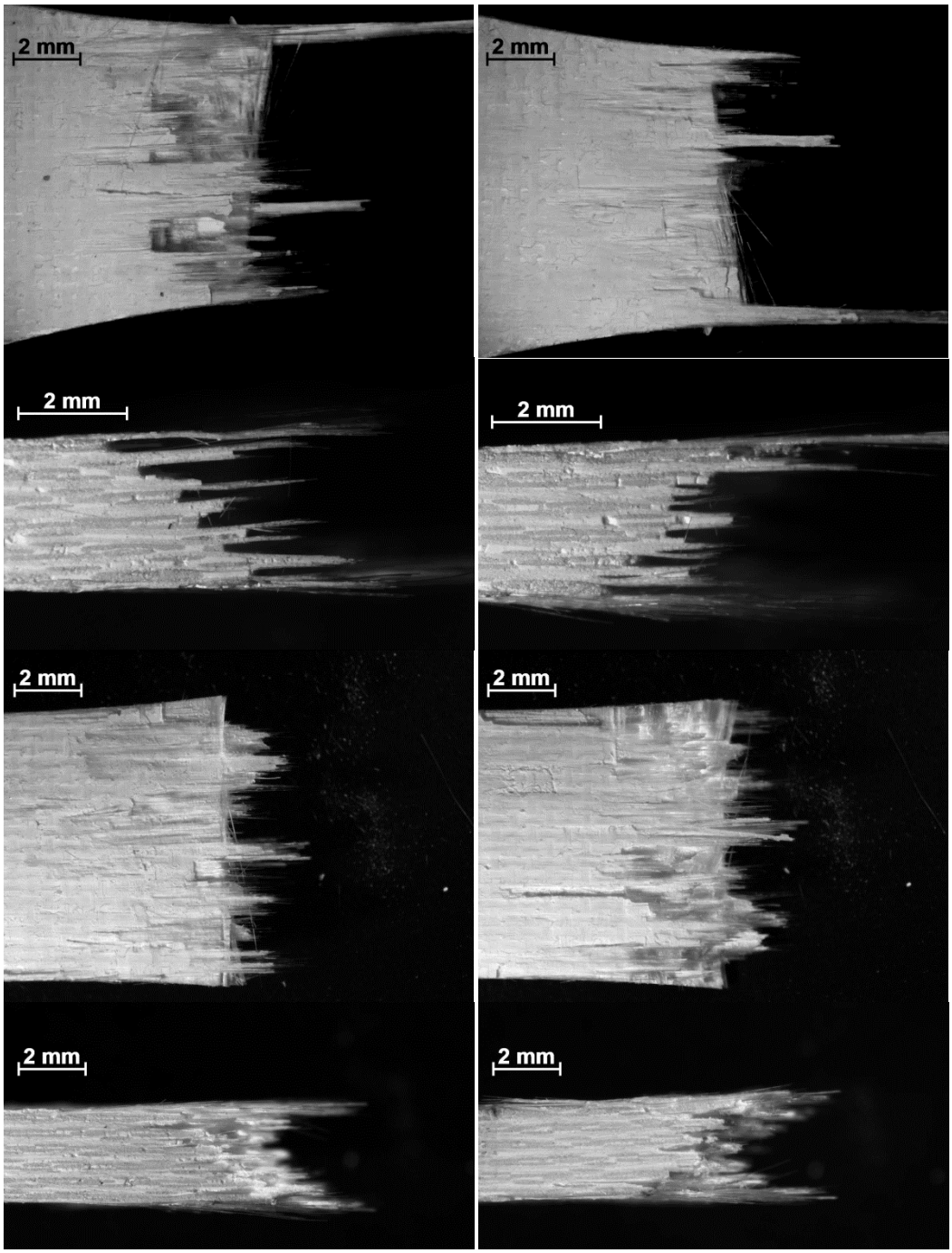

Figure E.1 - Optical micrographs of fracture surface of as-received N720/A composite obtained in tensile tests (Specimen 5)

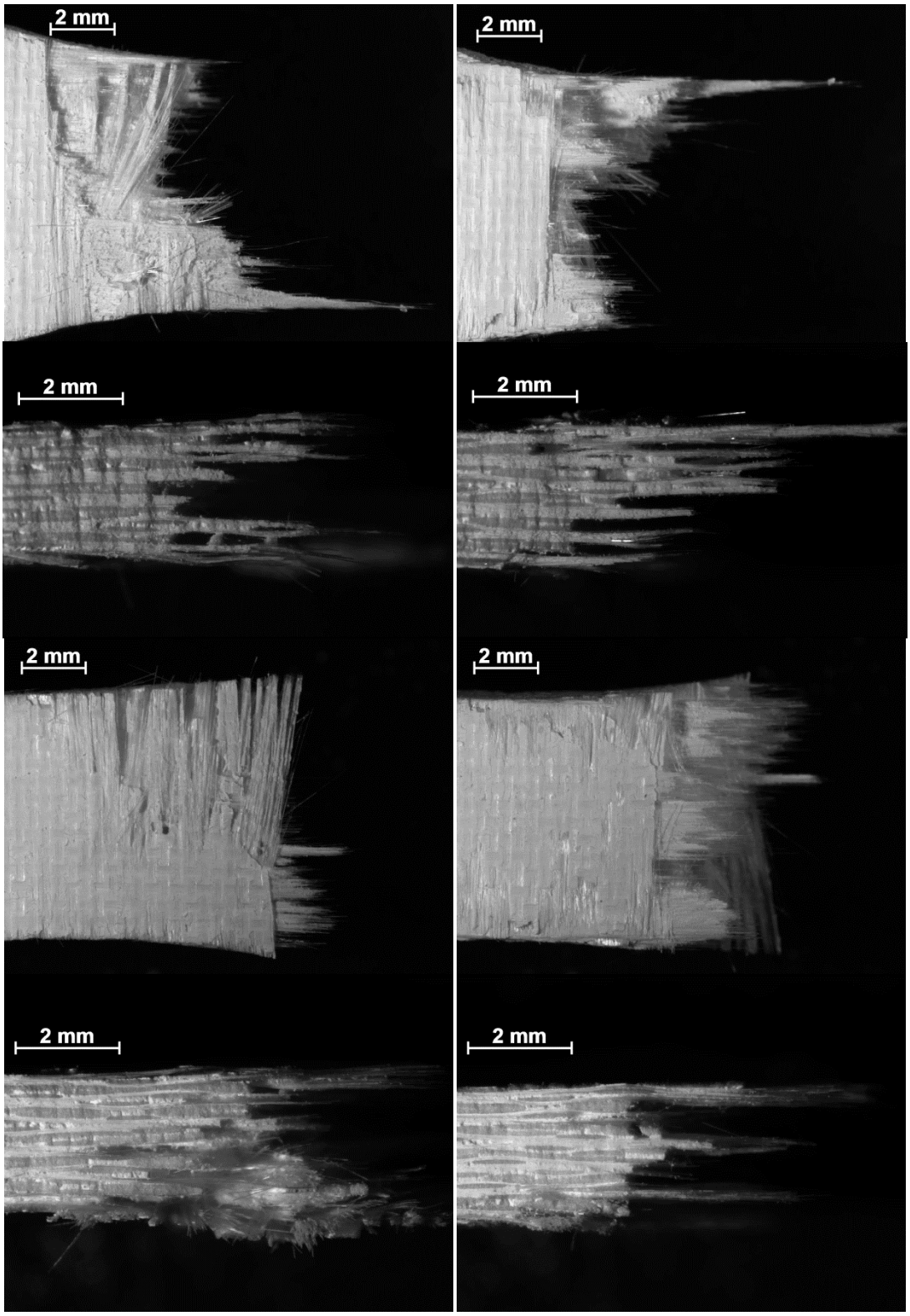

Figure E.2 - Optical micrographs of fracture surface of N720/A composite obtained in tensile tests after prior heat treatment of 100 h at 1200°C (Specimen 1)

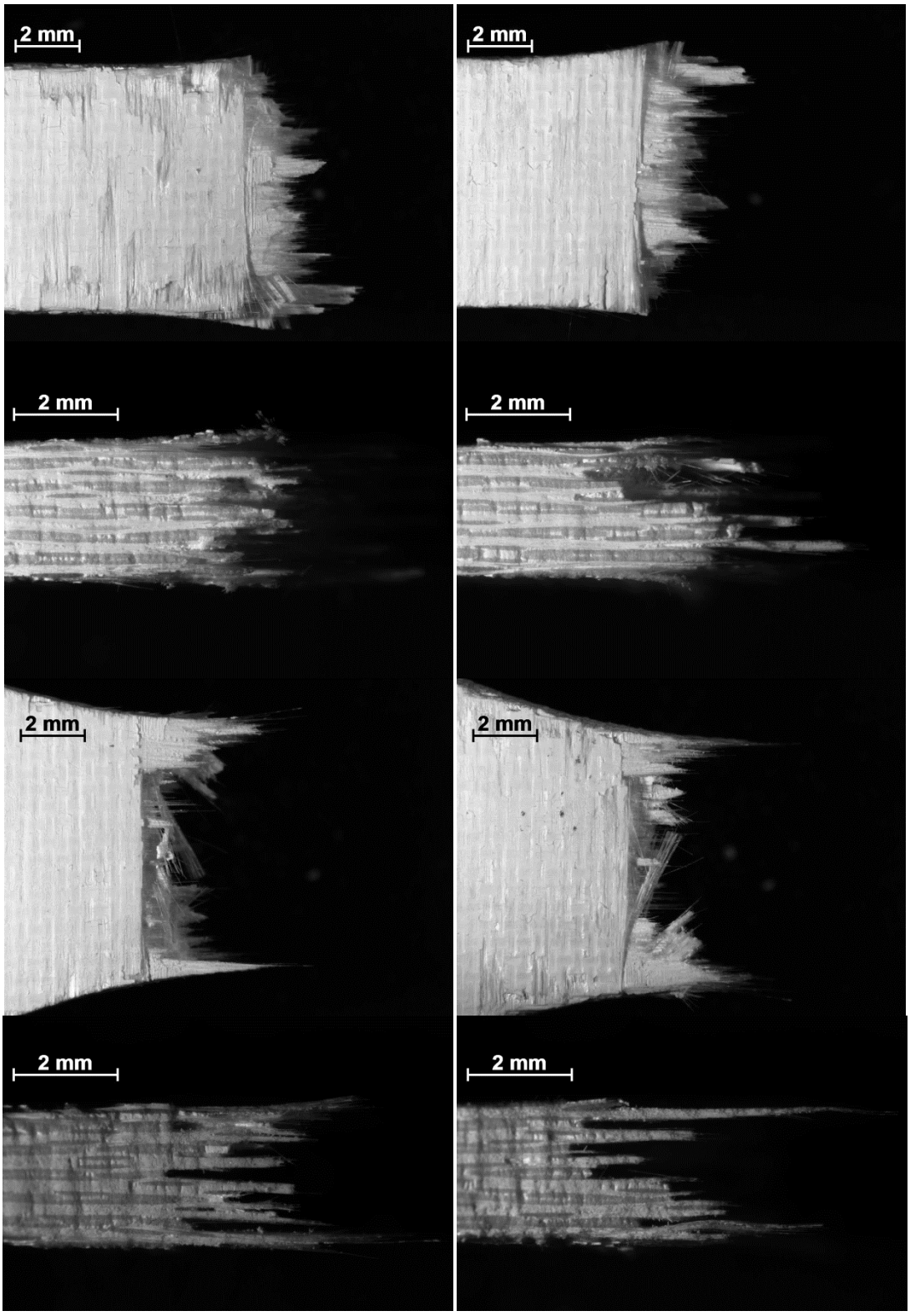

Figure E.3 - Optical micrographs of fracture surface of N720/A composite obtained in tensile tests after prior heat treatment of 100 h at 1200°C (Specimen 2)

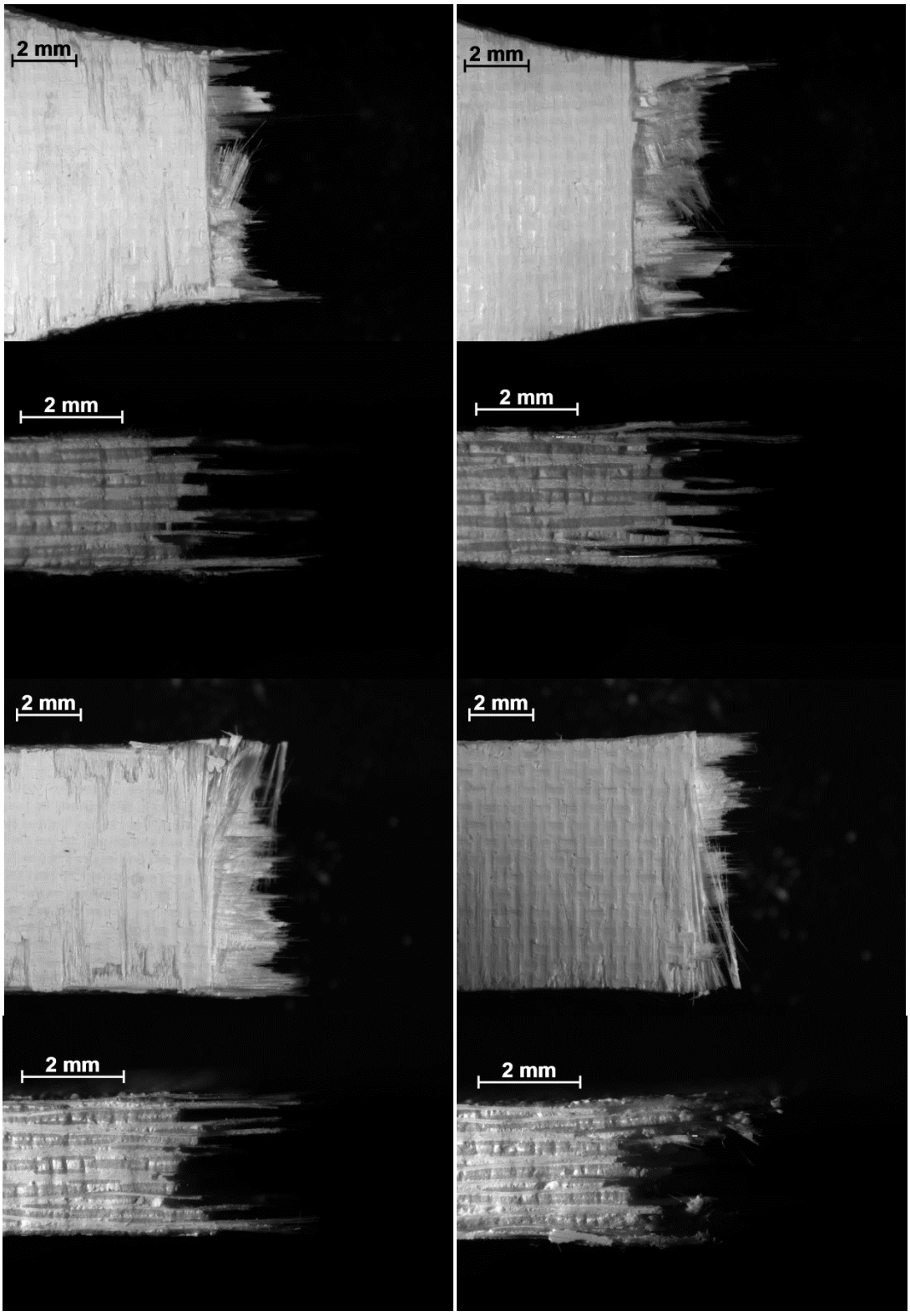

Figure E.4 - Optical micrographs of fracture surface of N720/A composite obtained in tensile tests after prior heat treatment of 10 h at 1300°C (Specimen 2)

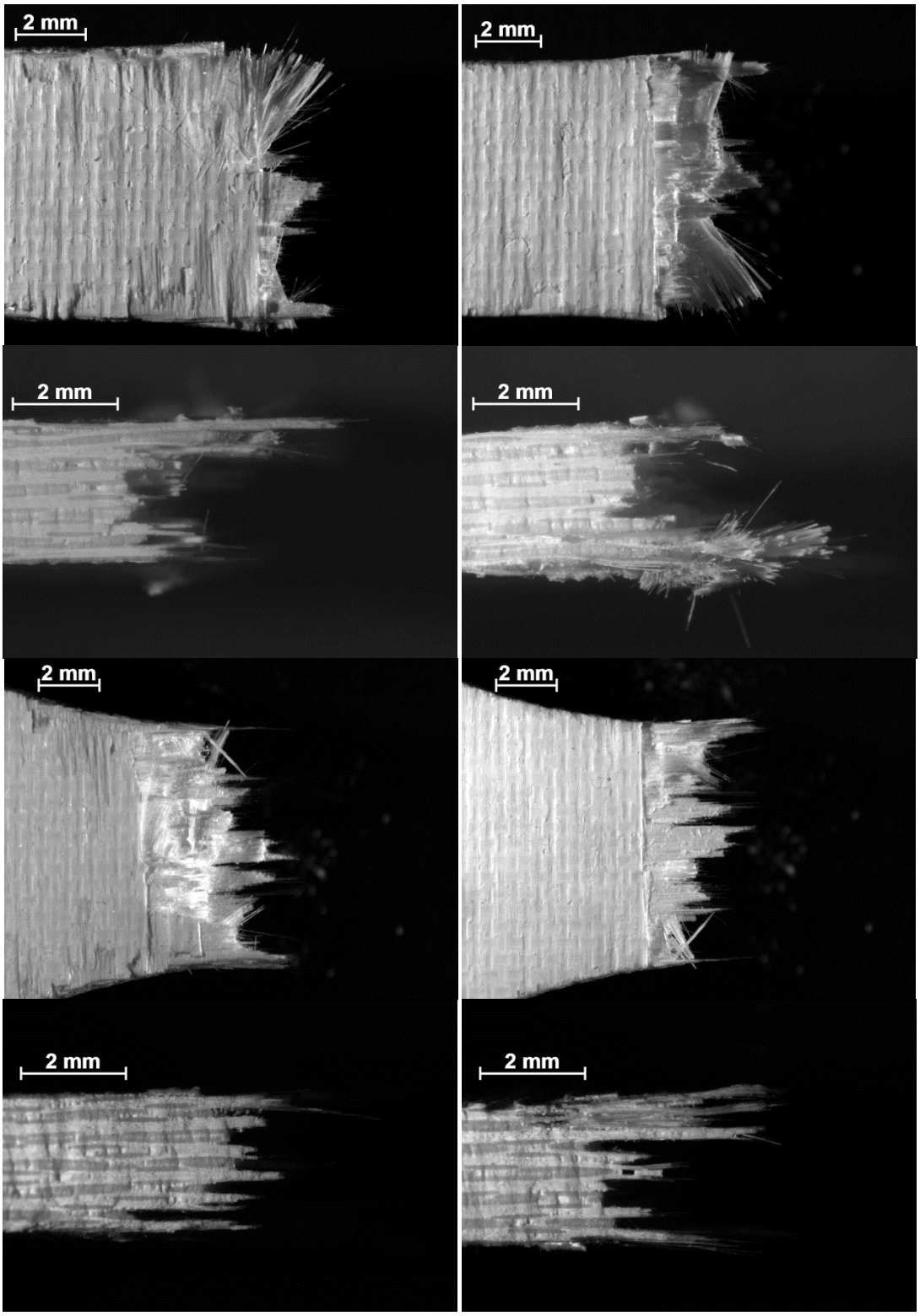

Figure E.5 - Optical micrographs of fracture surface of N720/A composite obtained in tensile tests after prior heat treatment of 10 h at 1300°C (Specimen 3)

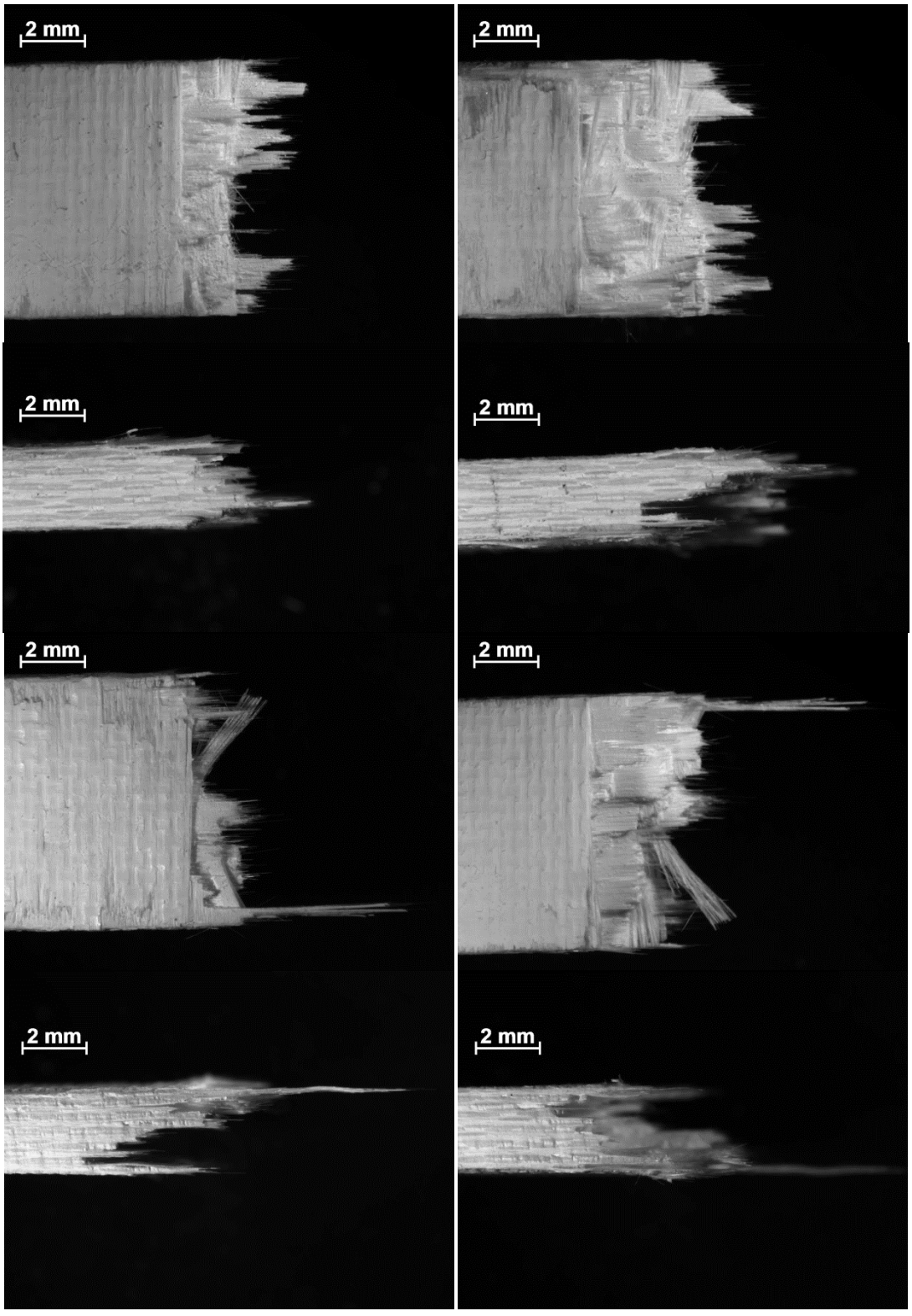

Figure E.6 - Optical micrographs of fracture surface of N720/A composite obtained in tensile tests after prior heat treatment of 20 h at 1300°C (Specimen 1)

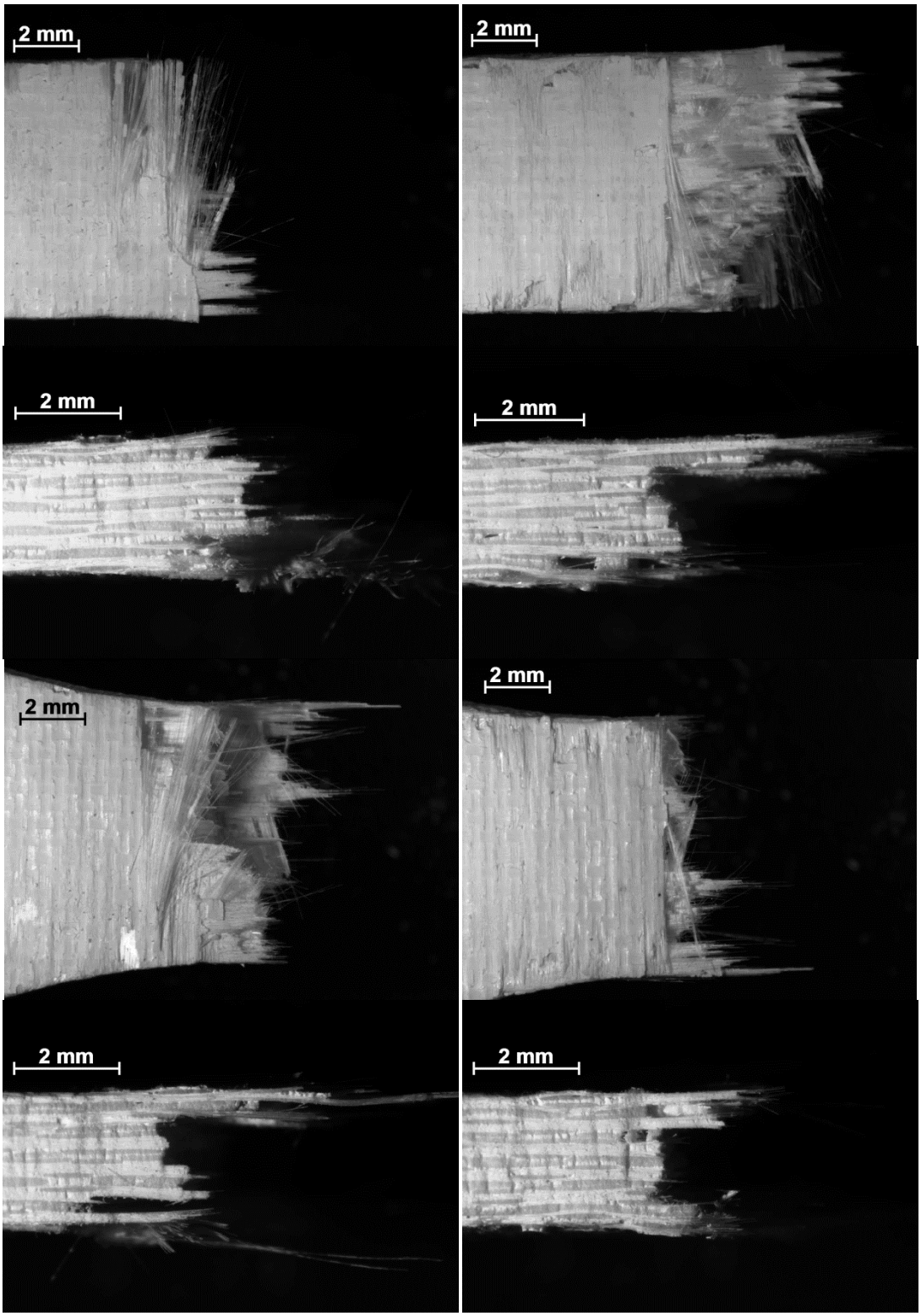

Figure E.7 - Optical micrographs of fracture surface of N720/A composite obtained in tensile tests after prior heat treatment of 20 h at 1300°C (Specimen 6)

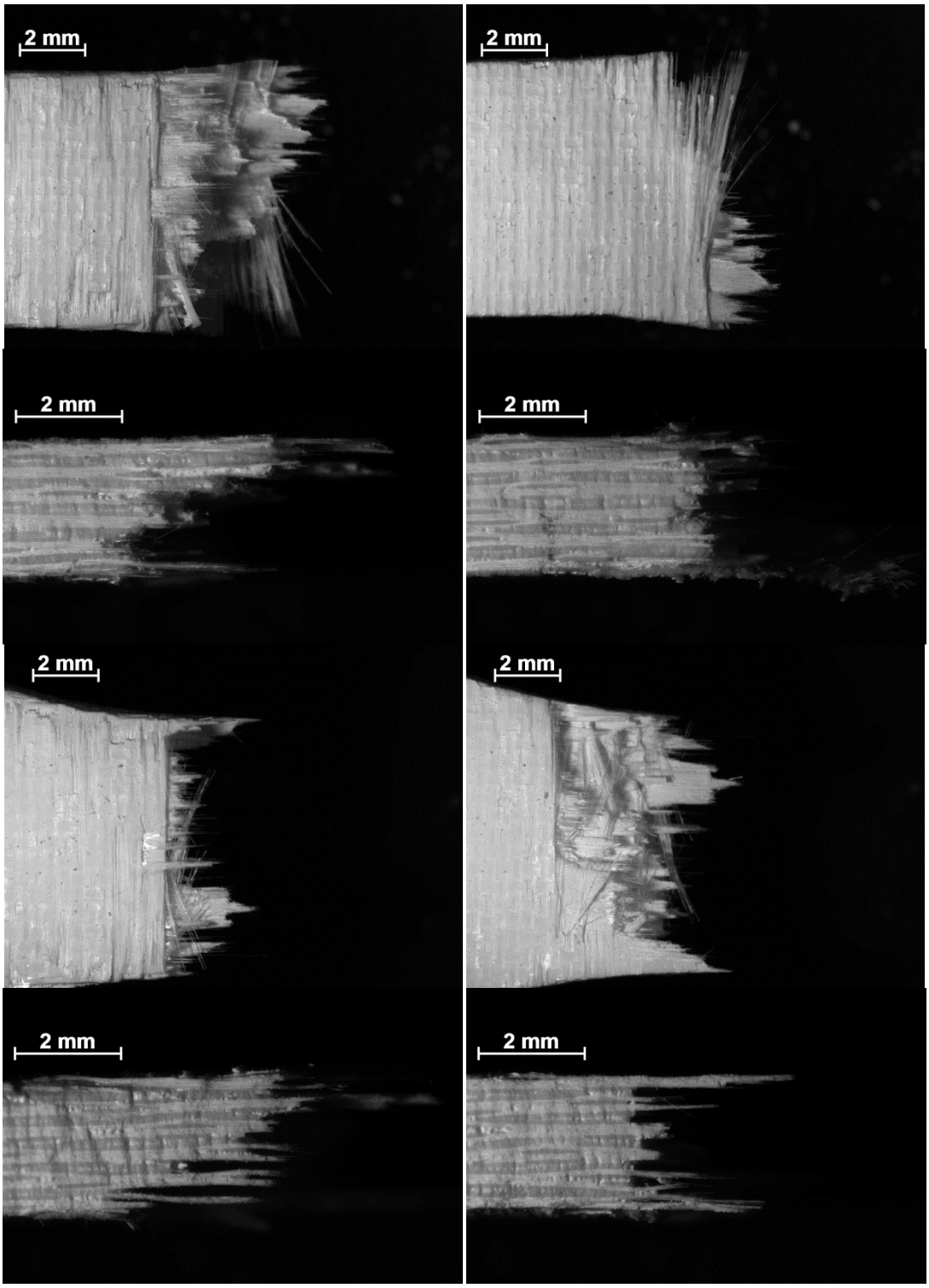

Figure E.8 - Optical micrographs of fracture surface of N720/A composite obtained in tensile tests after prior heat treatment of 40 h at 1300°C (Specimen 4)

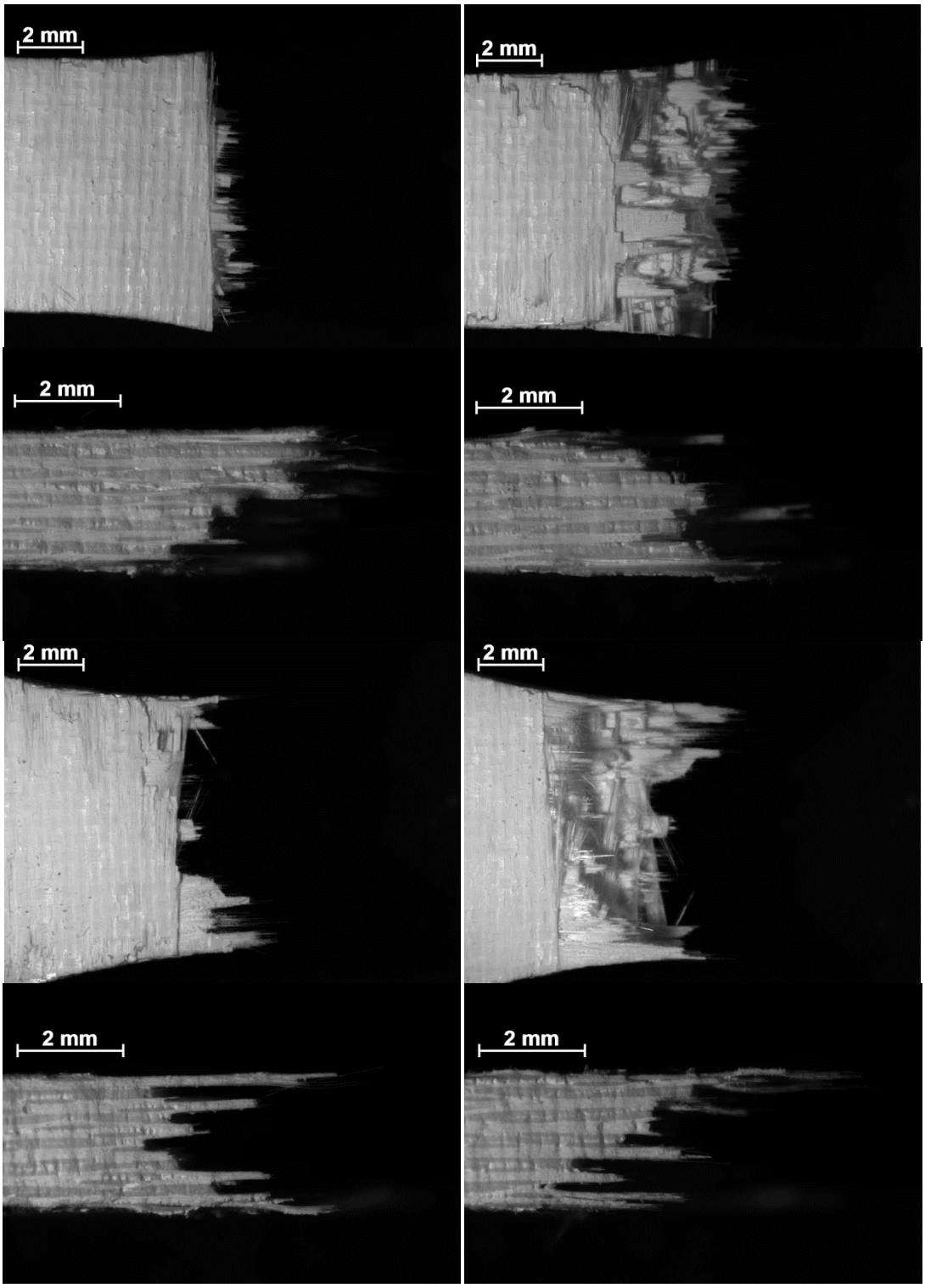

Figure E.9 - Optical micrographs of fracture surface of N720/A composite obtained in tensile tests after prior heat treatment of 40 h at 1300°C (Specimen 5)

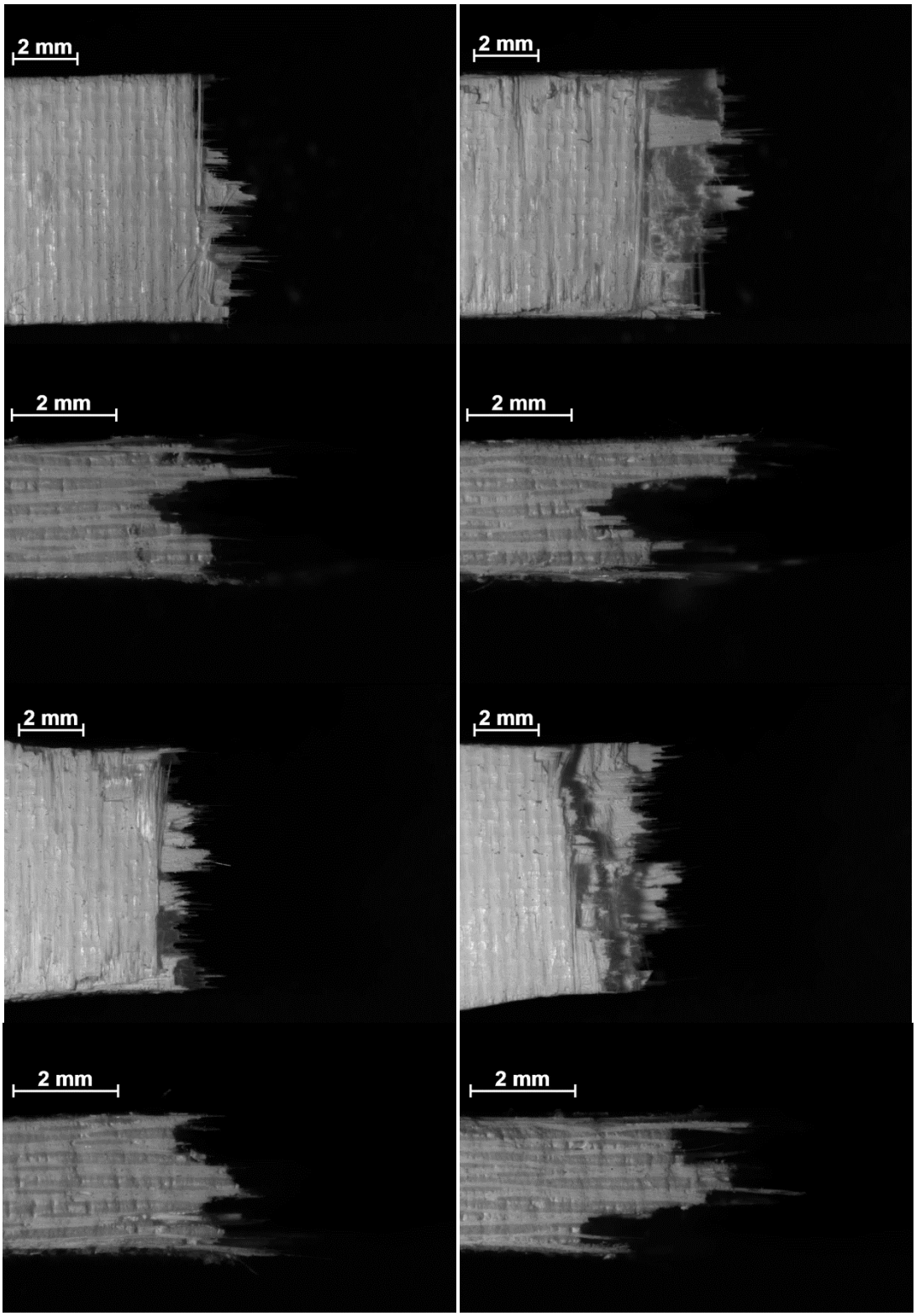

Figure E.10 - Optical micrographs of fracture surface of N720/A composite obtained in tensile tests after prior heat treatment of 100 h at 1300°C (Specimen 3)

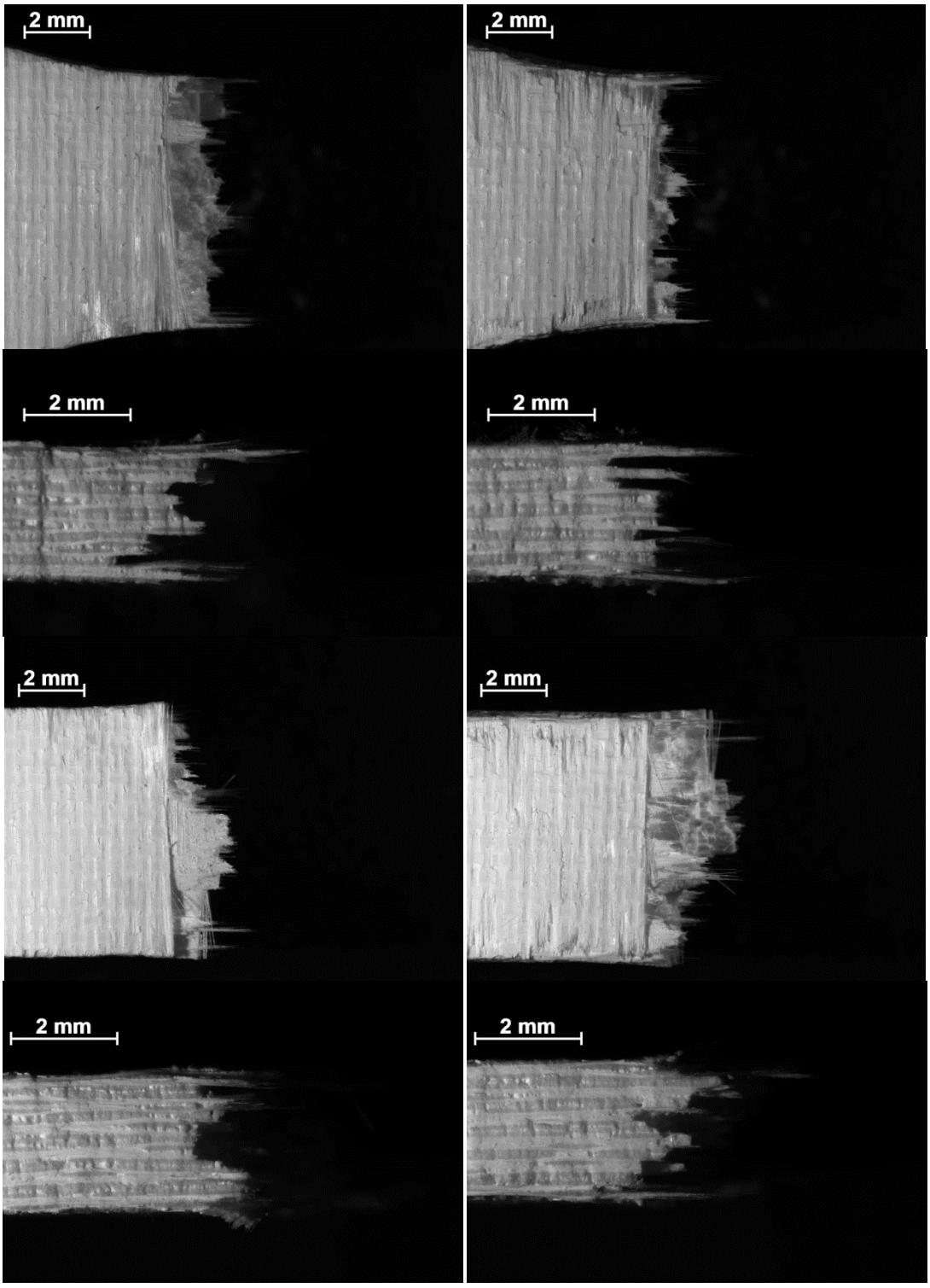

Figure E.11 - Optical micrographs of fracture surface of N720/A composite obtained in tensile tests after prior heat treatment of 100 h at 1300°C (Specimen 6)

Appendix F - Additional SEM Micrographs of N610/AS Fracture Surfaces

Appendix F presents additional SEM micrographs of the fracture surfaces of N610/AS specimens produced in tensile tests.

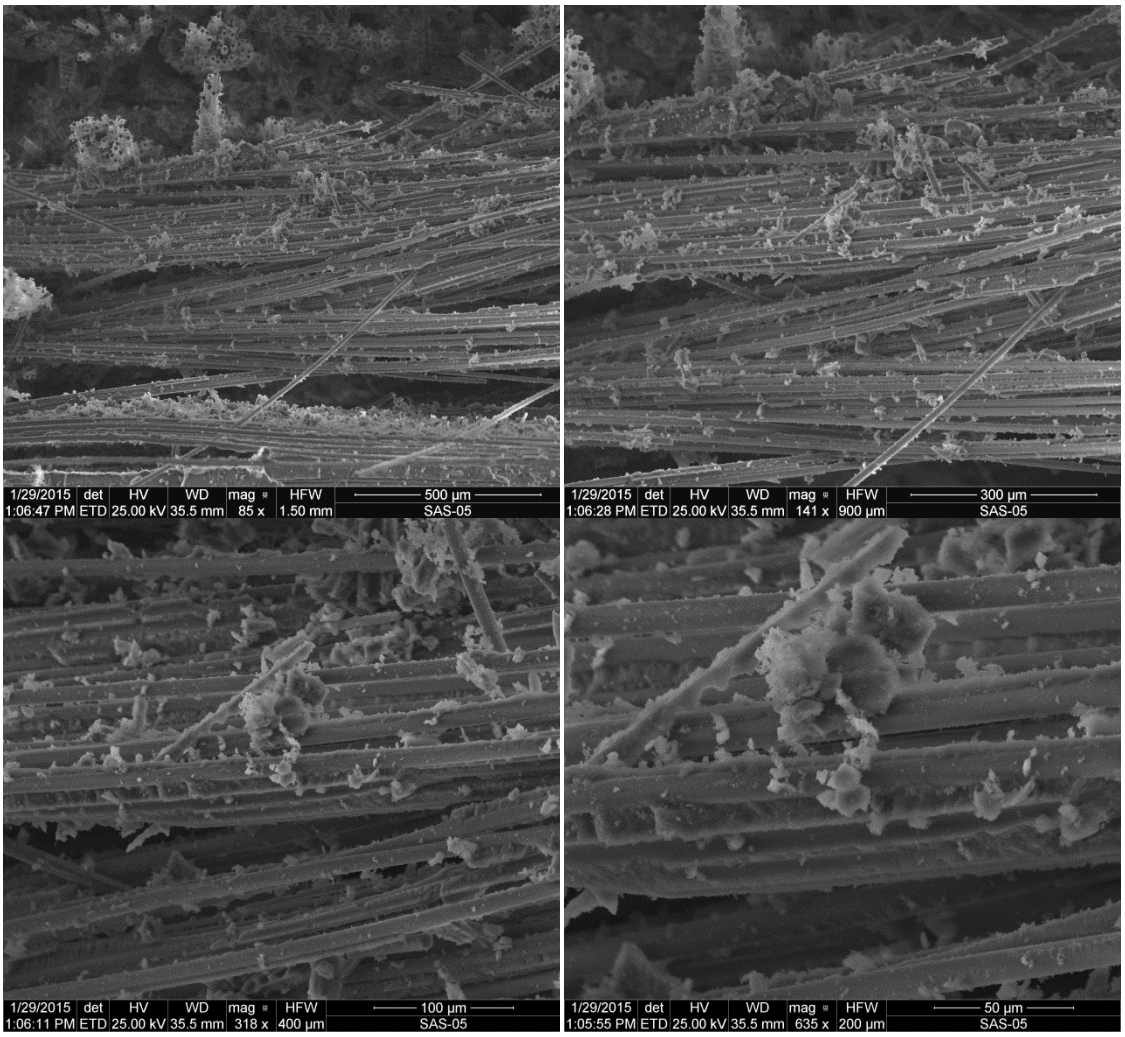

Figure F.1 – SEM micrographs of fracture surface of as-received N610/AS composite obtained in tensile tests (Specimen 5)

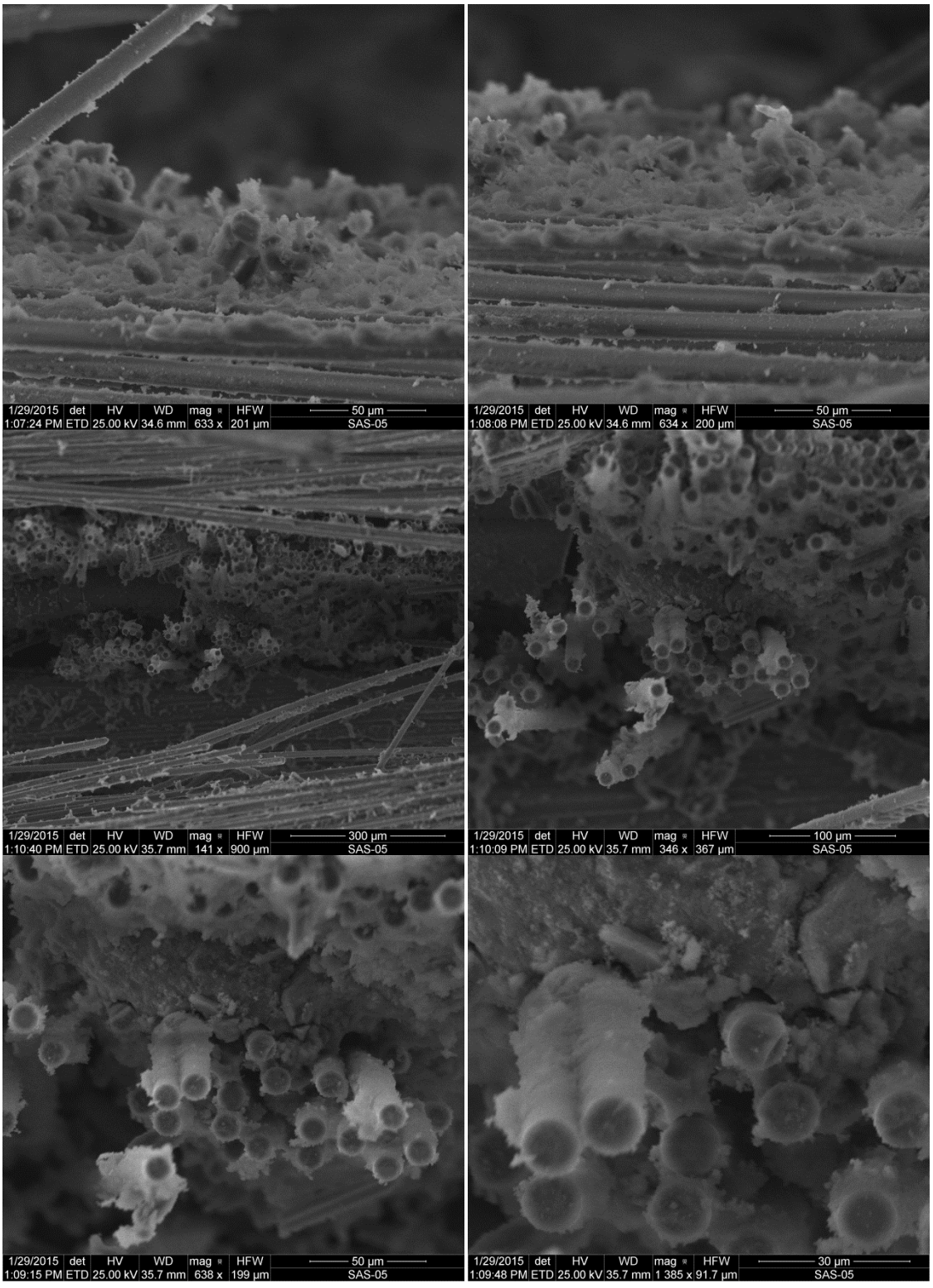

Figure F.2 – SEM micrographs of fracture surface of as-received N610/AS composite obtained in tensile tests (Specimen 5)

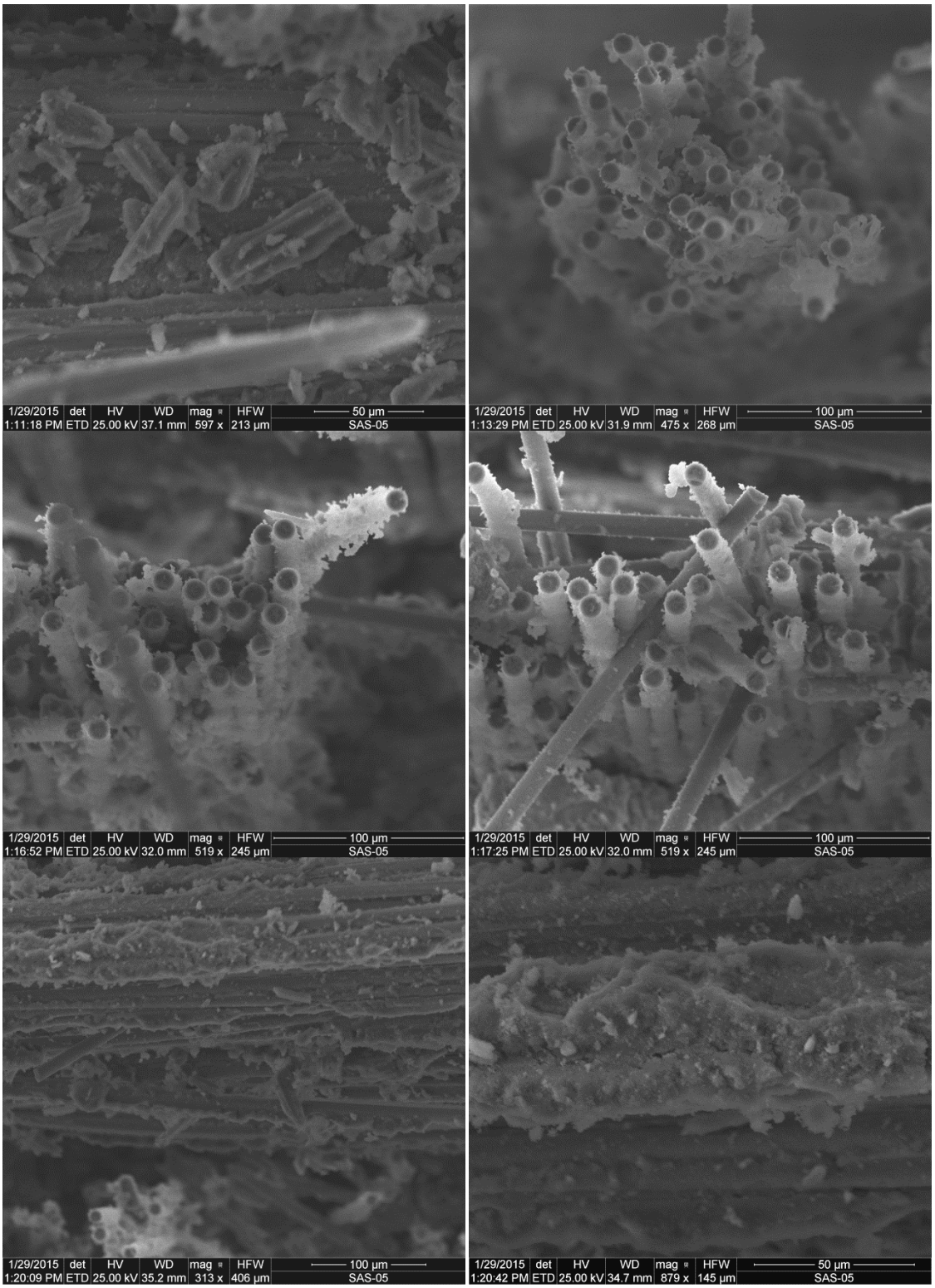

Figure F.3 – SEM micrographs of fracture surface of as-received N610/AS composite obtained in tensile tests (Specimen 5)

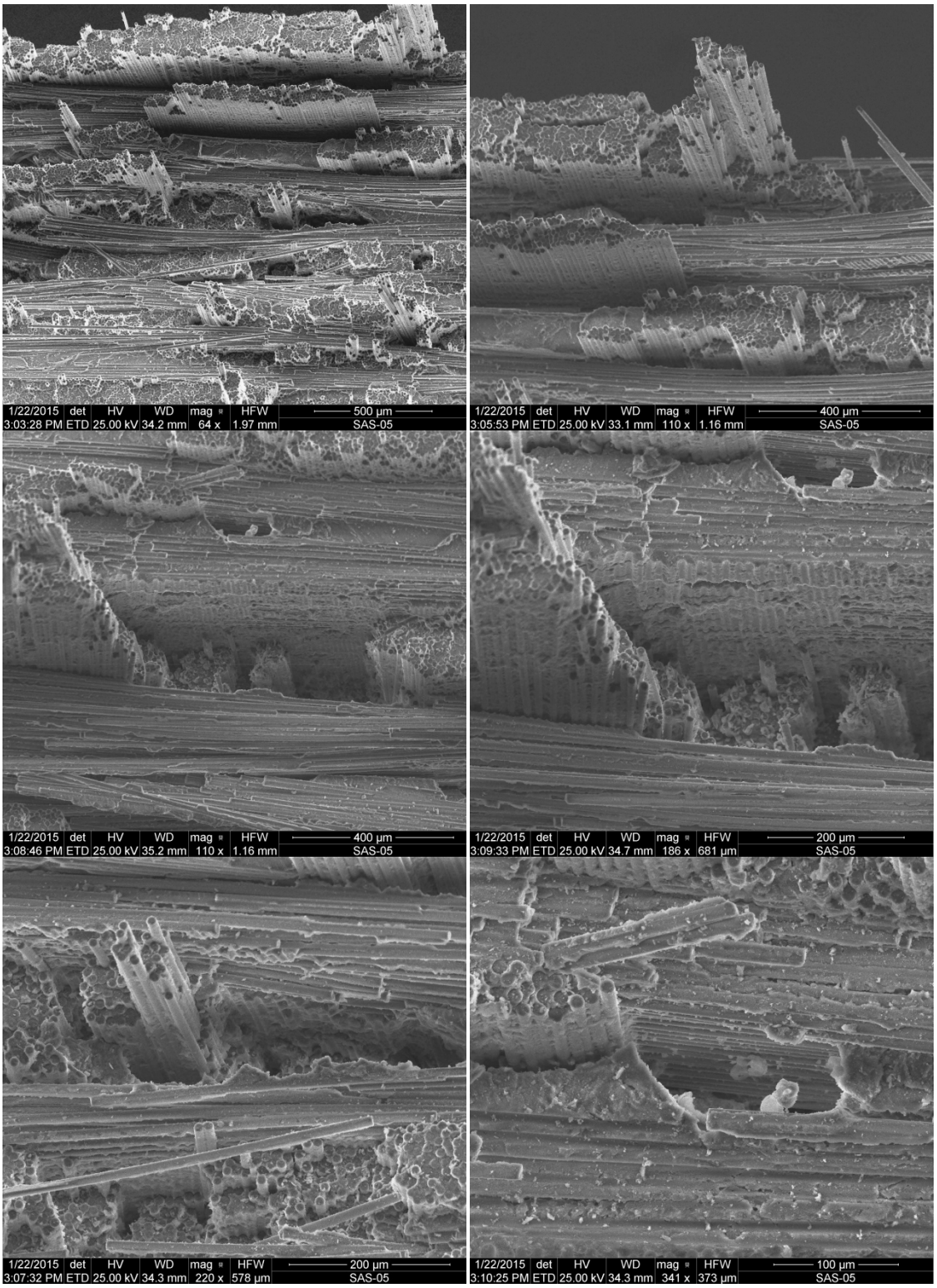

Figure F.4 – SEM micrographs of fracture surface of N610/AS composite obtained in tensile tests after prior heat treatment of 100 h at 1100°C (Specimen 5)

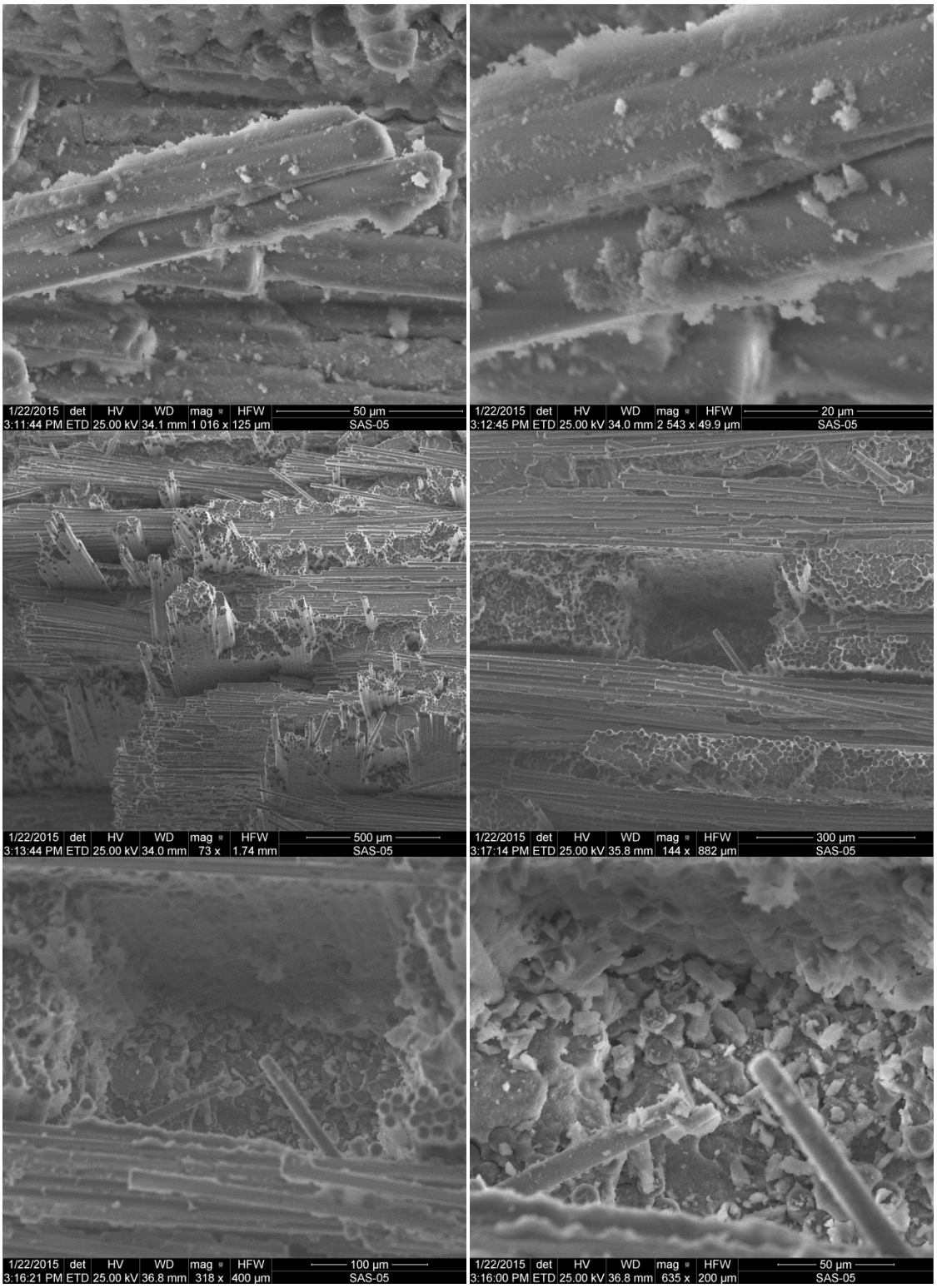

Figure F.5 – SEM micrographs of fracture surface of N610/AS composite obtained in tensile tests after prior heat treatment of 100 h at 1100°C (Specimen 5)

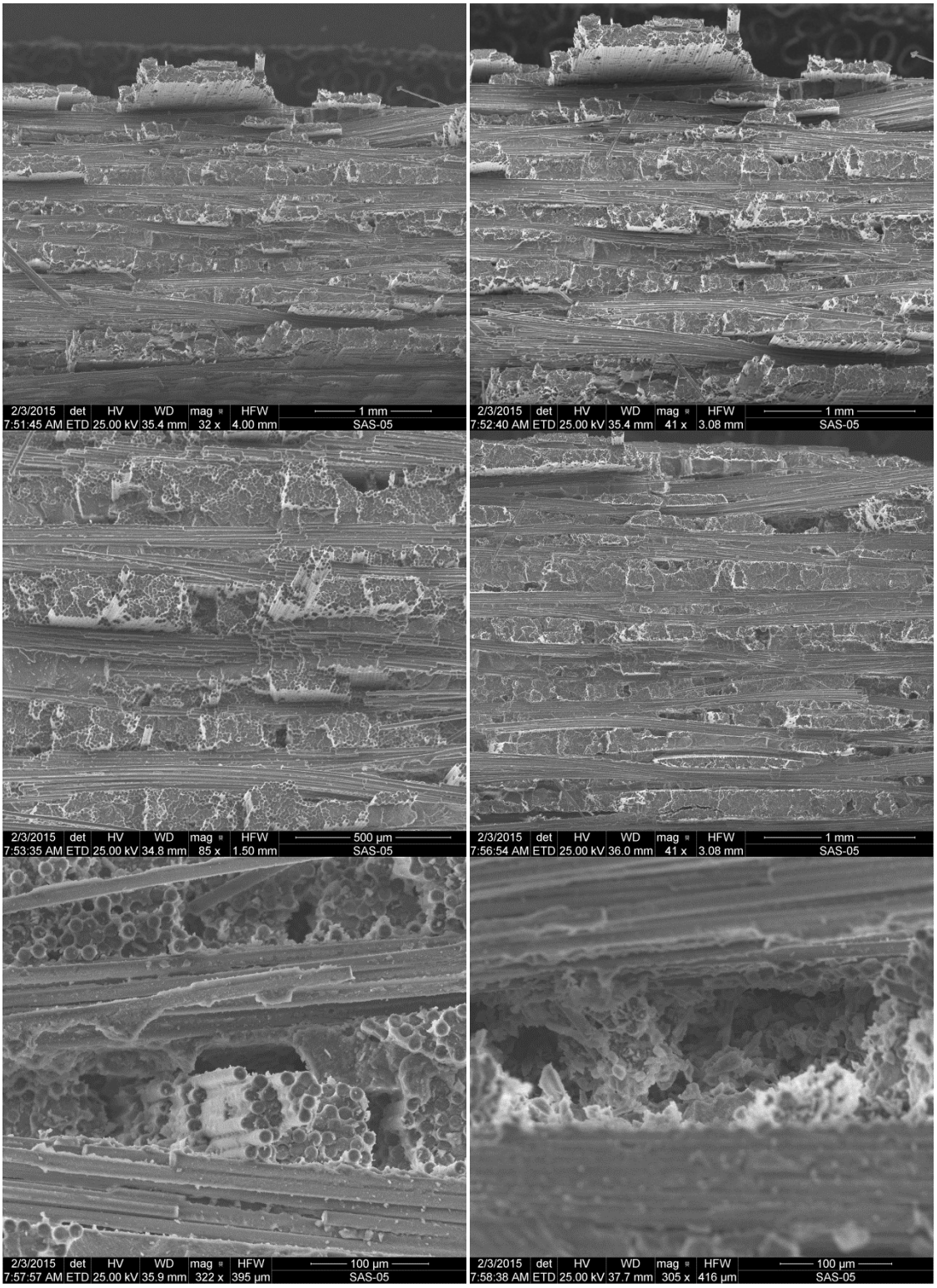

Figure F.6 – SEM micrographs of fracture surface of N610/AS composite obtained in tensile tests after prior heat treatment of 100 h at 1100°C (Specimen 5)

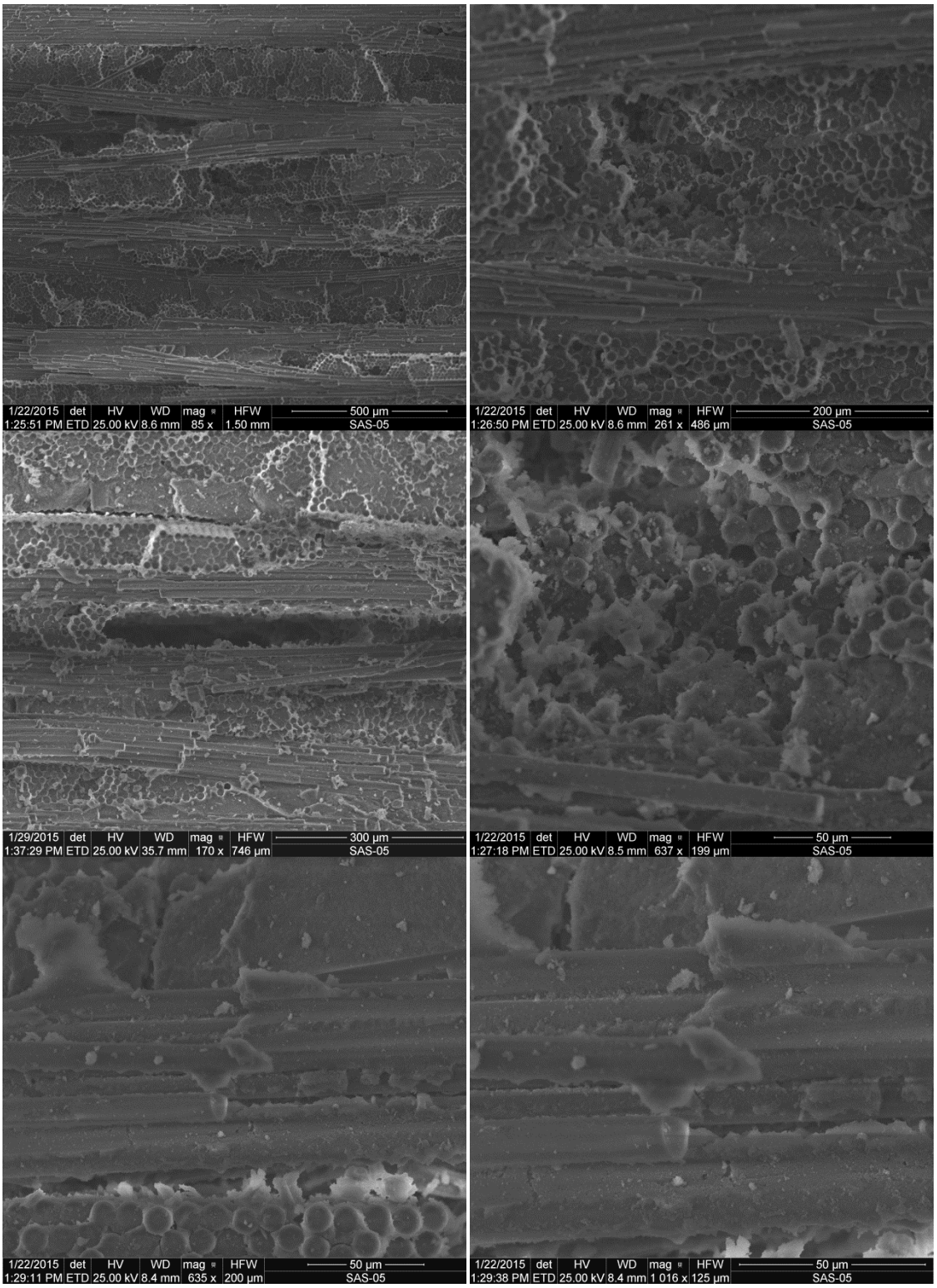

Figure F.7 – SEM micrographs of fracture surface of N610/AS composite obtained in tensile tests after prior heat treatment of 10 h at 1200°C (Specimen 4)

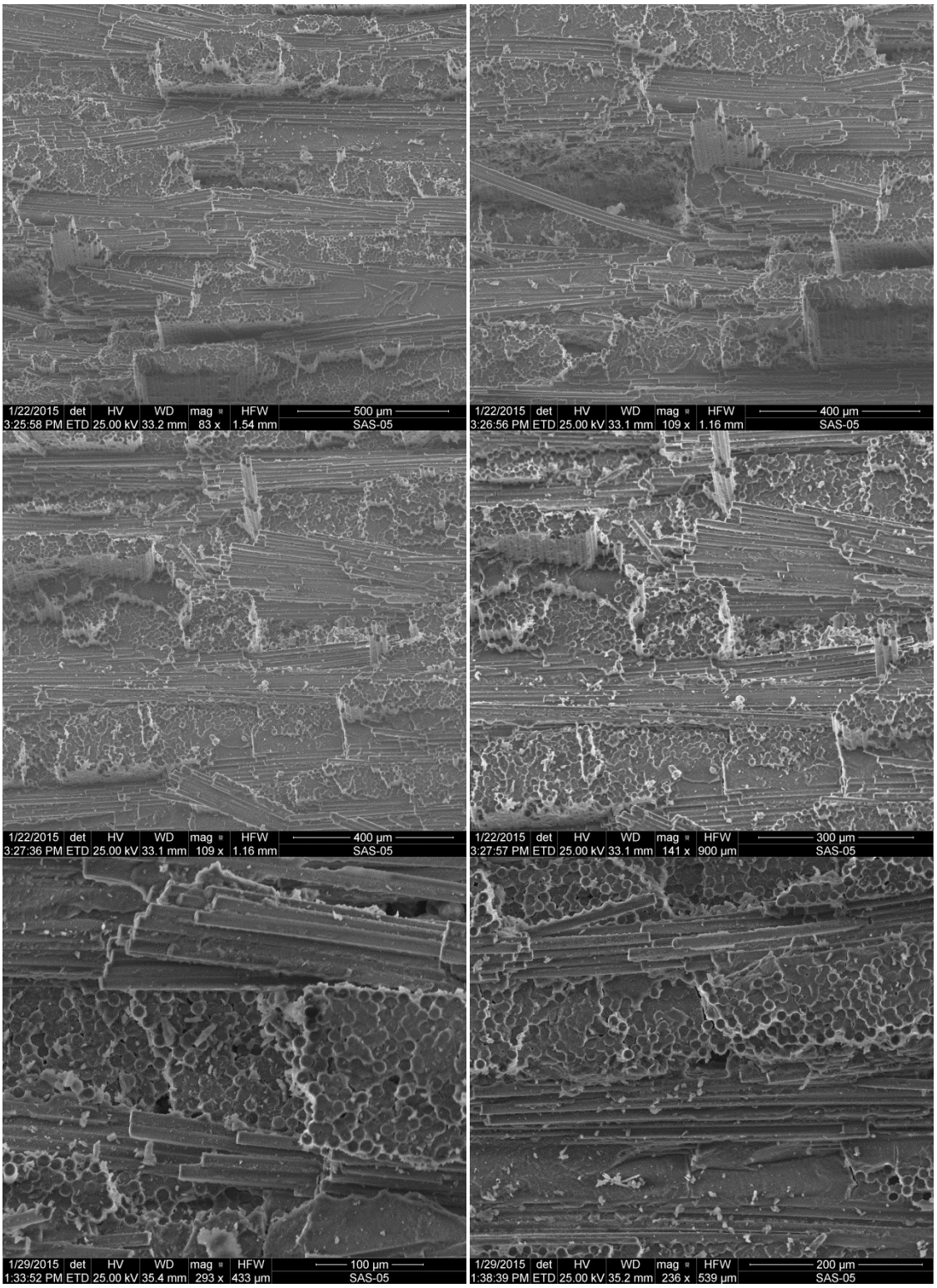

Figure F.8 – SEM micrographs of fracture surface of N610/AS composite obtained in tensile tests after prior heat treatment of 10 h at 1200°C (Specimen 4)

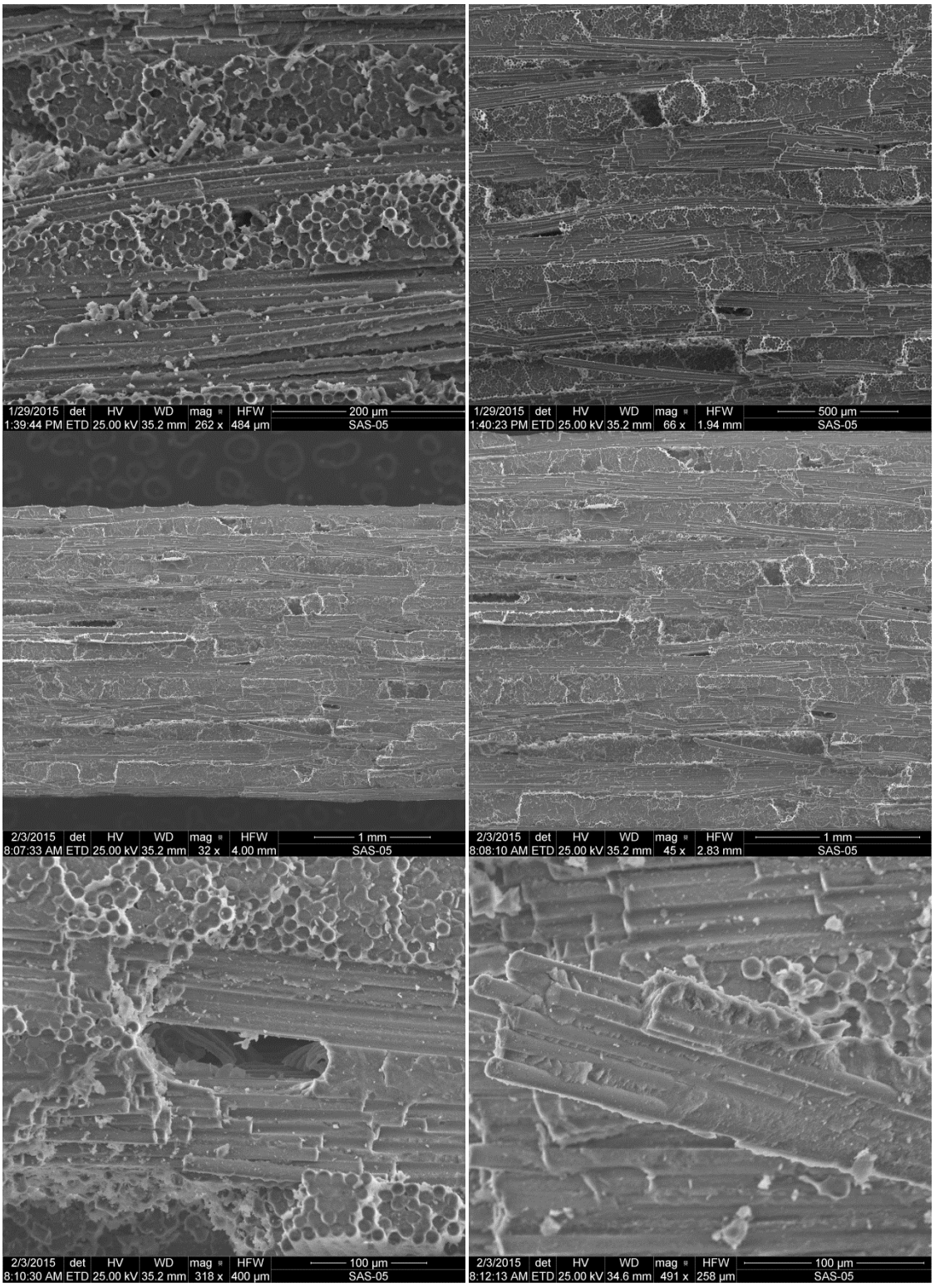

Figure F.9 – SEM micrographs of fracture surface of N610/AS composite obtained in tensile tests after prior heat treatment of 10 h at 1200°C (Specimen 4)

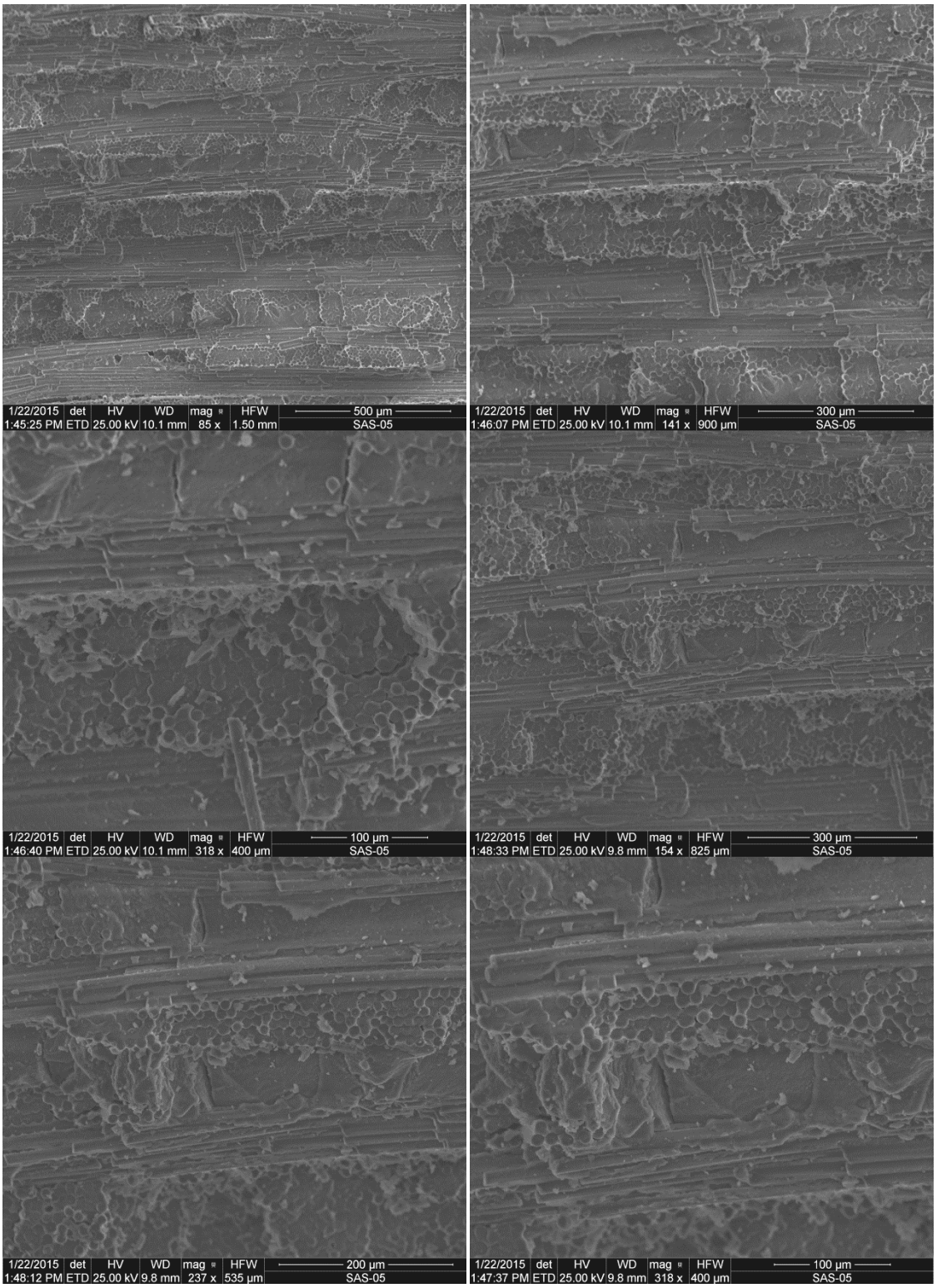

Figure F.10 – SEM micrographs of fracture surface of N610/AS composite obtained in tensile tests after prior heat treatment of 20 h at 1200°C (Specimen 5)

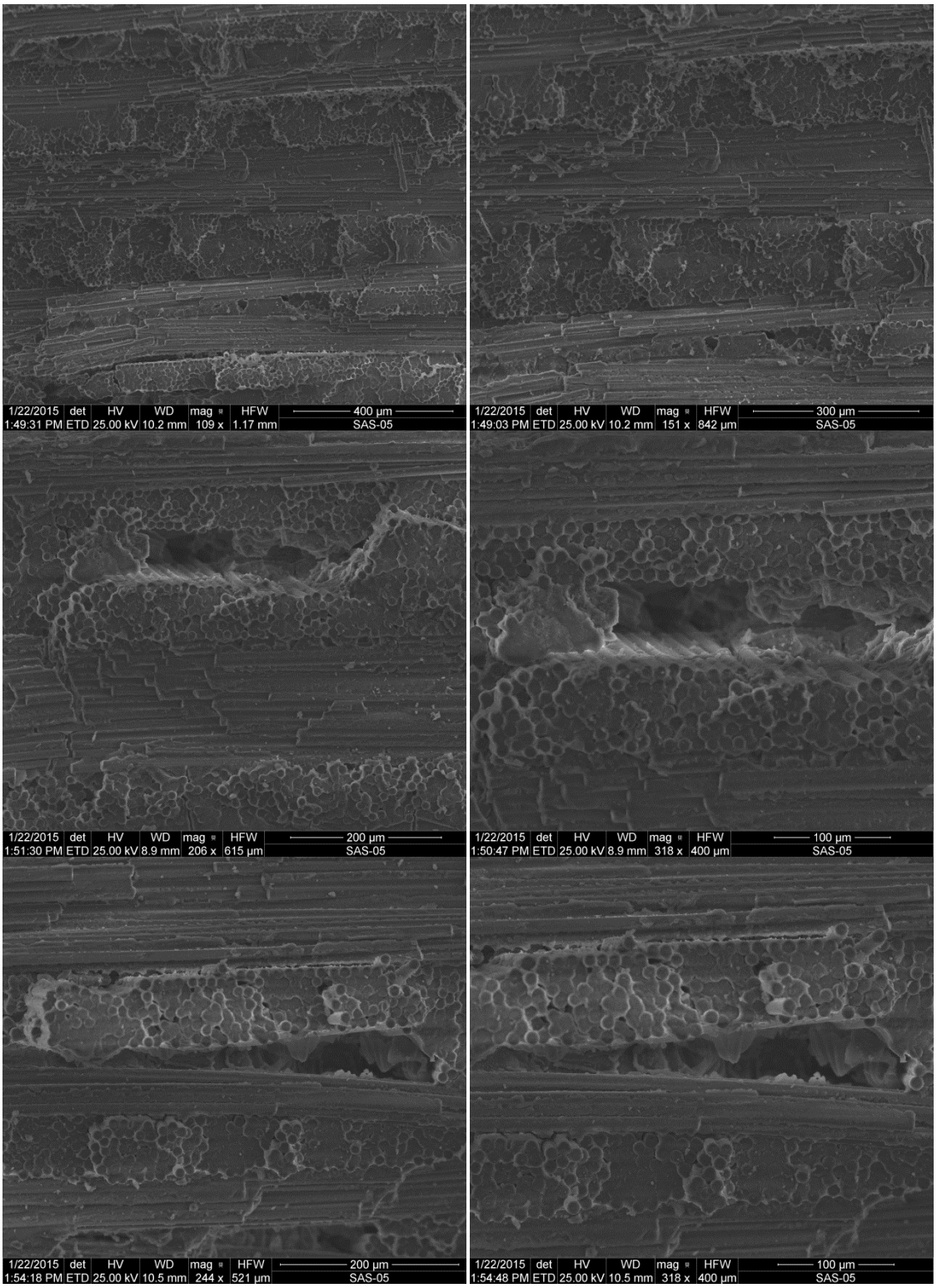

Figure F.11 – SEM micrographs of fracture surface of N610/AS composite obtained in tensile tests after prior heat treatment of 20 h at 1200°C (Specimen 5)

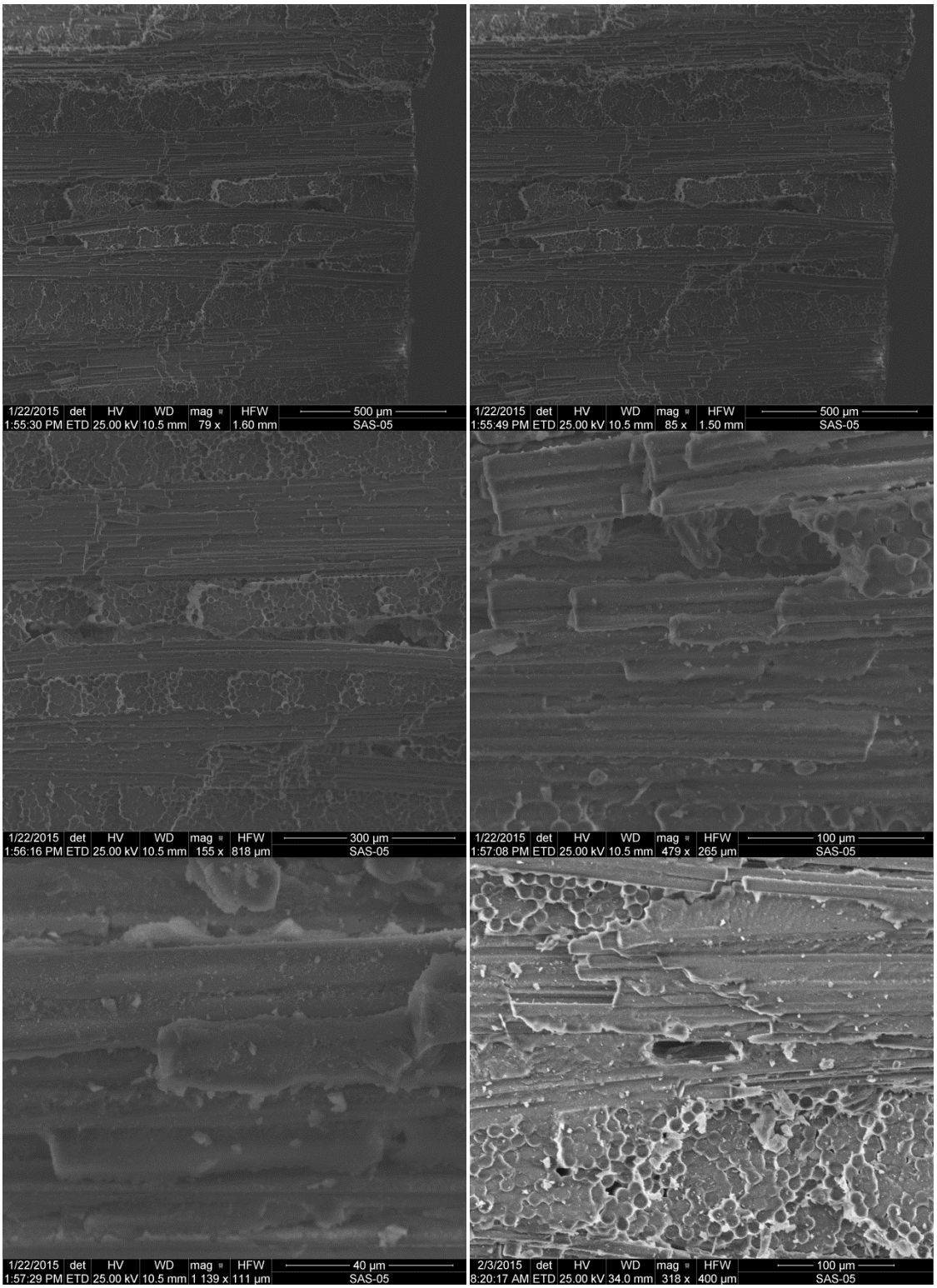

Figure F.12 – SEM micrographs of fracture surface of N610/AS composite obtained in tensile tests after prior heat treatment of 20 h at 1200°C (Specimen 5)

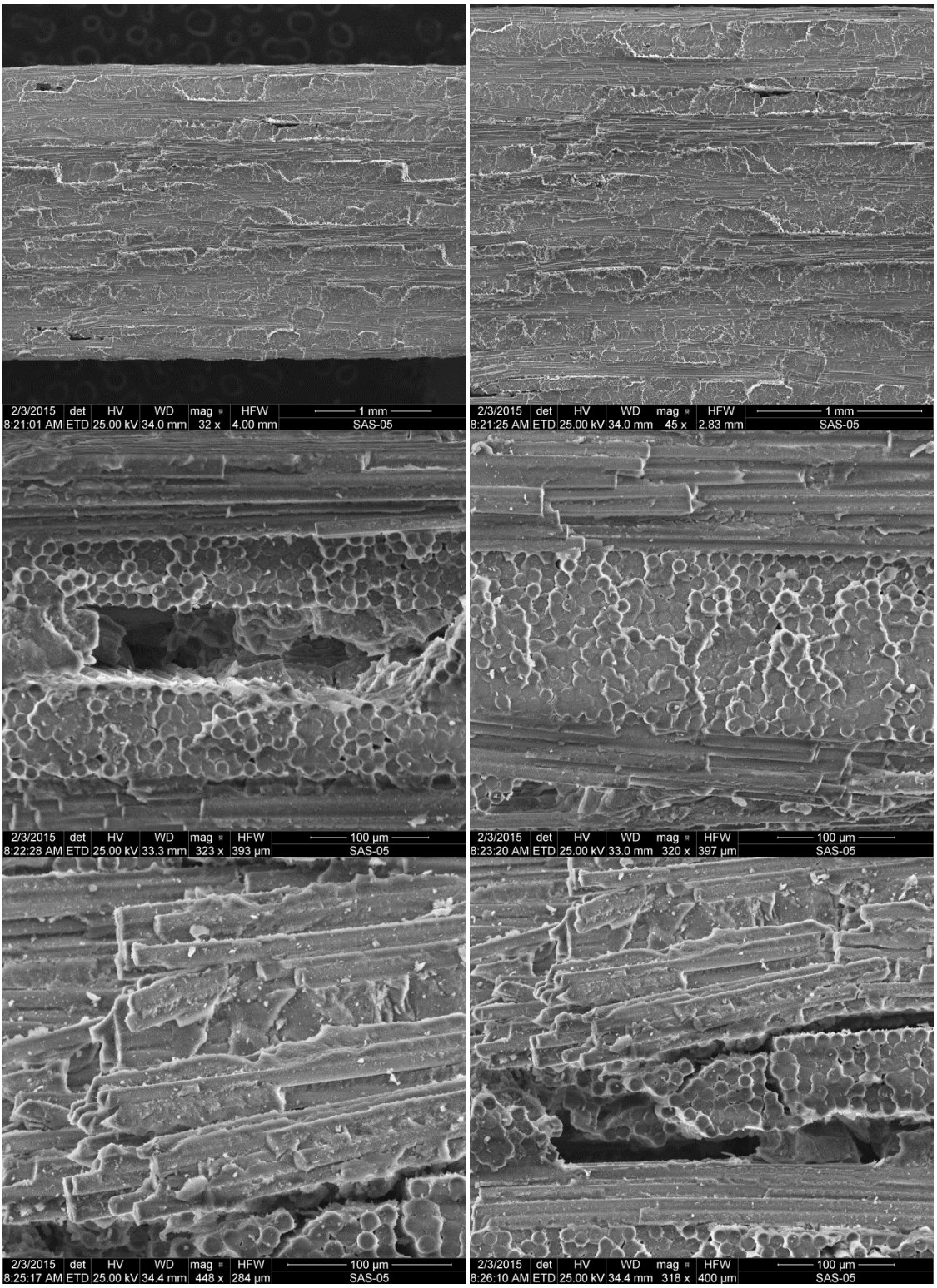

Figure F.13 – SEM micrographs of fracture surface of N610/AS composite obtained in tensile tests after prior heat treatment of 20 h at 1200°C (Specimen 5)

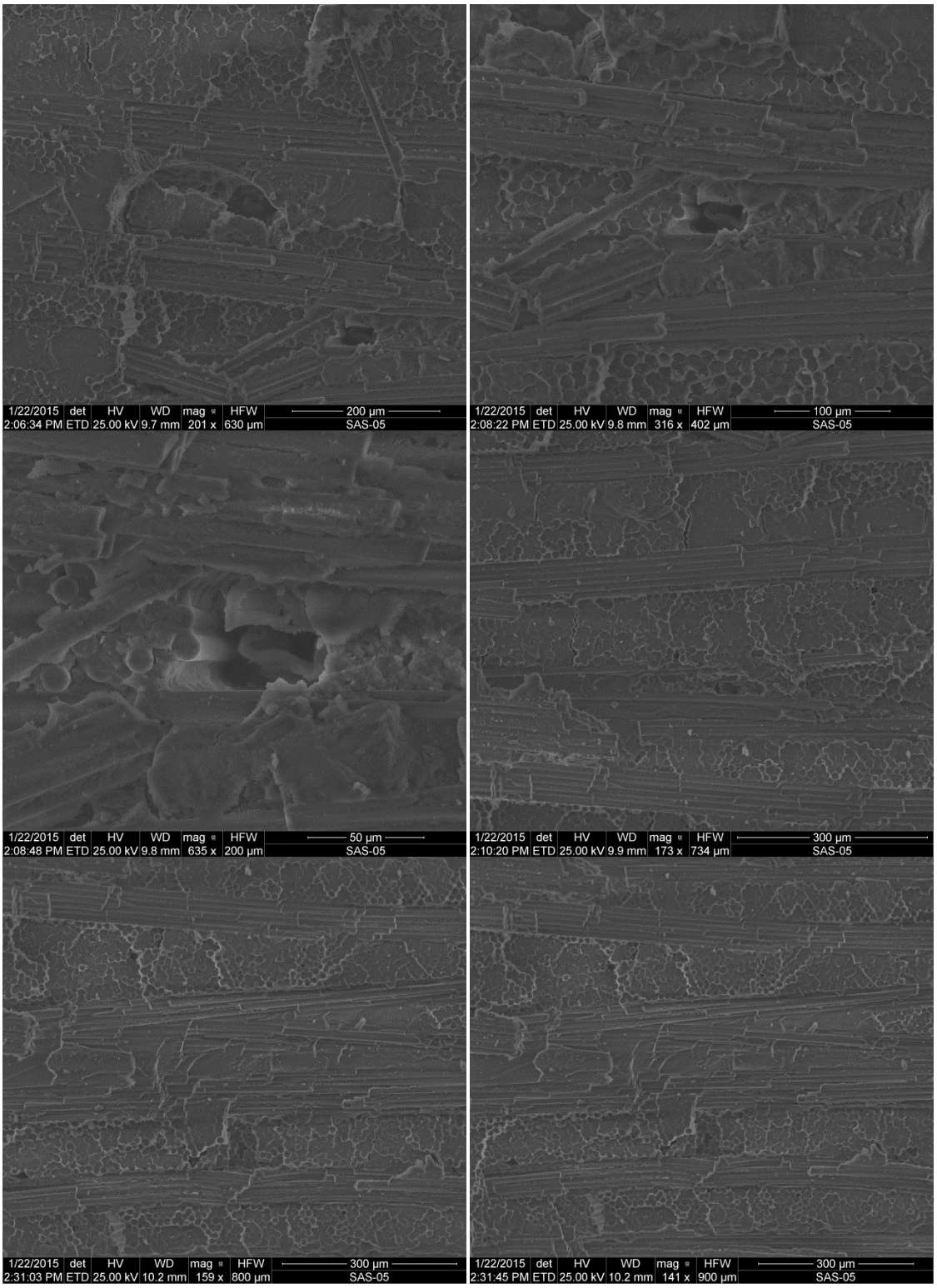

Figure F.14 – SEM micrographs of fracture surface of N610/AS composite obtained in tensile tests after prior heat treatment of 40 h at 1200°C (Specimen 6)

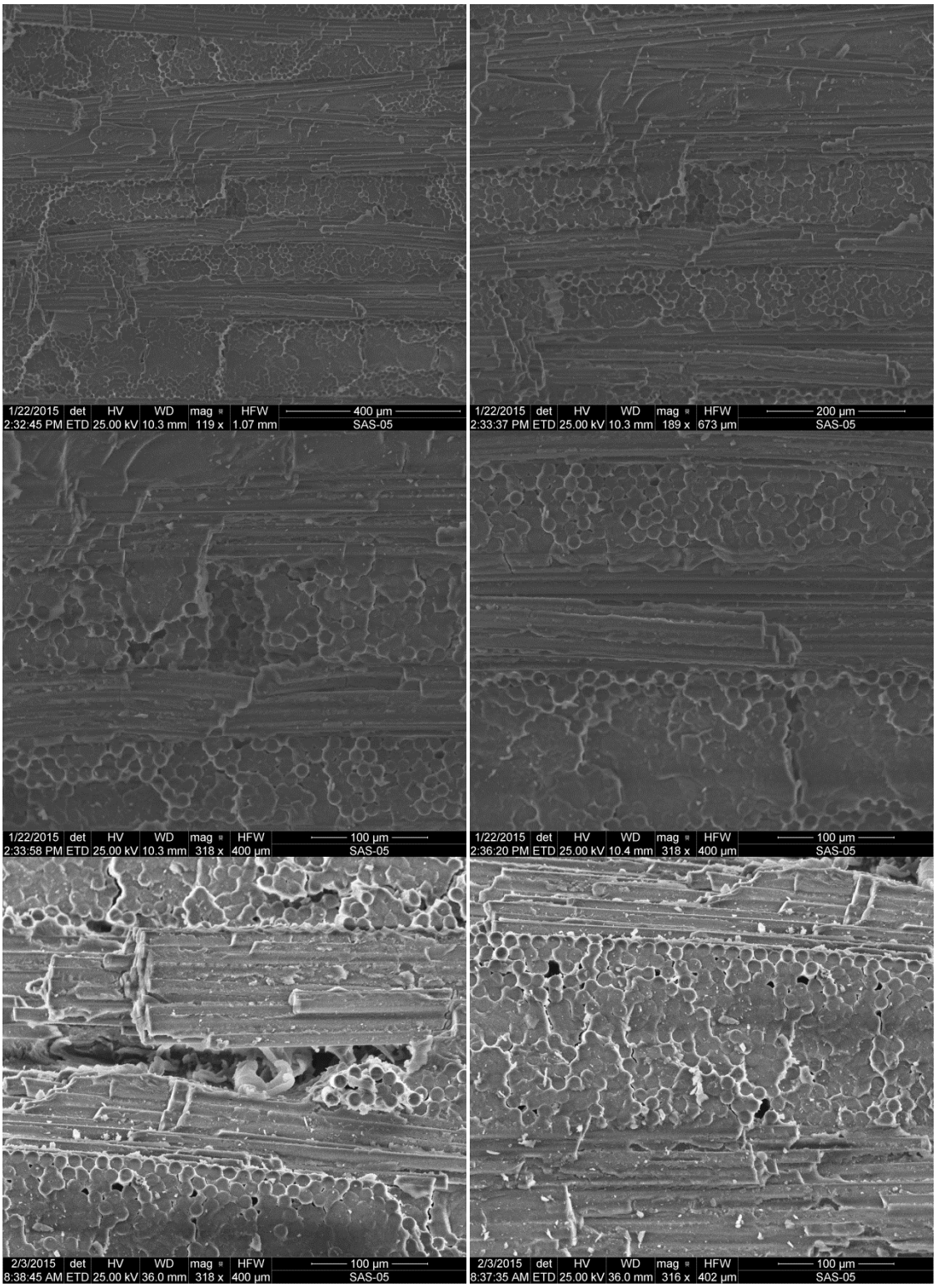

Figure F.15 – SEM micrographs of fracture surface of N610/AS composite obtained in tensile tests after prior heat treatment of 40 h at 1200°C (Specimen 6)

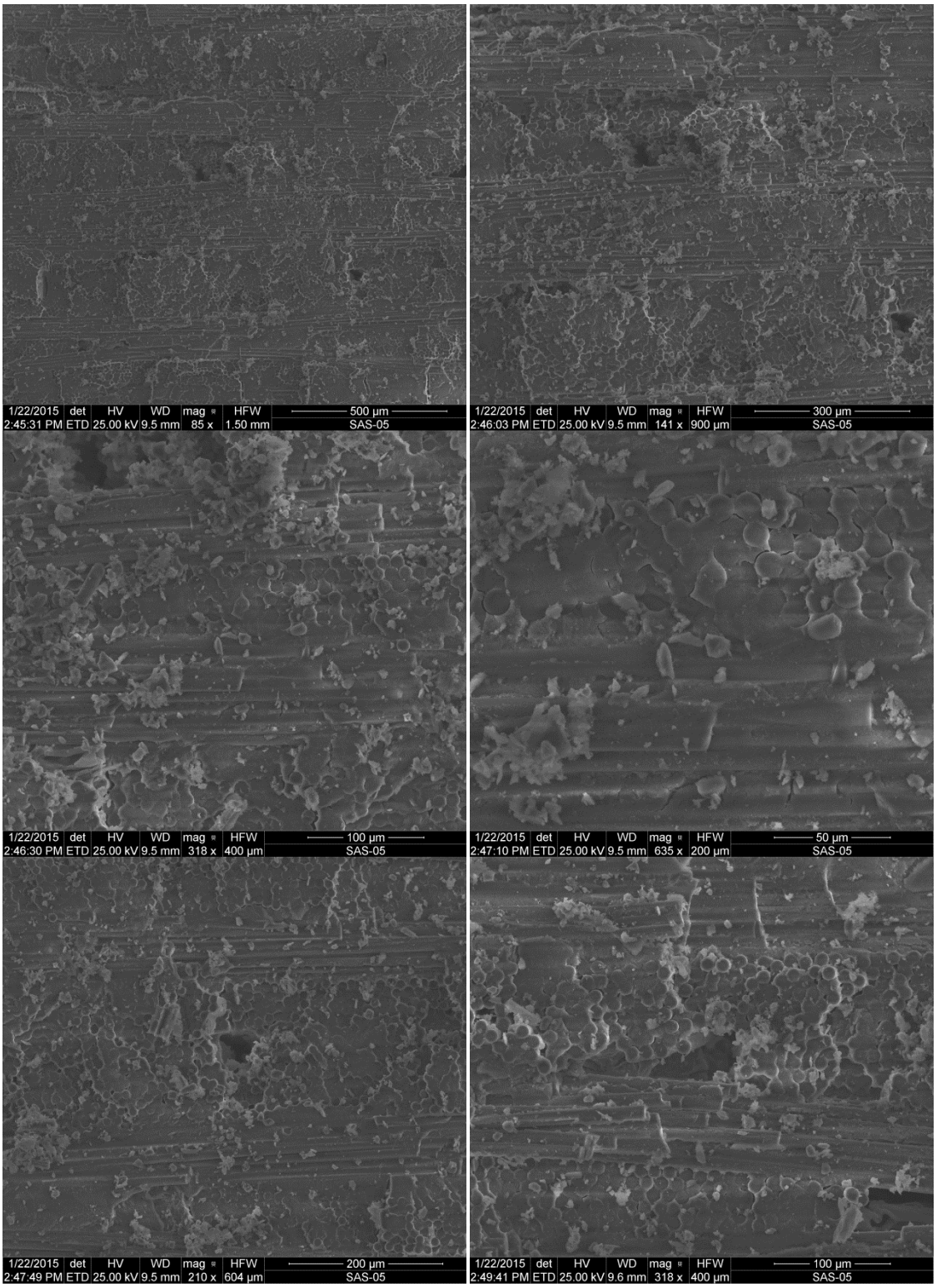

Figure F.16 – SEM micrographs of fracture surface of N610/AS composite obtained in tensile tests after prior heat treatment of 100 h at 1200°C (Specimen 3)

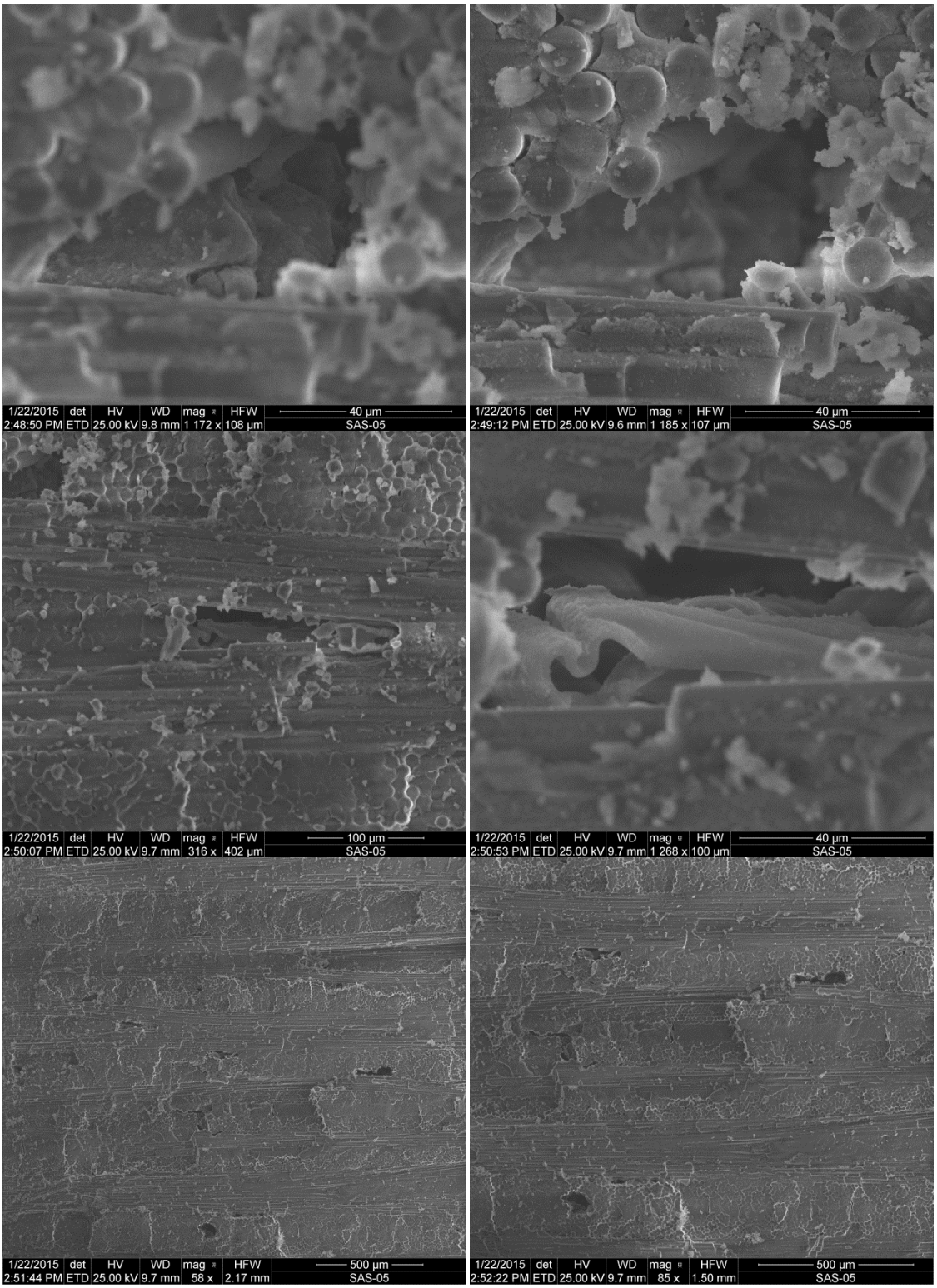

Figure F.17 – SEM micrographs of fracture surface of N610/AS composite obtained in tensile tests after prior heat treatment of 100 h at 1200°C (Specimen 3)

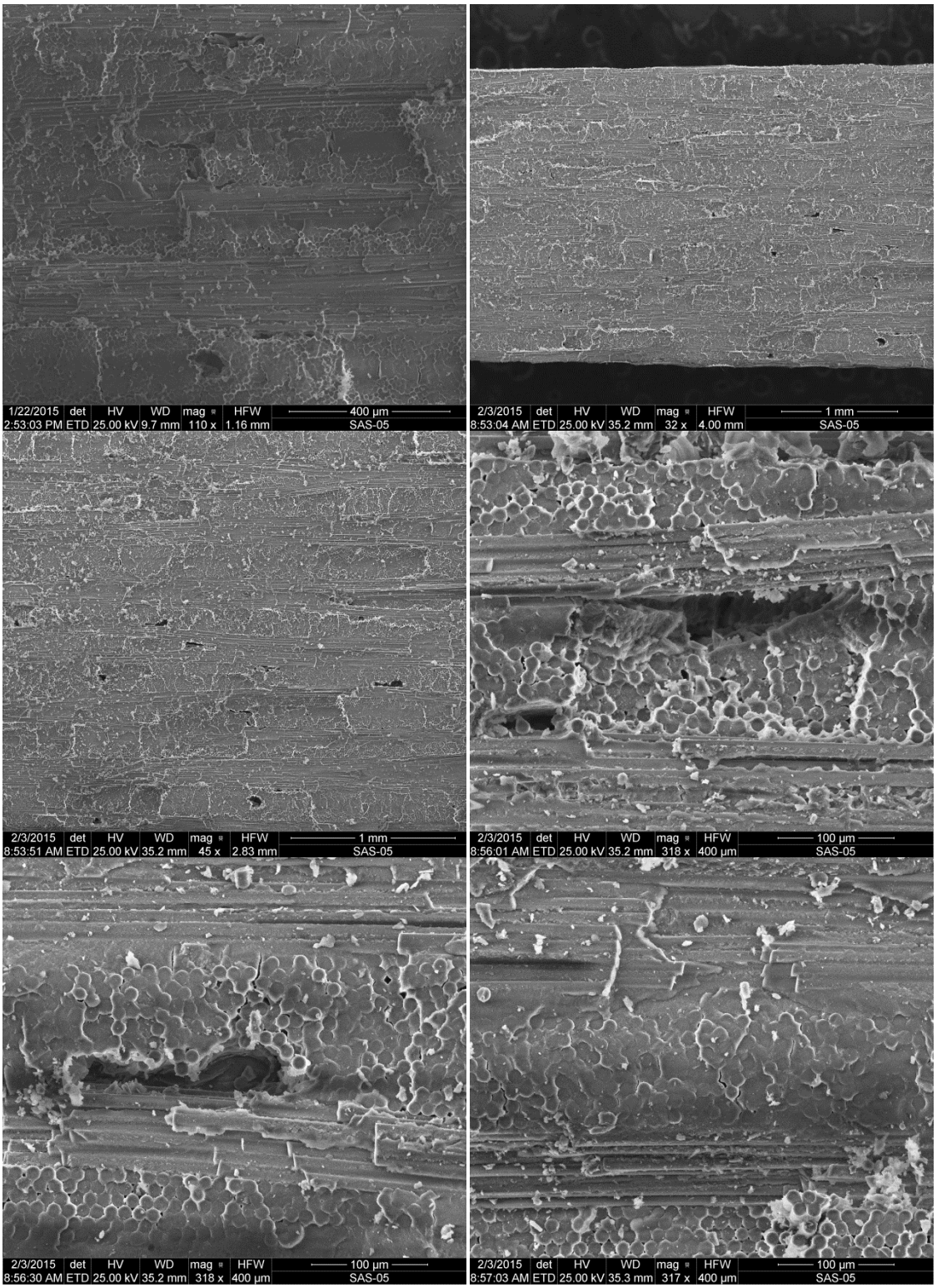

Figure F.18 – SEM micrographs of fracture surface of N610/AS composite obtained in tensile tests after prior heat treatment of 100 h at 1200°C (Specimen 3)

Appendix G - Additional SEM Micrographs of N720/AS Fracture Surfaces

Appendix G presents additional SEM micrographs of the fracture surfaces of N720/AS specimens produced in tensile tests.

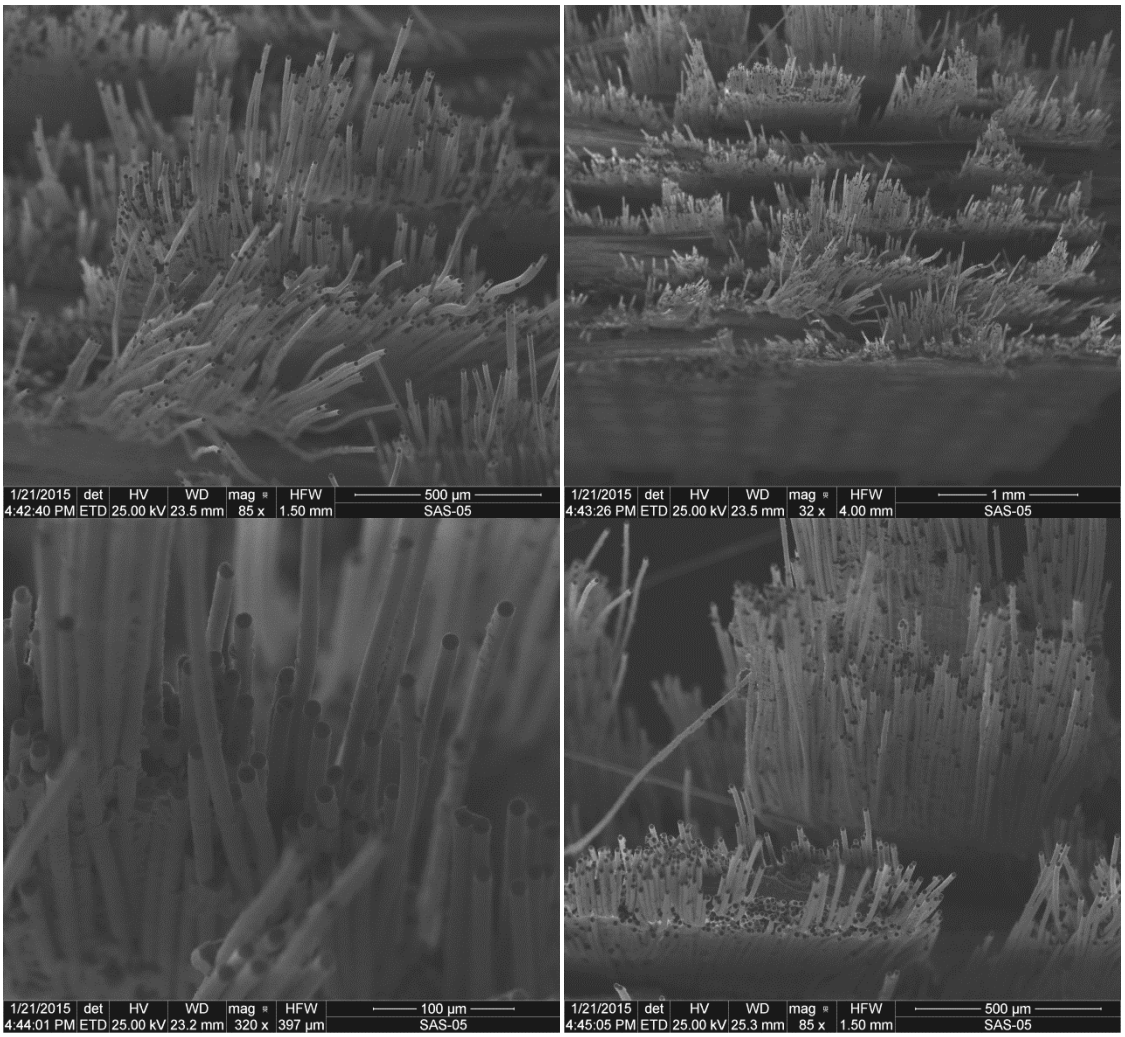

Figure G.1 – SEM micrographs of fracture surface of as-received N720/AS composite obtained in tensile tests (Specimen 6)

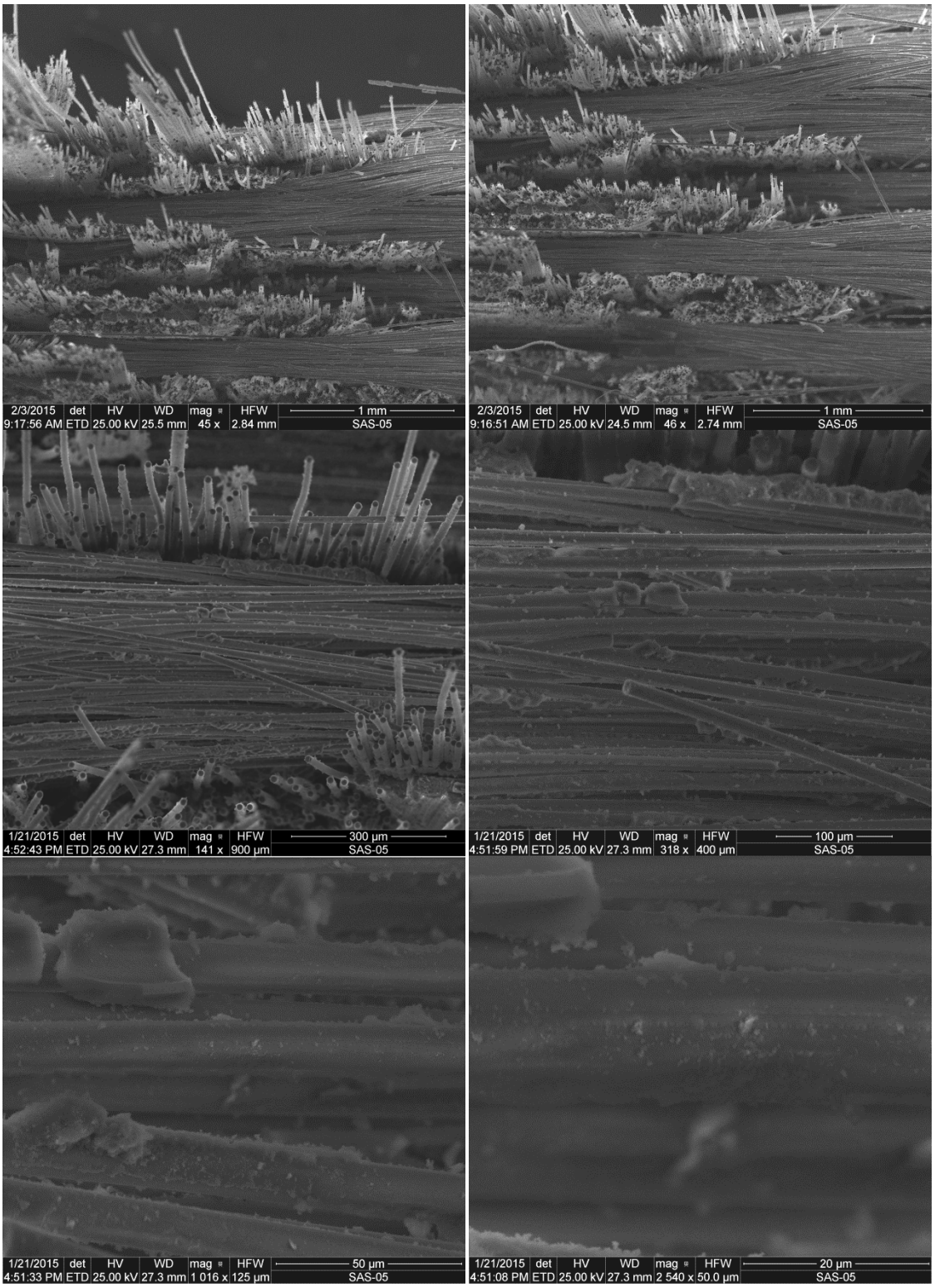

Figure G.2 – SEM micrographs of fracture surface of as-received N720/AS composite obtained in tensile tests (Specimen 6)

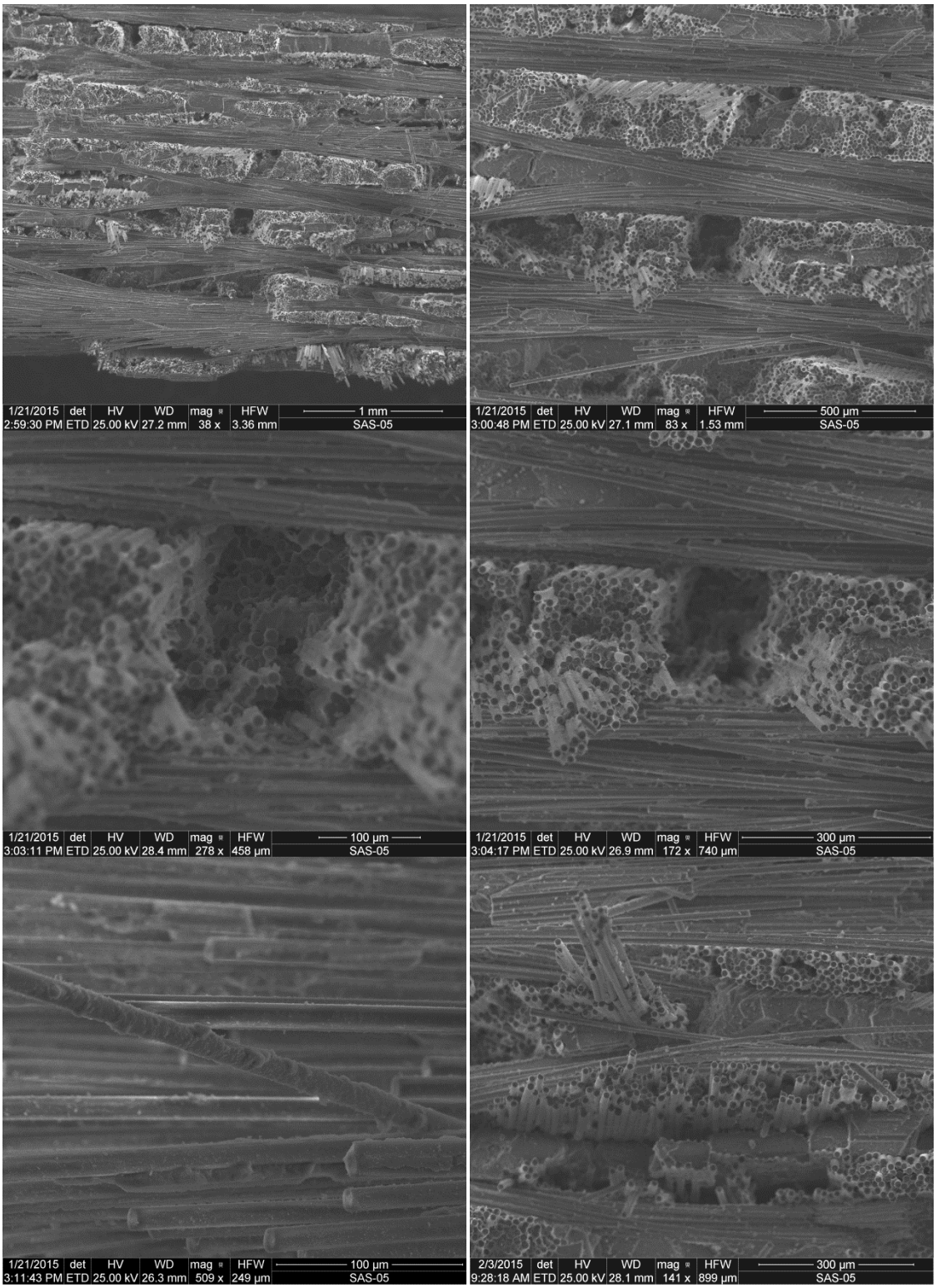

Figure G.3 – SEM micrographs of fracture surface of N720/AS composite obtained in tensile tests after prior heat treatment of 100 h at 1100°C (Specimen 5)

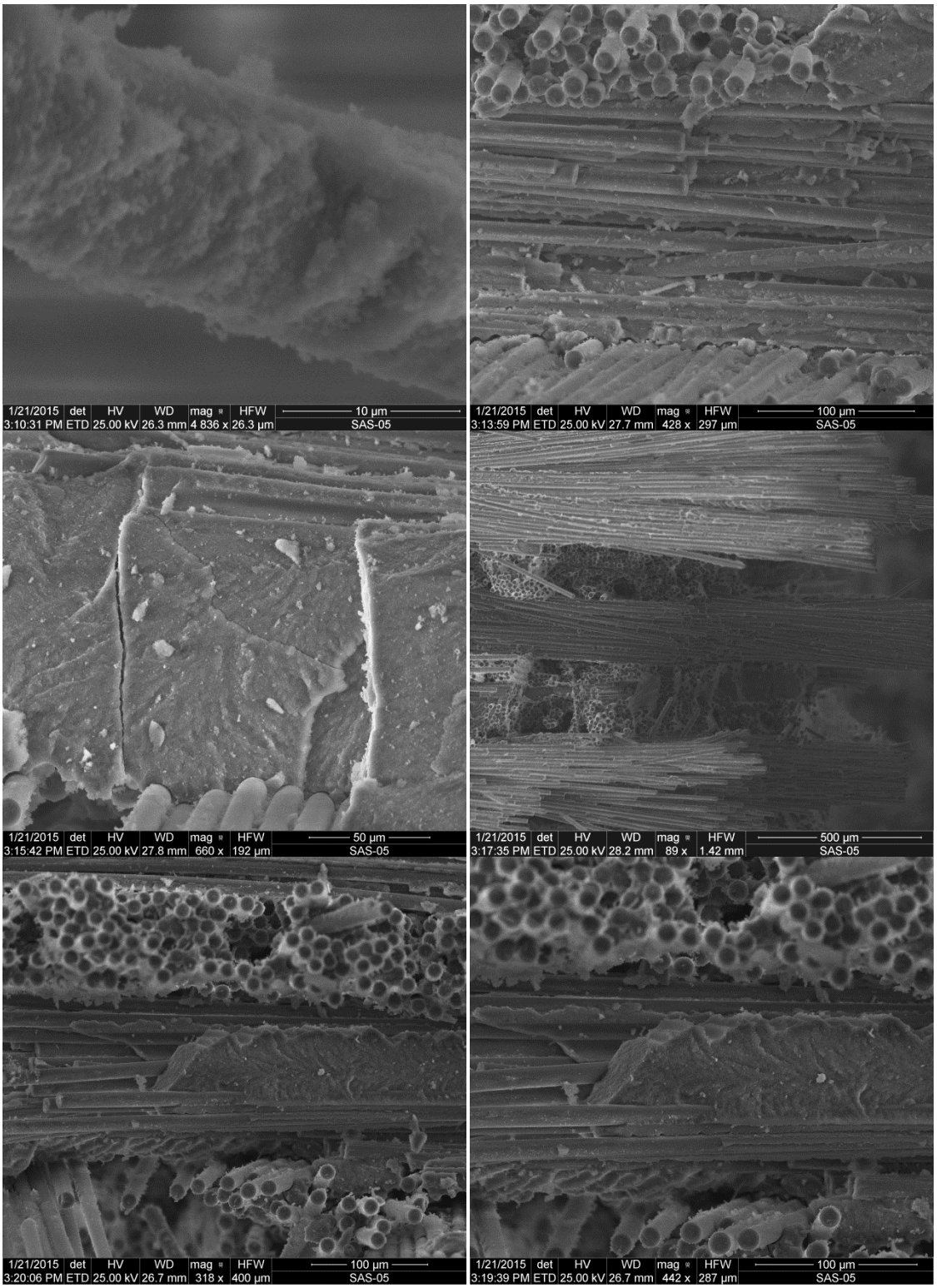

Figure G.4 – SEM micrographs of fracture surface of N720/AS composite obtained in tensile tests after prior heat treatment of 100 h at 1100°C (Specimen 5)

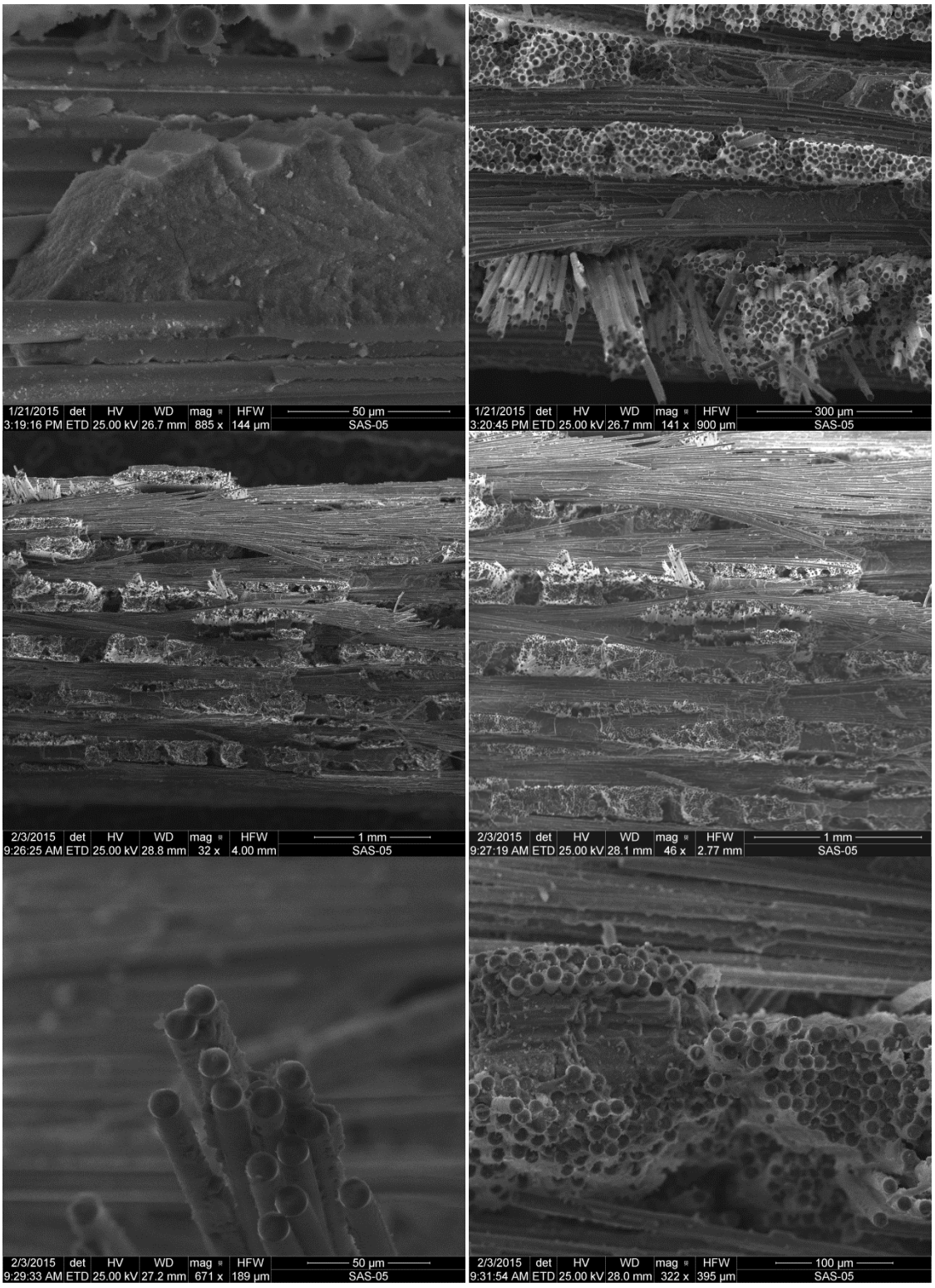

Figure G.5 – SEM micrographs of fracture surface of N720/AS composite obtained in tensile tests after prior heat treatment of 100 h at 1100°C (Specimen 5)

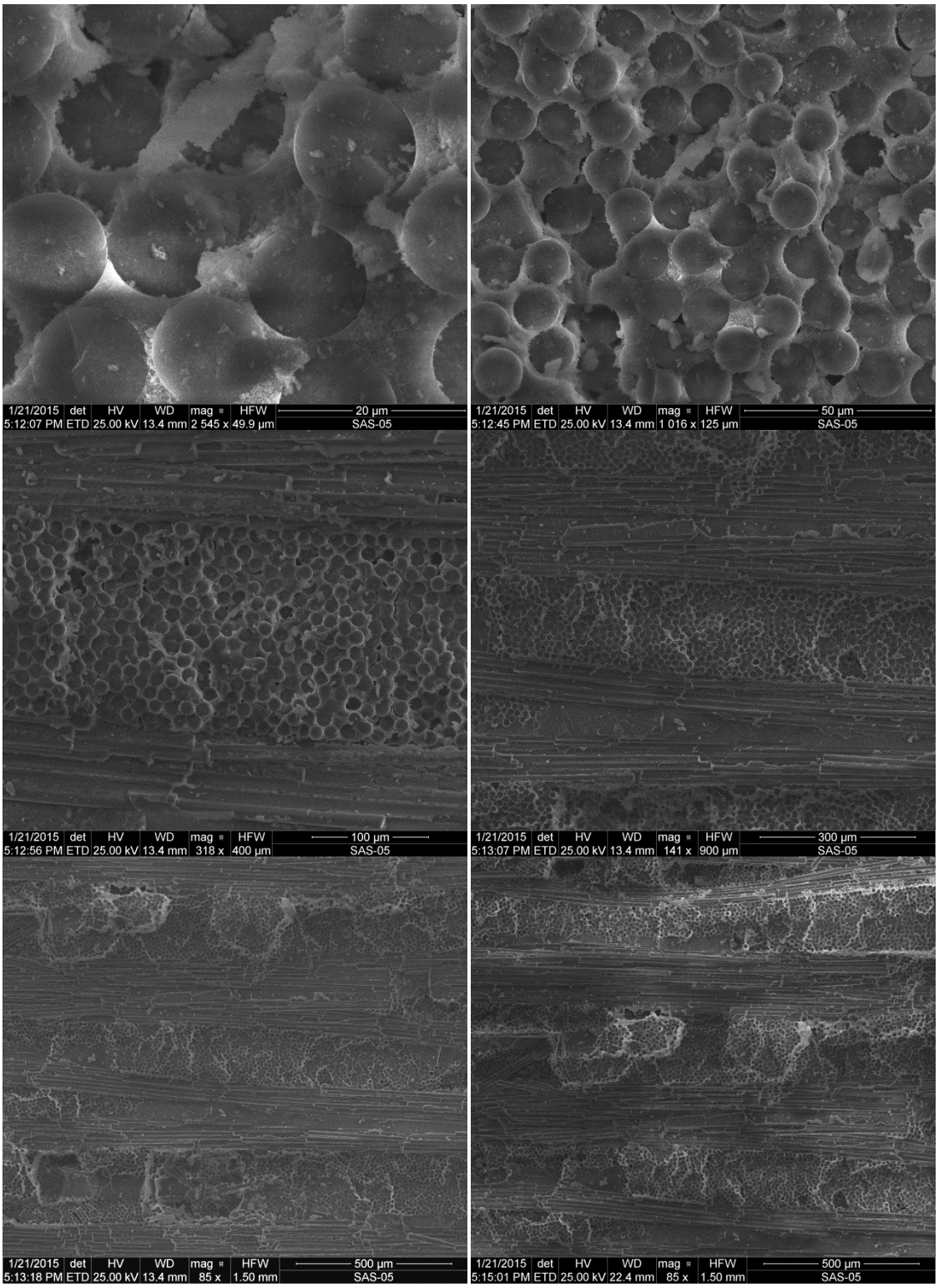

Figure G.6 – SEM micrographs of fracture surface of N720/AS composite obtained in tensile tests after heat treatment of 10 h at 1200°C (Specimen 5)

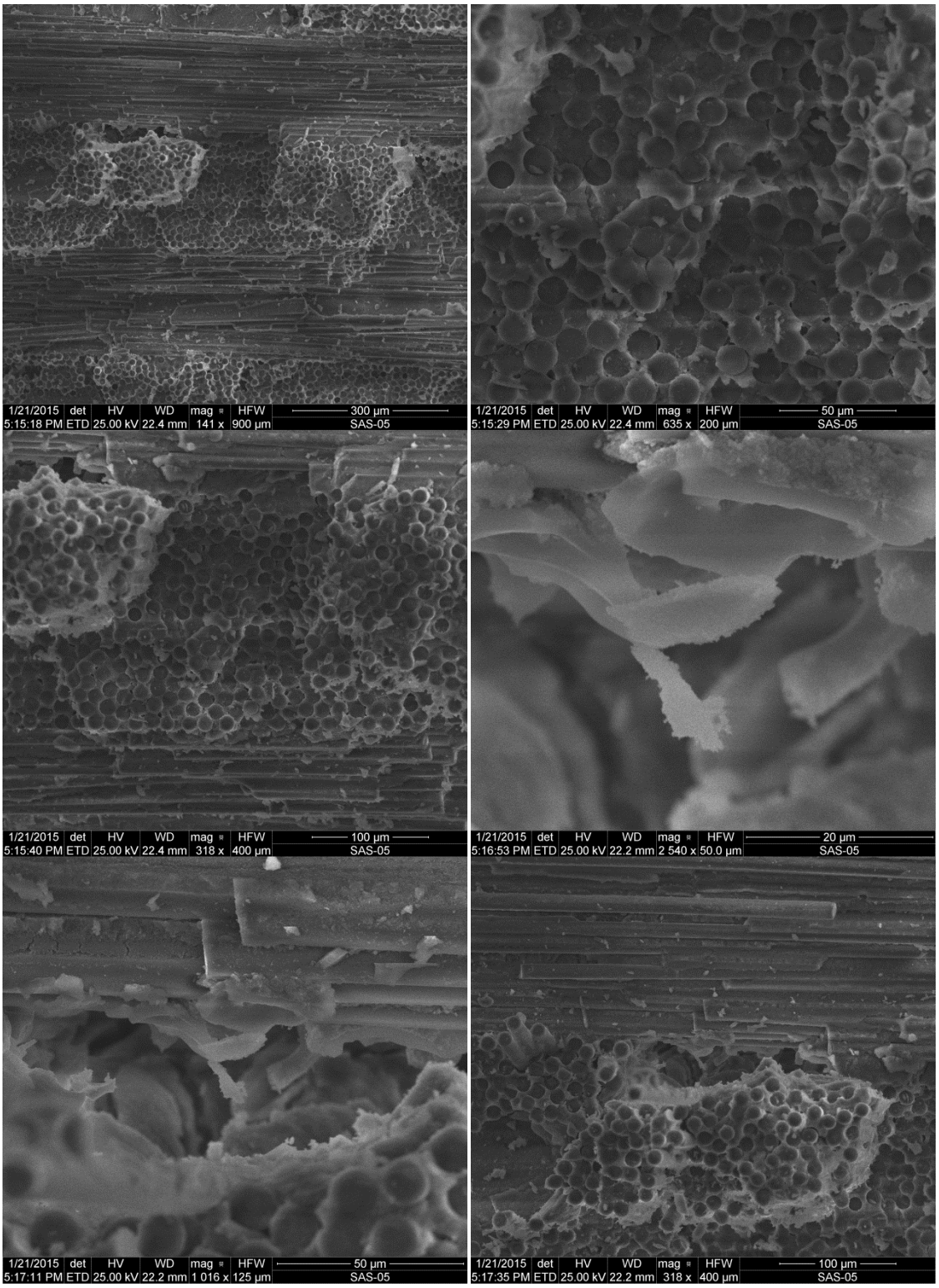

Figure G.7 – SEM micrographs of fracture surface of N720/AS composite obtained in tensile tests after heat treatment of 10 h at 1200°C (Specimen 5)

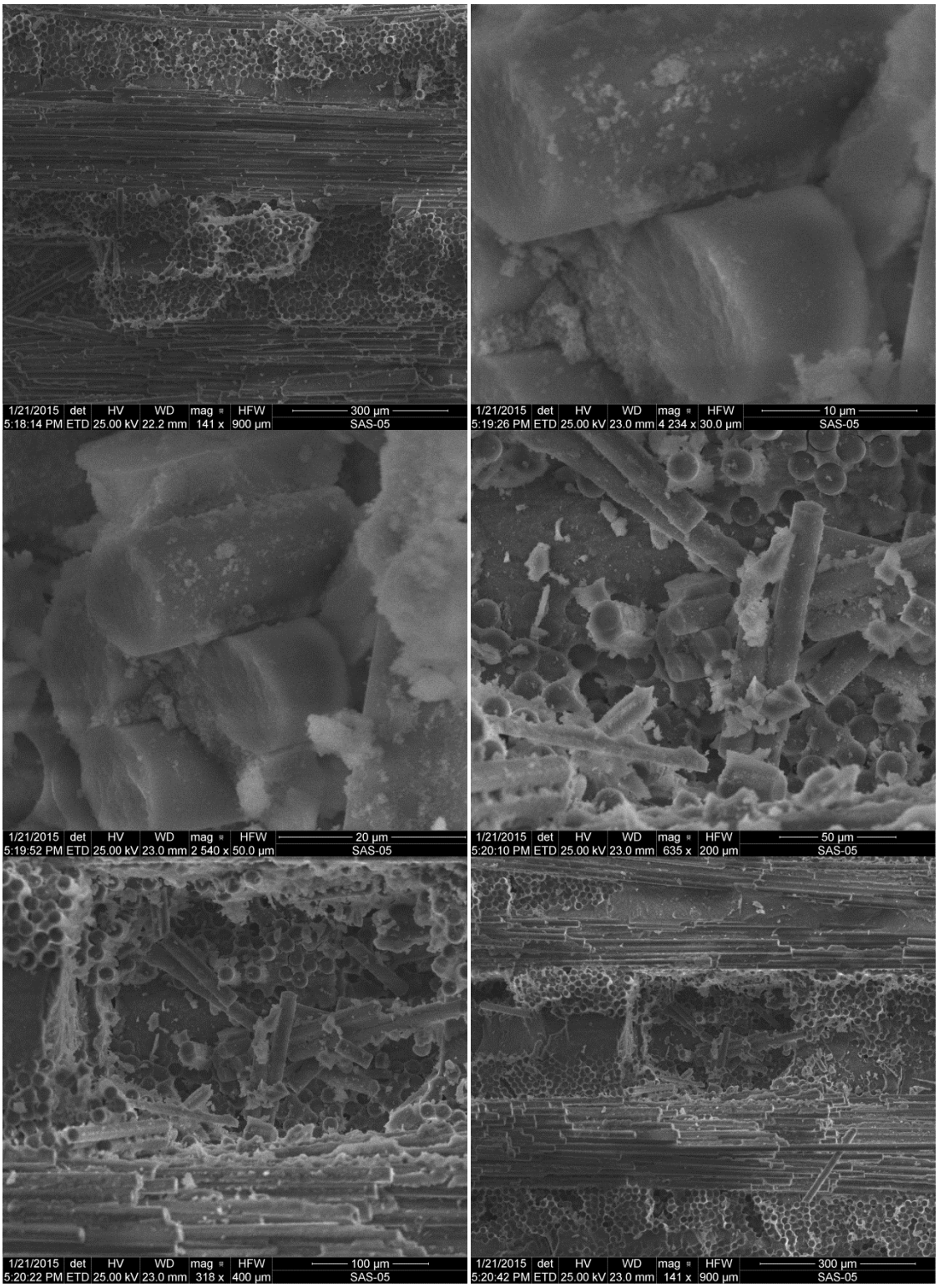

Figure G.8 – SEM micrographs of fracture surface of N720/AS composite obtained in tensile tests after heat treatment of 10 h at 1200°C (Specimen 5)

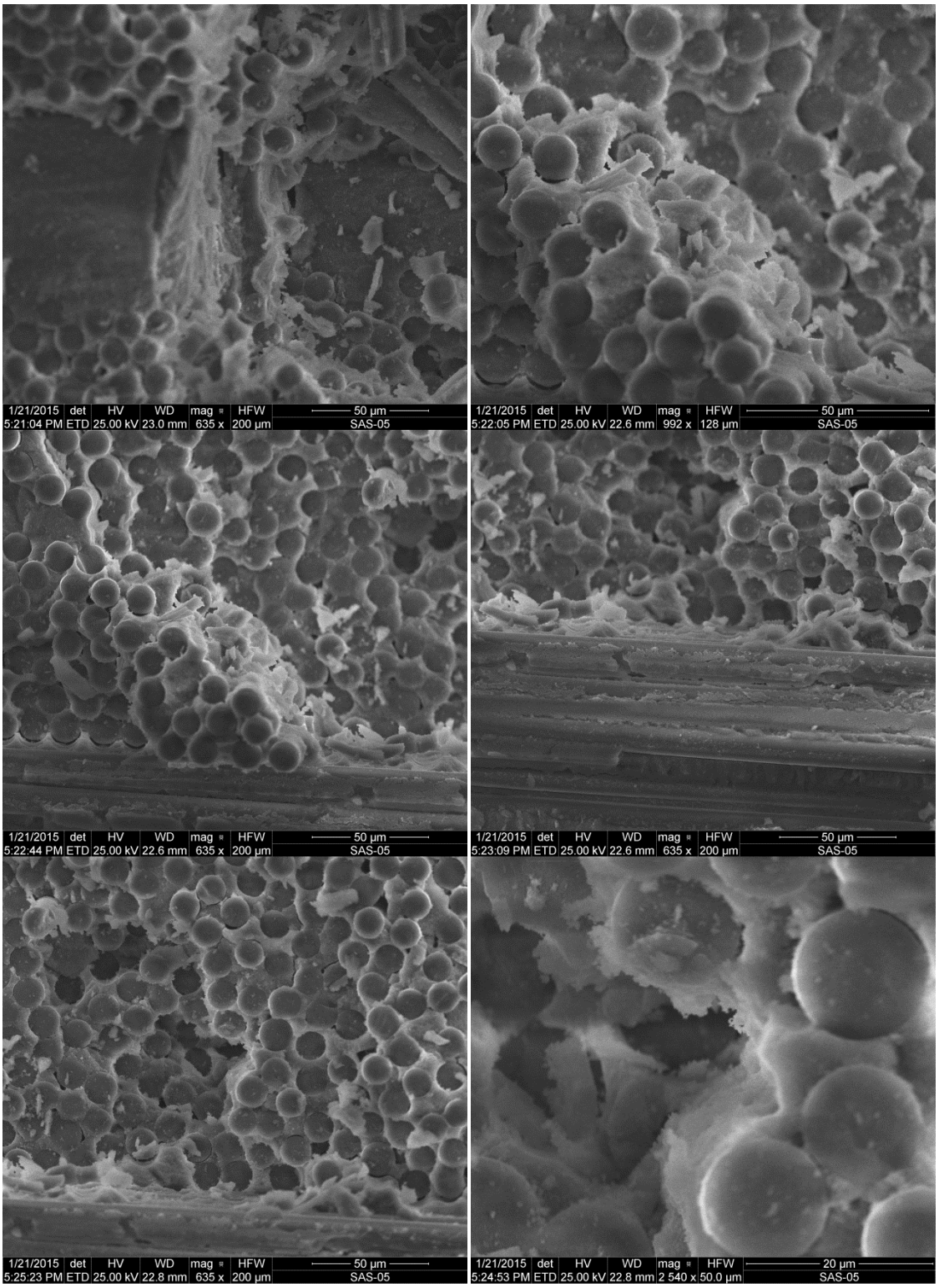

Figure G.9 – SEM micrographs of fracture surface of N720/AS composite obtained in tensile tests after heat treatment of 10 h at 1200°C (Specimen 5)

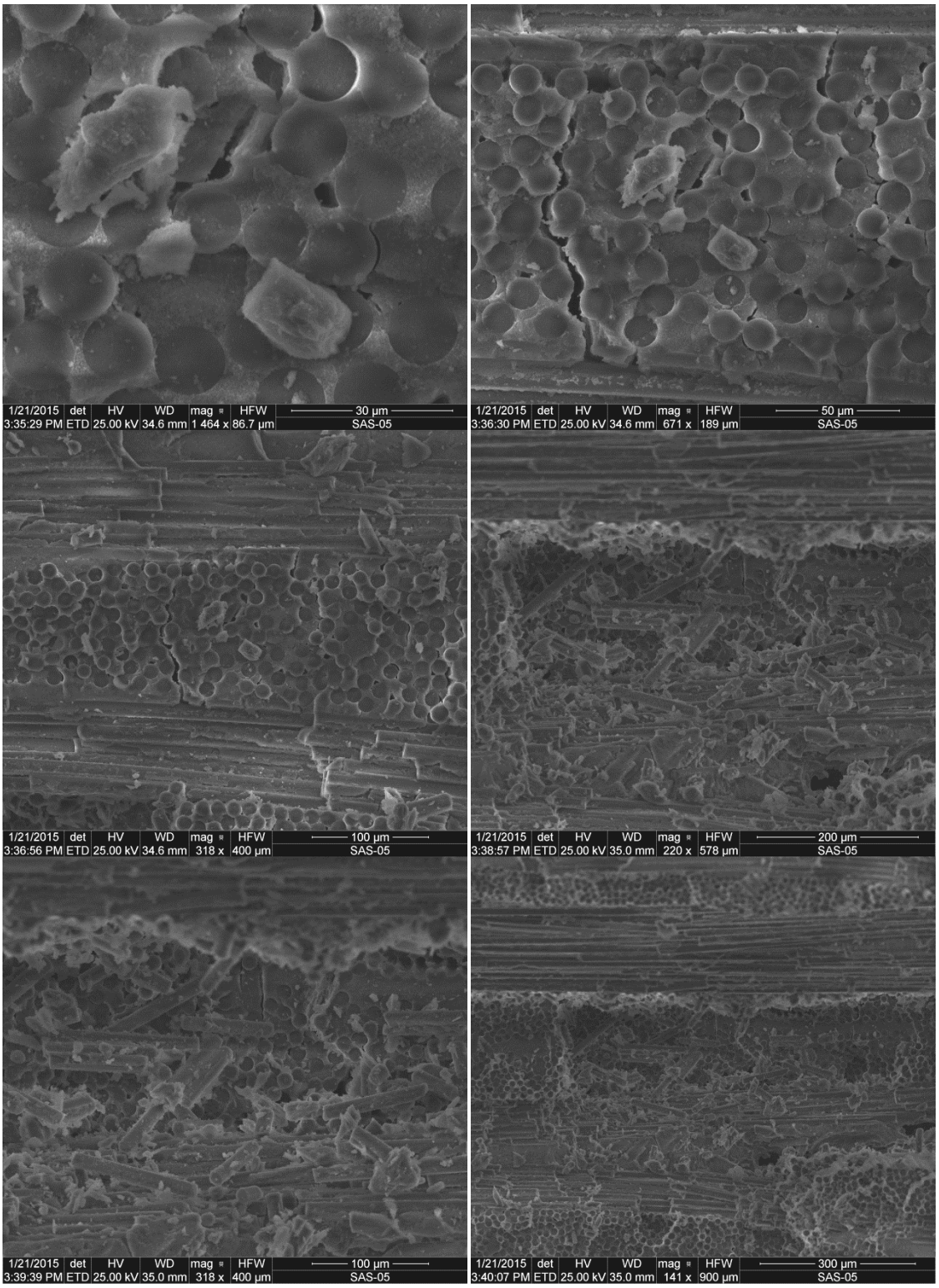

Figure G.10 – SEM micrographs of fracture surface of N720/AS composite obtained in tensile tests after heat treatment of 20 h at 1200°C (Specimen 2)

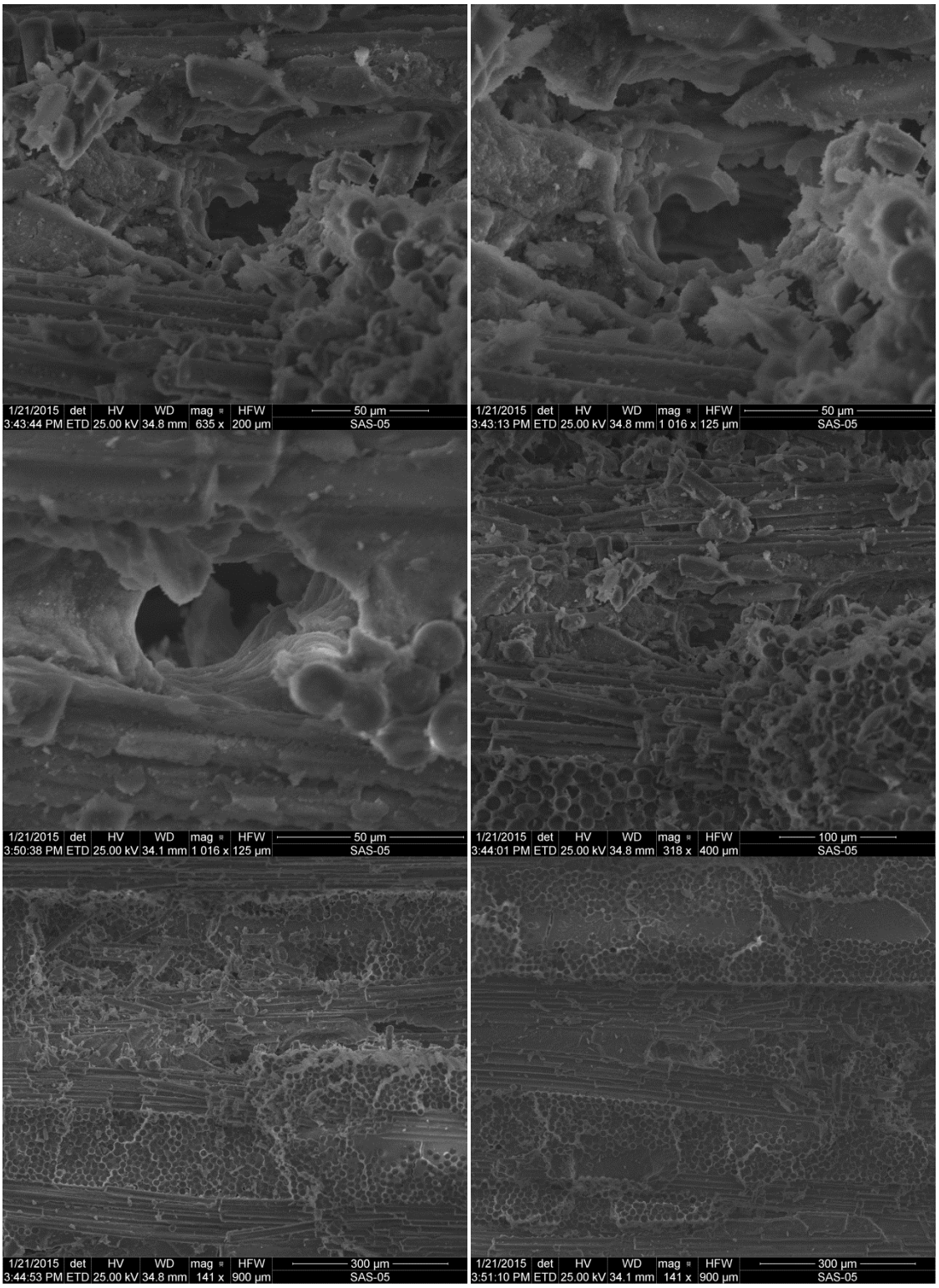

Figure G.11 – SEM micrographs of fracture surface of N720/AS composite obtained in tensile tests after heat treatment of 20 h at 1200°C (Specimen 2)

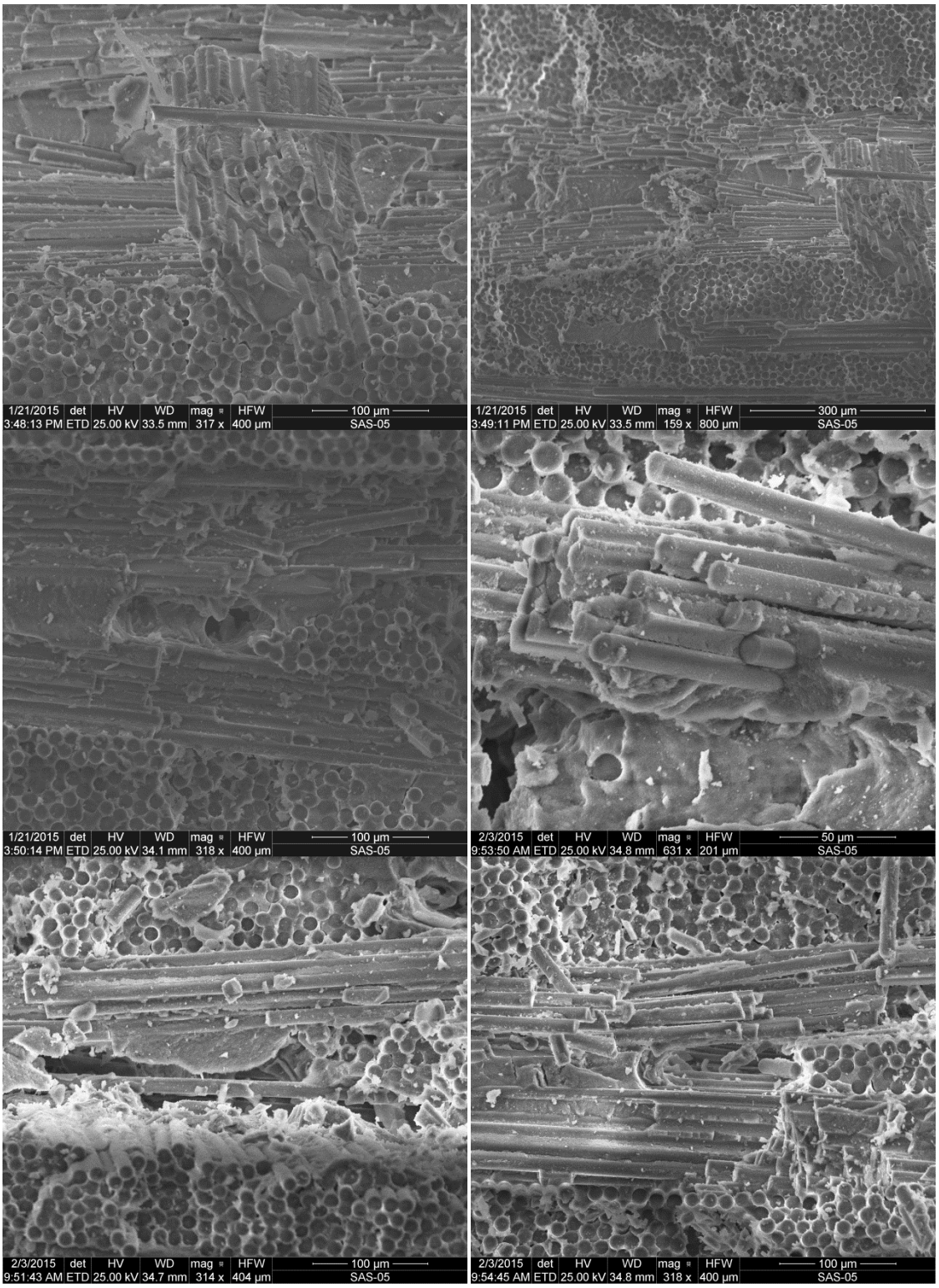

Figure G.12 – SEM micrographs of fracture surface of N720/AS composite obtained in tensile tests after heat treatment of 20 h at 1200°C (Specimen 2)

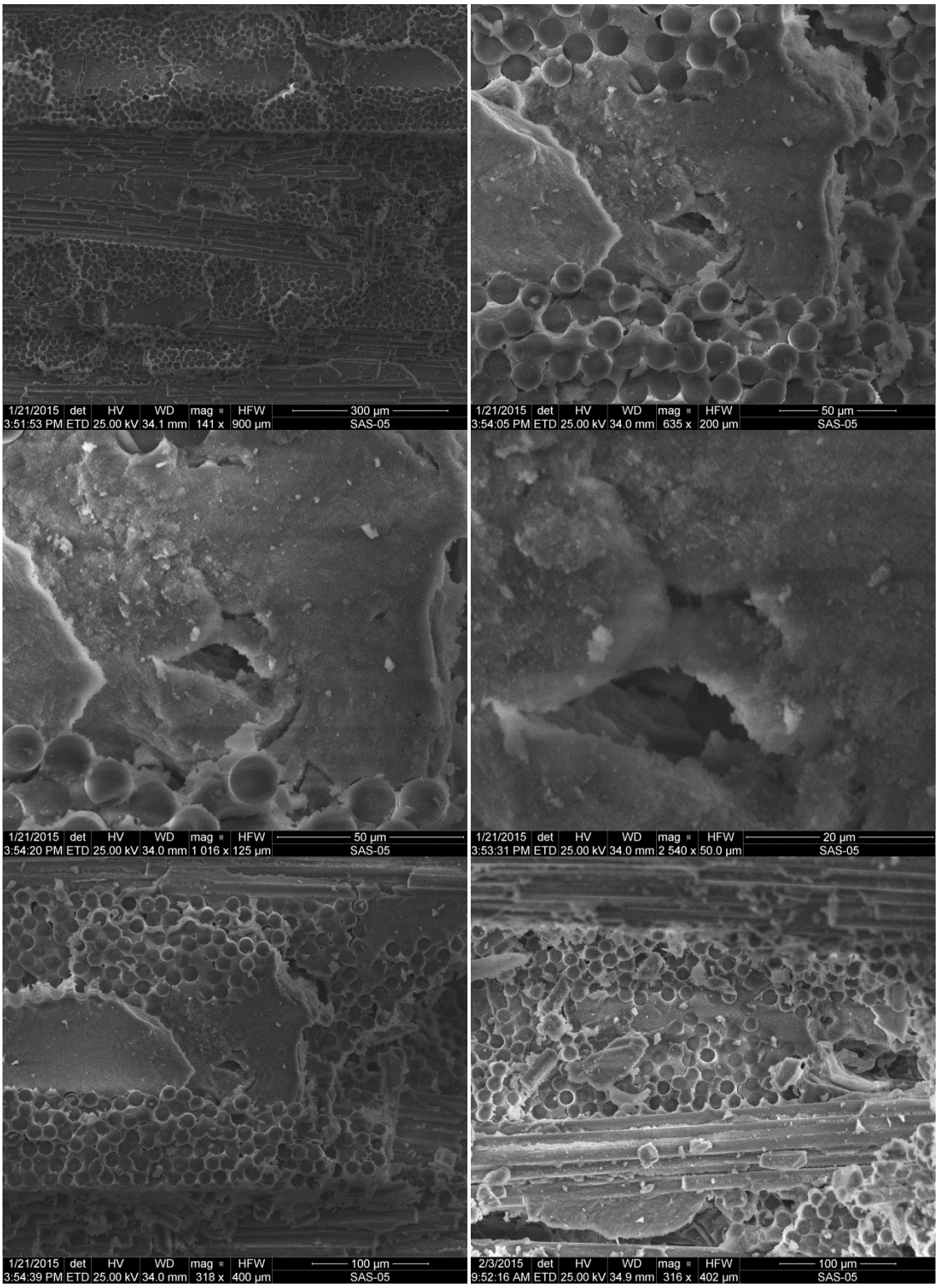

Figure G.13 – SEM micrographs of fracture surface of N720/AS composite obtained in tensile tests after heat treatment of 20 h at 1200°C (Specimen 2)

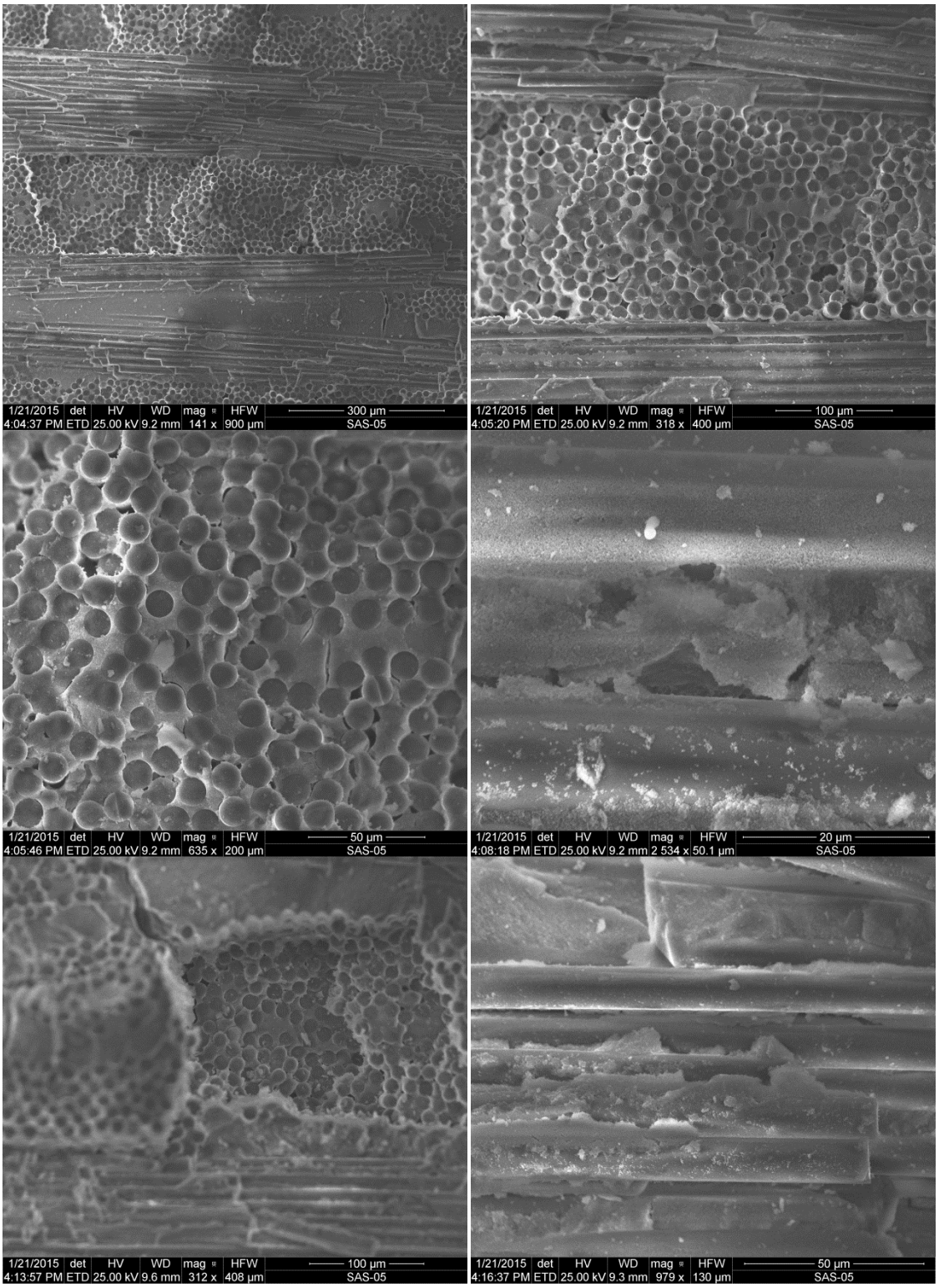

Figure G.14 – SEM micrographs of fracture surface of N720/AS composite obtained in tensile tests after heat treatment of 40 h at 1200°C (Specimen 3)

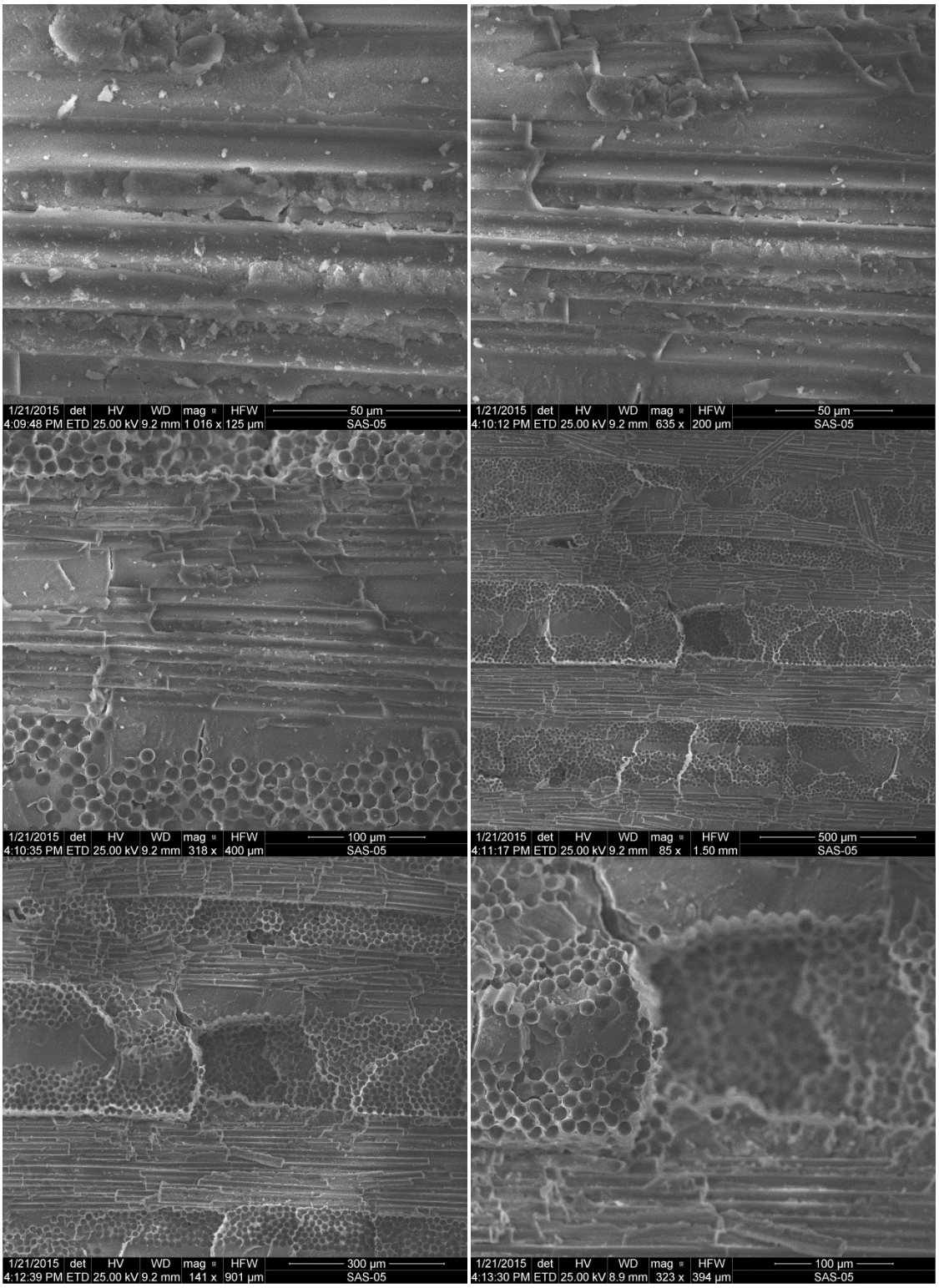

Figure G.15 – SEM micrographs of fracture surface of N720/AS composite obtained in tensile tests after heat treatment of 40 h at 1200°C (Specimen 3)

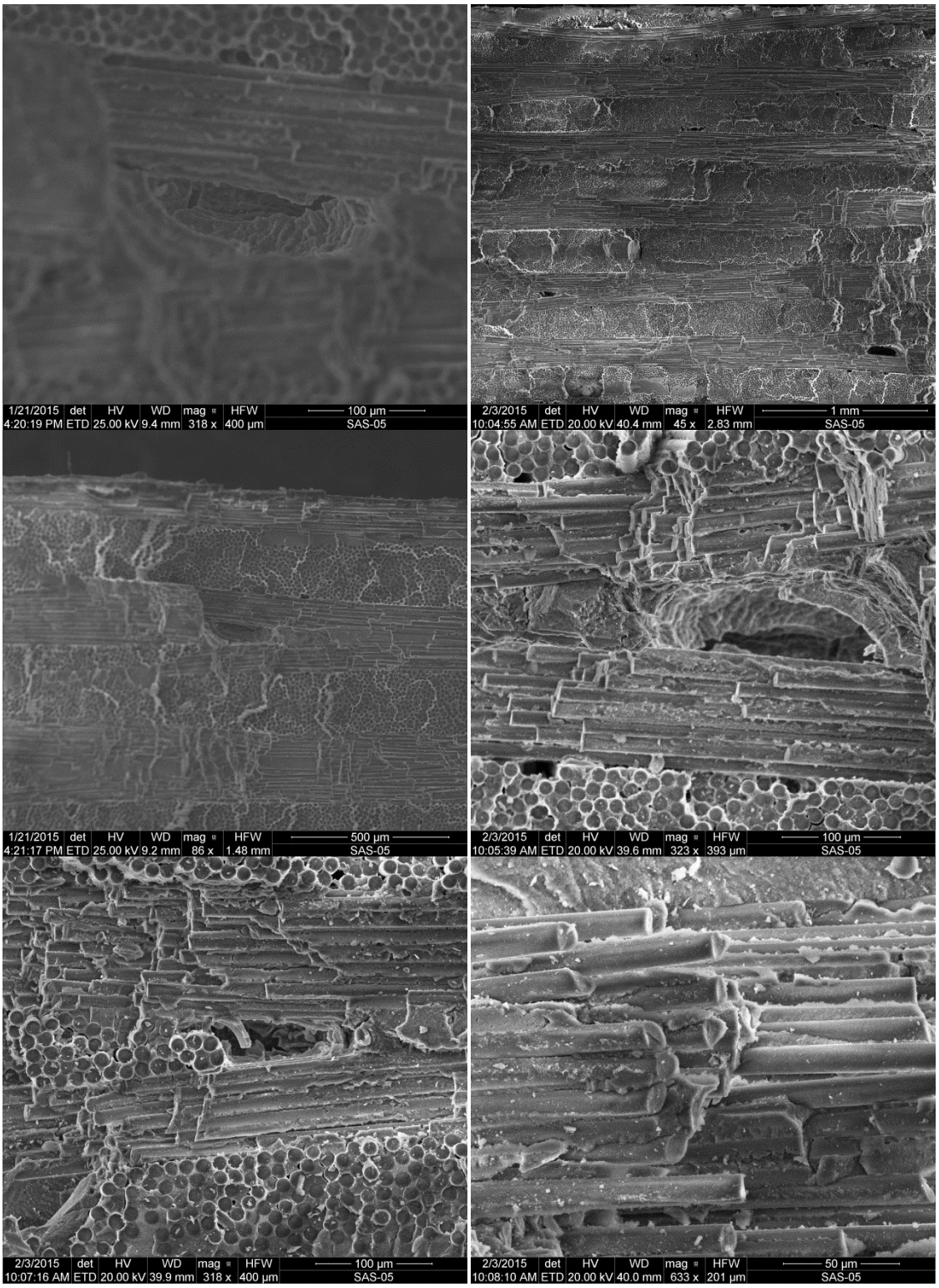

Figure G.16 – SEM micrographs of fracture surface of N720/AS composite obtained in tensile tests after heat treatment of 40 h at 1200°C (Specimen 3)

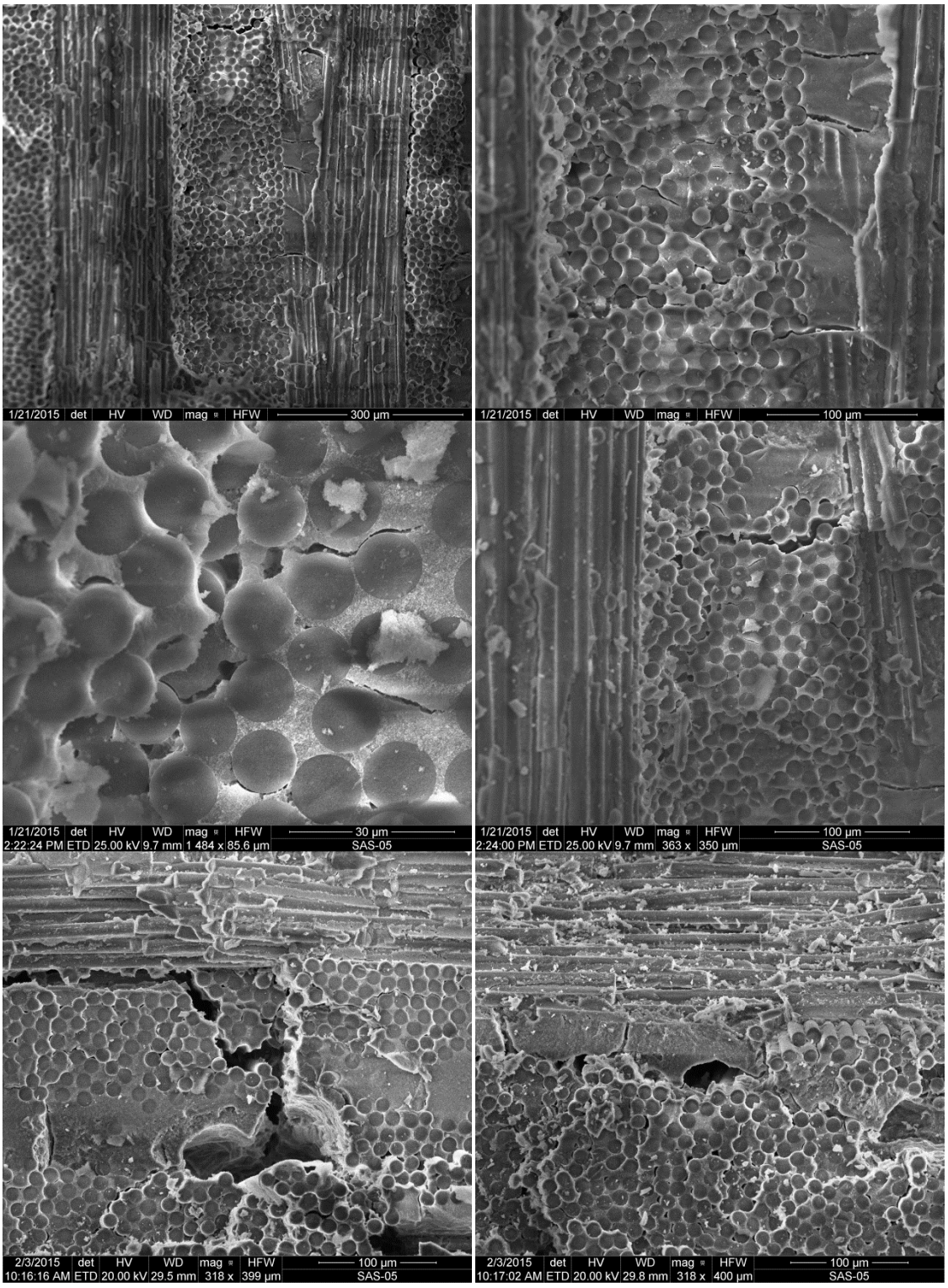

Figure G.17 – SEM micrographs of fracture surface of N720/AS composite obtained in tensile tests after heat treatment of 100 h at 1200°C (Specimen 4)

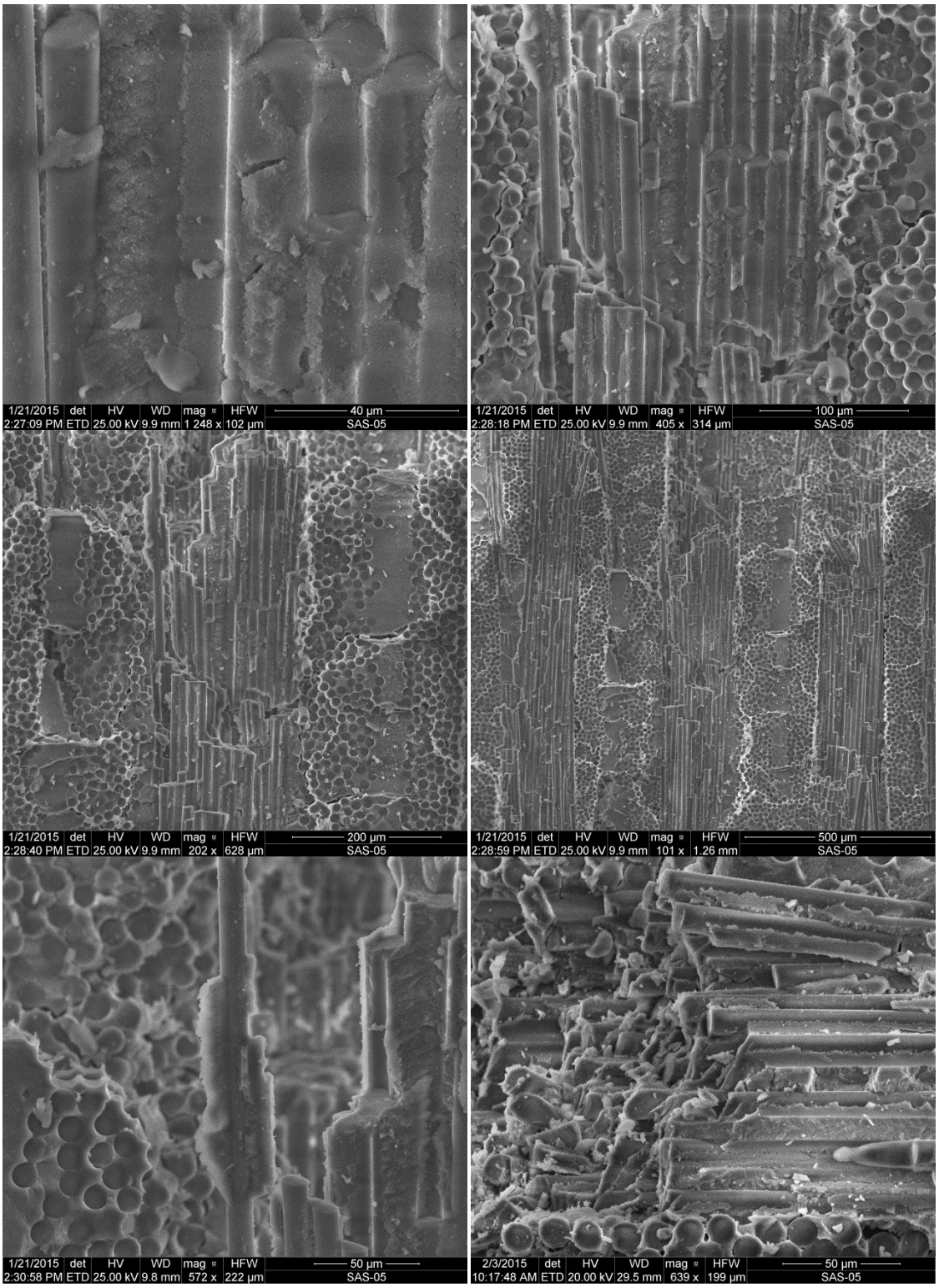

Figure G.18 – SEM micrographs of fracture surface of N720/AS composite obtained in tensile tests after heat treatment of 100 h at 1200°C (Specimen 4)

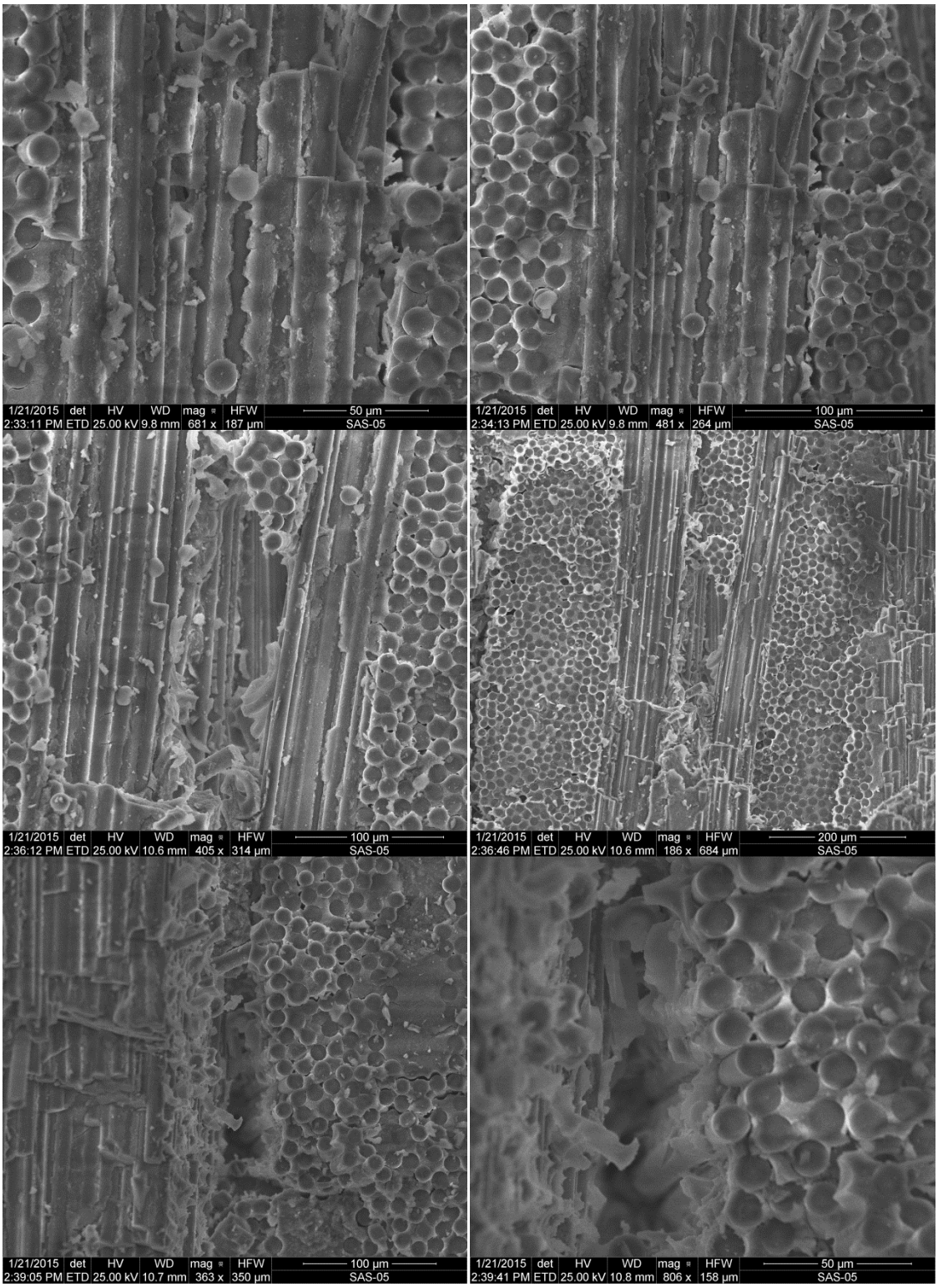

Figure G.19 – SEM micrographs of fracture surface of N720/AS composite obtained in tensile tests after heat treatment of 100 h at 1200°C (Specimen 4)

Appendix H - Additional SEM Micrographs of N720/A Fracture Surfaces

Appendix H presents additional SEM micrographs of the fracture surfaces of N720/A specimens produced in tensile tests.

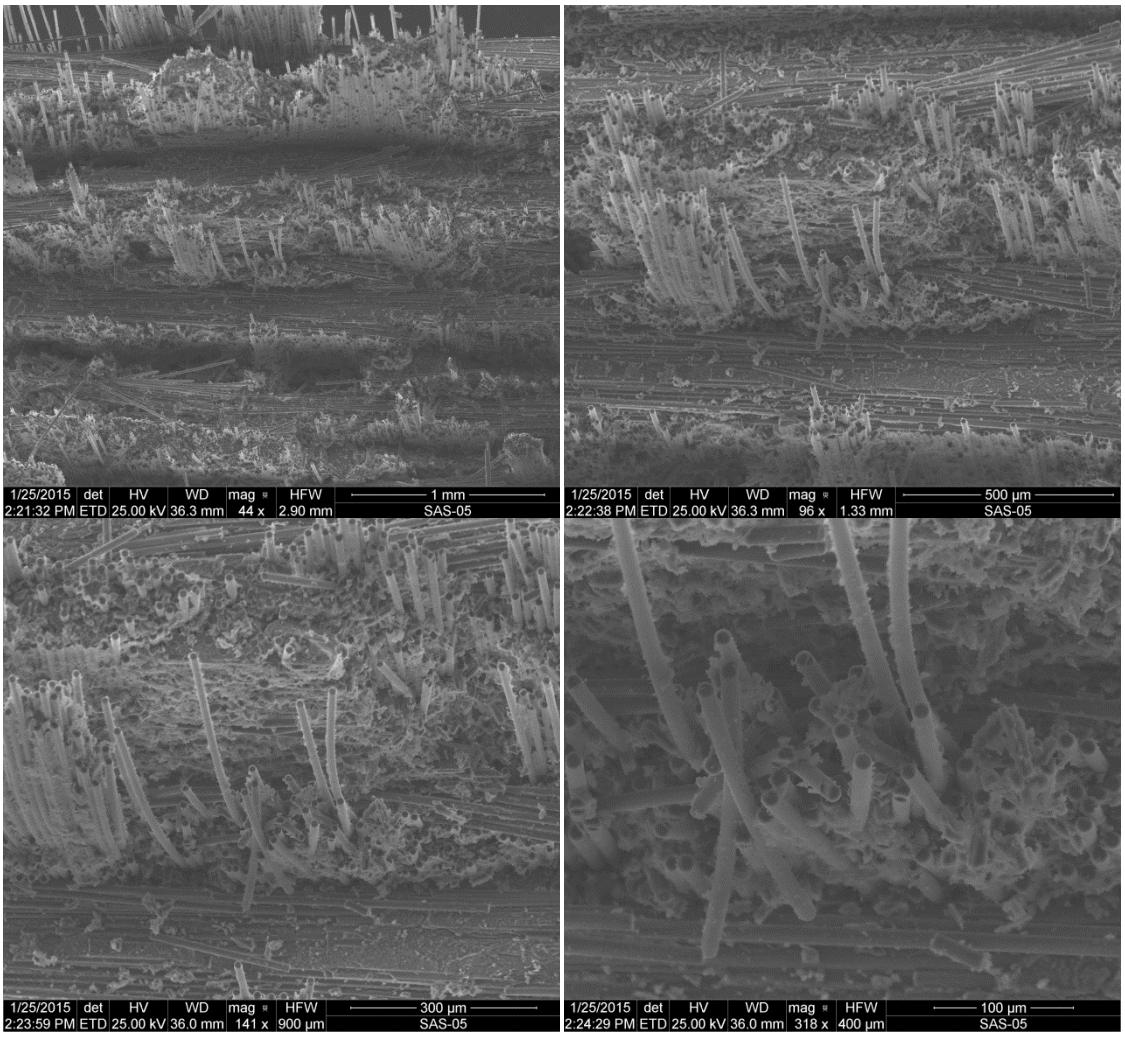

Figure H.1 – SEM micrographs of fracture surface of as-received N720/A composite obtained in tensile tests (Specimen 5)

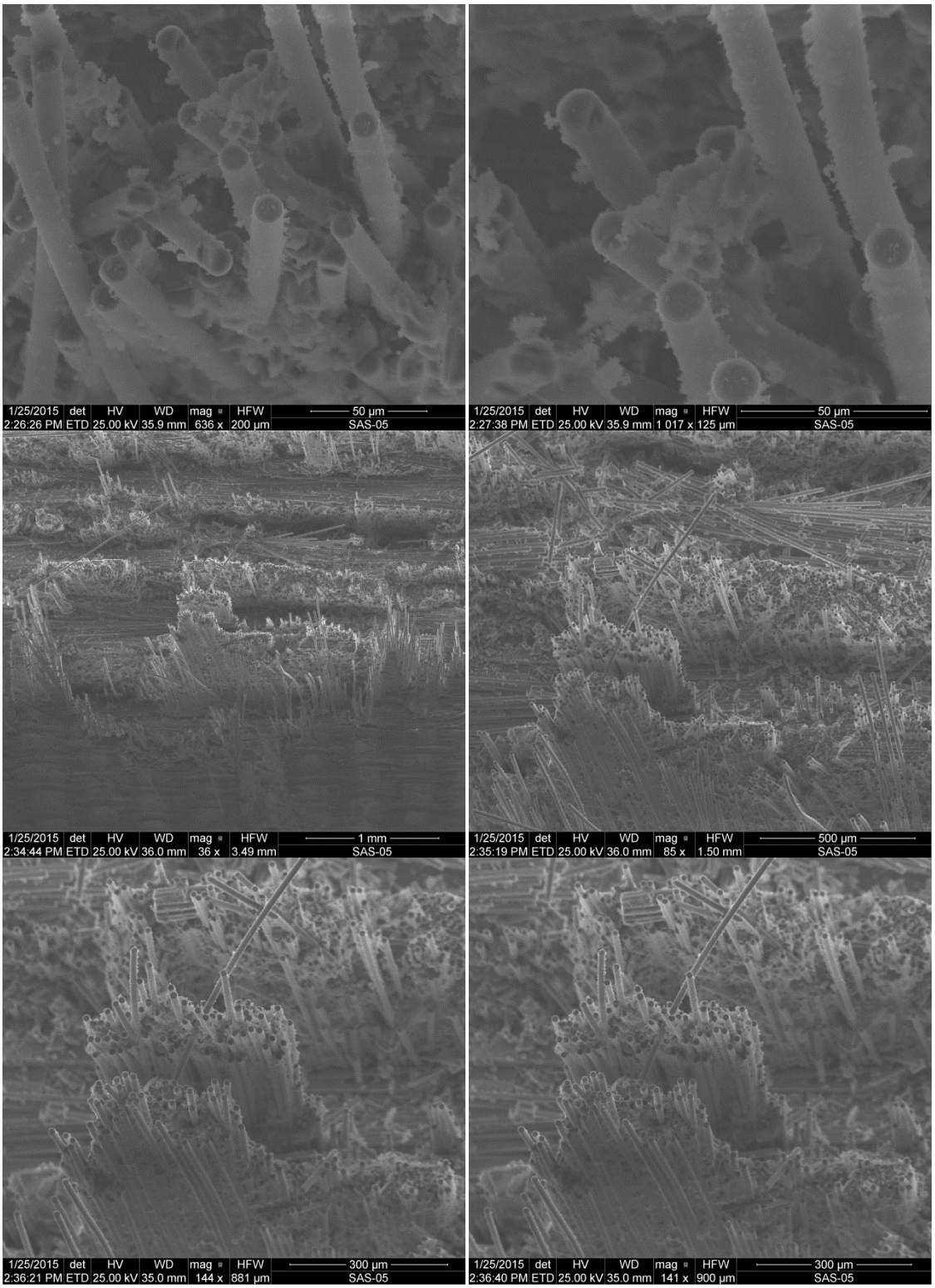

Figure H.2 – SEM micrographs of fracture surface of as-received N720/A composite obtained in tensile tests (Specimen 5)

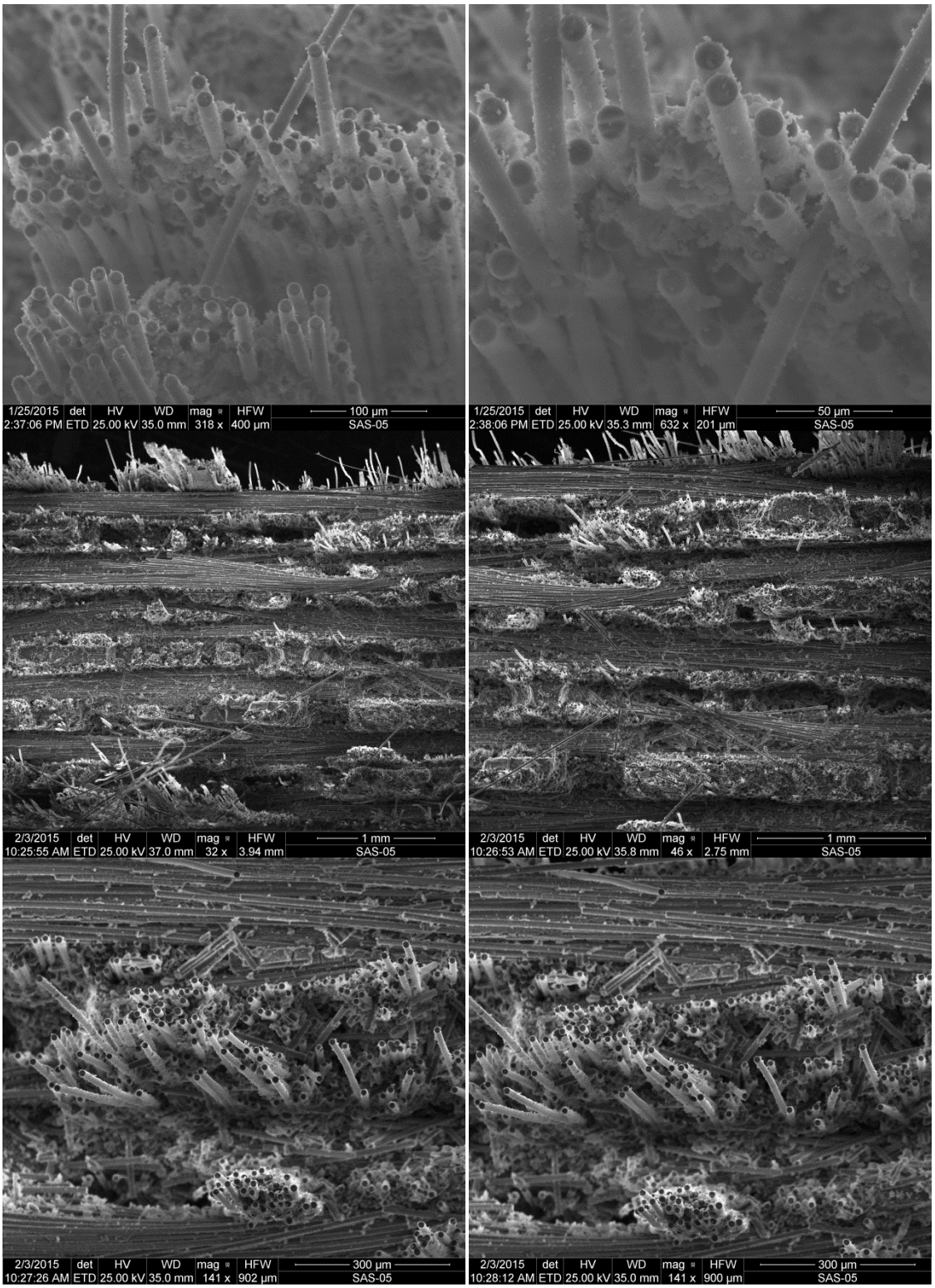

Figure H.3 – SEM micrographs of fracture surface of as-received N720/A composite obtained in tensile tests (Specimen 5)

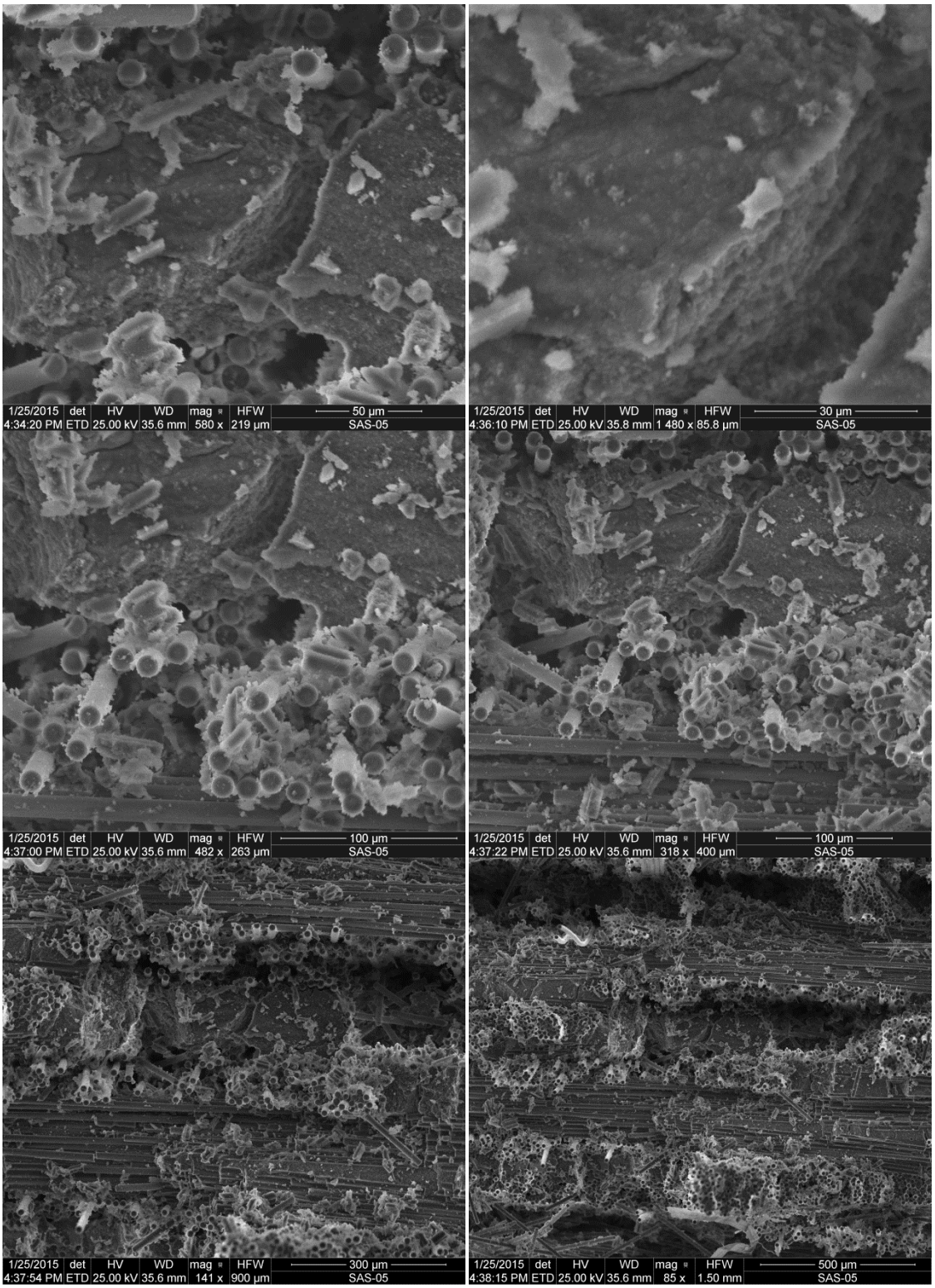

Figure H.4 – SEM micrographs of fracture surface of N720/A composite obtained in tensile tests after heat treatment of 100 h at 1200°C (Specimen 2)

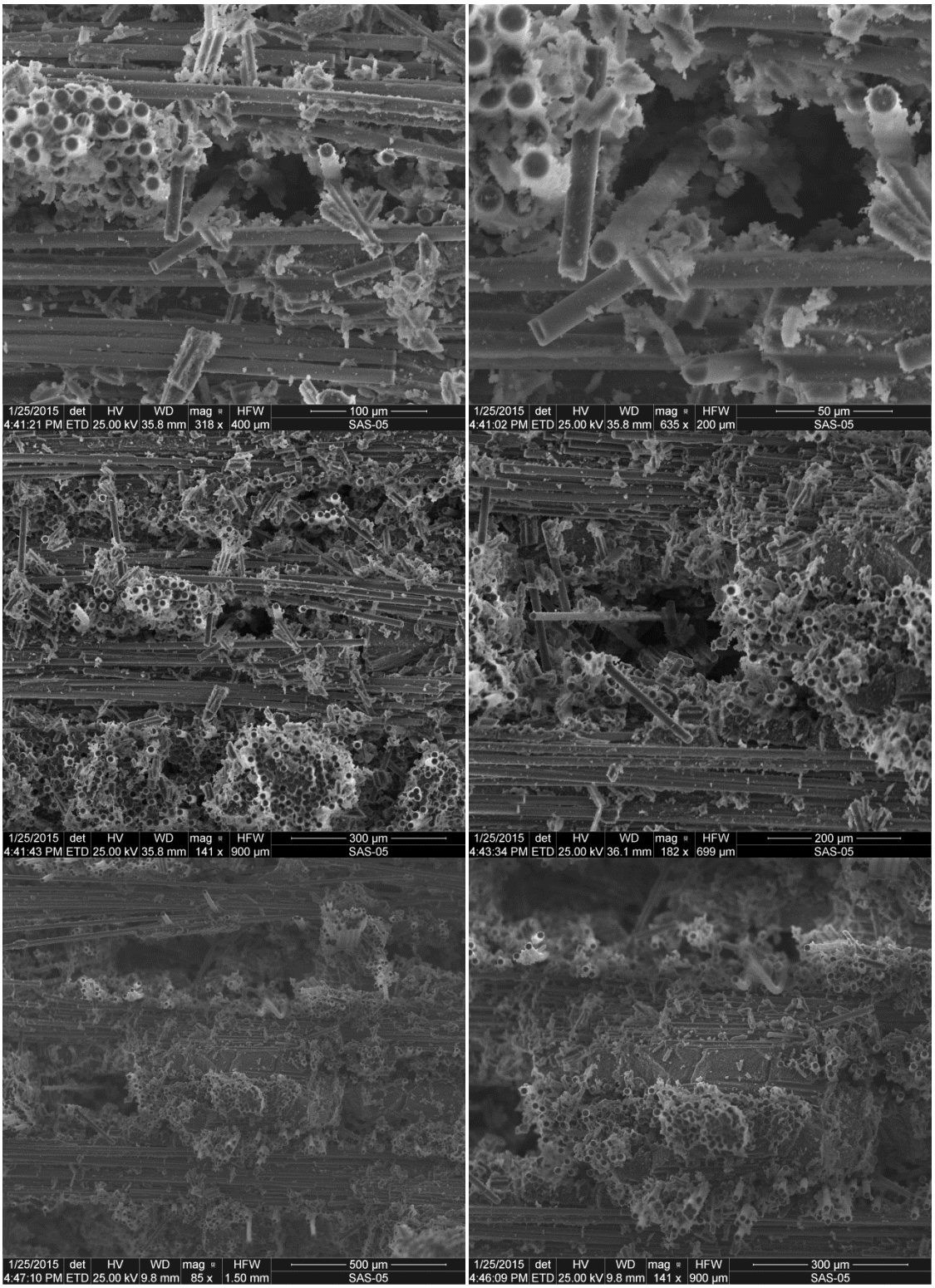

Figure H.5 – SEM micrographs of fracture surface of N720/A composite obtained in tensile tests after heat treatment of 100 h at 1200°C (Specimen 2)

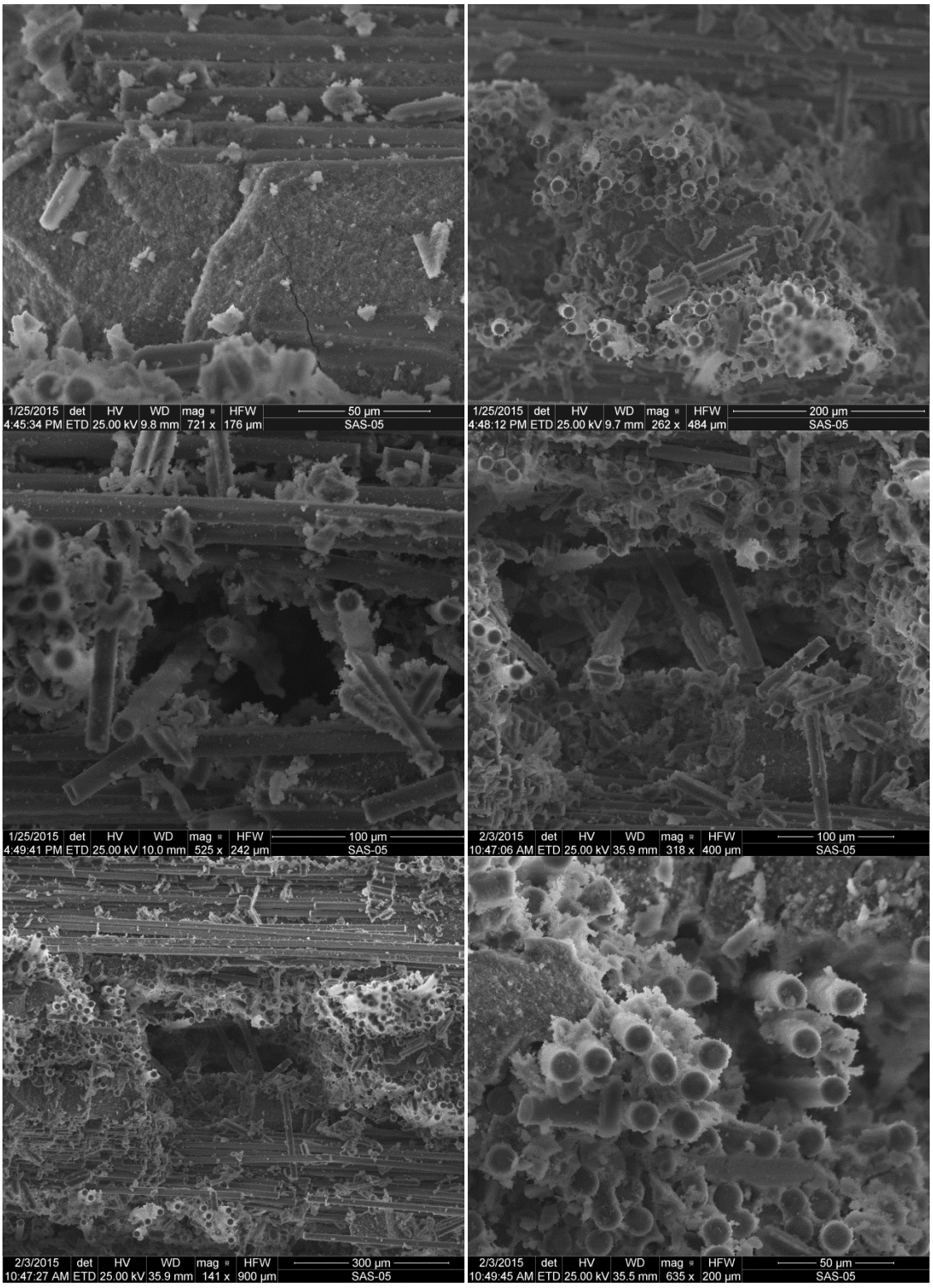

Figure H.6 – SEM micrographs of fracture surface of N720/A composite obtained in tensile tests after heat treatment of 100 h at 1200°C (Specimen 2)

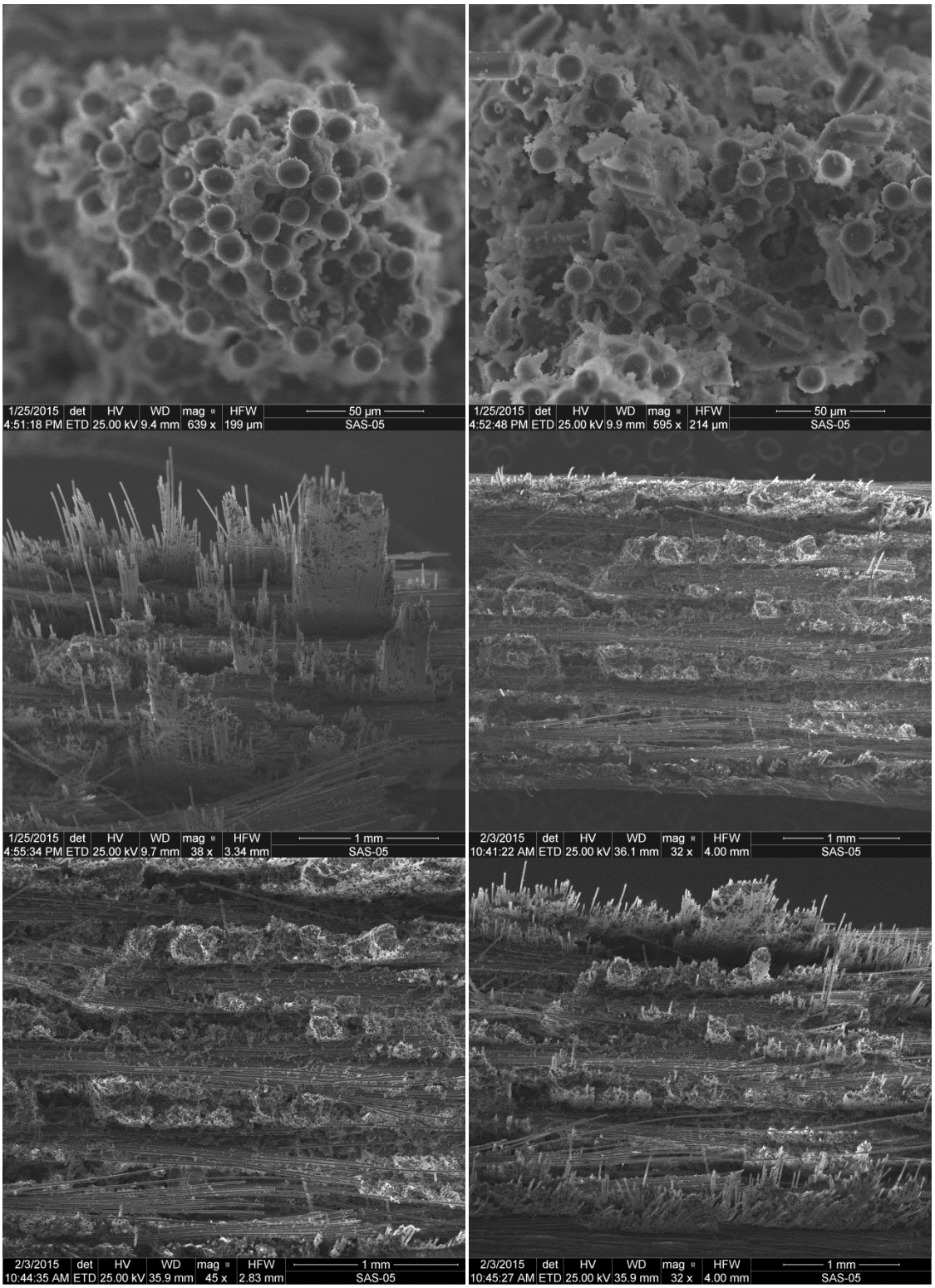

Figure H.7 – SEM micrographs of fracture surface of N720/A composite obtained in tensile tests after heat treatment of 100 h at 1200°C (Specimen 2)

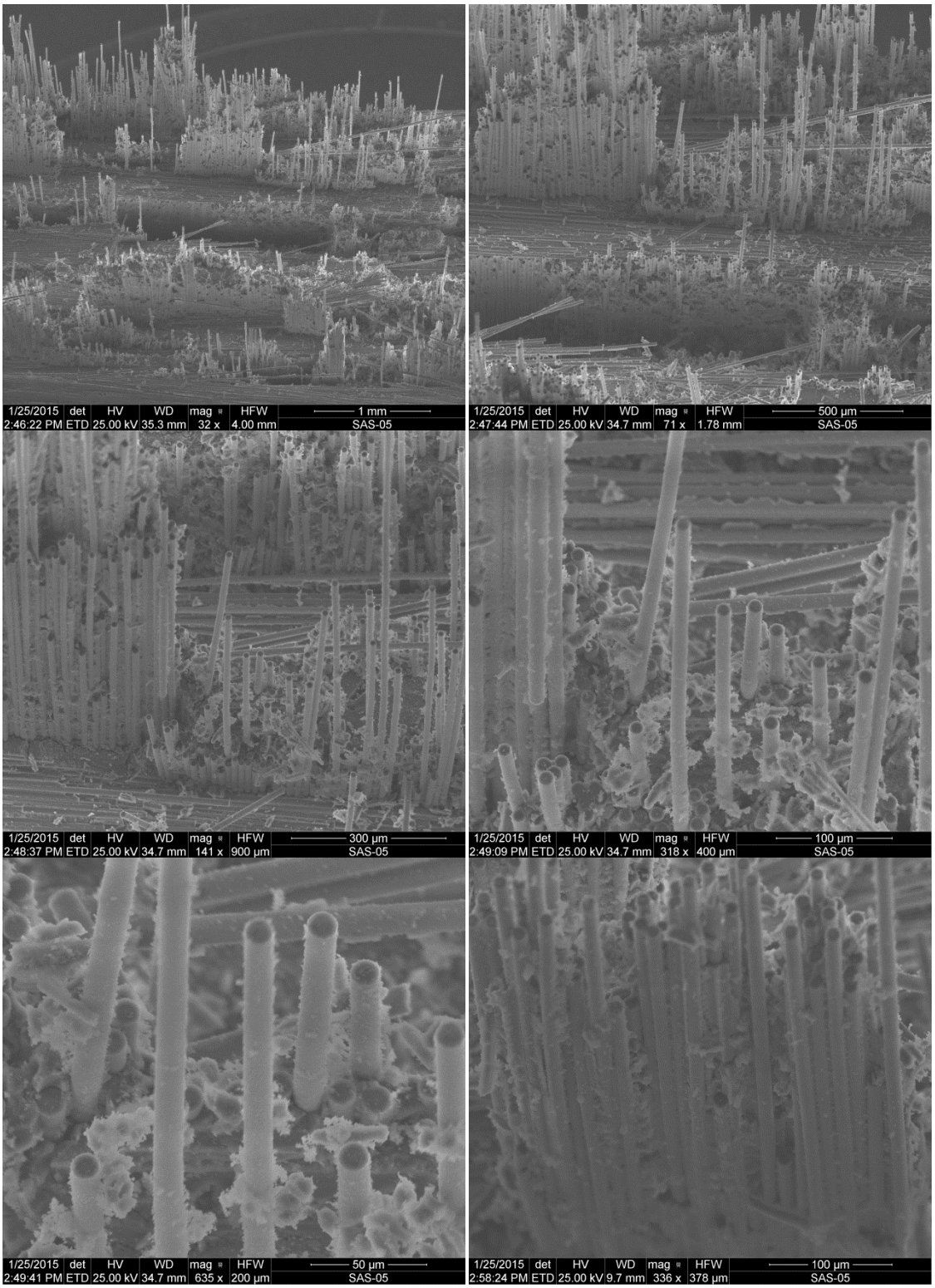

Figure H.8 – SEM micrographs of fracture surface of N720/A composite obtained in tensile tests after heat treatment of 10 h at 1300°C (Specimen 2)

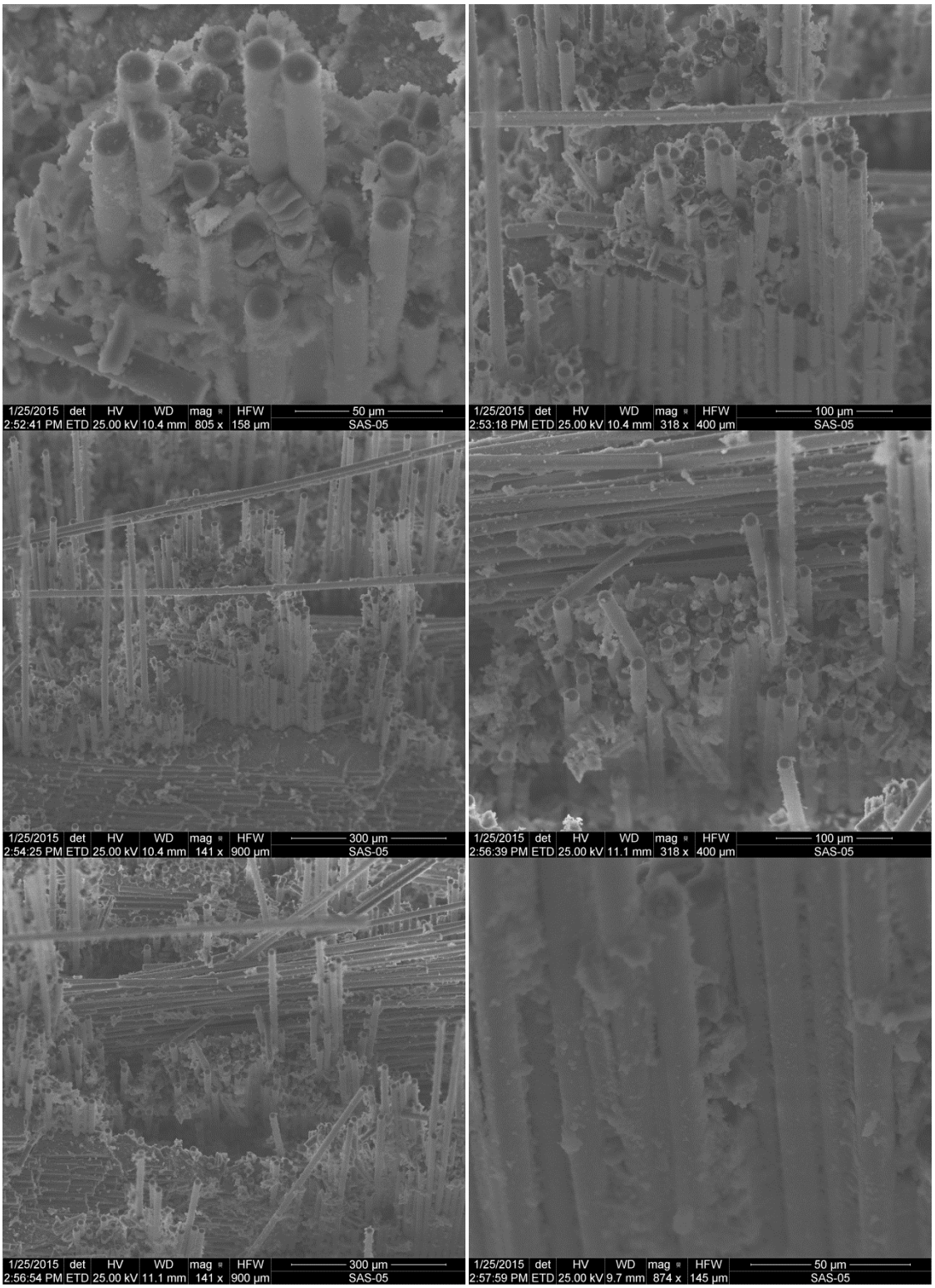

Figure H.9 – SEM micrographs of fracture surface of N720/A composite obtained in tensile tests after heat treatment of 10 h at 1300°C (Specimen 2)

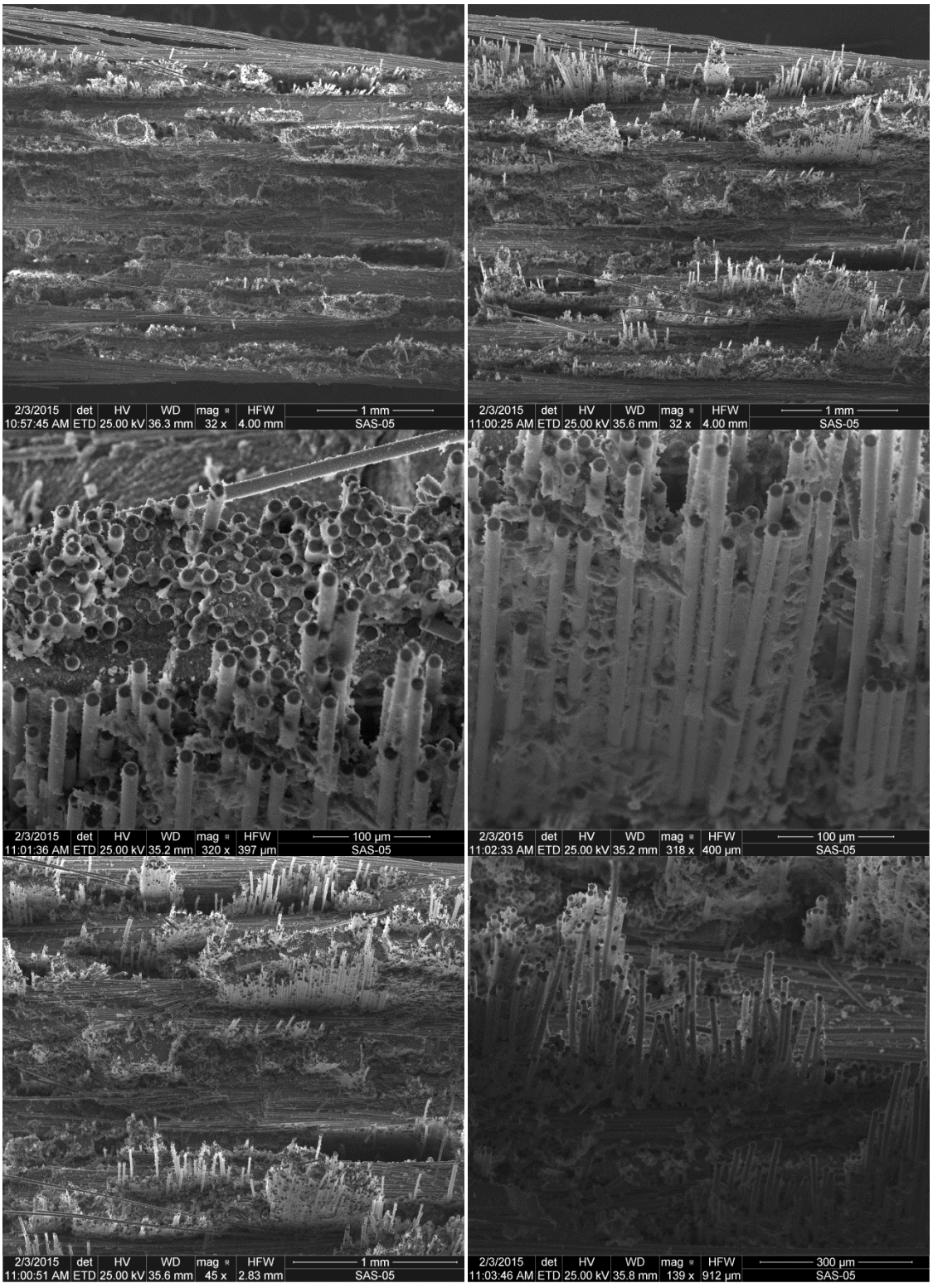

Figure H.10 – SEM micrographs of fracture surface of N720/A composite obtained in tensile tests after heat treatment of 10 h at 1300°C (Specimen 2)

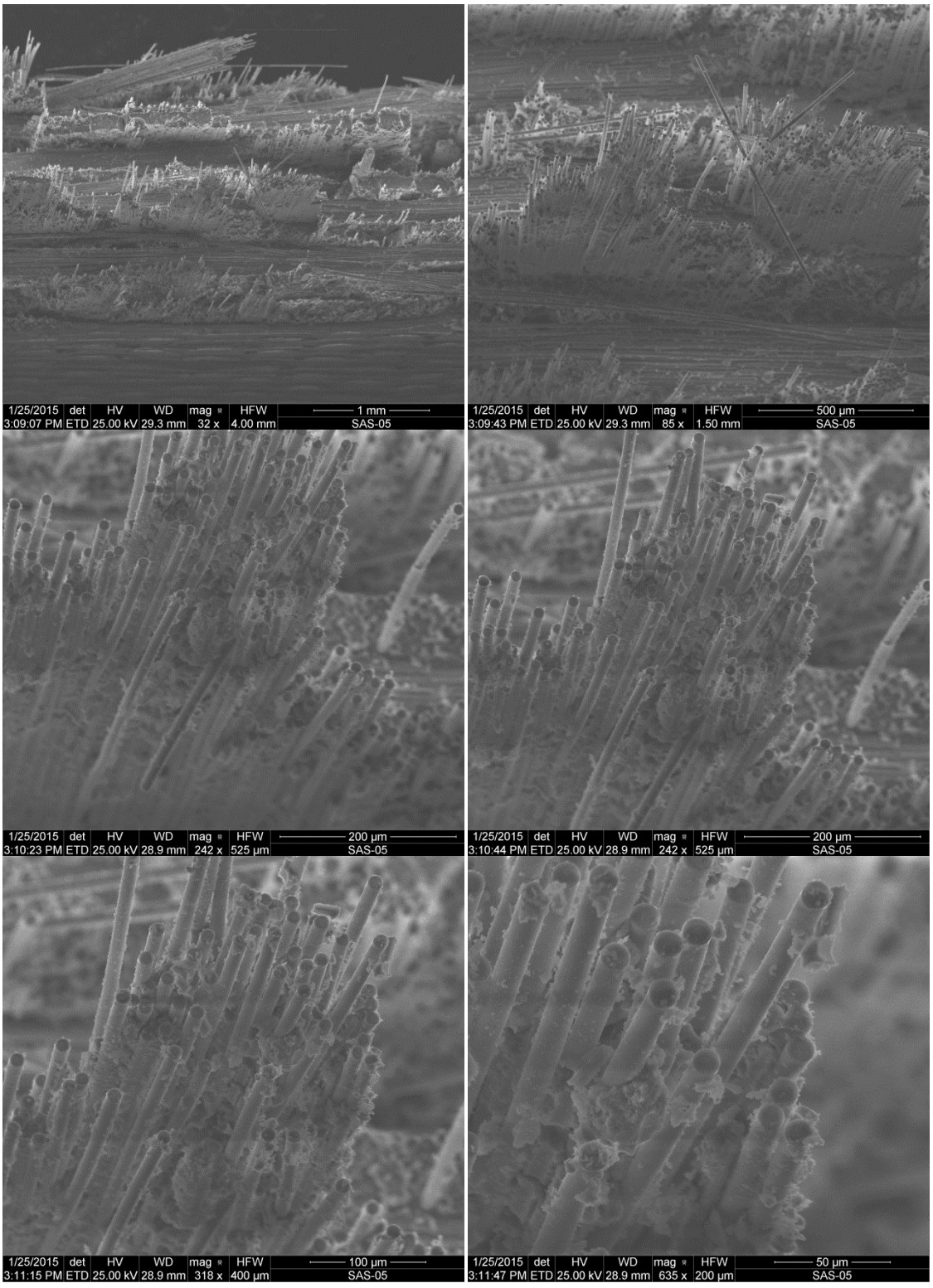

Figure H.11 – SEM micrographs of fracture surface of N720/A composite obtained in tensile tests after heat treatment of 20 h at 1300°C (Specimen 1)

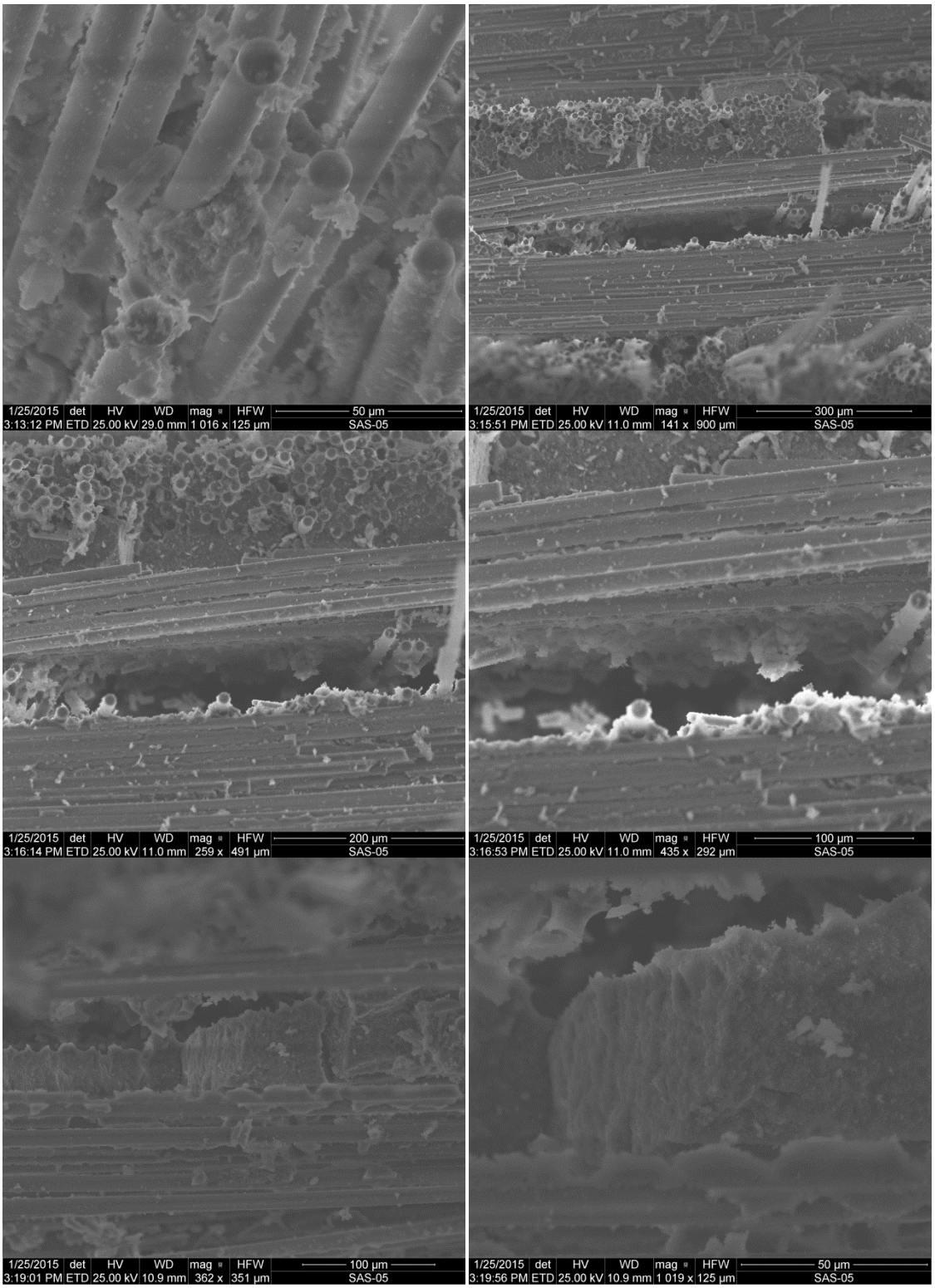

Figure H.12 – SEM micrographs of fracture surface of N720/A composite obtained in tensile tests after heat treatment of 20 h at 1300°C (Specimen 1)

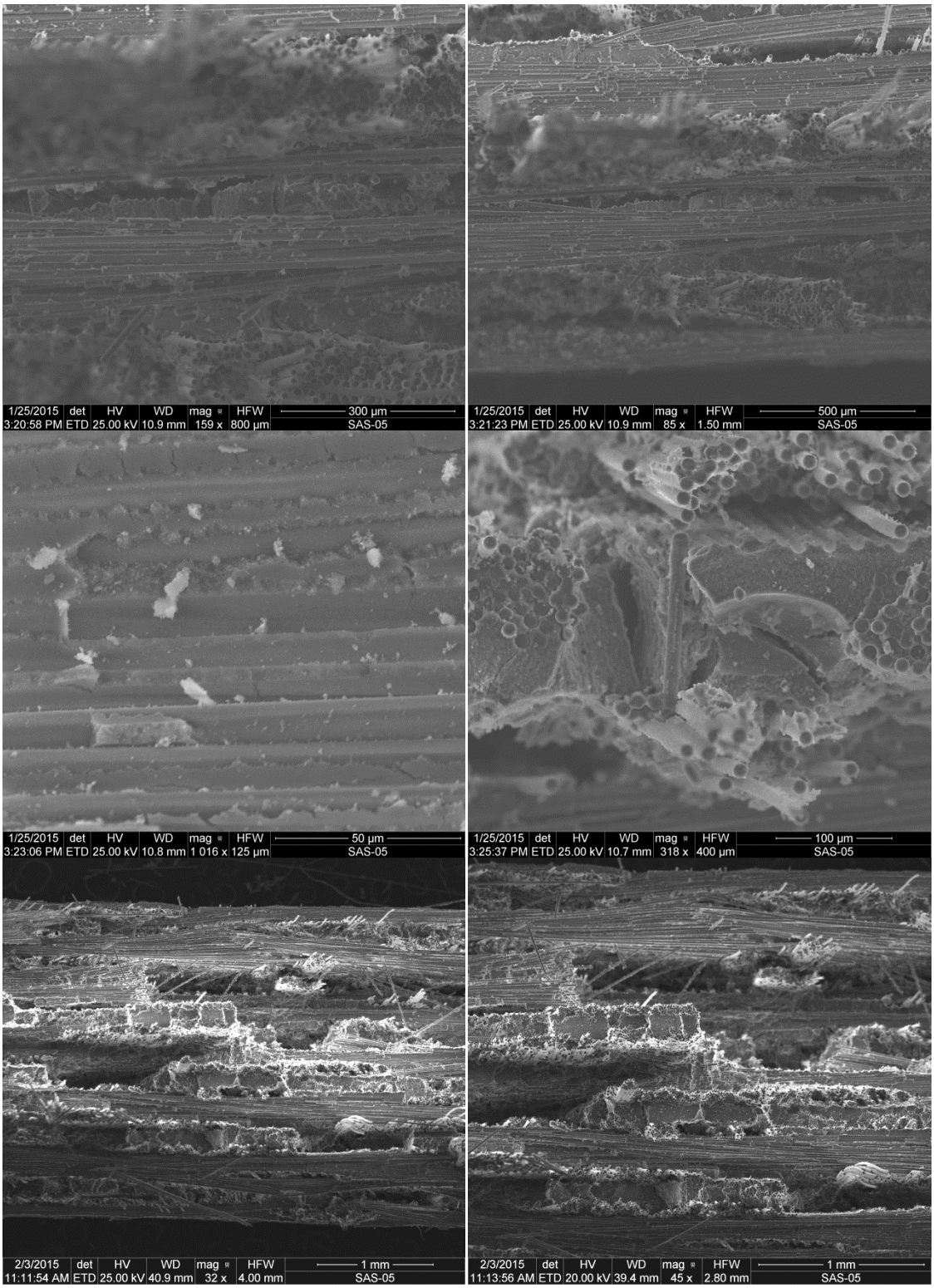

Figure H.13 – SEM micrographs of fracture surface of N720/A composite obtained in tensile tests after heat treatment of 20 h at 1300°C (Specimen 1)

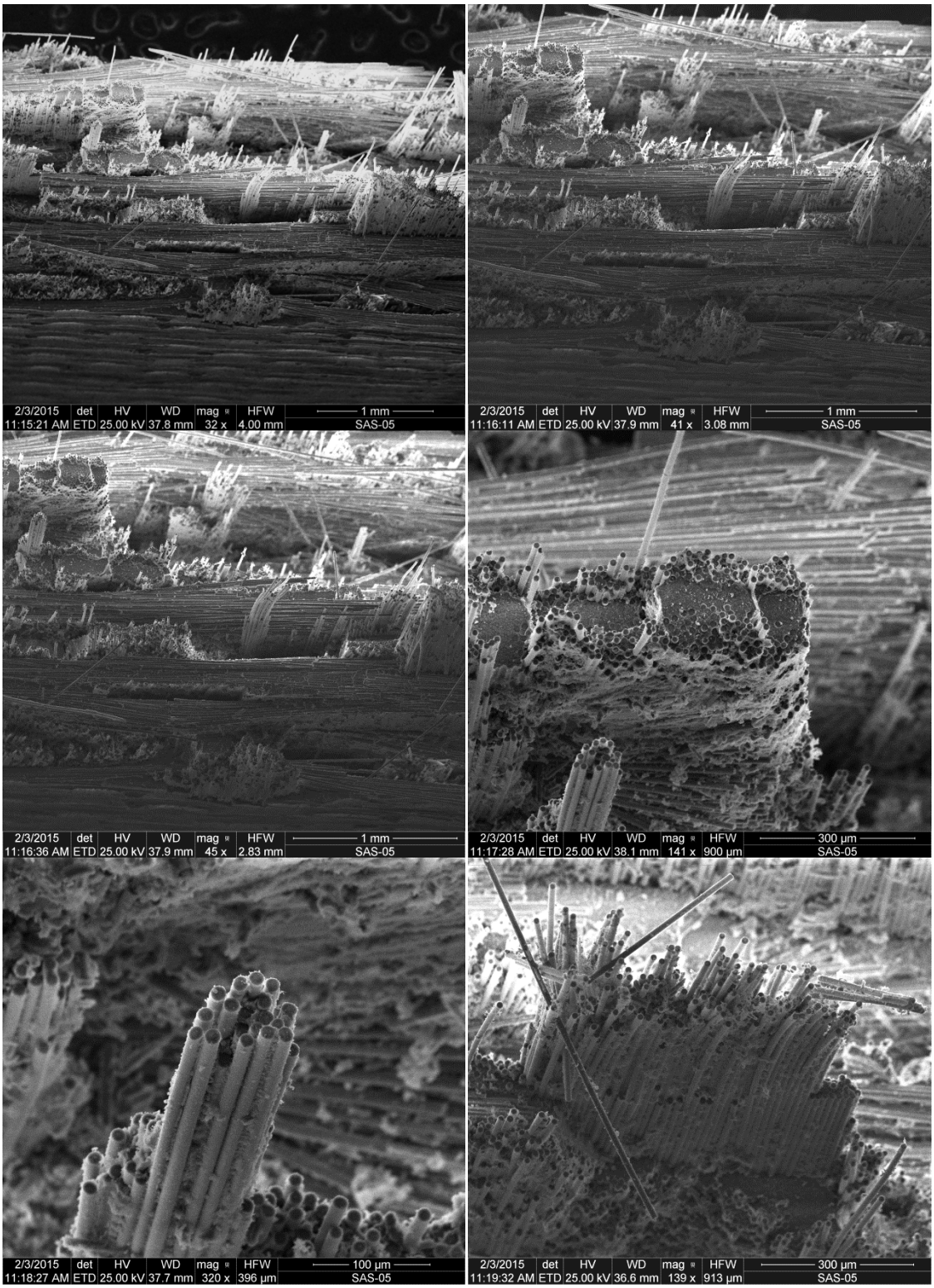

Figure H.14 – SEM micrographs of fracture surface of N720/A composite obtained in tensile tests after heat treatment of 20 h at 1300°C (Specimen 1)

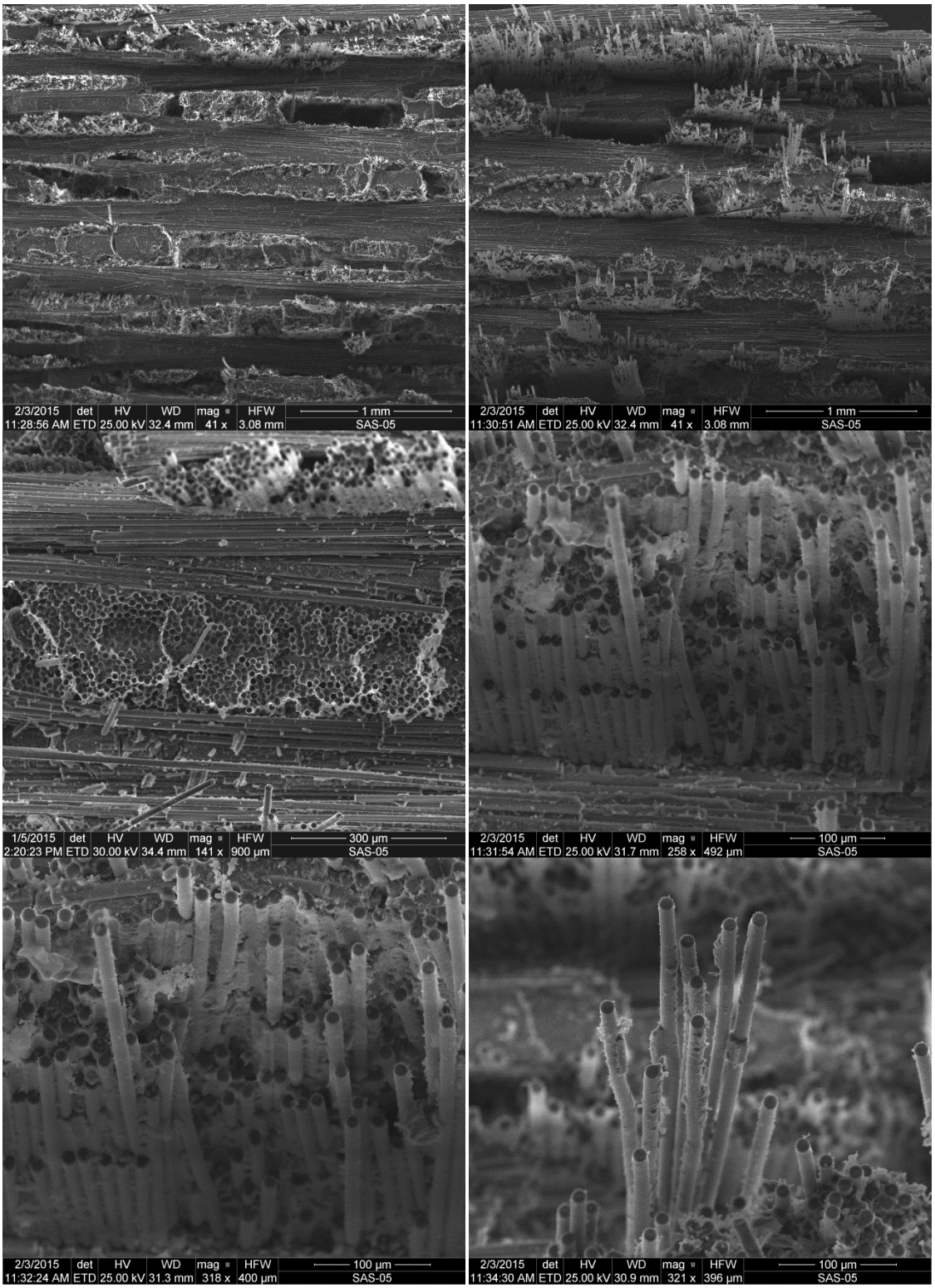

Figure H.15 – SEM micrographs of fracture surface of N720/A composite obtained in tensile tests after heat treatment of 40 h at 1300°C (Specimen 5)

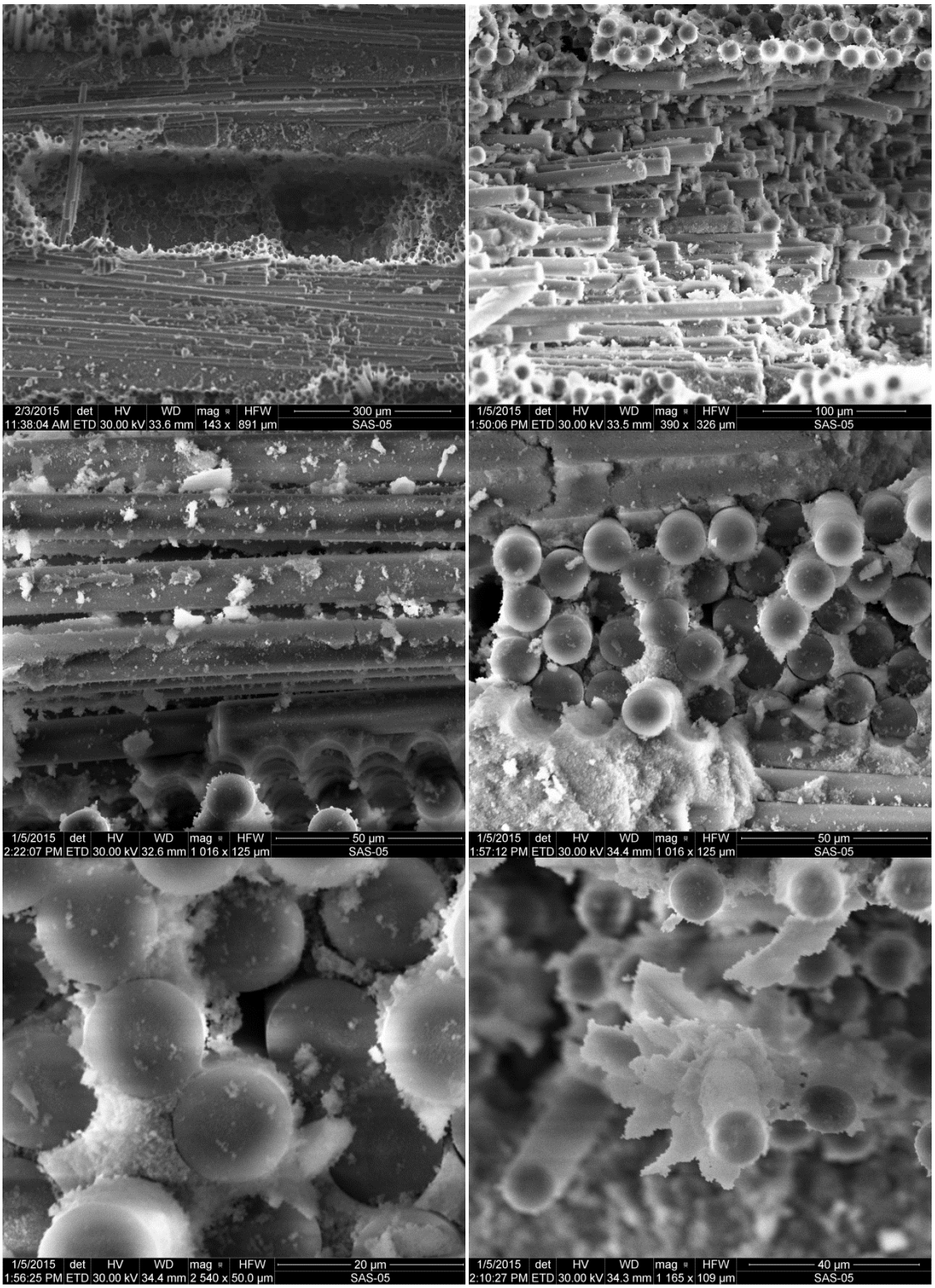

Figure H.16 – SEM micrographs of fracture surface of N720/A composite obtained in tensile tests after heat treatment of 40 h at 1300°C (Specimen 5)

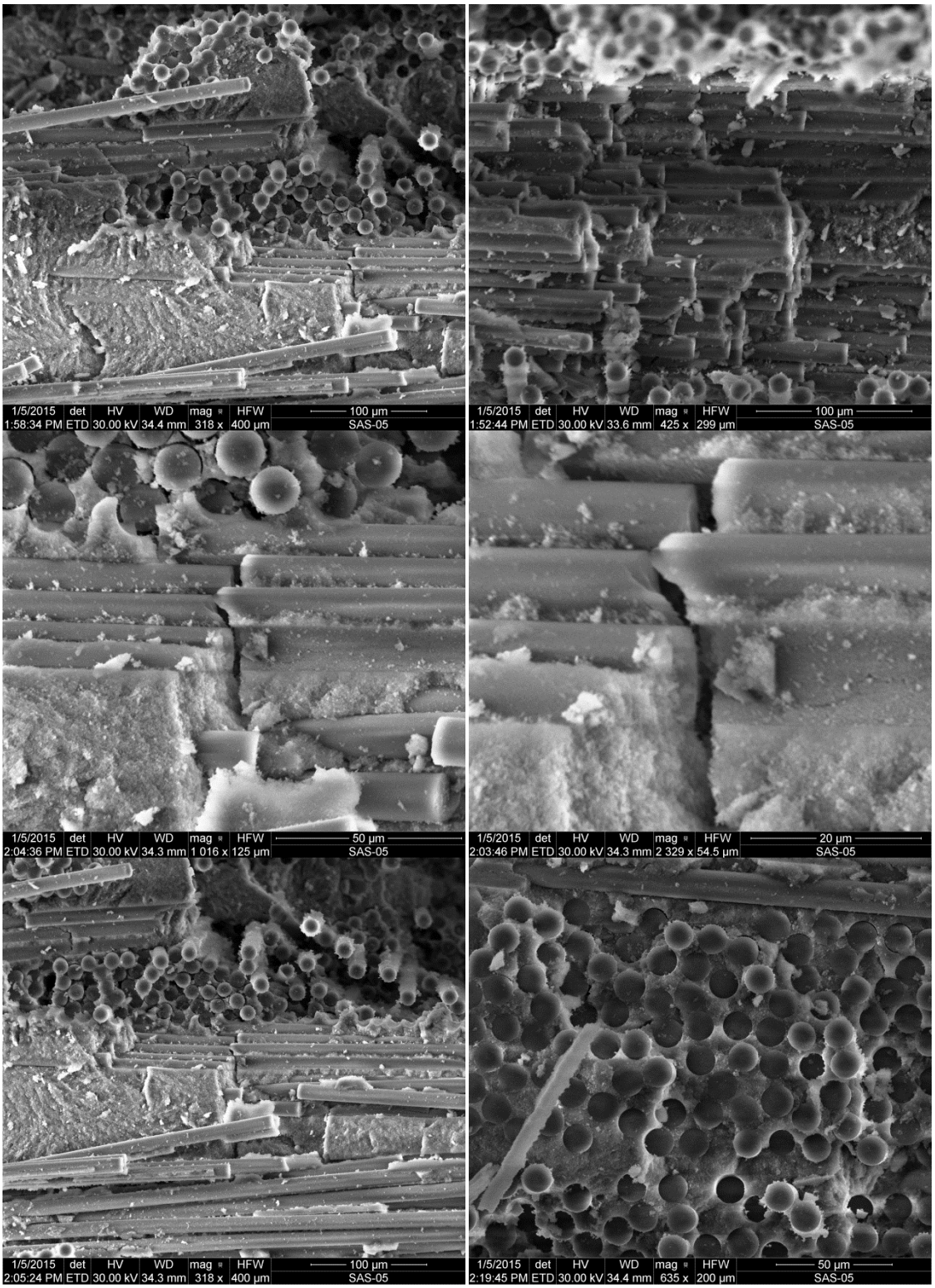

Figure H.17 – SEM micrographs of fracture surface of N720/A composite obtained in tensile tests after heat treatment of 40 h at 1300°C (Specimen 5)

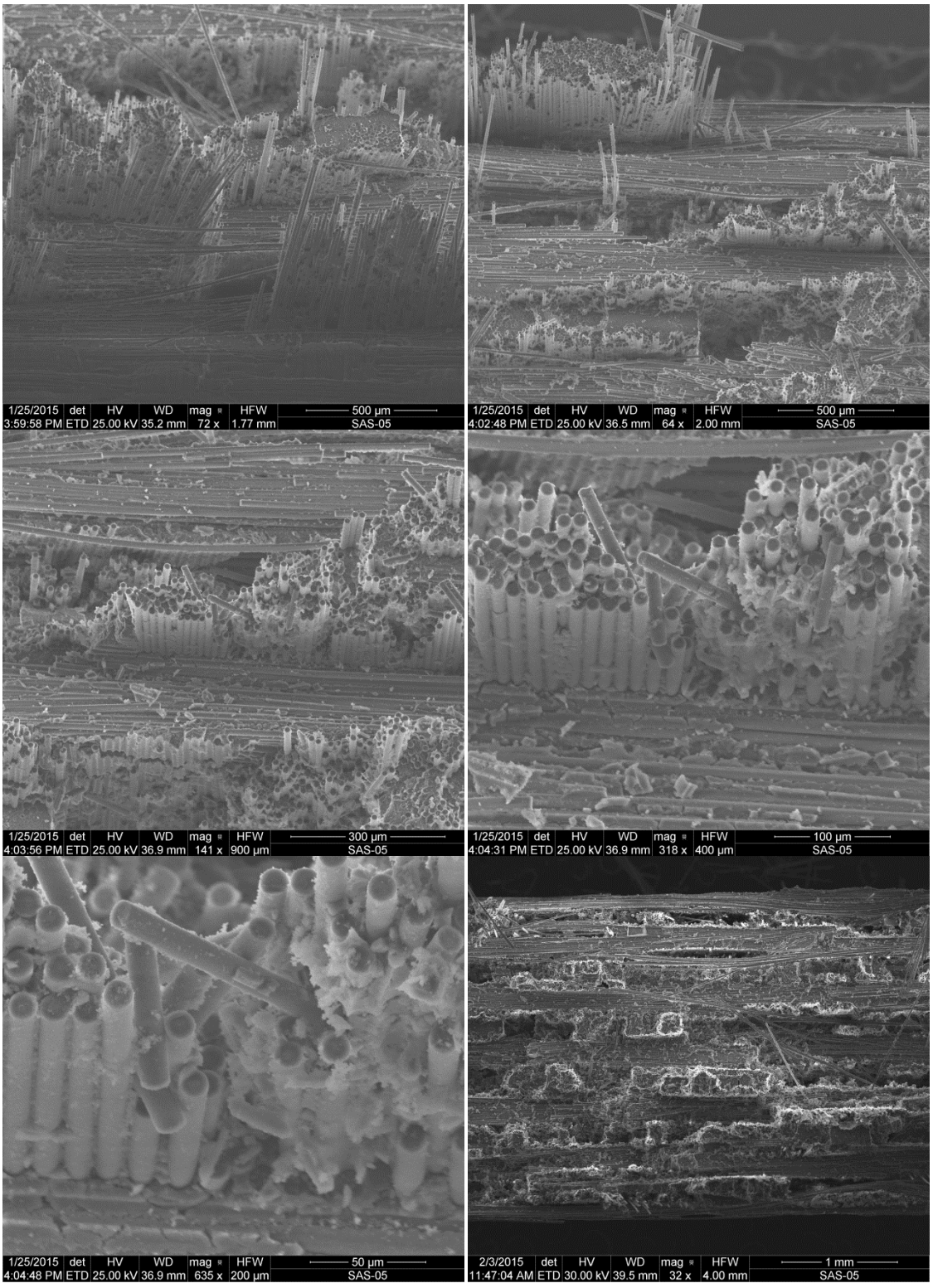

Figure H.18 – SEM micrographs of fracture surface of N720/A composite obtained in tensile tests after heat treatment of 100 h at 1300°C (Specimen 3)

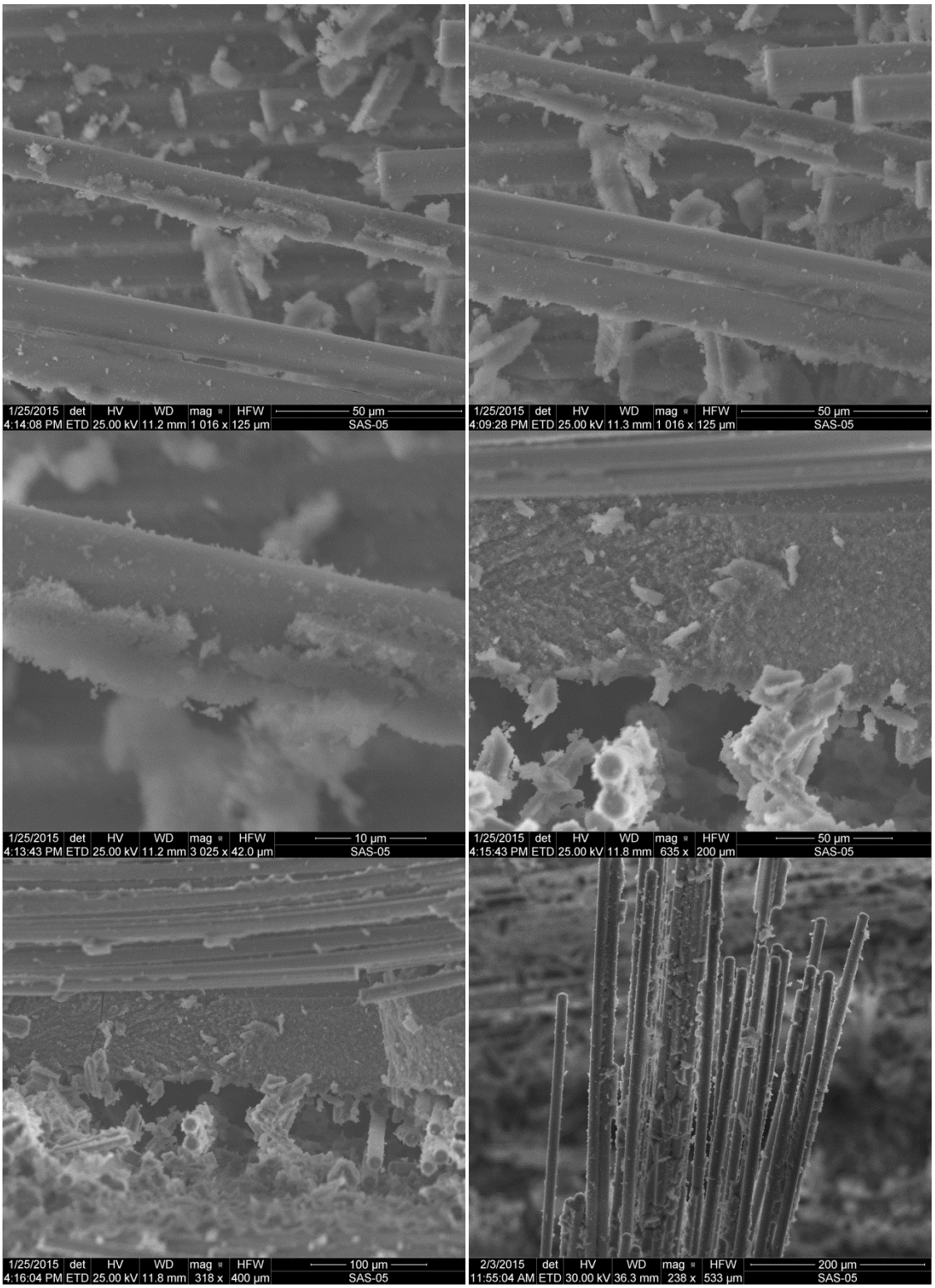

Figure H.19 – SEM micrographs of fracture surface of N720/A composite obtained in tensile tests after heat treatment of 100 h at 1300°C (Specimen 3)

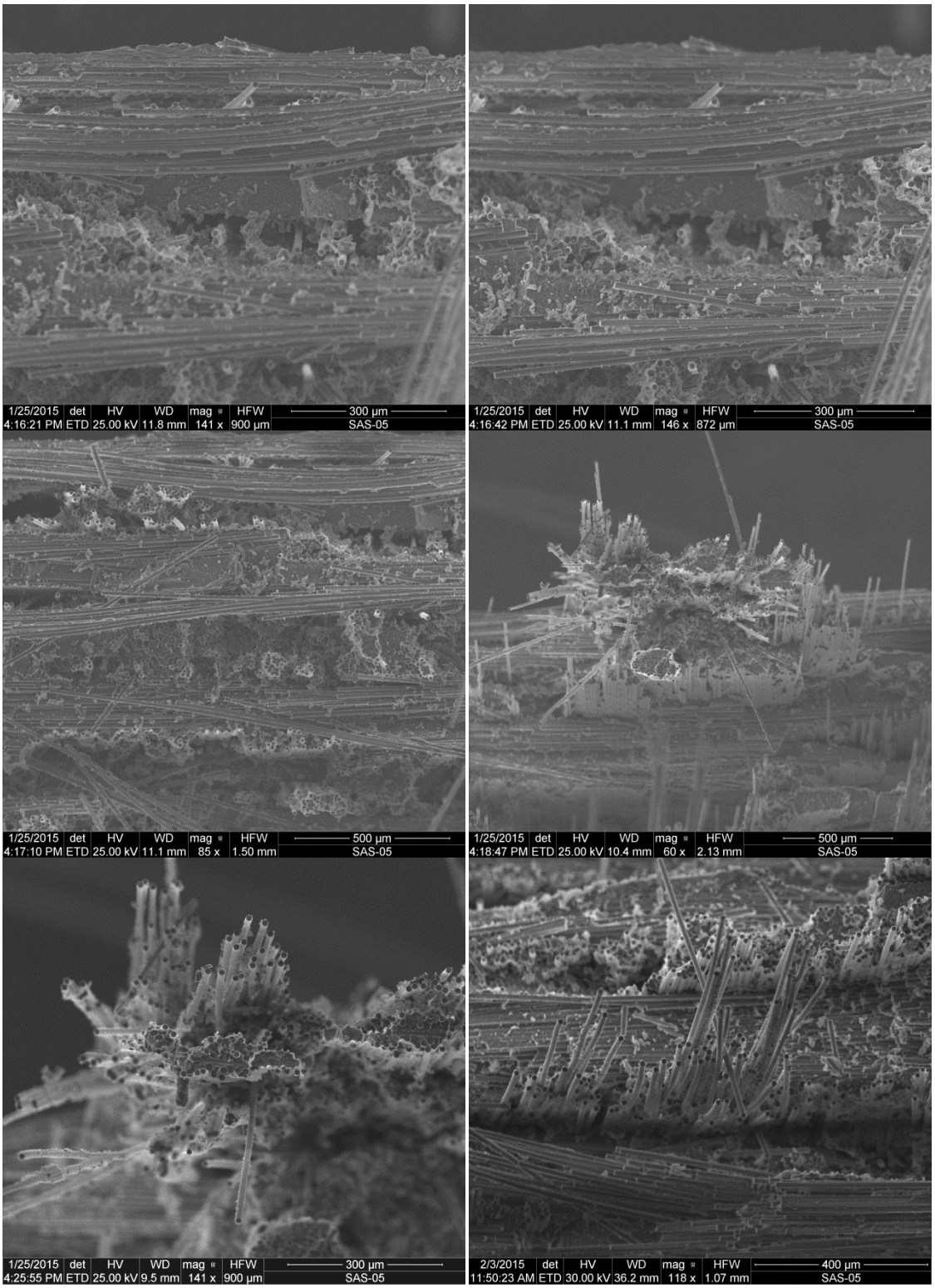

Figure H.20 – SEM micrographs of fracture surface of N720/A composite obtained in tensile tests after heat treatment of 100 h at 1300°C (Specimen 3)

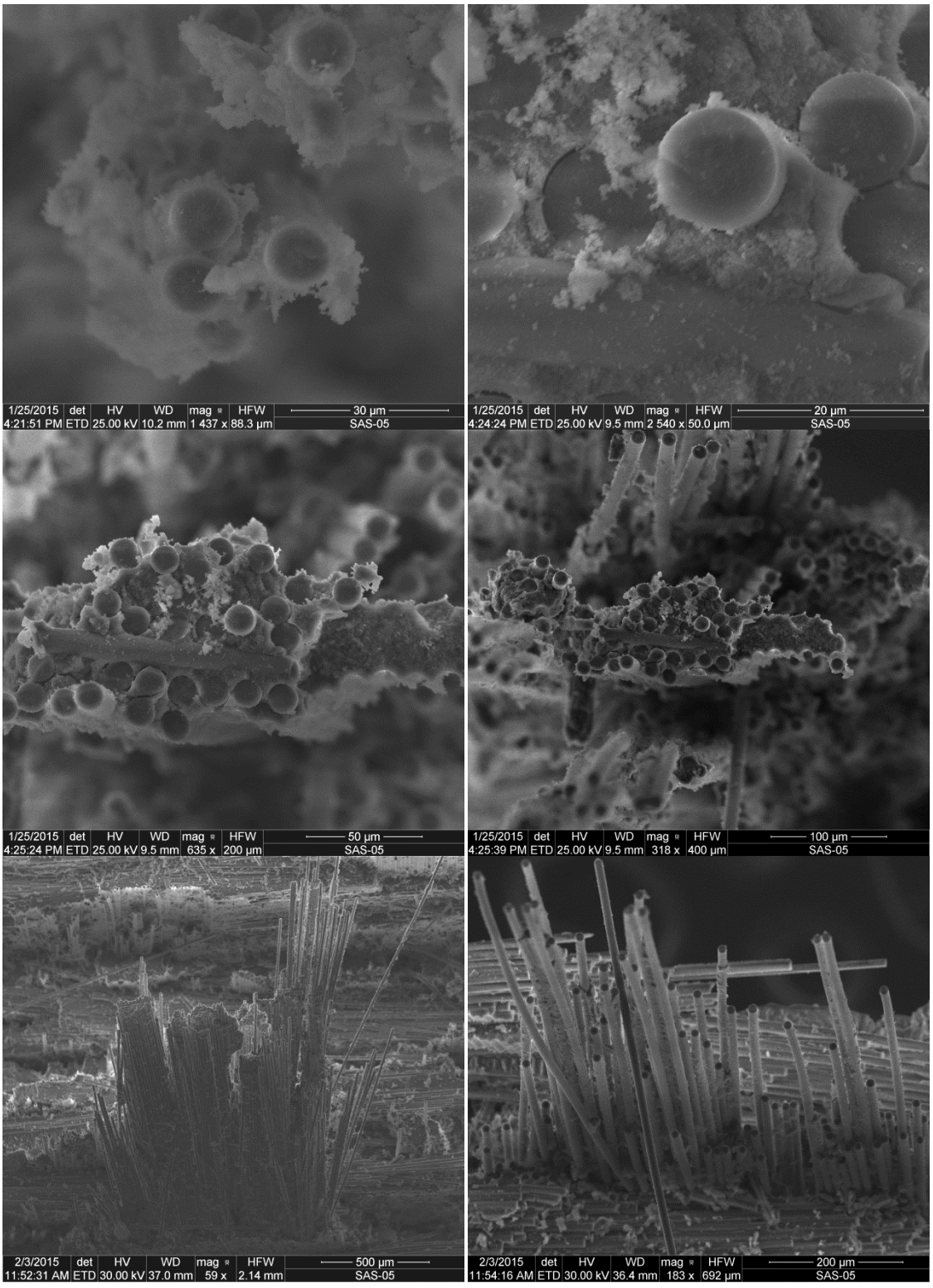

Figure H.21 – SEM micrographs of fracture surface of N720/A composite obtained in tensile tests after heat treatment of 100 h at 1300°C (Specimen 3)

References

[1] I. Cookson, "Sector Outperforms: 2008 M&A Activity Matches Prior-Year Record," *Aerospace Components,* pp. 1-5, February 2009.

[2] M. Ruggles-Wrenn, "Environmental Effects on Oxide/Oxide Composites," in *Ceramic Matrix Composites: Materials, Modeling and Technology*, N. P. Bansal and J. Lamon, Eds., John Wiley & Sons, Inc, 2014, pp. 295-333.

[3] A. Silnes, "The American Ceramic Society," 19 May 2014. [Online]. Available: http://ceramics.org/learn-about-ceramics/history-of-ceramics. [Accessed Jan 2015].

[4] K. K. Chawla, Ceramic Matrix Composites, London: Chapman & Hall, 1993.

[5] M. T. Pope, "Creep Behavior in Interlaminar Shear of a CVI SiC/SiC Composite at Elveated Temperature in Air and in Steam," Air Force Institute of Technology, Wright-Patterson AFB, OH, 2012.

[6] R. A. Jurf and S. C. Butner, "Advances in Oxide-Oxide CMC," *J. Engineering for Gas Turbines and Power, Trans. ASME,* vol. 122, pp. 202-205, 2000.

[7] I. COI Ceramics, "http://www.coiceramics.com/oxidepg.html," [Online]. Available: http://www.coiceramics.com/oxidepg.html. [Accessed Jan 2015].

[8] D. M. Wilson, D. C. Lunenburg and S. L. Lieder, "High Temperature Properies of Nextel 610 and Alumina-Based Nanocomposite Fibers," *Ceramic Engineering and Science Proceedings,* vol. 14, p. 609, 1993.

[9] D. M. Wilson, "Statistical Tensile Strength of Nextel 610 and Nextel 720 Fibers," *Journal of Materials Science,* vol. 32, p. 2535, 1997.

[10] D. M. Wilson and L. R. Visser, "High Performance Oxide Fibers for Metal and Ceramic Composites," *Composites Part A,* vol. 32, pp. 1143-1153, 2001.

[11] A. R. Bunsell and M. H. Berger, "Fine Diameter Ceramic Fibres," *Journal of the European Ceramic Society,* vol. 20, p. 2249, 2000.

[12] S. R. Hilburn, "Experimental Investigation of Mechnical Behavior of an Oxide/Oxide Ceramic Composite in Interlaminar Shear and Under Combined Tension-Tension Loading," Air Force Institute of Technology, Wright-Patterson AFB, OH, 2014.

[13] D. M. Wilson, S. L. Lieder and D. C. Lunenburg, "Microstructure and High Temperature Properties of Nextel 720 Fibers," *Ceramic Engineering and Science Proceedings,* vol. 16, p. 1005, 1995.

[14] C. Milz, J. Goering and H. Schneider, "Mechanical and Microstructural Properties of nextel 720 Relating to its Suitability for High Temperature Application in CMCs," *Ceramic Engineering and Science Proceedings,* vol. A20, p. 191, 1999.

[15] R. S. Hay, E. E. Boakye, M. D. Petry, Y. Berta, K. Von Lehmden and J. Welch, "Grain Growth and Tensile Strength of 3M Nextel 720 after Thermal Exposure," *Ceramic Engineering and Science Proceedings,* vol. 20, no. 3, pp. 153-163, 1999.

[16] "3M Ceramic Textiles Technical Notebook," 3M Ceramic Fibers and Textiles, St. Paul, MN, 2001.

[17] F. Deleglise, M. H. Berger, D. Jeulin and A. R. Bunsell, "Microstructural Stability and Room Temperature Mechanical Properies of the Nextel 720 Fibre," *Journal of the European Ceramic Society,* vol. 21, no. 5, pp. 569-580, 2001.

[18] F. Deleglise, M. H. Berger and A. R. Bunsell, "Microstructural Evolution Under Load and High Temperature Deformation Mechanisms of a Mullite/Alumina Fibre," *Journal of the European Ceramic Society,* vol. 22, pp. 1501-1512, 2002.

[19] G. W. Sherer, "Coarsening in a Viscous Matrix," *Journal of the American Ceramic Society,* vol. 81, pp. 49-54, 1998.

[20] R. K. Bordia and A. Jagota, "Crack Growth and Damage in Constrained Sintering Films," *Journal of the American Ceramic Society,* vol. 76, pp. 2475-85, 1993.

[21] M. B. Ruggles-Wrenn, P. Koutsoukos and S. S. Baek, "Effects of Environment on Creep Behavior of Two Oxide/Oxide Ceramic-Matrix Composites at 1200°C," *J. Mater Sci,* vol. 43, pp. 6734-6746, 2008.

[22] H. Fujita, G. Jefferson, R. M. McMeeking and F. W. Zok, "Mullite/Alumina Mixtures for Use as Porous Matrices in Oxide Fiber Composites," *American Ceramic Society,* vol. 87, no. 2, pp. 261-267, 2004.

[23] H. Fujita, C. G. Levi, F. W. Zok and G. Jefferson, "Controlling Mechanical Properties of Porous Mullite/Alumina Mixtures via Precursor-Derived Alumina," *Journal of the American Ceramic Society,* vol. 88, no. 2, pp. 367-75, 2005.

[24] M. B. Ruggles-Wrenn and J. C. Braun, "Effects of steam environment on creep behavior of NextelTM720/alumina ceramic composite at elevated temperature," *Materials Science and Engineering,* vol. 497, pp. 101-110, 2008.

[25] E. Volkmann, M. D. Barros, K. Tushtev, W. C. Pritzkow, D. Koch, J. Goring, C. Wilhelmi, G. Grathwohl and K. Rezwan, "Influence of the Matrix Composition and the Processing Conditions on the Grain Size Evolution of Nextel 610 Fibers in Ceramic Matrix Composites after Heat Treatment," *Advanced Engineering Materials,* 2014.

[26] M. L. Antti, E. Lara-Curzio and R. Warren, "Thermal Degradation of an Oxide Fibre (Nextel 720)/Aluminosilicate Composite," *European Ceramic Society 24,* 2004.

[27] D. J. Buchanan, R. John and L. P. Zawada, "Off-Axis Creep Behavior of Oxide/Oxide Nextel 720/AS-0," *Composites Science and Technology 68,* 2008.

[28] E. A. Carelli, H. Fugita, J. Y. Yang and F. W. Zok, "Effects of Thermal Aging on the Mechanical Properties of a Porous-Matrix Ceramic Composite," *American Ceramic Society,* vol. 85, no. 3, pp. 595-602, 2002.

[29] R. J. Kerans, G. E. Fair and T. A. Parthasarathy, "Damage Progression in Ceramic Composites," Air Force Research Laboratory, Wright-Patterson AFB, OH, 2005.

[30] G. Fair, "Ceramic Composites for Structural Aerospace Applications: Processing and Properties," Air Force Research Laboratory, Wright-Patterson AFB, OH, 2008.

[31] J. M. Mehrman, M. B. Ruggles-Wrenn and S. S. Baek, "Influence of Hold Times on the Elevated-Temperature Fatigue Behavior of an Oxide-Oxide Ceramic Composite in Air and in Steam Environment," *Composite Science and Technology,* vol. 67, pp. 1425-1438, 2007.

[32] M. B. Ruggles-Wrenn, G. Hetrick and S. S. Baek, "Effects of Frequency and Environment on Fatigue Behavior of an Oxide-Oxide Ceramic Composite at 1200°C," *International Journal of Fatigue,* vol. 30, pp. 502-516, 2008.

[33] T. Ishikawa, "Advances in Inorganic Fibers," *Adv Polym Sci,* vol. 178, pp. 109-144, 2005.

[34] E. Volkmann, K. Tushtev, D. Koch, C. Wilhelmi, J. Goring and K. Rezwan, "Assessment of Three Oxide/Oxide Ceramic Matrix Composites: Mechanical Performance and Long-Term Stability," Composite Part A: Applied Science and Manufacturing.

[35] E. Volkmann, A. Dentel, K. Tushtev, C. Wilhelmi and K. Rezwan, "Influence of Heat Treatment and Fiber Orientation on the Damage Threshold and the Fracture Behavior of Nextel Fiber-Reinforced Mullite-SiOC Matrix Composites Analysed by Acoustic Emission Monitoring," *J Mater Sci,* 2014.

[36] E. Volkmann, L. L. Evangelista, K. Tushtev, D. Koch, C. Wilhelmi and K. Rezwan, "Oxidation-induced Microstructural Changes of a Polymer-Derived Nextel TM 610 Ceramic Composite and Impact on the Mechanical Performance," *J Mater Sci,* vol. 49, pp. 710-719, 2014.

[37] Y. Wang, H. Cheng, H. Liu and J. Wang, "Effects of Sintering Temperature on Mechanical Properties of 3D Mullite Fiber (ALF FB3) Reinforced Mullite Composites," *Ceramics International,* vol. 39, pp. 9229-9235, 2013.

[38] M. B. Ruggles-Wrenn, S. Mall, C. A. Eber and L. B. Harlan, "Composites Part A," *Effects of Steam Environment on High-Temperature Mechanical Behavior of Nextel TM 720/Alumina (N720/A) Continuous Fiber Ceramic Composite,* vol. 37, pp. 2029-2040, 2006.

REPORT DOCUMENTATION PAGE

Form Approved
OMB No. 074-0188

PLEASE DO NOT RETURN YOUR FORM TO THE ABOVE ADDRESS.

1. REPORT DATE *(DD-MM-YYYY)*	2. REPORT TYPE	3. DATES COVERED *(From – To)*
26-03-2015	Master's Thesis	October 2013 – March 2015

TITLE AND SUBTITLE

Effect of Prior Exposure at Elevated Temperatures on Tensile Properties and Stress-Strain Behavior of Three Oxide/Oxide Ceramic Matrix Composites

5a. CONTRACT NUMBER

5b. GRANT NUMBER

5c. PROGRAM ELEMENT NUMBER

6. AUTHOR(S)

Hull, Christopher J., Captain, USAF.

5d. PROJECT NUMBER

5e. TASK NUMBER

5f. WORK UNIT NUMBER

7. PERFORMING ORGANIZATION NAMES(S) AND ADDRESS(S)

Air Force Institute of Technology
Graduate School of Engineering and Management (AFIT/ENY)
2950 Hobson Way, Building 640
WPAFB OH 45433-8865

8. PERFORMING ORGANIZATION REPORT NUMBER

AFIT-ENY-MS-15-M-228

9. SPONSORING/MONITORING AGENCY NAME(S) AND ADDRESS(ES)

Air Force Research Lab/RXCC
LtCol Chad Ryther
2977 Hobson Way, Bldg 655
WPAFB OH 45433-7734
(937)656-9153 chad.ryther@us.af.mil

Air Force Research Lab/RXCC
Dr. Richard Hall
2977 Hobson Way, Bldg 655
WPAFB OH 45433-7734
(937)255-9097 richard.hall.16@us.af.mil

10. SPONSOR/MONITOR'S ACRONYM(S)
AFRL/RXCC

11. SPONSOR/MONITOR'S REPORT NUMBER(S)

12. DISTRIBUTION/AVAILABILITY STATEMENT

DISTRIBUTION STATEMENT A:
APPROVED FOR PUBLIC RELEASE; DISTRIBUTION UNLIMITED

13. SUPPLEMENTARY NOTES

14. ABSTRACT

Thermal stability of three oxide-oxide ceramic matrix composites was studied. The materials studied were Nextel™610/aluminosilicate (N610/AS), Nextel™720/aluminosilicate (N720/AS), and Nextel™720/Alumina (N720/A), commercially available oxide-oxide ceramic composites (COI Ceramics, San Diego, CA). The N610/AS composite consists of a porous aluminosilicate matrix reinforced with laminated woven alumina N610 fibers. The N720/AS and N720/A composites consist of a porous oxide matrix reinforced with laminated, woven mullite/alumina (Nextel™720) fibers. The matrix materials are aluminosilicate in N720/AS and alumina in N720/A. All three composites have no interface between the fibers and matrix, and rely on the porous matrix for flaw tolerance. The N610/AS and N720/AS CMCs were heat treated in laboratory air for 100 h at 1100°C and for 10, 20, 40 and 100 h at 1200°C. The N720/A CMC was heat treated in laboratory air for 100 h at 1200°C and for 10, 20, 40 and 100 h at 1300°C. The room-temperature tensile properties of all composites were measured after each type of heat treatment. Effects of prior heat treatment on tensile strength were evaluated. Heat treatment at 1100°C had little effect on tensile strength of the N610/AS and N720/AS composites, while heat treatment at 1200°C caused dramatic loss of tensile strength. Poor strength retention after heat treatment at 1200°C is attributed to degradation of the aluminosilicate matrix. The N720/A composite exhibited excellent thermal stability, retaining about 90% of its tensile strength after heat treatment at 1300°C. Results indicate that the aluminosilicate matrix is considerably more susceptible to localized densification and coarsening of the porosity than the alumina matrix.

15. SUBJECT TERMS

Ceramic Matrix Composites, Composite Materials, Ceramic Fibers, Ceramic Materials, Fiber Reinforced Composites, Alumina, Aluminosilicate, Oxides, Nextel™ 610 Fiber, Nextel™ 720 Fiber, Elevated Temperature

16. SECURITY CLASSIFICATION OF:			17. LIMITATION OF ABSTRACT	18. NUMBER OF PAGES	19a. NAME OF RESPONSIBLE PERSON
a. REPORT	b. ABSTRACT	c. THIS PAGE			Dr. Marina Ruggles-Wrenn, (AFIT/ENY)
U	U	U	UU	191	19b. TELEPHONE NUMBER *(Include area code)* (937) 255-3636, ext 4641 (Marina.Ruggles-Wrenn@afit.edu)

Standard Form 298 (Rev. 8-98)
Prescribed by ANSI Std. Z39-18